A Survey of Semiconductor Radiation Techniques

Edited by L.S. SMIRNOV

MIR PUBLISHERS
MOSCOW

Prof SMIRNOV, L. S., D.Sc.
(Physics and Mathematics)

A specialist in physics of semiconductors and dielectrics was among the pioneers of a new and promising field, that of radiation physics and technology. Since 1954, he has been actively working in research of radiation effects in semiconductors. At present, Professor Smirnov is with the Institute of Physics of the USSR Academy of Sciences, Siberian Branch, and is head of a section currently engaged in the execution of comprehensive programs aimed at developing basic methods using particle radiation for localized control of properties of semiconductors in micro- and optoelectronics applications. Among the methods are ion implantation, annealing of semiconductors by pulsed radiation, radiation enhanced diffusion, etc.

Prior to his present position, professor Smirnov was with the Lebedev Institute of Physics of the USSR Academy of Sciences, the first USSR scientific center ever to start an investigation of ionization processes and radiation-induced defects in semiconductors.

This book gives an outline of the evolution of semiconductor radiation technology and introduces the reader to the pertinent works done by the experts of the Institute of Physics of the Siberian Branch of the USSR Academy of Sciences.

The authors who contributed to writing this book are prof. L. S. Smirnov, D.Sc. (Phys. and Math.), V. V. Bolotov, A. V. Vasilyev, G. A. Kachurin, N. B. Pridachin, and V. F. Stas', all Cand. Sc. (Phys. and Math.).

A Survey of Semiconductor Radiation Techniques

Edited by L.S.SMIRNOV

ИЗДАТЕЛЬСТВО
МИР

В. В БОЛОТОВ, А. В. ВАСИЛЬЕВ, А. В. ДВУРЕЧЕНСКИЙ, Г. А. КАЧУРИН,
Н. Б. ПРИДАЧИН, Л. С. СМИРНОВ, В. Ф. СТАСЬ

ВОПРОСЫ РАДИАЦИОННОЙ ТЕХНОЛОГИИ ПОЛУПРОВОДНИКОВ

Издательство «Наука»
Сибирское отделение

V. V. BOLOTOV, A. V. VASILYEV, A. V. DVURECHENSKY,
G. A. KACHURIN, N.B. PRIDACHIN, L. S. SMIRNOV,
V. F. STAS'

A Survey of Semiconductor Radiation Techniques

Edited by Prof. L. S. SMIRNOV

MIR PUBLISHERS MOSCOW

Translated from the Russian by Igor Frolov

First published 1983
Revised from the 1980 Russian edition

На английском языке

© Издательство «Наука», 1980
© English translation, Mir Publishers, 1983

PREFACE

Semiconductor materials show temporary and metastable changes in their electrophysical, optical and luminescent properties when irradiated with elementary particles and quanta. Although apparently simple, the radiation methods found application only after many years of extensive studies. While the research is still under way, a qualitative generalized model of the radiation processes has emerged with the effective means of control of said processes defined and developed, which allows obtaining the required fairly stable changes in characteristics of crystals and films. Considering radiation from the viewpoint of its technological applicability, one is primarily concerned with the stability of the effects achieved.

Thin layer doping by ion bombardment, radiation compensation of the material, injection of radiative recombination centers, control of the photoconductivity spectra and nonequilibrium carrier lifetime, and doping by nuclear transmutation are but a few examples that illustrate the importance of radiation methods to semiconductor technology. Many new methods, e.g. ionic synthesis, employment of amorphous and disordered layers, radiation-enhanced diffusion, etc., are still under development. A very promising trend in the radiation techniques is the development of combination methods of crystal processing, e.g., thermal treatment under radiation, radiation concurrent with laser action, radiation under pressure, growing crystals in radiation fields, though this is one of the areas where a further work is obviously required.

The properties of crystals change as a result of any imperfection (e.g., vacancies, interstitial atoms, their clusters, impurities, etc.) or deviation from the initial state of the crystal lattice.

So, the notion of radiation defect implies any change caused to the crystal structure by radiation. Sometimes, it is better to use the term "active center" instead of "radiation defect" as more descriptive of the role of this phenomenon in the crystal.

Historically, the use of the radiation methods in semiconductor technology had been first suggested in the 50s after the advent of the electron (n-p conversion for germanium) and neutron (doping by nuclear transmutation) irradiation techniques. At that stage, however, such methods did not receive immediate developmental effort due to an incomplete knowledge of the ghost effects involved in radiation processes, and, mainly, due to the availability of competing methods. On the contrary, the semiconductor doping by ion implantation, first described by M. M. Bredov and W. Shockley, rapidly gained wide acceptance despite the fact that many implications of this method remained unclear, since its advantages such as

reproducibility of results and their little dependence on the inherent inhomogeneities of the material yielded an immediate positive effect.

At present, the new, more stringent requirements for homogeneity of semiconductor materials and for contamination-free processing environment as well as the need for developing the methods of localized control of semiconductor properties and for hardening, semiconductor devices against the effects of thermal and radiation fields have prompted a keen interest to the radiation methods. It is not unlikely that among the major reasons have been, on the one hand, the examples of successful employment of the radiation methods and, on the other hand, the inability, in many instances, of the existing standard techniques to provide an adequate answer to technological problems.

The basic theory of radiation methods is presented in a number of books on the physics of semiconductor radiation processes. In the present publication prepared by a group of research workers of the Semiconductor Physics Institute of the Siberian Branch of the USSR Academy of Sciences, a survey of the current trends in the semiconductor radiation techniques is given and an attempt is made at summarizing the available material on radiation damage and radiation control in semiconductors and at analyzing the drawbacks and merits of each radiation method. This information combined with that on the existing standard methods forms the core of a new and promising field of semiconductor technology, the semiconductor radiation technology.

Despite the continuing intensive studies of radiation effects in semiconductors, many important problems still await their solution. This refers, first of all, to the role of the ionization processes, stability of the defect clusters, the influence of impurities on amorphization and crystallization attendant with ion bombardment. The problems grow in complexity when new materials, compound semiconductors, semiconductor-dielectric systems, etc. are coming into use, as this expands the range of possible technological solutions and practical designs. All this makes us quite confident of an interesting future for the radiation technology.

It is hoped that translation of this book into English will contribute to the popularization of the radiation physics and technology and to the concentration of efforts on the problems that await their solution.

L. S. Smirnov

CONTENTS

Preface 5

Chapter 1. **Characteristics of Radiation Defects** 9

1.1. Introduction 9
1.2. Point Defects 16
1.3. Disordered Regions 25
1.4. Disordered Layers 33

References 43

Chapter 2. **Defect Inventory Control in Defect Centers** 51

2.1. Species of Particles and Their Energy 51
2.2. Importance of Crystal Prehistory 59
2.3. Importance of Radiation Intensity and Temperature 69

References 75

Chapter 3. **Radiation-Enhanced Diffusion (RED)** 80

3.1. General Information 80
3.2. Experimental Studies of RED in Semiconductors 85
3.3. Principles and Techniques of Radiation Control of Diffusion in Semiconductors 105

References 106

Chapter 4. **Possibilities of Technological Employment of Radiation Defects** 110

4.1. Control of Electrophysical Parameters 110
4.2. Local Levels 133
4.3. Employment of Disordered Layers 148

References 154

Chapter 5. **Status and Prospects of Ion Implantation in Semiconductors** 163

References 171

Chapter 6. **Ion Implantation in Indium Antimonide** 172

6.1. Basic Characteristics and Prospects of Employment of Indium Antimonide 172
6.2. Radiation Effects Caused by Corpuscular and Electromagnetic Irradiations 173
6.3. Behaviour and Properties of Radiation Defects Caused by Ion Bombardment 177
6.4. Behaviour of Implanted Impurities 184
6.5. Production of Semiconductor Device Structures by Ion Bombardment 190

References 195

Chapter 7. **High Dose and Current Density Effects in Ion Implantation of Semiconductors** 198

7.1. Attendant Factors Affecting High-Dose Ion Implantation 199
7.2. Structural Changes in Layers During Irradiation and Annealing 207
7.3. Electrical Characteristics of Layers 213
7.4. Impurity Profiles at Various Doses of Irradiation and Beam Current Densities 216

References 220

Chapter 8. **Laser Annealing of Implanted Layers** 225

8.1. Major Factors Affecting Implanted Layers During Laser Annealing 226
8.2. Laser Annealing of Implanted Silicon Layers 230
8.3. Laser Annealing of Implanted Layers in Gallium Arsenide 235
8.4. Redistribution of Impurity by Laser Annealing 238
8.5. Special Cases of Laser Treatment 243

References 246

Chapter 9. **Production of Thin Films by Ion and Molecular Beam Deposition** 249

9.1. Basic Methods of Film Synthesis Using Ion and Molecular Beams 249
9.2. Synthesis of Compounds by Ion Implantation 250
9.3. Synthesis of Compounds by Ion Implantation of Components into an Interlayer 255
9.4. Deposition of Films by Ion Beams 257
9.5. Molecular Beam Epitaxy 261

References 269

Chapter 10. **Doping by Nuclear Transmutation** 272

10.1. The Concept of Nuclear Reactions 273
10.2. Silicon Doping by Nuclear Transmutation 277
10.3. Germanium Doping by Nuclear Transmutation 282
10.4. Doping of Binary Compounds by Nuclear Transmutation 285
10.5. Advantages and Disadvantages of Nuclear Transmutation Doping 287

References 288

CHAPTER 1

CHARACTERISTICS OF RADIATION DEFECTS

Sec. 1.1. Introduction

The influence of high-level radiation (e.g., gamma rays, high-energy electrons, neutrons, ions) on semiconductor materials produces quasi-stable changes in the properties of such materials. These changes stem from resulting primary radiation-induced defects, such as vacancies, interstitials, disordered regions (DR) whose interaction with various imperfections of the crystal structure (say, dissolved impurities) gives rise to a wide range of active centers.

In discussion of the properties of radiation-induced defects, emphasis will be placed on silicon and germanium, the semiconductors that are best known and most extensively used in semiconductor device technology. The main interest will be focused on defects showing stability at room and higher temperatures, the property that readily lends itself to technological application. As the understanding of the nature of the radiation defects in other semiconductors (GaAs, InSb, SiC, etc.) of interest is practically lacking, the radiation defects in these materials will be considered in Ch. 4 which discusses the effects of radiation on various crystal characteristics.

The amount of energy lost by the particles impinging on the crystal and the mechanisms of such a loss vary with the particle species and its energy, which, in turn, alters the structural damage formation process. Tables 1.1 and 1.2 supply some data relating to

Table 1.1

Threshold and boundary (for electrons) energies of formation of radiation defects in some semiconducting materials

Material	Displaced atom	Boundary energy, keV	Threshold energy, eV	Irradiation temperature, K	References
Ge	Ge	360	14.5	289	[1, 19]
		380	15.6	300	[2, 19]
Si	Si	215	20.4	300	[3, 4, 19]
GaAs	Ga	228	8.8	—	[19]
	As	273	10.1	300	[19]
	Ga	—	17-18	77	[19]
InSb	In	247	5.8	77	[19]
	Sb	286	6.8	77	[19]
SiC	Si, C	—	17-30	—	[57]

Energy lost by fast particles in semiconductor material crystals

Particle	Energy E	Energy loss mechanisms
Electron	$E < E_{\text{bound}}$	1. Ionization 2. Excitation of atomic vibrations
Electron	$E \geqslant E_{\text{bound}}$	1. Ionization 2. Elastic scattering, formation of vacancies (V) and interstitials (I) 3. Bremsstrahlung

Table 1.2

Some relations	Qualitative relationships and clarifications	References
Ionization losses: $dE/dx = 2\pi Ne^4 Z/mc^2\beta^2 \times \{\ln[mc^2\beta^2 E/2I^2(1-\beta^2)] - [2\sqrt{(1-\beta^2)} - 1 + \beta^2]\ln 2 + 1 - \beta^2 + 0.125[1-\sqrt{(1-\beta^2)}]^2\}$	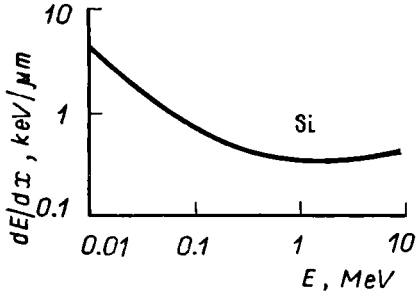	[7, 19]
Main energy losses are due to ionization (see relations for Ge and Si given as examples)	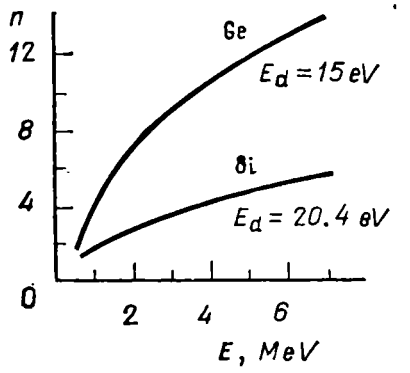	[7, 19]
	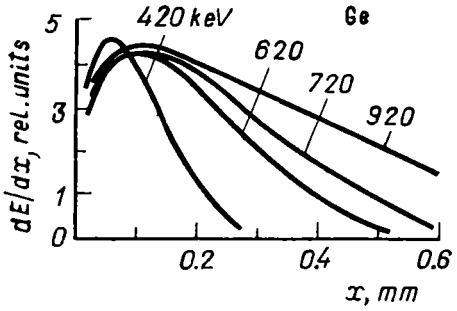	
A — a ratio of radiation losses to ionization losses: $A = E_0 Z/1600\ mc^2$ at $E = 25$ and 57 MeV for Ge and Si, respectively; ionization and bremsstrahlung losses are equal	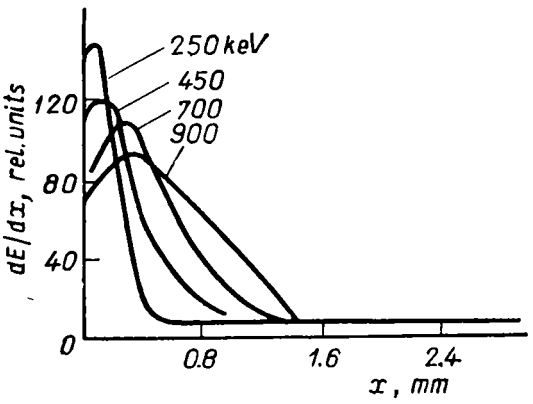	[7, 19, 61]

Particle	Energy E	Energy loss mechanisms
Electrons	$E \geqslant 10$ Mev	1. Ionization 2. Formation of V and I 3. Bremsstrahlung 4. Formation of DR 5. Nuclear reactions yielding high-energy products
Gamma-quanta	Co^{60} gamma-source, gamma radiation of reactor, $E \simeq 1$ to 10 MeV	1. Photo effect 2. Compton effect 3. Formation of electron-positron pairs
Bremsstrahlung gamma-radiation	$E \geqslant 15$-28 MeV	1. Photo effect 2. Compton effect 3. Formation of pairs 4. Photonuclear reactions, formation of DR by products of nuclear reactions
Thermal neutrons	$E \simeq 0.025$ eV	Nonelastic collisions with atomic nuclei, nuclear reactions yielding high-energy products

Table 1.2 Cont'd

Some relations	Qualitative relationships and clarifications	References
Number of displacements produced by recoil atom (after Kinchin and Pease) with energy E: $n = E/2E_d$		[5-7, 19]
Photo effect dominates at $E \leqslant 1$ MeV Probability of Compton effect grows with increase in Z, energy of compton-electron may be close to E of gamma-quantum Formation of pairs begins at $E > 1.02$ MeV. For materials with low Z (Ge and Si) and for gamma-radiation of Co^{60} and reactor, Compton effect dominates over photo effect and formation of pairs. Vacancies and interstitials form as a result of internal irradiation of the crystal with compton-electrons, photo electrons, and components of electron-positron pairs	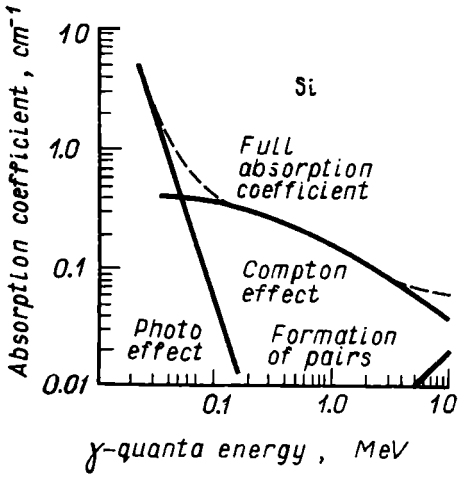	[7]
In Si, photonuclear reactions occur at $E > 15$ MeV; in Ge, at $E > 25$ MeV	Probability of formation of V and I under gamma-radiation is lower than that under electron irradiation by about two orders of magnitude (since first it is required to generate a high-energy electron)	[8, 9, 10]
Interaction cross-sections are extremely large: about 10^{-19} cm^2. Both elementary defects, such as V and I appearing due to gamma-radiation	Examples of nuclear reactions in Si and Ge: $^{30}Si\,(n, \gamma)^{31}Si \xrightarrow[2.6\ h]{\beta} {}^{31}P$ $^{74}Ge\,(n, \gamma)^{75}Ge \xrightarrow[82\ min]{\beta} {}^{75}As$	[7, 58]

Particle	Energy E	Energy loss mechanisms
Fast neutrons	$E > 100$ keV	Elastic scattering at atomic nuclei
High-energy neutrons	$E \gtrsim 5$ MeV	1. Elastic scattering at atomic nuclei 2. Nuclear reactions
Protons and other light ions	$E \leqslant 5$-10 keV	1. Ionization 2. Elementary defects (V and I)
(mass of ion is below that of atom of semiconductor material)	$E > 10$-30 keV $E > 10$-20 MeV	1. Ionization 2. Elementary defects 3. Complex defects of DR type 4. Nuclear reactions
Heavy ions		

Note. Symbols: E_d — threshold energy for formation of defects (see Table 1.1); coordinate system; $\beta = v/c$; I — mean ionization potential (11.5 Z eV in silicon);

Table 1.2 Cont'd

Some relations	Qualitative relationships and clarifications	References
background and formation of light-weight reaction products, and complex ones (e.g., DR) arise		
Various structural defects appear; defects of DR type dominate	Number of displacements caused by recoil atom with energy E; $n = E/2E_d$	[5, 7]
Reactions, such as (n, p), (n, α), (n, d) occur	Fast neutrons arising from fission have energy from 0 to 15 MeV; mean energy, 2 MeV	[5, 7]
At beginning of light ion path, main losses are caused by ionization. Losses grow as the particle movement is retarded during elastic scattering	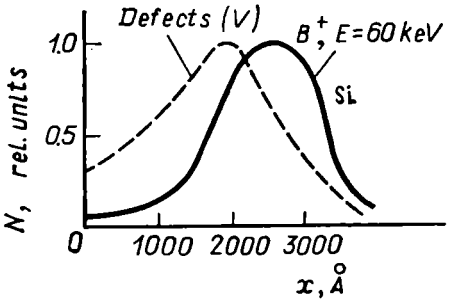	[11] [11, 12]
Main energy losses are due to elastic displacements (60-80%)		[11]

θ_A and φ_A — angles determining the movement of the recoil atom in the spherical
n — number of displaced atoms, cm^{-1}. Other symbols are universally adopted ones.

the threshold energy and basic mechanisms whereby different particles lose their energy.

Sec. 1.2. Point Defects

From the technological viewpoint, it is important to know the properties of such point defects as the atoms of chemical impurities, vacancies and interstitial atoms and their complexes. The behaviour of doping impurities in crystals received detailed treatment in many papers [13-20, 26, 59, 60]. Tables 1.3 and 1.4 present the contents of uncontrollable impurities in germanium and silicon.

Irradiation of the crystal with high-energy particles results in emergence of non-equilibrium defects, such as vacancies and interstitials (the components of the Frenkel pair), disordered regions (DR), complexes of intrinsic defects with impurities, etc. As was implied above, to form the Frenkel pair, the atom should be imparted a certain amount of energy called the *threshold energy*. So far, the threshold

Table 1.3

Contents of some impurities in pure silicon

Impurity	Method of growing crystals	Impurity content, at/cm^3	Measurement technique	References
H	Czochralski method	$1.7 \cdot 10^{19}$	Mass spectroscopy	[21]
O	Same	$1.5 \cdot 10^{19}$	Same	[21]
O	Same	$5\text{-}7 \cdot 10^{17}\text{-}2 \cdot 10^{18}$	IR spectroscopy	—
C	Same	$1.1 \cdot 10^{19}$	Mass spectroscopy	[21]
C	Same	$1 \cdot 10^{16}\text{-}3 \cdot 10^{17}$	IR spectroscopy	—
O	Same	$2 \cdot 10^{17}\text{-}10^{18}$	Activation analysis	[22]
C	Same	$3 \cdot 10^{16}\text{-}3 \cdot 10^{17}$	Same	[22]
O	Zone refining in vacuum	$1 \cdot 10^{15}\text{-}3 \cdot 10^{15}$	Same	[22]
O	Zone refining in Ar	$5 \cdot 10^{15}\text{-}2 \cdot 10^{16}$	Same	[22]
C	Zone refining in vacuum and Ar	$3 \cdot 10^{15}\text{-}4 \cdot 10^{16}$	Same	[22]
O	Zone refining	$< 10^{16}$	IR spectroscopy	—
C	Zone refining	$1 \cdot 10^{16}\text{-}10^{17}$	Same	—
O	Decomposition of silane	$< 10^{16}$	Same	—
C	Same	$\leqslant 3 \cdot 10^{16}$	Same	—

Table 1.4

Contents of some impurities in pure germanium

Impurity	Impurity content, at/cm³	Measurement technique	References
O	$\sim 10^{16}$	IR spectroscopy	[24]
H	$2.5 \cdot 10^{18}$	Mass spectroscopy	[21]
O	$3.6 \cdot 10^{18}$	Same	[21]
C	$2.3 \cdot 10^{18}$	Same	[21]
	$\sim 10^{18}$	Same	[21]
	$\sim 3 \cdot 10^{19}$	Same	[25]
Ca	$\sim 9 \cdot 10^{19}$	Same	[25]
	$\sim 3 \cdot 10^{18}$	Same	[25]
Ba	$\sim 9 \cdot 10^{18}$	Same	[25]
H	$\sim 3 \cdot 10^{18}$	Vacuum melting	[13]
Mg	$3.6 \cdot 10^{18}$-$2.83 \cdot 10^{19}$	Mass spectroscopy	[140]
Fe	$1.4 \cdot 10^{17}$-$7.9 \cdot 10^{18}$	Same	[140]
Co	$4.4 \cdot 10^{16}$-$1.37 \cdot 10^{17}$	Same	[140]
Ni	$4.4 \cdot 10^{16}$-$1.86 \cdot 10^{17}$	Same	[140]
Cu	$4.4 \cdot 10^{16}$-$1.81 \cdot 10^{17}$	Same	[140]
Au	$4.4 \cdot 10^{16}$-$1.37 \cdot 10^{17}$	Same	[140]

Note. All crystals are grown by the Czochralski method.

energies have been reliably established for a large number of semiconductor materials [19] (see Table 1.1). However, the problem is being investigated at present [27]. Fairly recently [19], it was found that many factors contributed to the formation of the Frenkel defect in semiconductors (the atoms of several coordination spheres take part in the process). Also, a decrease in the threshold energy with a rising temperature and its anisotropy were discovered. The values of the defect formation threshold energy, E_d (in eV), most reliably established at 300 K are 20.4 for silicon and $\simeq$15 for germanium [19] (see Table 1.1).

The remarkable mobility of vacancies and interstitials and the emergence of defect associations which arise from their interactions with the crystal impurity, with each other and with various crystal imperfections present a severe problem in the study of the characteristics of primary defects [19]. Extra low temperatures are required to "freeze" the thermal motion of the particles and permit observation of free vacancies and interstitials. In this respect, even the temperatures of 0.5 to 1.5 K are insufficient to restrict the movement of the interstitials in silicon [19, 28, 29]. For some data relating to

Table 1.5

Properties of free vacancy in silicon

Material	Defect	Level, charge state	Level type*	σ_n, σ_p, cm²	Annealing temperature, K	Migration activation energy, eV	References
		Conduction band					
	$V^=$	=			~ 90	0.18±0.02	[30, 31, 32]
n		—(E_C–0.09) eV	A	—			
	V^-	—			—	—	
		— ?	A	—			
	V^0	0			150		
p		—(E_V+ +0.11) eV**	D	$\sigma_p^0 = 5 \cdot 10^{-17}$		0.33±0.03	
	V^+	+at $E < (E_V +$ +0.045) eV**					
		Valence band					

* In tables 1.5-1.9: D — donor level, A—acceptor level.
** According to different authors.

the properties of primary defects in silicon and germanium refer to Tables 1.5-1.8.

Defect complexes form another large group of radiation defects. Defect associations arise as a result of interactions of intrinsic defects with one another and with impurities both doping and uncontrollable. When the components of the Frenkel pair interact with the impurities, this leads to the formation of defect complexes, such as the vacancy-impurity and interstitial-impurity pairs, and to a change in the position of the impurity in the crystal lattice, which takes the form of displacement of the impurity from the regular lattice site into an interstitial position by its own interstitial atom (the Watkins effect) [31, 42] as well as dissolution of the interstitial impurity in the radiation-induced vacancies [7], annihilation of vacancies and interstitials successively captured by the impurity atom (the annihilation center [19]).

To generate most defect complexes, the components of the Frenkel pair should migrate over long distances within the crystal. The efficiency of the generation process depends on the irradiation conditions (temperature, intensity of the stream of particles, etc.), the concentration of reacting components and energy spent in the proc-

Table 1.6

Properties of free vacancy in germanium

Material	Defect	Level, charge state	Level type	Annealing temperature, K	Migration activation energy, eV	References
		Conduction band				
n	$V^=$	$=?$		~ 80	~ 0.2*	[19, 36, 37]
		—(E_C—0.21—0.27)eV	A	—	0.006-0.04**	[19, 37]
	V^-	—?		—	~ 0.09**	[39, 41]
p		—?	A	~ 140	~ 0.1**	[19, 40]
	V^0	0				
		Valence band				

* Results of experimental annealing.
** Results of experimental irradiation.

Table 1.7

Properties of free interstitial in silicon

Material	Defect	Level, charge state	Level type	Annealing temperature, K	Migration activation energy, eV	References
		Conduction band				
		----------	Chemical			
n	I^-		donor			
		—		~ 140-180	~ 0.3	[19, 34, 35, 42]
		—(E_C—0.4) eV	A			
—	I^0	0		540-600	~ 1.5	[34, 35]
		—(E_V+0.4) eV	D			
	I^+	+		370-420	~ 0.85	[34, 35]
p				$\leqslant 4$*	~ 0	[19, 31, 35, 42]
		----------	Chemical			
			acceptor			
		Valence band				

* It is assumed that the diffusion mechanism is adiathermal [33, 35].

Table 1.8

Properties of free interstitial in germanium

Material	Defect	Level, charge state	Level type	Annealing temperature, K	Migration activation energy, eV	References
		Conduction band				
n	$I^=$	=		27	0.05	[35]
		—	A			
		----------	Chemical donor			
	I^-	—		65	0.15	
		—	A			
—	I^0	0		$\leqslant 6$	0-0.0044*	
				220	—	
p		—	D			
	I^+	+		$\geqslant 77$	—	
		----------	Chemical acceptor			
		Valence band				

* It is assumed that the diffusion mechanism is adiathermal [35].

ess (for more detail, see [19]). The characteristics of some defect centers in silicon are given in Table 1.9.

Apart from the defects indicated in Table 1.9, it was discovered that silicon had other defect complexes [19, 51, 52, 53] whose nature and properties are at present lacking the full understanding.

The basic evidence on the formation of defect complexes in germanium has been derived from the investigations of the electrical, recombination and optical characteristics of the irradiated materials. In *n*-type germanium, the defects caused by electron and gamma [19, 41] radiation are known best. The main defects are the complexes that include a donor impurity and a vacancy.

Irradiation of *n*-type germanium results in the *n-p* conversion. Right after the conversion an energy level [41] emerges that changes its position within the energy gap in accordance with the donor impurity type: ($E_V + 0.1$ eV), ($E_V + 0.1$ eV), ($E_V + 0.12$ eV) and ($E_V + 0.16$ eV), when the dopant is phosphorus, arsenic, antimony

or bismuth, respectively. The authors of [41] attribute the emergence of the level to the *VVD* complex.

The EPR method has been instrumental in identifying the *VV*As complex ($T_{\text{anneal}} > 210$ °C) [54]. During annealing of the defects that occur after the *n-p* conversion (*VVD*) one observes a dependence of the annealing temperature on the covalent radius of the donor impurity: $\approx$ 240, 370, 430 and 490 K for P, As, Sb and Bi used as the doping agents, respectively.

A reliable theory explaining the nature of radiation-induced defects in *p*-type germanium is lacking. A series of experiments conducted on *p*-type germanium have pointed to an important role played by the displacement of the acceptor impurity by its own interstitial atoms (the Watkins effect) [55].

The efficiency with which any radiation defects are generated depends on intricate competing processes. Thus, in oxygen-free *n*-type Si irradiated with electrons of about 1-3 MeV, the main defects are the vacancy-donor impurity pair and the divacancy, whereas in *n*-type Si containing oxygen and having a low donor impurity content these are the vacancy-oxygen pair and the divacancy. In *p*-type silicon, the properties of the irradiated crystals are considerably affected by the vacancy-oxygen pairs, K-centers, and, probably, by the vacancy-acceptor impurity pairs (see Table 1.9).

The efficiency of generation of defect complexes changes with an increase in the radiation dose. Specifically, as the radiation dose reaches a certain limit, the number of complexes of a particular type becomes maximum. This phenomenon may be attributed to (1) exhaustion of the impurity that forms part of the complex, (2) thermal dissociation of the complex (at fairly high temperatures) and (3) occurrences of annihilation of vacancies and interstitials by the impurity [19].

Point defects may be annealed out by a number of techniques that include thermal dissociation, capture of a component of the Frenkel pair by its counterpart from a defect complex [19], and rearrangement of the defect with the resultant change in its properties. The conditions of annealing (the activation energy, E_A, annealing temperature, etc.) depend, to a considerable degree, on the defect inventory of the material, i.e., its prehistory (see Table 1.9). It should be emphasized that whether or not some defect (complex) can be annealed out depends not only on its own energy parameters but on similar parameters of other defects present in the crystals and taking part in the reactions [19].

An analysis of the data presented in Table 1.9 allows one to believe that the stability of defects is enhanced with an increase in their number, that is, with an enlargement of the defect complex.

The results thus achieved attest to the complexity of the processes involved in the formation and annealing of the radiation defects

Parameters of main radiation defects in silicon

Defect	Symbol	Charge state	Level, eV	Level type
Divacancy	V_2	$V_2^{=}$	$E_C-0.23$	A
		V_2^{-}	$E_C-0.4$	A
		V_2^{0}	$E_C-0.39$	A
		V_2^{+}	$E_V+0.21$	D
Vacancy-oxygen (*A*-center)	*V*-O	(*V*-O)$^-$	$E_C-0.18$	A
		(*V*-O)^0		
Vacancy-phosphorus (*E*-center)	*V*-P	(*V*-P)$^-$	E_C-0.44	A
		(*V*-P)^0		
	V-P_2	—	—	—
Vacancy-arsenic	*V*-As	(*V*-As)$^-$	—	A
		(*V*-As)^0		
	V-As_2	—	—	—
Vacancy-antimony	*V*-Sb	(*V*-Sb)$^-$	—	A
		(*V*-Sb)^0		
	V-Sb_2		—	—
Vacancy-bismuth	*V*-Bi	(*V*-Bi)$^-$	—	A
		(*V*-Bi)^0		
	V-Bi_2	—	—	—
Vacancy-aluminium	*V*-Al	(*V*-Al)^0	$E_V+0.48$	D
		(*V*-Al)$^+$		

Table 1.9

σ_n, σ_p, cm^2	Annealing temperature, K	Migration activation energy, eV	References
$\sigma_n^- = 2 \cdot 10^{-16}$?	~ 550, reorientable	$\leqslant 1.5$	[32, 42, 43, 44, 46]
$\sigma_n^0 = 4 \cdot 10^{-15}$	~ 140, non-reorientable		
$\sigma_p^0 = 2 \cdot 10^{-16}$	~ 610, in oxygen-free material		
$\sigma_n^0 = 10^{-14}$	600-620	1.3	[32, 42]
$\sigma_n^0 = 0.8\text{-}1 \cdot 10^{-15}$			[45]
$\sigma_n^0 = 2 \cdot 10^{-16}$			[45]
$\sigma_p^- = 2.5\text{-}4 \cdot 10^{-14}$			[45]
$\sigma_p^- = 5.5 \cdot 10^{-13}$			[45]
$\sigma_n \gg 10^{-16}$	420	1.25	[43, 45, 47, 48, 49]
$\sigma_p \sim 10^{-13}$		0.95	
—	400	0.93	
$\sigma_p = 4 \cdot 10^{-14}$	440	1.07	[43, 49]
—	400	1.27	[49]
—	460	1.28	[49]
—	400	1.84	[49]
—	470	1.46	[49]
—	400	2.22	[49]
$\sigma_p \gg 10^{-16}$	470	0.77	[32, 50]

Defect	Symbol	Charge state	Level, eV	Level type
Vacancy-boron	V-B	$(V\text{-B})^0$ $(V\text{-B})^+$	$E_V+0.45$	D
Vacancy-gallium	V-Ga	$(V\text{-Ga})^0$ $(V\text{-Ga})^+$	—	D
Vacancy-oxygen (K-center)	?(V-O-C)	$?(V\text{-O-C})^0$ $?(V\text{-O-C})^+$	$E_V+0.16$ $E_V+0.3$	D
Interstitial aluminium	Al_I	Al_I^0 Al_I^+ Al_I^{++}	— $E_V+0.25$	D D
Interstitial carbon	C_I	C_I^0 C_I^+	$E_V+0.27$	D
Interstitial carbon-regular carbon	C_I-C_S	$(C_I\text{-}C_S)^0$ $(C_I\text{-}C_S)^+$	$E_V+0.33$	D
Interstitial aluminium-regular aluminium	Al_I-Al_S	—	$E_V+0.23$	—
Interstitial boron-regular boron	B_I-B_S	—	$?E_C-0.26$	—
Divacancy-oxygen	V_2O	—	$?E_C-0.3$	—
Oxygen-trivacancy	V_3O	—	$?E_C-0.27$	—

and their dependence on many conditions. This complicates the theoretical analysis of the processes in general. There exist, however, certain techniques such as the quasichemical reaction method [19, 56, 93] that may be used for performing a quantitative analysis of the specific processes attendant with irradiation and annealing of radiation defects.

Table 1.9 Cont'd

σ_n, σ_p, cm^2	Annealing temperature, K	Migration activation energy, eV	References
—	300	0.42	[33, 50]
	~ 470	0.6	[33, 50]
— —	~ 570-620	—	[33, 43]
	~ 470	—	[32]
$\sigma_p = 7 \cdot 10^{-18}$	~ 470	—	
—		—	
$\sigma_p = 7 \cdot 10^{-18}$	~ 300	—	[32]
$\sigma_p = 8 \cdot 10^{-17}$	~ 670	—	[32]
—	520	—	[32]
—	~ 420	—	[32]
—	~ 570	—	[32]
—	~ 720	—	[32]

Sec. 1.3. Disordered Regions

The greater the energy and mass of the bombarding particle, the greater the energy imparted to the knocked-on atom. As a high-energy recoil atom slows down and comes to rest in a crystal it makes many violent secondary collisions with lattice atoms which results in the production of a large number of vacancies and inter-

stitials. At the end of the recoil atom path, the density of the defects produced by the atom becomes so high and the interactions between the individual point defects so strong, that the latter acquire some additional properties. As a consequence, a plurality of point defects thus formed within a small local volume leads to the emergence of a single extended defect having specific features. Such defects have been termed as disordered regions (DR). At present the properties of DR are being extensively studied. The physical nature of DR and their influence on the crystal parameters have been examined in a number of papers and reviews [5, 7, 11, 12, 19, 43]. In the present section we shall not only summarize the basic information on the properties of DR, important from the viewpoint of possible technological applications, but also dwell on some controversial issues that received of late much attention and development. A specific importance of DR to the electrophysical and other parameters of semiconductors is discussed in Ch. 4.

As in the case of the Frenkel pair, the threshold energy has been also proposed for the formation of DR. The values of this quantity widely differ with different authors. The DR formation threshold for silicon has been set at 5 keV [6], 10 keV [74], and 20 to 40 keV [75]. For germanium, the threshold energies range from 15 to 20 keV [65]. So wide a spread is not attributed to some peculiar features of experiment or calculation, but, rather, is explained [5] by the fact that it is impossible to find the precise limits for the DR formation energy threshold, since the sizes of the DRs and the population and density of defects in their cores vary largely with the energy and mass of the bombarding particle. Nevertheless, the notion of DR formation threshold has proved to be suitable enough for extensive use.

Irradiation of semiconducting materials with elementary particles of any kind produces, along with DR, a fairly large number of point defects (see Sec. 1.1). A ratio between the DR and point defect (PD) concentrations is intricately dependent on the energy and type of the bombarding particle, impurity-defect inventory of the irradiated material, and the irradiation conditions (dose, temperature, density of the beam of impinging particles, etc.). Since both the DR and PD change the properties of the irradiated crystals, when considering the practical application (e.g., simulation of the effect of space radiation), one has to distinguish between the DR and PD effects degrading the characteristics of the crystals and semiconductor devices. A number of papers have been devoted to the solution of this problem [5, 6, 66, 76, 77]. However, as was stated in [72, 92] and will be noted in our further discussion, there is a remarkably strong interaction between DR and PD both at the DR formation stage and during the subsequent processing of irradiated crystals (annealing, in particular).

The first DR model was suggested in [63, 64]. According to this model, a DR represents a spheroidal defect formation of radius r_1, surrounded with a space charge whose radius is r_2. Within the central area whose radius is r_0 ($r_0 < r_1 < r_2$), the Fermi level occupies the so-called limit position with the result that the electrical and recombination parameters in this area prove to be other than those in the "undisturbed" portion of the crystal. In this model, a DR acts as a potential well for the minority and a barrier for the majority carriers. A detailed description of the Gossik model is presented in [5].

Numerous attempts at using this model for interpretation of the results of, say, irradiation of silicon and germanium [5, 43] by neutrons have shown that the Gossik model cannot be employed for explaining many peculiar features of DR-containing crystals. Specifically, it was discovered that the dimensions of the DR in silicon depended on the presence of oxygen [5, 67], and in germanium, on the presence of lithium [73]. From this it is inferred that a DR represents a defect formation more complex than an ordinary concentration of point defects of the vacancy type.

The author of [68] has suggested a model where the DR represents a core filled with divacancies and surrounded by a shell containing vacancy-impurity complexes. This model [68] can explain a far greater number of experimental facts than the Gossik model [64].

An attempt at developing a coherent model explaining the formation and structure of a DR is made in papers [56, 69, 70, 72]. Assuming that the properties of DRs and their influence on the electrophysical parameters of the crystals are largely controlled by the impurity content and the inventory of the point defects emerging, along with the DRs, in the semiconductor material, the authors of [69, 72] break the DR formation process into four stages.

1. Cascade stage. The processes that occur at this stage are governed by the radiation parameters (energy, mass of the bombarding particle, etc.), not by the impurity content of the crystal and PDs appearing within the space concurrently with the formation of DR.

2. Post-cascade stage. During this stage, a DR vacancy core is being formed. The outer region whose radius is about 10^3 Å is a place where displaced interstitial atoms interact with PDs formed outside the active (cascade) volume as well as with the original chemical impurities. In the latter case, some impurity atoms may be displaced from the substitutional to the interstitial position (according to [31]), which results in a sharp rise of their diffusibility [14].

3. Quasi-chemical stage. At this stage, the impurity atoms, that were diffusing during the previous stage, migrate towards the sinks where the impurity is again immobilized. At the same time, the vacancies combine together in the DR core thereby stabilizing the DR.

In the DR periphery, an intricate enveloping structure (atmosphere) is formed. This structure consists of chemical impurity atoms and their complexes with vacancies and with one another.

4. Accommodation stage. The properties of the matrix continue to change as the radiation dose is increased. This comes as a result of introduction of point defects and interactions of these with the original crystal imperfections (impurities, in particular). At the same time, defect complexes are formed, some of them being electrically active thus changing the concentration of majority carriers. As a result, the position of the Fermi level is changed which leads to a change in the charge states of most defects, including those forming part of the DR. A difference between the energy states of the DR and the matrix, caused by the above factor, induces additional interactions of the DR with the surrounding medium. These interactions tend to recover the balance between the energy states of the DR and the matrix at each irradiation phase. In the case under consideration, the interactions are accomplished through the agency of an electronic subsystem. Besides, there is a direct interaction between the DR and PDs generated within the matrix. The collection of phenomena that arise at this stage after the DR has already formed and stabilized (stages 1-3) and persist throughout the irradiation time, affecting the DR peripheral structure only, may be called the processes of accommodation of the DR to the surrounding medium. These processes govern the nature of the influence of the DR on the electrical, recombination and other characteristics of semiconductor materials.

With DRs present in sufficiently large concentrations, their shells and, then, cores begin, under certain conditions, to overlap, which results in the crystal amorphization.

The processes of DR accommodation to the environment give rise to a situation when the DR develops an electric potential relative to the matrix [72]. A DR energy distribution pattern suggested by the authors of [72] is shown in Fig. 1.1. Here, the core is in the intrinsic state and the shell has an electric potential attracting the electrons. Similar patterns may be proposed for *p*-Si and for *n*- and *p*-Ge. Note that in contrast to the recombination theory of non-equilibrium carriers in DRs, developed in [5] according to the pattern suggested in [69, 72], here the recombination of electrons and holes occurs in the impurity-defect shell of the DR, not in its core, i.e., it is accomplished through the agency of the point defects forming the shell and seeming to have the properties somewhat different from the properties of the like defects in the matrix.

This means that in a pattern suggested in [69, 72], the DR consists of a core surrounded with an impurity-defect shell. At present, at least two types of DR cores are known, crystalline and amorphous [81]. The amorphous core forms, in some instances, spontaneously,

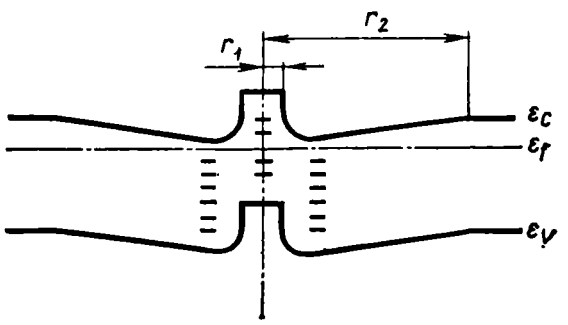

Fig. 1.1. Energy band model for a disordered region (DR).
Shown with dashed lines are the levels of recombination centers in the core and shell of the DR; $r_1 \ll r_2$

as a result of heavy ion irradiation (ion mass M_1 is greater than the mass of the target atom, M_2) with a comparatively low energy ($\leqslant$ 50 keV) [11, 81]. With most other kinds of radiation, e.g., light ions ($M_1 < M_2$), neutrons, electrons and gamma-rays, the DR core preserves its crystalline structure.

The dimensions of a DR core largely vary depending on the kind and energy of irradiation, the type of irradiated semiconductor and other factors [5, 12]. A number of experiments have shown a growth in the DR size with an increase in the energy of the bombarding particles [82, 83]. An average DR size in silicon and germanium is usually assumed to be equal to about 50 to 150 Å.

Some experimental data confirming the importance of stages 3 and 4 will be supplied further in the book.

The existence of the impurity-defect atmosphere around an extended defect of the DR type stems from the analogy with the macrodefects such as dislocations, interface or grain boundary. The presence of impurities around dislocations is a well established fact [26]. The analogy between DRs and dislocations is noted in [12, 72]. Dislocations and their impurity atmospheres effectively interact with PDs introduced by irradiation [84, 85, 86, 87]. A grain boundary [88, 89] or a dielectric-semiconductor interface [90] is the factor materially affecting the manner of defect production upon irradiation. These facts constitute a support for the assertion that the DR core-matrix interface will also affect the distribution of impurities and defects in the vicinity of the DR core, which will result in the formation of a shell with a greater content of impurities and impurity-defect complexes than in the matrix.

The existence of an impurity-defect shell around a DR is indirectly confirmed by the experiments showing a dependence of the DR properties on the type of irradiated material. According to [67], the DR radius in a silicon crystal grown by the Czochralski method exceeds that in a silicon crystal obtained by zone refining. The authors of [78], however, have arrived at the result which is directly contrary to the above one. It seems that besides oxygen, other impurities and/or defects play an important role in the DR forma-

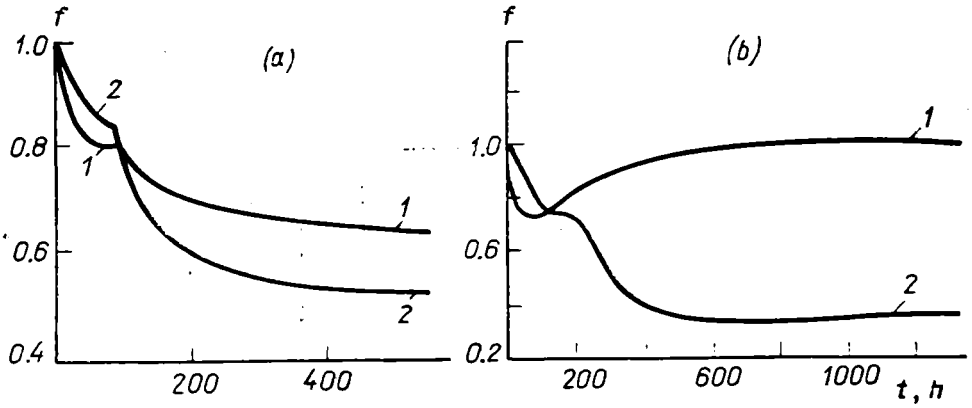

Fig. 1.2. Unannealed portion of reciprocal of lifetime in neutron irradiated *p-n-p* (1) and *n-p-n* (2) germanium transistors vs annealing time [91]. The initial sections of the curves represent annealing at 20 °C; then the annealing is at 36 °C (a) and at 36 °C within the Co^{60} gamma-radiation field (b)

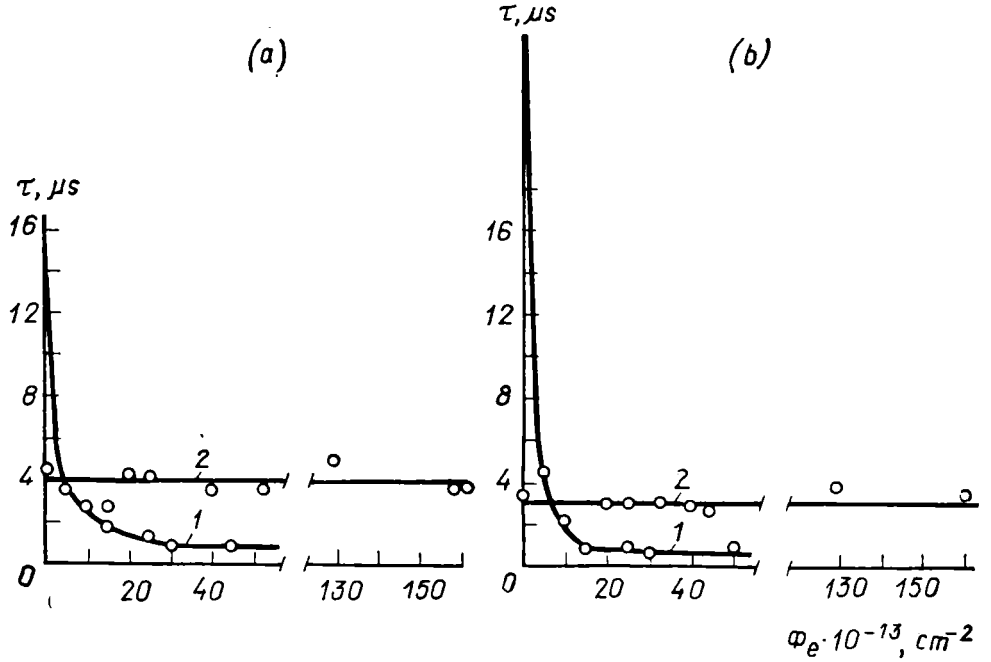

Fig. 1.3. Dose dependence of τ in silicon irradiated at 3.5 MeV [92]. *1*—an original sample; *2*—a sample first irradiated with neutrons at $\Phi_n = 10^{14}$ cm^{-2}; *a*—material: БКЭФ-1, $N_O \cong 2 \cdot 10^{17}$ cm^{-3}; *b*—material: КЭФ-1, $N_O \cong 9 \cdot 10^{17}$ cm^{-3}

tion processes. In [80] it was shown that DRs present in neutron irradiated *n*- and *p*-type silicon interacted with doping impurities. Note that the concentration of doping impurity in the investigated materials was comparatively low ($N_B \approx 7 \cdot 10^{16}$ cm^{-3}, $N_P \approx 2 \cdot 10^{16}$ cm^{-3}). In [98] is shown a relationship between the resistivity variations introduced by reactor neutron irradiation of silicon and the cobalt,

manganese or nickel impurity content in silicon.

Some papers have revealed an interaction between the DRs produced by, say, neutron irradiation, and PDs generated simultaneously or in succession by electron and gamma radiation with the energies sufficient only for generation of the PDs. The authors of [91] conducted an isothermal annealing of fused germanium *p-n-p* and *n-p-n* transistors irradiated by neutrons. Several samples were annealed in a gamma radiation field derived from a Co^{60} source. The result thus obtained (Fig. 1.2) was indicative of the effective interaction of the DRs introduced by the preliminary neutron irradiation with the PDs introduced by gamma irradiation.

Neutron irradiated silicon exhibits two series of absorption bands within the regions of 2-4 and 4.5-14.5 μm, associated with DR [78, 79, and 80]. Additional irradiation with 10 MeV electrons drastically decreases the absorption in both regions [79], which can be explained by annihilation of some defects in the DR core or shell upon interaction with the components of the Frenkel pairs introduced by electron irradiation.

The interactions of PDs introduced by 3.5 MeV electron irradiation with DRs resulting from a preliminary irradiation with reactor neutrons were investigated in papers [92, 94]. Fig. 1.3*a*, *b*, shows τ as a function of electron irradiation dose. The introduction of PDs by electron irradiation does not, for all practical purposes, produce additional recombination centers in the samples first irradiated with neutrons. The authors of [92] attribute the results thus obtained to the interactions of the vacancies arising from electron irradiation with the DRs introduced by a preliminary neutron irradiation. The same authors compare the effects of proton and neutron irradiations on τ in silicon. The data given in Table 1.10 are indicative of the effective interactions between DRs and PDs simultaneously introduced by proton irradiation.

The results of an isochronal reciprocal-of-lifetime annealing of silicon samples irradiated with 3.5 MeV electrons and subjected

Table 1.10

Carrier lifetime, τ, in neutron and electron irradiated silicon versus lifetime expected in proton irradiated silicon without interactions between DR and PD, μs

Material	Neutrons, $\Phi_n = 7 \cdot 10^{12}$ cm^{-2}	Protons	
		$\Phi_p = 5 \cdot 10^{12}$ cm^{-2}	without interactions
КЭФ-1	1.5±0.3	1.9±0.4	0.40
БКЭФ-1	1.3±0.2	2.5±0.5	0.45

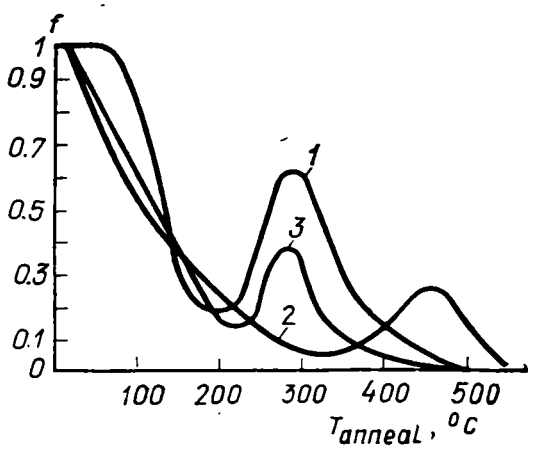

Fig. 1.4. Isochronal annealing of silicon (10 min).
Irradiation: *1*—electrons ($\Phi_e = 4.5. \times 10^{14}$ cm^{-2}); *2*—neutrons ($\Phi_n = 3.1. \times 10^{12}$ cm^{-2}); *3*—neutrons ($\Phi_n = 3.1 \times 10^{12}$ cm^{-2}) and electrons ($\Phi_e = 4.5. \times 10^{14}$ cm^{-2}). Material: ВКЭФ-1

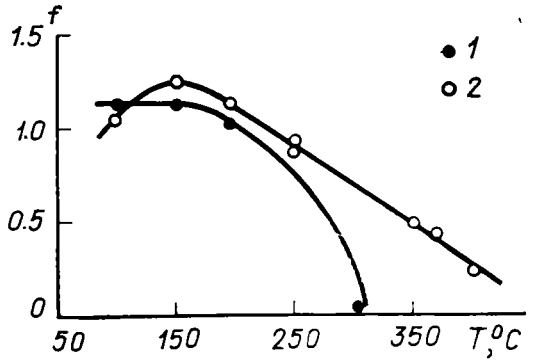

Fig. 1.5. Isochronal annealing of germanium proton irradiated at 660 MeV [12].
1—*n*-type germanium (Sb), $\Phi = (1\text{-}8) \times 10^{12}$ cm^{-2}; *2*—*p*-type irradiation-converted germanium, $\Phi = (1\text{-}3) \times 10^{14}$ cm^{-2}; $f = (n_0 - n_{anneal})/(n_0 - n_{irrad})$

to the reactor neutron and electron irradiation (after a preliminary neutron irradiation) are presented in Fig. 1.4.

The annealing behaviour (curve *2*) of the neutron irradiated material changes considerably after a repeated electron irradiation (curve *3*), which constitutes an additional support for the interaction of the PDs resulting from electron irradiation with the DRs arising in the crystal from neutron irradiation. What is obvious is the absence of clearly defined steps in annealing of the DR-containing material over a wide range of temperatures (curve *2*). The stepless character of DR annealing was noted by a number of experimenters [5, 12]. Figure 1.5 borrowed from [12] supplies an example of the stepless character of DR annealing in germanium irradiated with 660 MeV protons.

This arouses interest in the complete anneal temperature of DRs. The authors of [11], who conducted numerous experiments involving ion bombardment and ion implantation, argue that DRs are annealed out at about 300 °C in silicon and about 150-220 °C in germanium. The real picture, however, seems to be different.

It is noted in [68] that the existence of an impurity shell around a DR brings about a situation when a DR (in silicon) is to be completely annealed at a much higher temperature (about 700-800 °C).

The complex structure of a DR comprising a core and an impurity-defect shell leads inevitably to a wide variety of the processes involved in annealing out of crystals containing DRs.

It is quite probable that the main characteristics of the point defect complexes (the binding energy of the defects in a complex, the level of the complex in the forbidden zone, etc.) contained within the DR shell are different from the characteristics of the like defects in the matrix of the crystal. This is inferred from the existence of the deformation field around a DR [92, 95, 96] (one of the major causes of the formation of an impurity-defect shell around a DR) and from the interactions between defect centers. However, this is one of the areas where more experimental evidence is required. It is known (see for example [45]) that the *A*-center electron and hole capture cross-sections in silicon irradiated with reactor neutrons ($\sigma_n^0 = 7 \cdot 10^{-14}$ cm^2, $\sigma_p^- = 5.5 \cdot 10^{-13}$ cm^2) are by an order of magnitude greater than the values obtained from the experiments involving irradiation with 1 MeV electrons ($\sigma_n^0 = (0.8\text{-}1) \cdot 10^{-15}$ cm^2, $\sigma_p^- = (2.5\text{-}4) \cdot 10^{-14}$ cm^2. On electron irradiation, the divacancies in silicon are annealed out at about 240 °C [19], while on high-dose neutron irradiation, the annealing of the divacancies is completed at about 150 °C [97].

Sec. 1.4. Disordered Layers

Disordered layers (DL), like disordered regions (DR), are clusters of point defects, whose properties are dictated by the character of their interactions with one another. Disordered layers arise from overlapping of DRs within a part of the irradiated layer or from accumulation, under particular circumstances, of point defects into large concentrations. In this section, we consider the formation of DLs as a result of ion bombardment, their properties and the structural changes they undergo upon annealing. The priority given to the results of ion bombardment of semiconductors is explained by the fact that the processes of accumulation and rearrangement of defects during ion implantation are largely the same as those taking place, say, in neutron irradiation, though a higher (by three-four orders of magnitude) irradiation dose should be used in the latter case for obtaining similar results. That is why ion irradiation is used in study of the formation and properties of the DLs. In this respect, the most extensively used material is silicon. However, it has been shown by the experimental study of the formation, properties and anneal behaviour of the DLs, that the major conclusions derived on silicon are also true for Ge and GaAs.

The temperature at which the processes of interest take place constitutes a significant distinction. For example, crystallization of the amorphous layer in Si, Ge and GaAs occurs at about 600,

400 and 300 °C, respectively [11, 19]. There are some peculiarities inherent in the formation and annealing of DLs in InSb (see Chap. 6).

Formation of DLs. In our further discussion, the processes involved in the formation of DLs will be treated with reference to a specific yet fairly important and, for practical purposes, promising method of amorphization of semiconductor materials, namely, by ion irradiation (see, for instance, [19]).

As stated above, the DR is a most typical defect occurring in ion irradiated semiconductors. One can distinguish between several stages which make up the formation and stabilization of DRs (see Sec. 1.3). These stages are (1) an onset of a series of displacements (10^{-14} to 10^{-13} s), (2) a thermolysis of the excitation region and migration of the interstitials from the DR (10^{-11} to 10^{-10} s), (3) diffusion of the defects, their partial annihilation, formation of stable clusters of interstitials and vacancies as well as complexes with impurities, and (4) establishment of an equilibrium between the DR and the surrounding matrix.

The amorphization phase within an individual DR is largely dependent upon the second and third of the above processes. Indeed, in order for some region inside the crystal to change to an amorphous state, a certain critical concentration of defects is required with $7 \cdot 10^{19}$ cm^{-3} [99] and $4 \cdot 10^{19}$ cm^{-3} [100] for divacancies and tetravacancies, respectively. The concentration of the stable complexes emerging within a DR depends on the concentration of displacements produced by the ions and the temperature of the sample.

So, the number of displacements increases with the growth in the ion mass. As a consequence, the probability of interactions of the defects, resulting in complexes immobile at a given temperature also increases. A rise in the sample temperature promotes diffusion of the introduced Frenkel pair components, which in turn reduces the concentration of stable clusters formed in the process.

This means that during amorphization the second and third of the aforementioned stages of DR formation are opposed to each other and the efficiency of the processes depends on the irradiation conditions.

As a result, the amorphization mechanism also depends on the irradiation conditions, hence, on the efficiency of the processes under study. The amorphization of the irradiated crystal area may occur via (1) formation of amorphous regions directly in a separate DR, (2) interaction (overlapping) of various DRs resulting in their rearrangement, enlargement and formation of amorphous regions, and (3) sinking and accumulation of like-sign defects (vacancies or interstitials) in the vicinity of strong-field areas in the crystal (boundaries, lattice defects, etc.) [101].

For a selected crystal area to turn to an amorphous state it is essential that the vacancies and interstitials should be spatially

separated within this area [102, 103]. It is this condition that provides for accumulation of like-sign defects (vacancies or interstitials) in concentrations sufficient for a monocrystal to change to an amorphous state. Otherwise, annihilation of defects will bring about a saturation of the defect accumulation process at a low-content level.*

The spatial separation of vacancies and interstitials and their accumulation, within a certain region of the crystal, to the critical content will indicate the fact that the amorphization occurring via one of the above mechanisms is a heterogeneous process. The mechanism of homogeneous formation of the amorphous layer is thought of as having an amorphization nucleus appearing as a result of combination of point defects during migration. The nucleus thus formed attracts other mobile defects [104]. Such a process seems to depend on the concentration of mobile defects in the crystal and, hence, on the density of the ion beam. The dependence of the amorphization dose of the irradiated silicon layer [19] on the current density of the ion beam has not been found over a wide range of current densities, ion masses and temperatures of the substrate [105]. All these data allow one to conclude that the possibility of homogeneous formation of the amorphization nucleus in silicon is insignificant.

At room temperature of silicon samples, the first of the above listed amorphization mechanisms is realized through implantation of heavy ions (e.g., Sb^+ [128] or Xe^+ [106]), the second mechanism, through implantation of light- or medium-mass ions (e.g., O^+ [107] and Ar^+ [100]). Conventionally, one can use mass 60 to draw a boundary line between them [19].

The third mechanism has been revealed in the experiments involving irradiation of semiconductors with light ions. Thus, two amorphous layers [109-112] have been observed in silicon irradiated with ions (e.g., B^+, Ne^+). One of them was located in the semiconductor bulk and its position was dictated by the region of the maximum losses of energy by the implanted ions colliding with the host material atoms. The other amorphous layer was located near the surface and, as was shown by the results of special investigations, the emergence of this layer was attributed to the diffusion of the defects towards the surface and their accumulation to a concentration sufficient for semiconductor amorphization [111, 112].

The collection of defects near the surface and their accumulation to high concentrations are associated with the stresses in the surface layer. Changing the sign of elastic stresses near the surface through building up an oxide film by various methods encouraged

* It is believed that underestimation of this condition in the papers [142, 143] that have appeared recently complicates the understanding of the process of amorphization induced by ion irradiation.

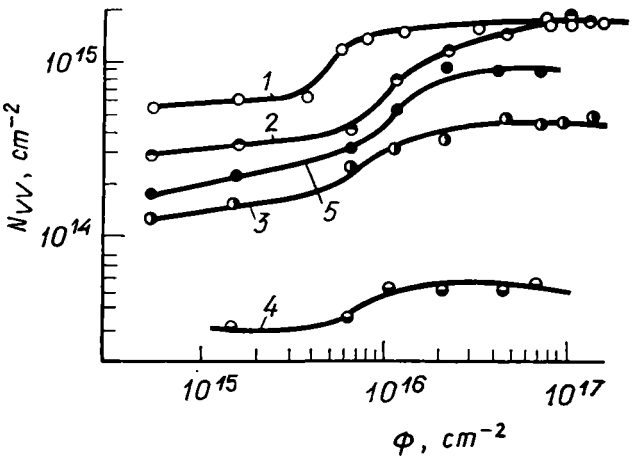

Fig. 1.6. Dose dependence of the number of VV-centers in a polycrystalline silicon film 1 μm thick when irradiated with H_2^+ ions at $E = 500$ keV (*1-4*) and with He^+ ions at $E = 1.2$ MeV (*5*) [101].
Original films (*1*, *5*) and those annealed at $T = 850$ (*2*), 1000 (*3*) and 1150 °C (*4*) were irradiated for 30 min

the replacement of a Frenkel pair component appearing in the vicinity of the semiconductor surface [90].

The third of the above described amorphization mechanisms is illustrated by the results of accumulation of paramagnetic vacancy centers (VV-centers appearing concurrently with amorphization [103, 108]) in the films of polycrystalline silicon [101]. Such films were irradiated with ions of hydrogen and helium at room temperature. Under preselected conditions (temperature, dose, ion energy), the implantation of such ions in a monocrystalline silicon did not result in the emergence of VV-centers. These centers appeared, however, in polycrystalline films (Fig. 1.6). With an increase in the dose, the number of VV-centers grew, in the films, to a certain value depending on the preliminary annealing temperature of the samples. The annealing seemed to take up the internal stresses in a polycrystalline silicon film, thereby reducing the number of sinks for the mobile defects generated by the irradiation. As a result, the number of VV-centers also decreased for the given H-ion irradiation dose.

The dose at which the irradiated semiconductor layer turns to an amorphous state depends strongly on the sample temperature during the bombardment. The available experimental evidence of the dependence $\Phi_a(T)$ is explained well enough by the Morehead and Crowder model based on the idea of an amorphous core formed inside the area surrounding the particle track. This idea is in conformity with the first of the above-mentioned mechanisms of amorphization of ion irradiated semiconductors. Though this mechanism does not play a decisive role in, say, irradiation of semiconductors with light- and medium-mass ions, the dependence $\Phi_a(T)$ obtained from the Morehead and Crowder model supplies a fairly good explanation of the experimental data in this case as well. With due consideration given for this, let us discuss the results of modifying the Morehead and Crowder model [105, 114].

Assume that for amorphization of a semiconductor layer whose thickness is $R_\perp$, N_1 ions are required. The irradiated area is A, the energy losses due to atomic collisions, $\langle d\nu/dR \rangle$, and R, the complete path of the particle. Then the energy liberated by the ion implantation is $N_1 [\langle d\nu/dR \rangle R]$ and is equal to the energy required for accumulation of displaced atoms in this semiconductor layer before the amorphization occurs, i.e.,

$$N_1 [\langle d\nu/dR \rangle R] = \alpha n_0 A R_\perp E_d \tag{1.1}$$

where n_0 is the atomic density of the semiconductor; E_d is the atom displacement threshold energy; α is the proportionality factor indicating the share of atoms to be displaced to turn the semiconductor to an amorphous state. From (1.1), we arrive at the amorphization dose, $\Phi_a^0 = N_1/A = \alpha n_0 R_\perp E_d/[\langle d\nu/dR \rangle R]$.

The amorphous (disordered) core surrounding the particle track has radius ρ that depends on the sample temperature during the irradiation, since over a period, τ, of the formation of a DR, during one of the four stages (see Sec. 1.3), the defects will diffuse from the DR thus reducing the radius of the amorphous core. In consequence, $\rho = \rho_0 - \rho_\perp$ where ρ_0 is the radius of the core at a low temperature when the diffusion of defects is insignificant; $\rho_\perp$ is the quantity determined by the length of the defect diffusion path over period τ. The diffusion coefficients is put down as $D_\nu = D_\nu^0 \exp(-E/kT)$, where E is the energy required to cause the migration of the defects. The value of τ is usually not known exactly but can be expressed in terms of another parameter found experimentally. With a specific temperature of a sample irradiated during T_∞, no amorphous layer is formed, i.e., $\rho = 0$. In this case, $\rho_0 = \rho_\perp$, hence, τ can be expressed in terms of T_∞. Taking into consideration that $\Phi_a \simeq (\pi\rho^2)^{-1}$, the temperature dependence of the amorphization dose will take the form

$$\Phi_a(T)/\Phi_a^0(T) = [1 - \exp(E/kT_\infty) \cdot \exp(-E/kT)]^{-2} \tag{1.2}$$

where $\Phi_a^0 \simeq (\pi\rho_0^2)^{-1}$; k is the Boltzmann constant. For example, with N^+ ions implanted in Si, $T_\infty = 400 \pm 30$ K, $E = 0.20 \pm \pm 0.06$ eV. For Ar^+ ions, $T_\infty = 540 \pm 30$ K, $E = 0.26 \pm 0.06$ eV, and for Kr^+ ions, $T_\infty = 725 \pm 30$ K, $E = 0.24 \pm 0.06$ eV [141].

Homogeneity of amorphous layers produced by ion bombardment. On ion bombardment of the crystals, amorphization occurs via the above-discussed mechanism either in the region of the maximum losses of energy due to atomic collisions, or near the surface acting as a sink for the mobile defects, or in both regions simultaneously. Thus, at the initial stages of irradiation, the bombarded layer has an irregular thickness. As the irradiation dose increases, the disordered areas expand and eventually the entire irradiated layer becomes amorphous. According to the data obtained by the EPR and reflection

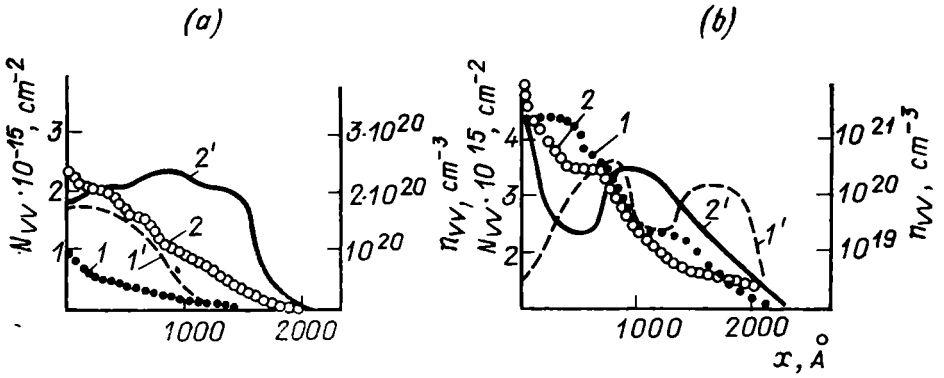

Fig. 1.7. Depth distribution of VV-centers in silicon irradiated with Ne^+ ions. $T_{meas} = 77$ K [101].
a—$E = 40$ keV, $\Phi = 10^{15}$ cm^{-2} (*1*, *1'*—integral and differential distributions, respectively), $\Phi = 6.25 \cdot 10^{16}$ cm^{-2} (*2*, *2'*); *b*—$E = 50$ keV, $\Phi = 1.87 \times 10^{17}$ cm^{-2} (*1*, *1'*), $\Phi = 3.12 \cdot 10^{17}$ cm^{-2} (*2*, *2'*)

electron diffraction techniques, this amorphous layer is fairly homogeneous. For example, in Ne^+-ion ($E = 50$ keV; $\Phi = 10^{15}$ cm^{-2}) irradiated silicon, VV-centers have uniform distribution throughout the thickness of the amorphous layer, except the depth distribution "tail" (Fig. 1.7*a*). With a further increase in the dose, however, the concentration of VV-centers begins to change. This shows up in, say, silicon samples irradiated to a dose of $2\text{-}3 \cdot 10^{17}$ cm^{-2} (Fig. 1.7*b*) [101, 115]. In this case, the homogeneity of the amorphous layer is strongly affected. Moreover, the amorphous layers with a comparatively uniform distribution of VV-centers in depth also lose their homogeneity after annealing. So, in Si irradiated with P^+ and Xe^+ ions, the VV-centers sited at different depths in the implanted layer anneal out dissimilarly, which is indicated by the displacement of the peak of the defect distribution profile curve deep inside the sample when the temperature increases (Fig. 1.8) [115, 116]. Besides, the comparison of the results obtained from irradiation of a semiconductor by P^+ and Xe^+ ions reveals that the displacement of the peak of the defect distribution curve is the greater the heavier the ion used to produce an amorphous layer. This is indicative of the fact that the displacement observed cannot be attributed to the proximity of the surface.

The information thus collected enables one to think that an amorphous layer produced by ion bombardment is inhomogeneous in these or other respects. The factors responsible for this are:

(1) the presence of stressed states originating from the sample surface, an impurity introduced by ion implantation, or the boundary between the amorphous layer and the matrix;

(2) a nonuniform distribution of ion energy losses caused by elastic and nonelastic collisions and, as a consequence, a nonuniform distribution of various defects in depth;

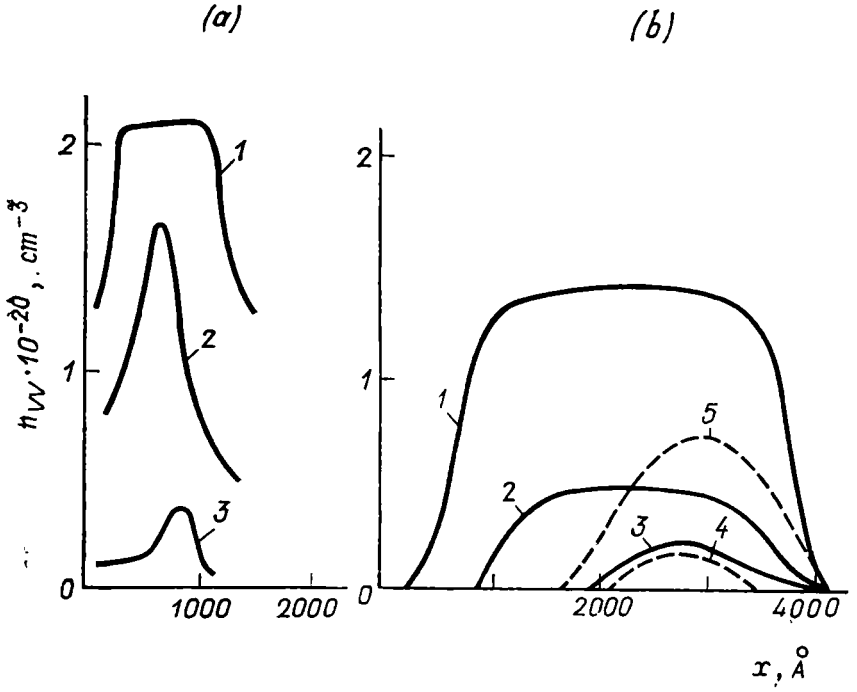

Fig. 1.8. Depth distribution of VV-centers in ion irradiated silicon [115, 116]. *a*—P^+, $E = 150$ keV, $\Phi = 10^{15}$ cm^{-2}; original sample (*1*), after 10-min annealing at 300 (2) and 400 °C (*3*); *b*—Xe^+, $E = 1$ MeV, $\Phi = 2 \cdot 10^{14}$ cm^{-2}, original sample (*1*), after 1-min annealing (*2*), 60-min annealing (*3*, *5*), 3600-min annealing (*4*) at 350 (*5*) and 500 °C (*1-4*)

(3) interactions of high-concentration impurities with lattice defects.

Apart from the experimental evidence presented here, there are other data obtained with the EPR, electrophysical, structural and optical techniques used for investigation of the amorphous layer properties. These data prompt a conclusion that the properties of an amorphous layer show their strong dependence on the conditions under which it has been produced, i.e., the species of the ion [117, 119-123], its energy [116, 124], dose [118, 119-121, 124-126], and the sample temperature during the irradiation [127]. Hence, one may speak about the "degree of amorphization" of an amorphous layer. This notion seems to imply, in the first place, the amount of defects in the amorphous layer and its impurity content and, secondly, a degree of change of the short-range order.

The notion of defect does apply not only to monocrystals but also to amorphous semiconductors. Depending on their production conditions and subsequent processing, the amorphous semiconductors contain various concentrations of microscopic pores. Among other purposes, the concentration of micropores may serve the purpose of determining the density of an amorphous conductor. In amorphous silicon, the density deficit may amount to 30% [129]. On the other

hand, it is possible to produce an amorphous silicon whose density will not differ from that of the monocrystal, that is, the concentration of micropores in this silicon will be obviously equal to zero [130]. This means that the micropores will represent, in this case, defects in an amorphous silicon. Some of the defects are paramagnetic (e.g., the VV-center which, according to [130], is a dominating defect in an amorphous silicon layer produced by sputtering).

When discussing the rearrangement of defects in amorphous silicon, we have to use the concepts of the vacancy, interstitial atom, whose applicability seems to be based on the short-range order analogy between the crystalline and amorphous semiconductors.

As may be seen from Fig. 1.7, the concentration of defects in an amorphous layer (vacancy clusters) varies as the irradiation dose increases. The concentration of vacancy clusters increases in one part of the amorphous layer and decreases in another part, which indicates a rearrangement of defects when an amorphous silicon sample is being irradiated. A short-range order change in an amorphous layer has been noted in [131]. This paper investigated the spectrum of a relative change in the reflection coefficient of the ion irradiated germanium.

Structural changes in amorphous layer due to annealing.

The defect annealing mechanisms. The mechanisms of annealing out the defects in ion irradiated semiconductor layers are explained on the basis of the following experimental evidence:

1. The condition of the affected layer at every instant of time is characterized by the presence of a fairly wide spectrum of defects of the vacancy and interstitial types, whose stabilizing temperature varies with the structure of the defect over a wide range (for example, for Si, over a range of 100 to 700 °C [132, 133]; at a temperature in excess of 700°C, the layer usually restores its ordered nature).
2. The ratio (spectrum) of various defects to one another depends on the conditions of formation of the disordered layer, such as the dose, ion species, and may change in the course of annealing.
3. The temperature at which the defects are annealed out rises with an increase in the sizes of the defects (see Sec. 1.2 and [132, 133]).
4. The mobile products of dissociation of the lower temperature defect types interact with the clusters revealing stability at a given temperature.

The third one of the above items is not quite clear. It seems that, considering the energy involved in the process, it is easier to accomplish a dissociation of, say, a vacancy cluster into a vacancy and some remainder to be utilized by a larger defect. It has been already noted, however, that certain experimental data support the opinion that the annealing temperature increases with an increase in the size of the defect association. It is likely that these data indicate a pro-

cess more complex than the above dissociation of a cluster into an elementary defect and a remainder.

Using the aforementioned propositions as a basis, the authors of [124] have suggested two patterns for annealing out defects. The first pattern assumes that the defect spectrum includes the vacancy-type clusters only, while the thermal dissociation of the defect clusters into a vacancy and a remainder occurs at a temperature which is the higher the larger the size of the cluster. As the smaller (less stable) clusters disintegrate, the vacancies interact with the larger complexes and, also, sink inside the crystal. According to this pattern, the vacancy-type clusters grow in size due to dissociation of the smaller defects.

In the second pattern it is inferred that the annealing results in interstitial atoms whose interactions with the vacancy-type clusters decrease the cluster size by annihilation of the interstitial atom and the vacancy. The sources of the interstitials are the ion irradiated layer and that region within the crystal, which borders on the disordered layer.

The above patterns have the following mathematical expressions:

$$(1)\quad W_k \xrightarrow{\nu_k} W_{k-1}+V \quad (2\leqslant k<Q),$$

$$W_k+V \xrightarrow{\lambda_k} W_{k+1} \quad (k\geqslant Q>2),$$

$$V \xrightarrow{\text{diffusion}} (V)-\text{sinks};$$

$$(2)\quad (\text{I})-\text{sources} \xrightarrow{\text{generation}} I,$$

$$W_{k+1}+I \xrightarrow{\eta_k} W_{k-1} \quad (k\geqslant 2)$$

$$V \xrightarrow{\text{diffusion}} (V)-\text{sinks}.$$

Here, V is the monovacancy; I is the interstitial atom; W_k, the vacancy-type cluster consisting of k vacancies; ν_k, speed constants of the thermal dissociation of the smaller clusters $(2\leqslant k<Q)$; λ_k, speed constants of the reverse reaction for the larger vacancy clusters $(k\geqslant Q)$. The magnitude of Q depends on the annealing temperature and increases with an increase in the temperature.

Solution of a system of kinetic equations corresponding to the above patterns covers all the defects present in the layer, their thermal stability, depth distribution, etc. [134]. No such data exist as yet for an amorphous conductor. Nevertheless, the qualitative conclusions derived from the solution prove to be quite useful.

Crystallization of an amorphous layer. If the amorphous layer begins at the surface of the irradiated semiconductor and has a monocrystal-amorphous state interface on one side only (unlike the so-called latent amorphous layer that is separated from the surface with a monocrystalline interlayer), the crystallization process is essen-

tially an epitaxial ordering on a monocrystalline substrate [11]. For latent amorphous layers, the ordering proceeds on two sides: on the side of the sample bulk and on the side of the surface. In the first case, the amorphous layer can be investigated more easily and the results of the investigation are unambiguous. The main points of interest to the investigators of the amorphous layer crystallization process are how the crystallization rate changes with time, and if it does not change, what is the crystallization activation energy and whether or not the crystallization rate is affected by the position (orientation) of the substrate and by the impurity content in the amorphous layer.

To answer all these questions, the authors of [122, 123, 135, and 136] have conducted a detailed experimental research. The subject matter was a crystallization of an amorphous layer in silicon. The disorder measurement technique was based on the channelling effect. The amorphization of silicon has been accomplished through Si^+ ion bombardment with the energy successively changed from 50 to 250 keV to produce a sufficiently extended layer. The total dose amounted to $8 \cdot 10^{15}$ cm^{-2}, the thickness of the amorphous layer, 4600 Å. The sample temperature during the irradiation was maintained at about 77 K. The subsequent isothermal annealing was conducted in vacuum at temperatures ranging from 475 to 575 °C.

It is an established fact that the amorphous state-monocrystal interface movement is a linear function of time for the matrix orientations ⟨100⟩ and ⟨110⟩. At 550 °C and with the Si plane ⟨100⟩, the crystallization rate amounted to 80 Å/min. For the plane ⟨110⟩, the rate proved to be three times as small as for the plane ⟨100⟩. The energy required for activization of the amorphous layer ordering process for these two orientations equals 2.3 ± 0.1 eV.

For crystallization of an amorphous layer sited on a substrate with the plane ⟨111⟩, the speed of the movement of the monocrystal-amorphous state interface was the least for the three investigated orientations, and its value changed with time. Introduction of various impurities into a silicon amorphous layer strongly affects the crystallization rate (for details see Chap. 7).

According to the electronographic research data, in GaAs irradiated with nitrogen ions crystallization of an amorphous layer proceeds epitaxially off the monocrystalline substrate [137]. In contrast to Si, GaAs shows no marked dependence of the ordering process on the orientation of the sample for the planes ⟨100⟩, ⟨110⟩ and ⟨111⟩ [138].

Another distinction of GaAs from Si resides in that during an isochronous annealing of semiconductors, the crystallization of the amorphous layer in silicon occurs within a rather narrow temperature range, whereas in GaAs, this range is much wider [139].

References

1. Smirnov, L. S., Glazunov, P. A. Volume distribution of lattice defects in germanium crystals irradiated with fast electrons. *Fiz. tverd. tela*, 1959, 1, 9, pp. 1376-1378 (in Russian).
2. Lofferski, J. J., Rappaport, P. Radiation damage in Ge and Si detected by carrier lifetime changes: damage threshold. *Phys. Rev.*, 1958, 111, 2, pp. 432-441 (in Russian).
3. Gerasimenko, N. N., Dvurechensky, A. V., Panov, V. I., Smirnov, L. S. On threshold energy of formation of radiation defects in semiconductors. *Fizika i tekhnol. polupr.*, 1971, 5, 8, pp. 1644-1646; ibidem, 1972, 6, 5, p. 991 (in Russian).
4. Panov, V. I., Smirnov, L. S. On importance of collective processes in formation of primary radiation defects in silicon. *Fizika i tekhnol. polupr.*, 1971, 5, 1, pp. 212-215 (in Russian).
5. Konopleva, R. F., Litvinov, V. L., Ukhin, N. A. *Characteristics of Radiation Damage in Semiconductors Bombarded with High-Energy Particles.* Moscow, Atomizdat, 1971, 174 pages (in Russian).
6. Ivanov, G. M., Sirota, N. N. On the relative role of disordered regions in damage of electron irradiated silicon. In: *Radiation Defects in Semiconductors.* Minsk, Belorussian State University, 1972, pp. 56-57 (in Russian).
7. Vavilov, V. S., Ukhin, N. A. *Radiation Effects in Semiconductors and Semiconductor Devices.* Moscow, Atomizdat, 1969, 310 pages (in Russian).
8. Ivanov, N. A., Kasimov, V. I., Kosmach, V. F., Kuznetzov, P. F., Luganov, P. F., Ostroumov, V. I., Tkachev, V. D. Formation of disordered regions in silicon irradiated with high-energy gamma rays. *Fizika i tekhnol. polupr.* 1975, 9, 12, pp. 2369-2371 (in Russian).
9. Ivanov, N. A., Komarov, S. R., Kosmach, V. F., Ostroumov, V. I. Number of Frenkel defects in germanium irradiated with high-energy gamma-rays. *Fizika i tekhnol. polupr.*, 1977, 11, 4, pp. 762-763 (in Russian).
10. Abdullayev, A., Vitovsky, N. A., Mashovets, T. V. On the size of the cross-section of the Frenkel pair formation process in gamma irradiated semiconductors. *Fizika i tekhnol. polupr.*, 1974, 8, 11, pp. 2203-2205 (in Russian).
11. Mayer, J., Eriksson, L., Davies, J. *Ion Implantation in Semiconductors. Silicon and Germanium*, New York, 1970.
12. Konopleva, R. F., Ostroumov, V. N. *Interactions of High-Energy Charged Particles with Germanium and Silicon.* Moscow, Atomizdat, 1975, 127 pages (in Russian).
13. Glazov, V. M., Zemskov, V. S. *Physico-chemical Basis of Semiconductor Doping.* Moscow, Nauka, 1967, 371 pages (in Russian).
14. Boltaks, B. I. *Diffusion in Semiconductors.* Moscow, Fizmatgiz, 1961, 462 pages (in Russian).
15. Boltaks, B. I. *Diffusion and Point Defects in Semiconductors.* Leningrad, Nauka, 1972, 384 pages (in Russian).
16. Milns, A. *Deep Impurities in Semiconductors.* New York, 1973, 526 pages.
17. Fistul, V. I. *Dissociation of Oversaturated Semiconductor Solid Solutions.* Moscow, Metallurgiya, 1977, 239 pages (in Russian).
18. *Atomic Diffusion in Semiconductors.* Ed. by D. Shaw. London-New-York, 1973, 607 pages.
19. *Physical Processes in Irradiated Semiconductors.* Ed. by L. S. Smirnov. Novosibirsk, Nauka, 1977, 256 pages (in Russian).
20. Bolotov, V. V., Vasilyev, A. V., Smirnov, L. S. Reactions in crystals as factor determining diffusion processes. *Fizika i tekhnol. polupr.*, 1974, 8, 6, pp. 1175-1181 (in Russian).
21. Papazian, H. A., Wolsky, S. P. Volatile impurities in silicon and germanium. *J. Appl. Phys.*, 1956, 27, 12, p. 1561.

22. Nozaki, T., Yatsurugi, Y., Akijama, N. Concentration and behaviour of carbon in semiconductor silicon. *J. Electrochem. Soc.*, 1970, **117**, 12, pp. 1566-1568.
23. Kaiser, W., Keck, P. H., Lange, C. F. Infrared absorption and oxygen content in silicon and germanium. *Phys. Rev.*, 1956, **101**, 4, pp. 1264-1268.
24. Shershel, V. A., Bessonova, N. V., Sidorenko, P. V. On behaviour and interaction of oxygen with donor impurities in germanium. *Nauchn. trudy Giredmeta*, 1974, 51, pp. 163-167 (in Russian).
25. Sokolov, E. B., Prokofyeva, V. K., Glavin, G. G. On "self-compensation" of impurities in Germanium. *Izv. AN SSSR. Neorganicheskie materialy*, 1966, **11**, 12, p. 2262 (in Russian).
26. Friedel, J. *Dislocations*. Oxford, 1964, 491 pages.
27. Vitovsky, N. A., Mustafakulov, D., Checkmareva, A. P. On magnitude of threshold energy for atom displacement in semiconductors. *Fizika i tekhnol. polupr.*, 1977, **11**, 9, pp. 1747-1753 (in Russian).
28. Gwozdz, P. S., Kochler, J. C. Changes in AC conductivity of silicon with electron irradiation at 0.5 K. *Phys. Rev., B*, 1972, 6, 12, pp. 4571-4574.
29. Mc Keighen, R. E., Kochler, J. C. Electron irradiation effects in silicon at liquid-helium temperatures using AC conductivity. *Phys. Rev., B*, 1971, **4**, 2, pp. 462-476.
30. Watkins, G. D. An EPR study of the lattice vacancy in silicon. *J. Phys. Soc. Japan*, 1963, **18**, Suppl. II, pp. 22-27.
31. Watkins, G. D. EPR studies of the lattice vacancy and low temperature damage processes in silicon. In: *Lattice Defects in Semiconductors*. Conf. Ser. No. 23, Inst. of Phys., London-Bristol, 1975, pp. 1-22.
32. Kimerling, L. C. Defect states in electron bombarded silicon: capacitance transient analysis. In: *Radiation Effects in Semiconductors*. Conf. Ser. No. 31, Inst. of Phys. London-Bristol, 1977, pp. 221-230.
33. Corbett, J. W., Bourgoin, J. C., Cheng, L. J., Corelli, J. C., Lee, Y. H., Mooney, P. M., Weigel, C. The status of defect studies in silicon. In: *Radiation Effects in Semiconductors*. Conf. Ser. No. 31, Inst. of Phys. London Bristol, 1977, pp. 1-11.
34. Seeger, A., Föll, H., Frank, W. Self-interstitials, vacancies and their clusters in silicon and germanium. In: *Radiation Effects in Semiconductors*. Conf. Ser. No. 31, Inst. of Phys. London-Bristol, 1978, pp. 12-27.
35. Frank, W. The nature of interstitials in silicon and germanium. In: *Lattice Defects in Semiconductors*. Conf. Ser. No. 23, Inst. of Phys. London-Bristol, 1975, pp. 23-43.
36. Whan, R. E. Evidence for low-temperature motion of vacancies in germanium. *Appl. Phys. Lett.*, 1965, **6**, 11, pp. 221-223.
37. Whan, R. E. Investigations of oxygen-defects interactions between 25 and 700 K in irradiated germanium. *Phys. Rev.*, 1965, **140**, 2A, pp. A690-A698.
38. Bolotov, V. V., Vasilyev, A. V., Smirnov, L. S. On the energy of migration of elementary defects in germanium and silicon. *Fizika i tekhnol. polupr.*, 1974, 8, 3, pp. 518-521 (in Russian).
39. Vitovsky, N. A., Yemtsev, V. V., Mashovets, T. V., Morozov, Yu. G. The kinetics of interactions of radiation-induced structural point defects with impurity atoms in semiconductors. *Fizika i tekhnol. polupr.*, 1974, 8, 11, pp. 2276-2279.
40. Saito, H., Fukuoka, N., Tatsumi, Y. Annealing of point defects in *p*-type germanium after electron irradiation at liquid nitrogen temperature. In: *Radiation Effects in Semiconductors*. Ed. by J. W. Corbett, G. D. Watkins, London-N.Y.-Paris, Gordon and Breach Science Publishers, 1971, pp. 81-85.
41. Mashovets, T. V. Point defects in germanium: reliable and questionable. In: *Radiation Effects in Semiconductors*. Conf. Ser. No. 31, Inst. of Phys. London-Bristol, 1977, pp. 30-44.
42. Watkins G. D. The interaction of irradiation-produced defects with impurities and other defects in semiconductors. EPR studies in silicon. In: *Ra-*

diation Effects in Semiconductor Components. Toulouse, *Journees D'Electronique*, 1967, pp. A1-A9.
43. Konozenko, I. D., Semenyuk, A. K., Khivrich, V. I. *Radiation Effects in Silicon*, Kiev, Naukova dumka, 1974, p. 199 (in Russian).
44. Cheng, L. J., Corelli, J. C. 1, 8-, 3,3-, and 3,9-μ bands in irradiated silicon: correlations with the divacancy., *Phys. Rev.*, 1966, **152**, 2, pp. 761-774.
45. *Compensated Silicon.* Ed. by B. I. Boltaks, Leningrad, Nauka, 1972, 121 pages (in Russian).
46. Hasiguti R. R., Ishino, S. Defect mobility and annealing in irradiated germanium and silicon. In: *Radiation Damage in Semiconductors*, Paris-Royanmont, Dunod, 1965, pp. 259-274.
47. Kimerling, L. C., Carnes, C. R. Annealing of electron irradiated *n*-type silicon: illumination and fluence dependence. *J. Appl. Phys.*, 1971, **42**, 9, pp. 3548-3552.
48. Kimerling, L. C. De Angelis, H. M., Carnes, C. P. Annealing of electron irradiated *n*-type silicon. *Phys. Rev., B*, 1971, 3, 2, pp. 427-432.
49. Hirata, M., Hirata, M., Saito, H. The interactions of point defects with impurities in silicon. *J. Phys. Soc. Japan*, 1969, **27**, 2, pp. 405-414.
50. Mukashev, B. N. *A Study of Radiation Damage in Silicon Doped with Different Donor and Acceptor Impurities.* Institute of Physics of High Energies of Kazakh SSR Academy of Sciences. Alma-Ata, 1972 (in Russian).
51. Panov, V. I., Smirnov, L. S., Tishkovsky, E. G. On competition for capture and transfer of vacancies between defect formations in silicon. *Fizika i tekhnol. polupr.*, 1972, **6**, 4, pp. 673-676.
52. Brower, K. L. Structure of multiple-vacancy (oxygen) centers in irradiated silicon. *Rad. Eff.*, 1971, 8, pp. 213-219.
53. Lee, Y. N., Corbett, J. W. EPR study of defects in neutron irradiated silicon: quenched in alignment under 110-uniaxial stress. *Phys. Rev.*, 1974, 9, 10, pp. 4351-4361.
54. Hasiguti, R. R., Tanaka, K., Takanaski, S. ESR studies of electron irradiation damage and its annealing in As-doped *n*-type germanium. In: *Radiation Effects in Semiconductors*, N. Y., Plenum Press, 1968, pp. 89-98.
55. Hikari, A., Cleland, J. W., Crawford, J. H. Experimental evidence for production and annihilation of interstitial impurities in electron irradiated *n*-type germanium. In: *Radiation Damage in Semiconductors*, N.Y., Plenum Press, 1968, pp. 224-231.
56. Lenchenko, V. M. Activation of quasi-chemical processes in solids by nuclear irradiation. Part 1. Mechanisms for activation events of diffusion and displacement of atoms. Part 2. Quasi-chemical processes of radiation-induced defect formation in semiconductors. In: *Physico-chemical Problems of Solids*, Krasnoyarsk, 1975, pp. 3-32 (in Russian).
57. Choyke, W. J. A review of radiation damage in SiC. In: *Radiation Effects in Semiconductors.* Conf. Ser. No. 31, Inst. of Phys. London-Bristol, 1977, pp. 58-69.
58. Baranskii, T. I., Klochkov, V. P., Potykevich, I. V. *Semiconductor Electronics. Properties of Materials* (a handbook), Kiev, Naukova dumka, 1975, p. 703 (in Russian).
59. Smirnov, L. S. On the reactions in the crystals. In: *Defects in Semiconductor Structure*, Novosibirsk, Inst. of Semicond. Phys. of USSR Academy of Sciences, 1973, pp. 201-207 (in Russian).
60. Medvedev, S. A. *Introduction into Technology of Semiconductor Materials*, Moscow, Vysshaya shkola, 1970, p. 503 (in Russian).
61. Vavilov, V. S., Kolomenskaya, T. I., Vintovkin, S. I., Chukichev, M. V. On the generation of non-equilibrium carriers by fast electron irradiation. *Pribory i tekhn. eksperimenta*, 1964, 5, pp. 79-90.
62. Kinchin, G. H., Pease, R. S. Displacement of atoms in solids by irradiation. *Uspekhi fiz. nauk*, 1956, **60**, 4, pp. 590-615 (Russian translation).

63. Crawford, J. H., Cleland, J. W. Nature of bombardment damage and energy levels in semiconductors. *J. Appl. Phys.*, 1959, 30, 8, pp. 1204-1213.
64. Gossik, B. R. Disordered regions in semiconductors bombarded by fast neutrons. *J. Appl. Phys.*, 1959, 30, 8, pp. 1214-1218.
65. Abiev, A. K., Ukhin, N. A. Low-temperature irradiation of germanium with 28 MeV electrons. *Fizika i tekhnol. polupr.*, 1970, 4, 3, pp. 484-489 (in Russian).
66. Starostin, K. L. Temperature dependence of electron concentration decrease rate in *n*-Ge and *n*-Si irradiated with fast neutrons. *Fizika i tekhnol. polupr.*, 1970, 4, 9, pp. 1823-1824 (in Russian).
67. Sadikov, V. P., Ukhin, N. A. Influence of impurity content on rate of electron mobility change during neutron irradiation. In: *Conference on radiation physics of non-metallic crystals*, Kiev, 1969, p. 9 (in Russian).
68. Ukhin, N. A. A model of disordered regions in silicon, produced by fast neutrons. *Fizika i tekhnol. polupr.*, 1972, 6, 5, pp. 931-934 (in Russian).
69. Baranov, A. I., Smirnov, L. S. Resonance scattering of carriers in disordered regions in semiconductors. In: *Radiation Defects in Semiconductors*, Minsk, Belorussian State University, 1972, pp. 237-238 (in Russian).
70. Lenchenko, V. M. On anomalously high mobility of implants in semiconductors and associated defects. In: *Physical Chemistry in Microelectronics*, Krasnoyarsk, 1976, pp. 21-29 (in Russian).
71. Lenchenko, V. M., Akilov, Yu. Z. Computer-aided investigation of displacement cascade structure in Ge, Si and PbS. *Fizika i tekhnol. polupr.*, 1971, 5, 3, pp. 397-402 (in Russian).
72. Baranov, A. I., Smirnov, L. S. On interactions of disordered regions with environment in semiconductors. *Fizika i tekhnol. polupr.*, 1973, 7, 11, pp. 2227-2229 (in Russian).
73. Sinishchuk, I. K., Reznikov, M. Ya. Interactions of lithium with disordered regions produced by fast neutrons in *n*-type germanium. *Fizika i tekhnol. polupr.*, 1973, 7, 9, pp. 1689-1692 (in Russian).
74. Vinetskii, V. L., Kondrachuk, A. V. On threshold of formation of radiation defect clusters in semiconductors. *Fizika i tekhnol. polupr.*, 1976, 10, 2, pp. 366-367 (in Russian).
75. Gorodetskii, S. M., Kreinin, L. B. Influence of disordered regions on recombination in irradiated *p*-type silicon. *Fizika i tekhnol. polupr.*, 1974, 8, 4, pp. 667-671 (in Russian).
76. Akishin, A. I., Gorodetskii, S. M., Grigoryeva, G. M., Kreinin, L. B., Nazarov, V. G. On selection of the assortment of irradiations to simulate the effect of space radiation on photoelectrical photoconverters. In: *Study of Space Materials and Technology*, Moscow, Nauka, 1977, pp. 149-157 (in Russian).
77. Lugakov, P. F., Tkachev, V. D., Shusha, V. V. Recombination in high-energy gamma radiated *n*-type silicon. *Fizika i tekhnol. polupr.*, 1977, 11, 10, pp. 1960-1963 (in Russian).
78. Koval, Yu. P., Mordkovich, V. N., Temper, E. M., Kharchenko, V. A. Optical properties of neutron irradiated silicon. *Fizika i tekhnol. polupr.*, 1972, 6, 7, pp. 1317-1322 (in Russian).
79. Mordkovich, V. N., Soloviev, S. P., Temper, E. M., Kharchenko, V. A. On the radiation annealing of defects in neutron irradiated silicon. *Fizika i tekhnol. polupr.*, 1974, 8, 5, pp. 1024-1025 (in Russian).
80. Temper, E. M. The peculiarities of formation of defects in high-dose neutron irradiated silicon. *Fizika i tekhnol. polupr.*, 1977, 11, 4, pp. 772-774 (in Russian).
81. Gibbons, J. F. Ion implantation in semiconductors. Part II. Damage production and annealing. *Proc. IEEE*, 1972, 60, 9, pp. 1062-1096.
82. Konopleva, R. F., Novikov, S. R., Ryvkin, S. M. On the levels of defects produced in Ge by monoenergetic neutrons. *Fiz. tverd. tela*, 1964, 6, 7, pp. 2022-2025 (in Russian).

83. Konopleva, R. F., Novikov, S. R., Rubinova, E. E., Sadikov, V. P., Ukhin, N. A. Annealing processes in high energy proton-irradiated *n*-Ge. *Fizika i tekhnol. polupr.*, 1970, 4, 8, pp. 1517-1523 (in Russian).
84. Khainovskaya, V. V., Smirnov, L. S. Interactions of radiation defects with dislocations in germanium. *Fiz. tverd. tela*, 1966, 8, 12, pp. 3403-3404 (in Russian).
85. Smirnov, L. S., Stas, V. F., Khainovskaya, V. V. Influence of dislocations on the kinetics of accumulation of radiation defects in germanium. *Fizika i tekhnol. polupr.*, 1971, 5, 1, pp. 85-90 (in Russian).
86. Drigo, E. D., Safronov, L. N., Smirnov, L. S. The role of the impurity atmospheres in radiative recombination at dislocations in germanium. *Fizika i tekhnol. polupr.*, 1972, 6, 9, pp. 1787-1790 (in Russian).
87. Glazman, V. B., Safronov, L. N., Smirnov, L. S. Influence of dislocations in germanium on depth of damage (layer of defects) during ion implantation. *Fizika i tekhnol. polupr.*, 1975, 9, 11, pp. 2222-2223 (in Russian).
88. Bolotov, V. V., Vasilyev, A. V., Misurkin, O. G., Potapova, L. P., Shirov, D. G. Fast electron irradiation effect on surface properties of germanium. *Izv. AN Latv. SSR. Ser. fiz. i tekhn. nauk*, 1973, 5, pp. 50-52.
89. Bolotov, V. V., Vasilyev, A. V., Misurkin, O. G., Potapova, L. P., Shirov, D. G. Influence of gas atmosphere on changes in surface electrostatic potential of germanium irradiated with fast electrons. *Izv. AN Latv. SSR. Ser. fiz. i tekhn. nauk*, 1973, 5, p. 119 (in Russian).
90. Romanov, S. I., Smirnov, L. S. On the interaction of point defects with SiO_2-Si Boundary. *Fizika i tekhnol. polupr.*, 10, 5, pp. 876-881 (in Russian).
91. Ukhin, N. A. On the interactions of defects produced by neutron irradiation in germanium with elementary defects injected by gamma radiation. In: *Radiation Physics of Non-metallic Crystals*. V. III, part 1, Kiev, Naukova dumka, 1971, pp. 193-196 (in Russian).
92. Bolotov, V. V., Vasilyev, A. V., Kozhevnikov, V. P., Smagulova, S. A., Smirnov, L. S. Interaction of disordered regions with point defects in *n*-type silicon. *Fizika i tekhnol. polupr.*, 1978, 12, 6, pp. 1104-1108 (in Russian).
93. Vinetskii, V. L., Yaskovets, I. I. On determination of effective rate of formation of radiation defects. In: *Radiation Physics of Non-metallic Crystals*. V. III, part 1, Kiev, Naukova dumka, 1971, pp. 142-146 (in Russian).
94. Bolotov, V. V., Vasilyev, A. V., Kozhevnikov, V. P., Smagulova, S. A., Smirnov, L. S. Interactions of disordered regions with point defects in *n*-type silicon. In: *Proc. of International Conf. on Ion Implantation in Semiconductors*, Central Inst. of Nuclear Research, Drezden, 1978, 1, pp. 219-225 (in Russian).
95. Rolle, M. E., Corelli, J. C. Study of atomic disorder produced by fast neutrons in Si using infrared spectroscopy. *J. Appl. Phys.*, 1976, 47, 1, pp. 37-42.
96. Totterdell, D. H. J., Newman, R. C. The effect of irradiation-induced lattice strain on the width of local mode absorption line in Si. *J. Phys., C: Sol. St. Phys.*, 1975, 8, 5, pp. 589-598.
97. Newman, R. C., Totterdell, D. H. J. An optical study of defects in silicon irradiated with fast neutrons. *J. Phys., C: Sol. St. Phys.*, 1975, 8, 12. pp. 3944-3954.
98. Bakhadyrkhanov, M. K., Zainabidinov, S. Influence of neutron irradiation on electrical properties of silicon doped with nickel, cobalt or manganese. *Fizika i tekhnol. polupr.*, 1977, 11, 10, pp. 2051-2053 (in Russian).
99. Stein, H. J., Vook, F. L., Brice, D. K., Borders, J. A., Picraux, S. T. Infrared studies of the crystallinity in ion implanted silicon. *Rad. Eff.*, 1970, 6, 1, pp. 19-26.
100. Gerasimenko, N. N., Dvurechensky, A. V., Lebedev, G. P. Interaction of defects produced by ion bombardment. *Fizika i tekhnol. polupr.*, 1973, 7, 12, pp. 2297-2300 (in Russian).

101. Dvurechensky, A. V., Smirnov, L. S. Production and rearrangement of radiation defects in ion implanted semiconductors. *Rad. Eff.*, 1978, 37, 3, 4, pp. 173-178.
102. Pridachin, N. B., Smirnov, L. S. Peculiarities of accumulation of radiation defects in ion bombarded crystals. *Fizika i tekhnol. polupr.*, 1971, 5, 1, pp. 166-168 (in Russian).
103. Gerasimenko, N. N., Dvurechensky, A. V., Smirnov, L. S. EPR study of defect formation in ion irradiated silicon. *Fizika i tekhnol. polupr.* 1971, 5, 9, pp. 1700-1705 (in Russian).
104. Thompson, M. *Defects and radiation damage in metals*, Cambridge, 1969, 384 pages.
105. Dennis, J. R., Hale, E. B. Amorphization of silicon by ion implantation: homogeneous or heterogeneous nucleation, *Rad. Eff.*, 1976, 30, pp. 219-225.
106. Gerasimenko, N. N., Gudayev, G. A., Dvurechensky, A. V., Smirnov, L. S., Sokolov, S. A. Amorphization of silicon by heavy ion irradiation. *Fizika i tekhnol. polupr.*, 1976, 10, 7, pp. 1237-1241 (in Russian).
107. Brower, K. L., Beezhold, W. Electron paramagnetic resonance of the lattice damage in oxygen-implanted silicon. *J. Appl. Phys.*, 1972, 43, 8, pp. 3499-3506.
108. Crowder, B. L., Title, R. S., Brodsky, M. H., Pettit, G. D. ESR and optical studies of ion-implanted silicon. *Appl. Phys. Lett.*, 1970, 16, 5, pp. 205-208.
109. Romanov, S. I., Smirnov, L. S. Production of disordered layers by ion bombardment of crystals. *Fizika i tekhnol. polupr.*, 1972, 6, 8, pp. 1631-1634 (in Russian).
110. Gerasimov, A. I., Zorin, E. I., Pavlov, P. V., Tetelbaum, D. I. On the peculiarities of silicon amorphization at ion bombardment. *Phys. Stat. Sol.* (*a*), 1972, 12, 2, pp. 679-685.
111. Gashtold, V. N., Gerasimenko, N. N., Dvurechensky, A. V., Smirnov, L. S. Defect profiles at ion implantation in silicon. *Fizika i tekhnol. polupr.*, 1975, 9, 5, pp. 835-839 (in Russian).
112. Abroyan, I. A., Titov, A. I., Khlebalkin, A. V. Formation of near-the-surface peak of structural damage at ion irradiation. *Fizika i tekhnol. polupr.*, 1977, 11, 6, pp. 1204-1206 (in Russian).
113. Morehead, F. F., Crowder, B. L. Model for the formation of amorphous Si by ion bombardment. *Rad. Eff.*, 1970, 6, 1, 2, pp. 27-32.
114. Dennis, J. R., Woodward, G. K., Hale, E. B. Vacancy motion in ion-implanted silicon. In: *Lattice Defects in Semiconductors. Conf. Ser., No. 23*, Inst. of Phys., London-Bristol, 1975.
115. Gerasimenko, N. N., Dvurechensky, A. V., Mashin, A. I., Khokhlov, A. F. Heterogeneity of amorphous layer produced by ion bombardment of semiconductor. *Fizika i tekhnol. polupr.*, 1977, 11, 1, pp. 190-192 (in Russian).
116. Gerasimenko, N. N., Dvurechensky, A. V., Romanov, S. I., Smirnov, L. S. The study of defect formation in ion-implanted silicon. In: *Radiation Damage and Defects in Semiconductors. Conf. Ser. No.* 16, Inst. of Phys., London-Bristol, 1972, pp. 72-80.
117. Vikhrev, B. I., Gerasimenko, N. N., Dvurechensky, A. V., Smirnov, L. S. Interaction of hydrogen atoms in silicon with defects produced by ion bombardment. *Fizika i tekhnol. polupr.*, 1974, 8, 7, pp. 1345-1348 (in Russian).
118. Christodoulides, C. E., Grant, W. A., Williams, J. S. Dose dependence of residual lattice disorder in ion-implanted and annealed silicon. *Appl. Phys., Lett.*, 1977, 30, 7, pp. 322-323.
119. Gerasimenko, N. N., Dvurechensky, A. V., Romanov, S. I., Smirnov, L. S. Interaction of defects and impurity upon ion implantation in silicon. *Fizika i tekhnol. polupr.*, 1972, 6, 10, pp. 1978-1981 (in Russian).

120. Kräutle, H. Study of the annealing behaviour of high-dose implants in Si and Ge crystals. *Rad. Eff.*, 1975, 24, 3, 4, pp. 255-262.
121. Dvurechensky, A. V., Gerasimenko, N. N., Romanov, S. I., Smirnov, L. S. High-dose effects in ion implantation. *Rad. Eff.*, 1976, 30, 2, pp. 69-72.
122. Csepregi, L., Kennedy, E. F., Gallagher, T. J., Mayer, J. W., Sigmon, T. W. Reordering of amorphous layer of Si implanted with P, As, B ions. *J. Appl. Phys.*, 1977, 48, 10, pp. 4234-4240.
123. Kennedy, E. F., Csepregi, L., Mayer, J. W., Sigmon, T. W. Influence of O, C, N and noble gases on the crystallization of amorphous Si layers. *J. Appl. Phys.*, 1977, 48, 10, pp. 4241-4246.
124. Baranov, A. I., Gerasimenko, N. N., Dvurechensky, A. V., Smirnov, L. S. Annealing of large vacancy clusters. *Fizika i tekhnol. polupr.*, 1977, 11, 1, pp. 94-99 (in Russian).
125. Baeri, P., Campisano, S. U., Cianola, G., Foti, G., Rimini, E. Influence of implanted dose on the recrystallization of Si amorphous layer. *Appl. Phys. Lett.*, 1975, 26, 4, pp. 154-155.
126. Golansky, A., Fiderkiewicz, A., Rzewuski, H., Lefeld-Sosnovska, M., Gronkowski, J., Grötzschel, R., Kreissing, U., Bartseh, H. Particularities of crystalline to amorphous state conversion in Si heavily damaged by 140 keV Si^{++} ions. *Phys. Stat. Sol.* (*a*), 1976, 38, 1, pp. 139-141.
127. Csepregi, L., Kennedy, E. F., Lau, S. S., Mayer, J. W., Sigmon, T. W. Disorder produced by high-dose implantation in Si. *Appl. Phys. Lett.*, 1976, 29, 10, pp. 645-648.
128. Baranova, E. C., Gusev, V. M., Martynenko, Yu. V., Starinin, C. V., Haibullin, I. B. On silicon amorphization during different mass ion implantation. *Rad. Eff.*, 1973, 18, 1, pp. 21-26.
129. Brodsky, M. H. Relations between structure and optical and electrical properties of amorphous Si and Ge films. *J. Vac. Sci. Technol.*, 1971, 8, pp. 125-134.
130. Brodsky, M. H., Kaplan, D., Zeigler, J. F. The densities of amorphous Si films by nuclear backscattering. *Appl. Phys. Lett.*, 1972, 21, 7, pp. 305-307.
131. Novozhilov, O. A., Meshcherskaya, L. I., Novikov, S. R. Influence of short-range order changes during ion bombardment on optical properties of germanium. *Fizika i tekhnol. polupr.*, 1975, 9, 11, pp. 2234-2237 (in Russian).
132. Lee, Y.-H., Kim, Y. M., Corbett, J. W., New ESR spectra in neutron-irradiated Si. *Rad. Eff.*, 1972, 15, 1, 2, pp. 77-84.
133. Lee, Y.-H., Brosious, P. R., Corbett, J. W. New ESR spectra in neutron-irradiated silicon II. *Rad. Eff.*, 1974, 22, 3, pp. 169-172.
134. Baranov, A. I. Annealing of complex defects in irradiated semiconductors. In: *Radiation Defects in Semiconductors.* Ed. by L. S. Smirnov, Novosibirsk, Nauka, 1979 (in Russian).
135. Csepregi, L., Mayer, J. W., Sigmon, T. W. Channeling effect measurement of the recrystallization of amorphous Si layers on crystal Si. *Phys. Lett.*, 1975, 54A, 2, pp. 157-158.
136. Csepregi, L., Mayer, J. W., Sigmon, T. W. Regrowth behaviour of ion-implanted amorphous layers on ⟨111⟩ silicon. *Appl. Phys. Lett.*, 1976, 29, 2, pp. 92-93.
137. Mazey, D. J., Nelson, R. S. Electron microscope investigation of damage structure in GaAs bombarded with neon ions. *Rad. Eff.*, 1969, 1, 4, pp. 229-239.
138. Gamo, K., Inada, T., Mayer, J. W., Eisen, F. H., Rhodes, C. G. Reordering of implanted amorphous layers in GaAs. *Rad. Eff.*, 1977, 33, 2, pp. 85-89.
139. Picraux, S. T. Disorder annealing in III-V semiconductors after ion implantation at low temperatures. *Rad. Eff.*, 1973, 17, 3-4, p. 261.

140. Kalandadze, G. I., Karumidze, G. S., Kervalishvily, P. J. On impurity background in detector germanium. *Fizika i tekhnol. polupr.*, 1978, **12**, 5, pp. 904-906 (in Russian).
141. Dennis, I. R., Hale, E. B. Crystalline to amorphous transformation in ion-implanted silicon: a composite model. *J. Appl. Phys.*, 1978, **49**, 3, pp. 1119-1127.
142. Zhukovsky, P. V., Stelmakh, V. F., Tkachev, V. D. Amorphization of semiconductor materials as a process of attainment of limit concentration of point defects. *Fizika i tekhnol. polupr.*, 1976, **10**, 11, pp. 2223-2225 (in Russian).
143. Zhukovsky, P. V., Stelmakh, V. F., Tkachev, V. D. Amorphization of silicon on irradiation with oxygen ions at $E < 5$ KeV. *Fizika i tekhnol. polupr.*, 1977, **11**, 4, pp. 793-795 (in Russian).

CHAPTER 2

DEFECT INVENTORY CONTROL IN DEFECT CENTERS

The employment of the radiation methods for technological purposes calls for control of the inventory of the defects formed, on the one hand, and for a search of the ways of optimizing the technological process, on the other. To accomplish this, one need not only know the properties of the radiation defects but also be capable of utilizing the presently established [4] relations between the rates of their formation and annealing and various external factors, such as the impurity content and defect inventory of the material, the radiation parameters (type, energy, intensity, dose) and the temperature. In this chapter, as in Chapter 1, emphasis is placed on silicon and germanium.

Sec. 2.1. Species of Particles and Their Energy

Where different species and energies of the particles are used to affect the parameters of the semiconductor materials and devices, the following results are obtained: (1) a different number of elementary structural defects (V and I) are generated per incident particle. In this case, the rates of production of secondary radiation defects are changed and a possibility arises for formation of disordered regions; (2) the sizes and thermal stability of developing defects are changed; (3) the ionization attendant upon the irradiation process varies in amount and in distribution in the crystal and (4) the spatial distribution of defects in the crystal is changed.

In this section, we shall consider major radiation defects produced in silicon when irradiated with different particle species.

An increase in the energy of electrons bombarding the crystal above $E_{\text{threshold}}$ leads to a rise in the number of vacancies and interstitials as well as of defect complexes of which these are a part (see Table 2.1). The studies of the relationship between the particle energy and the rate of production of defect complexes that include Frenkel pair components, such as vacancies, have made it possible to determine, fairly accurately, the threshold energy required for production of vacancies (V) and interstitials (I) (Fig. 2.1) [4].

Table 2.1

Defect center production rate in silicon versus energy

Electron energy, Mev	Defect	Production rate, cm^{-1}	Material* (ρ, ohm·cm, N, cm^{-3})	Irradiation conditions (T_{irrad}, K, j, $\mu A/cm^2$)	Measurement technique	Crystal orientation	References
0.7	V-O	$\sim 1.0 \cdot 10^{-1}$	n-Si (P), $N_P \sim 2 \cdot 10^{15}$, $5 \cdot 10^{16}$	$T_{irrad} \leqslant 340$, $j = 3$	EPR	—	[1]
1.0	V-O	$\sim 1.3 \cdot 10^{-1}$	Same	Same	Same	—	[1]
1.2	V-O	$\sim 1.5 \cdot 10^{-1}$	Same	Same	Same	—	[1]
2.2	V-O	$3.2 \cdot 10^{-1}$	n-Si (P), $\rho = 15$	$T_{irrad} = T_{cr}$, $\Phi = 8 \cdot 10^{14}$-10^{17} cm^{-2}	Hall effect	—	[2]
2.2	V-O	$4.4 \cdot 10^{-1}$	Same	Same	EPR	—	[2]
2.2	V-O	$1.7 \cdot 10^{-1}$	n-Si (P), ρ-40-75	Same	Hall effect	—	[2]
2.2	V-O	$2.6 \cdot 10^{-1}$	Same	Same	EPR	—	[2]
14	V-O	$1.3 \cdot 10^{-1}$-$3 \cdot 10^{-1}$	n-Si (P), $N_P \sim 2 \cdot 10^{15}$, $5 \cdot 10^{16}$	$T_{irrad} \leqslant 340$, $j = 3$	Same	—	[1]
52	V-O	$1.3 \cdot 10^{-1}$-$5 \cdot 10^{-1}$	Same	Same	Same	—	[1]
1.0	V-P	$1.8 \cdot 10^{-2}$	n-Si (P), $\rho = 4$	—	Hall effect	—	[3]
1.0	V-P	$8.3 \cdot 10^{-3}$	n-Si (P), $\rho = 7$	—	Same	—	[3]
2.2	V-P	$3.7 \cdot 10^{-2}$	n-Si (P), $\rho = 15$	$T_{irrad} = 300$	Same	—	[2]
0.7	V-V	$\approx 1.5 \cdot 10^{-3}$**	p-Si (B), $N_B = 2 \cdot 10^{16}$	$T_{irrad} \leqslant 340$, $j = 3$	EPR	—	[1]
0.85	V-V	$2 \cdot 10^{-3}$ $2.5 \cdot 10^{-3}$	Same	Same	Same	⟨110⟩, ⟨111⟩, ⟨100⟩	[1]
~1.0	V-V	$4.3 \cdot 10^{-3}$ $2.5 \cdot 10^{-3}$	Same	Same	Same	⟨111⟩, ⟨100⟩, ⟨110⟩	[1]
~1.2	V-V	$5.5 \cdot 10^{-3}$ $6.0 \cdot 10^{-3}$ $7 \cdot 10^{-3}$	Same	Same	Same	⟨110⟩ ⟨111⟩ ⟨100⟩	
~1.4	V-V	$7.8 \cdot 10^{-3}$ $8.5 \cdot 10^{-3}$ $9.2 \cdot 10^{-3}$	Same	Same	Same	⟨111⟩ ⟨110⟩ ⟨100⟩	[1]
14	V-V	$2.5 \cdot 10^{-2}$	Same	Same	Same	—	[1]
52	V-V	$4 \cdot 10^{-2}$	Same	Same	Same	—	[1]

* Grown by the Czochralski method.
** Same for all crystal orientations.

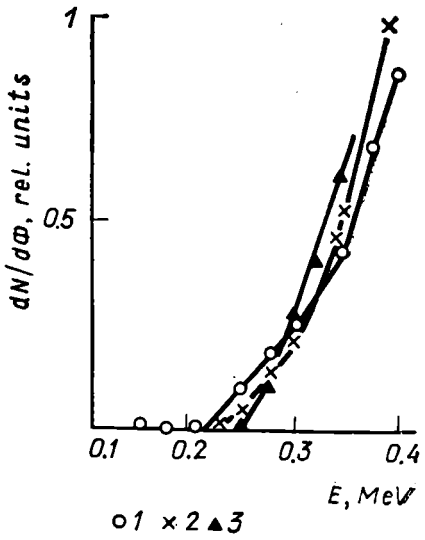

Fig. 2.1. *V*-O complex production rate in silicon vs fast electron energy [4].
Crystal orientation: *1*—⟨111⟩; *2*—⟨100⟩; *3*—⟨110⟩. Material: КЭФ-1. Fast electron beam density: 0.3 μA/cm²

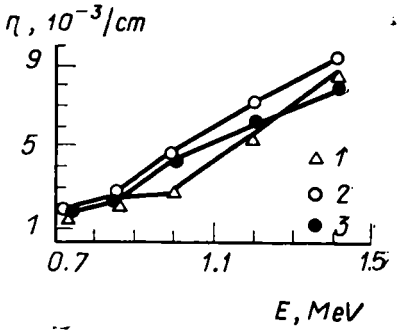

Fig. 2.2. Divacancy production rate in silicon vs electron energy [1].
Crystal orientation: *1*—⟨110⟩; *2*—⟨100⟩; *3*—⟨111⟩. Silicon of *p*-type, boron doped, $N_B = 2 \cdot 10^{16}$ cm^{-3}. Irradiation temperature, about 70 °C; electron beam density, 3 μA/cm²

There is a certain probability for generation, as a result of a single scattering action produced by a bombarding electron, of more complex defects, such as divacancies (*V*-*V*), tetravacancies, etc. (see Section 1.2) [1, 5]. As can be seen from Fig. 2.2 and Table 2.1, the rate of production of divacancies is by one order of magnitude lower than the rates of production of the *V*-O and *V*-P complexes. However, for their production the divacancies depend more heavily on the energy of the bombarding particle.

The investigations of the relationships existing between the energies of the bombarding particles and the rates of production of the *V*-O and *V*-*V* complexes in silicon [1, 5] have helped establish a slight anisotropy for the rates of production of such defects (see Figs. 2.1 and 2.2), associated with the anisotropy of the threshold energies of formation of *V* and *V*-*V*.

The defect production rate ($\Delta N/\Delta\Phi$, cm^{-1}, where ΔN is the change in the defect concentration, cm^{-3}, at irradiation dose $\Delta\Phi$, cm^{-2}) is found from the linear sections of the dose dependence curve, i.e., the sections illustrating the nature of the comparatively low

radiation doses. With an increase in the radiation dose, the impurity that forms part of the defect complex begins to show clear signs of depletion, which, combined with the thermal dissociation of the complex and annihilation of defects (see Section 1.1), reduces the defect production rate and causes a subsequent saturation of the complex concentration [4, 6].

Some investigators [7-9] have observed changes in the parameters of the crystal irradiated with electrons having energies below $E_{\text{threshold}}$ ("subthreshold" effects). At present, it is argued that the "subthreshold" effects are caused by structural rearrangements in the crystal [4]. This viewpoint becomes more convincing if one considers that semiconductor crystals do not maintain their thermodynamic balance after being grown [10, 11]. In this case, the ionizing radiation with an energy below $E_{\text{threshold}}$ promotes structural rearrangements in the crystals [4, 10] and causes a change in their parameters. Such processes are likely to be very important in objects with strong heterogeneity, such as semiconductor devices having *p-n* junctions, metal-dielectric-semiconductor interfaces, etc.

With electron energies higher than 10 MeV, disordered regions appear in Ge and Si along with point defects.

Irradiation of semiconductors with gamma rays amounts to an internal irradiation with electrons. From the practical viewpoint, of particular interest is the gamma radiation derived from a Co^{60} source (1.25 MeV), a gamma background of a nuclear reactor or gamma bremsstrahlung.

Table 2.2 supplies the reference data on the rates of production of defect centers with gamma radiation (Co^{60} source). The inventory and properties of the point defects produced with electron and gamma (Co^{60}) radiations are identical [1, 12-16].

The reactor gamma-background also results in the formation of point defects for the most part [17]. Irradiation of semiconductors with high-energy gamma rays (15-25 MeV and higher, gamma bremsstrahlung) results in a complex structural damage, such as the disordered region.

Irradiation of semiconductor materials with fast reactor neutrons results in the formation of both point defects and disordered regions. The comparison of the defect production rates obtained with the electron and neutron irradiations (see Table 2.2) shows a sharp rise in the number of divacancies for neutron irradiation, while the rates of production of defect complexes involving one vacancy (e.g., the *V*-O complex) are practically the same for both types of irradiation. According to [18], the rate of production of divacancies exceeds that of *A*-centers 13 and 40 times, depending on the concentration of oxygen (see Table 2.2) during neutron irradiation, and only three times during irradiation with 52-MeV electrons, which is sufficient for production of disordered regions [1].

Table 2.2

Comparison of vacancy complex production rates in gamma electron and neutron irradiated samples

Type and energy of irradiation	Defect	Material* (ρ,ohm·cm, N, cm^{-3}	Production rate, cm^{-1}	Irradiation conditions (T_{irrad}, K; j, μA/cm^2)	Measurement technique	References
Co^{60} gamma irradiation	V-O	n-Si (P), $\rho=2$, $N_O=(5\pm1)\cdot10^{17}$	$1.35\cdot10^{-3}$	$T_{irrad}=311$, intensity $1.0\cdot10^{12}$ kV/cm^{2}s	Hall effect	[12]
Same	V-P	Same	$1.2\cdot10^{-4}$	Same	Same	[12]
Same	V-O	n-Si (P), $\rho=11$, $N_O=5\cdot10^{17}$	$9.5\cdot10^{-4}$	Same	Same	[12]
Same	V-P	Same	$4.0\cdot10^{-5}$	Same	Same	[12, 13]
Same	V-?	p-Si (B), $\rho=5$, Z	$5.0\cdot10^{-5}$	Same	Same	[14]
Same	V-?	p-Si (B), $\rho=15$, Z	$2.0\cdot10^{-5}$	Same	Same	[14]
Electrons, MeV						
1	V-O	n-Si (P), $N_P=$ $2\cdot10^{15}$-$5\cdot10^{16}$, Cz	$1.3\cdot10^{-1}$	$T_{irrad}\leqslant340$	EPR	[1]
4.5	V-O	n-Si (P), $\rho=16$	$1.0\cdot10^{-1}$	$T_{irrad}=273$	Hall effect	[12]
2.2	V-P	n-Si (P), $\rho=15$, Cz	$3.7\cdot10^{-2}$	$T_{irrad}\cong300$	Same	[2]
1	V-V	p-Si (B) $N_B=2\cdot10^{16}$, Cz	$3\text{-}4\cdot10^{-3}$	$T_{irrad}\leqslant340$	EPR	[1]
Fast reactor neutrons	V-V	p-Si (B), $N_B=$ $5\cdot10^{14}$, Cz and Z ($N_O\approx3\cdot10^{17}$ and $\leqslant10^{16}$, respectively)	5.7	$j=3$ $T_{irrad}=320$	IR-spectroscopy	[18]
Same	V-V	p-Si (B), $N_B\sim2\cdot10^{17}$, Z ($N_O=10^{16}$)	~6.4	Same	Same	[18]
Same	V-O	p-Si (B), $N_B\sim5\cdot10^{14}$, Cz	$1.4\cdot10^{-1}$	Same	Same	[18]
		$N_O=3\cdot10^{17}$	$4.3\cdot10^{-1}$	Same	Same	[18]
		$N_O=10^{18}$	2.3	$T_{irrad}=300$	Same	[20]
Same	V-V	p-Si (B), Cz				

* Cz – grown by the Czochralski method, Z – grown by zone refining.

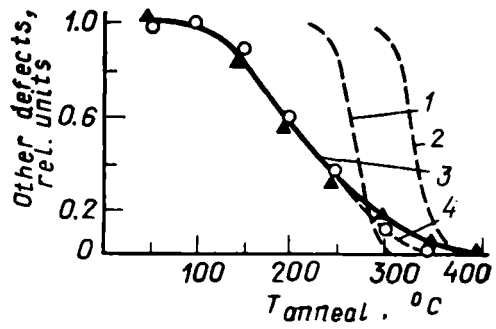

Fig. 2.3. Isochronal (15 min) annealing of a concentration of divacancies in silicon [18].

1, *3*—*p*-Si (B) grown by the Czochralski method, irradiated with 1.5-MeV electrons and neutrons, respectively; *2*, *4*—*p*-Si (B) produced by zone refining, irradiated with 1.5-MeV electrons and neutrons, respectively. Neutron irradiation temperature, about 50 °C

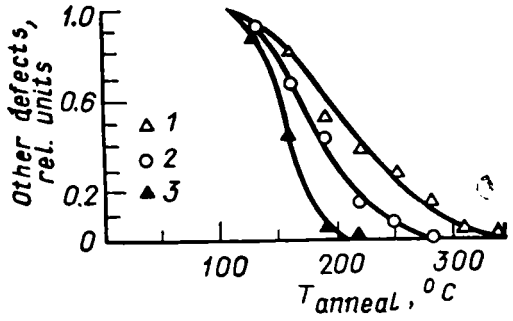

Fig. 2.4. Isochronal (30 min) annealing of a concentration of divacancies in neutron irradiated *p*-Si (B) [19].

Dose in cm^{-2}: *1*—10^{17}; *2*—10^{18}; *3*—10^{19}. Irradiation temperature, about 40 °C

In neutron irradiation, divacancies form in a heavily damaged (but crystalline [18, 19]) region, which is proved by the isochronal annealing experiments (Fig. 2.3). The investigations of the annealed structure have shown that the divacancies produced by neutron irradiation (in contrast to electron irradiation) can be annealed out at lower temperatures. An increase in the neutron dose shifts the annealing onset point towards still lower temperatures (Fig. 2.4). Another distinction of neutron irradiation from electron irradiation resides in that there is no effect of oxygen content on the annealing of 60% of divacancies, whereas the remaining 40% are annealed out much faster in an oxygen-containing material (see Fig. 2.3) [18]. The wealth of experimental data (a part of the data have been quoted above) have allowed the investigators to conclude that a DR core produced by neutron irradiation represents a pile up of vacancy complexes [19, 20], such as divacancies and other, more involved, formations [21].

As the neutron dose increases, the concentration of divacancies approaches the saturation point [18, 19]. For example, in *p*-Si with a boron content of about $2 \cdot 10^{17}$ cm^{-3}, the saturation point is reached at a neutron dose of about $4 \cdot 10^{16}$ cm^{-2} and a concentration of divacancies of about $2.7 \cdot 10^{16}$ [18]. According to other authors [19], the saturation point is reached only at doses of about 10^{18} to 10^{19} cm^{-2} as a result of DR overlapping. Such a difference in the results may be attributed to a high concentration of boron in the first case, since

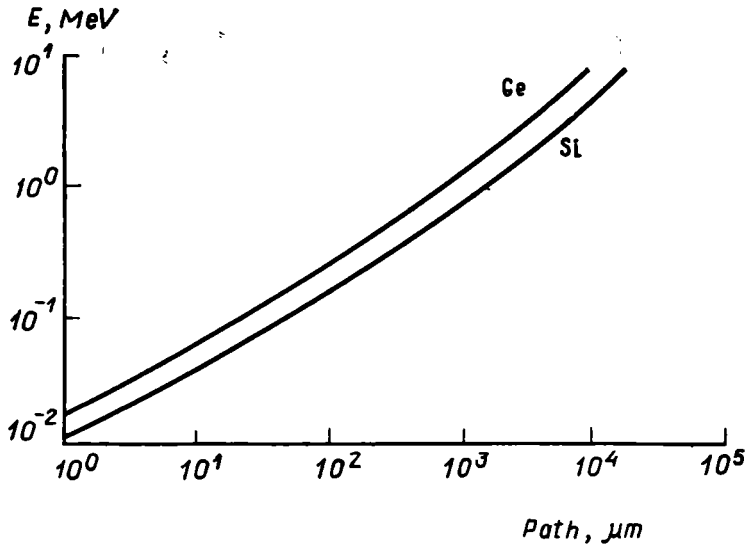

Fig. 2.5. Electron paths in silicon and germanium [17, 19].

here we have a higher rate of production of divacancies [18] (see Table 2.2).

Irradiation with slow neutrons having energies of about 0.025 eV leads to nuclear reactions in the crystal. This phenomenon has been employed in technology as a basis for the nuclear transmutation doping of semiconductors, i.e., production of an electrically active impurity as a result of the nuclear transmutation (see Chap. 10 for details) [22, 23].

Bombardment of crystals with light and heavy ions produces a complete set of structural defects, such as DRs (both with crystalline and amorphous cores, as described in Sec. 1.3), complexes of radiation defects [24-30], etc. As this takes place, an additional important factor comes into play, namely, a nonuniform depth distribution of implanted ions and produced defects (see, for example, [30]). Some authors argue that with light ion or proton irradiation (about 3 to 9 MeV energy), the spectrum of the damage produced in the crystal is similar to that appearing under neutron irradiation [24, 25].

Irradiation of Ge and Si with protons of extremely high energies (660 MeV and higher) results in the formation of large defects called by the authors of [29] as large diffused areas.

Irradiation of Si crystals with other comparatively light ions (say, oxygen) also produces defects typical of neutron irradiation [31, 32]. The heavier ions (say, Xe^+) produce disordered regions with an amorphous core. The processes involved in ion irradiation of semiconductors are considered in greater detail in Chapters 6 through 9. Here we shall restrict ourselves to just noting that on

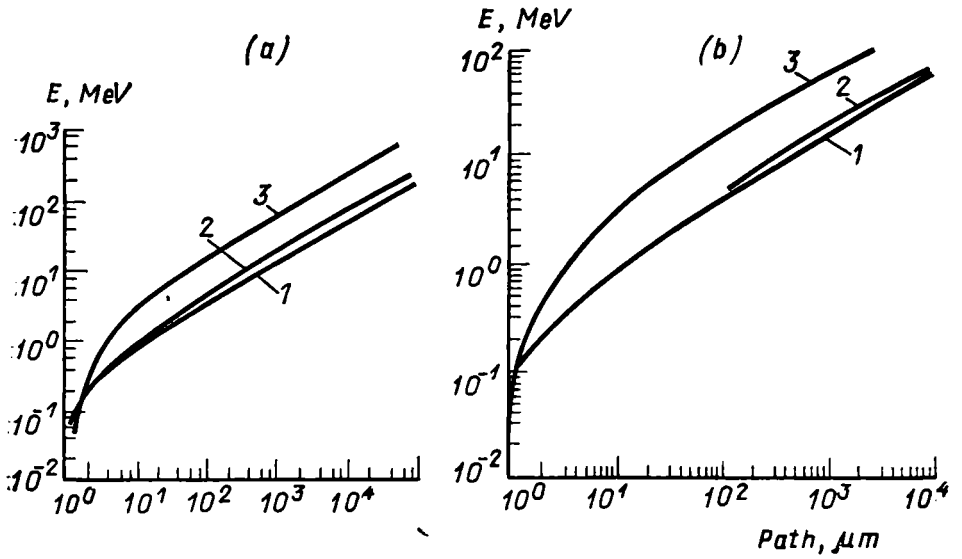

Fig. 2.6. Paths of charged particles in silicon (a) and germanium (b) [79, 80].
1—protons; *2*—deutrons; *3*—alpha-particles

ion bombardment of semiconductors the implanted impurity not only yields the desired doping effect but also takes an active part in the defect forming processes [30].

The changes in the species and energy of the bombarding particles do not always result in drastic changes in the nature of the damage thus induced. The authors of [33] note that the point defects dominate near the surface of a silicon sample if irradiated with neutrons, protons, ions of boron or phosphorus as well as with electrons or even with X-rays, which is indicative of the diffusion of defects and their accumulation near the sinks. The length of the particle path in the crystal depends on its species and energy (Figs. 2.5 and 2.6). The maximum depth at which the defects can be produced is somewhat less than the particle path [17, 30].

To conclude, let us indicate some uses of various particles for technological purposes. Gamma-quanta, electrons, fast neutrons are used for changing the parameters of semiconductor materials and devices in the desired manner and for simulating the damage caused by space radiation. Protons are helpful in injection of localized damage to change the optical properties of semiconductors and characteristics of semiconductor structures. Other ion species are used for ion-implanted doping, fusion, and control of the optical properties of the material. Slow neutrons are used in doping by nuclear transmutation.

Sec. 2.2. Importance of Crystal Prehistory

Among the factors that have a significant bearing on the processes of defect production by irradiation are:

(1) kind of doping impurity and its concentration;

(2) presence of inactive and uncontrollable impurities, their concentration and position in the crystal lattice (regular or interstitial, in aggregate, etc.);

(3) combination doping (the presence of two or more kinds of impurity, having their levels within the energy gap);

(4) presence of dislocations, a change in the impurity atmospheres;

(5) preliminary irradiation (e.g., introduction of disordered areas by neutron or ion irradiation);

(6) thermal treatment (hardening or preheating);

(7) boundaries, interfaces, presence of amorphous or disordered layers.

The above factors cause changes in the radiation-induced defect complexes and in the efficiency of their production.

Many investigators studied the importance of the doping impurities in the kinetics of production and annealing out of radiation defects in germanium [34-39] and silicon [12-14], [40-42]. Let us consider the basic experimental data.

In the crystals of the *n*-type silicon, grown by the Czochralski method (and containing a high concentration of oxygen, $N_O \approx \approx 10^{17}$ cm^{-3}), a change in the concentration of the charge carriers is largely dependent upon the formation of an *A*-center (level E_C— 0.17 eV), while in the crystals obtained by zone refining in vacuum, *E*-centers dominate (level E_C — 0.40 eV).

Earlier [34] it was shown that during gamma irradiation (Co^{60}) of *n*-type silicon doped with phosphorus ($N_P = 2.4 \cdot 10^{15}$ cm^{-3}) and containing oxygen in a concentration of $5 \cdot 10^{17}$ cm^{-3} the rate of formation of the *E*-centers ($2 \cdot 10^{-5}$ cm^{-1}) is way below that of the *A*-centers ($1.35 \cdot 10^{-3}$ cm^{-1}), the latter dropping to $6 \cdot 10^{-4}$ cm^{-1} as the concentration of phosphorus is decreased to 1.4×10^{14} cm^{-3}. The *E*-center formation rate grows with an increase in the concentration of phosphorus [41].

One paper [40] contains a detailed study of the dependence of the accumulation kinetics and annealing behaviour of *A*- and *E*-centers in silicon of *n*-type on the kind of doping impurity and oxygen content. The authors investigated the samples grown in quartz crucibles, containing oxygen $(5\text{-}7) \cdot 10^{17}$ cm^{-3}, doped with phosphorus ($\rho \approx$ 1-40 ohm·cm), arsenic or antimony ($\rho \approx 5$ ohm·cm), and the samples obtained by methods *I* and *II* of crucibleless zone refining, containing oxygen in concentrations of $\leqslant 2 \cdot 10^{16}$ and $\leqslant 1 \cdot 10^{15}$ cm^{-3}, respectively, and doped with phosphorus ($\rho \approx$ 5-40 ohm·cm). The

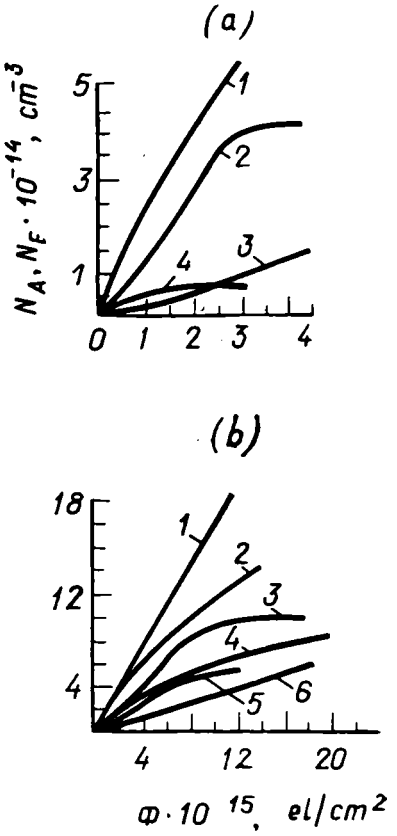

Fig. 2.7. Concentrations of A- and E-centers in silicon vs electron irradiation dose [40].

a—phosphorus-doped silicon: *1*, *4*—concentrations of E- and A-centers, respectively, in silicon samples produced by crucibleless zone refining method I, $N_P = 5.25 \cdot 10^{14}$ cm^{-3}; *2*, *3*—same in quartz crucible-grown silicon samples, $N_P = 5.45 \cdot 10^{14}$ cm^{-3}; *b*—silicon samples grown in quartz crucibles: *1*, *3*, *5*—concentrations of A-centers; *2*, *4*, *6*—concentrations of E-centers (*1*, *4*—in a sample with $N_P = 6.4 \cdot 10^{15}$ cm^{-3}; *3*, *6*—in a sample with $N_{As} = 1.65 \cdot 10^{15}$ cm^{-3}; *2*, *5*—in a sample with $N_{Sb} = 2.1 \cdot 10^{15}$ cm^{-3}); $T_{irrad} = 77$ K, $T_{anneal} = 380$ K

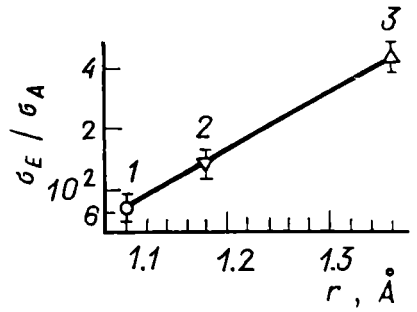

Fig. 2.8. E- and A-center formation cross-sections ratios vs covalent radius of donor impurity in silicon grown in quartz crucibles [40].

Samples doped with phosphorus at $N_P = 5.45 \cdot 10^{14}$ and $6.6 \cdot 10^{15}$ cm^{-3} (*1*); samples doped with arsenic at $N_{As} = 1.65 \cdot 10^{15}$ cm^{-3} (*2*); samples doped with antimony at $N_{Sb} = 2.1 \cdot 10^{15}$ cm^{-3} (*3*)

samples were irradiated with 1.5-MeV electrons at temperatures ranging from 77 to 500 K. Of major interest were the changes stable at room and higher temperatures.

Figure 2.7*a* is an illustration of a well known fact: in silicon with a high concentration of oxygen, the rate of introduction of A-centers is far in excess of that of E-centers, while the reverse is true for oxygen-free silicon. From Fig. 2.7*b*, the authors of [40] have concluded that the E-center formation cross-section grows with an increase in the covalent radius of the donor impurity:

$$\sigma_E = \sigma_0 \exp [A (r_D - r_{Si})],$$

where $A = (6.5 \pm 0.7)$ Å^{-1}; r_{Di} r_{Si} = tetrahedral covalence radii of the donor and silicon atoms, respectively; $\sigma_0 = \pi R^2$, $R \sim 50$ Å

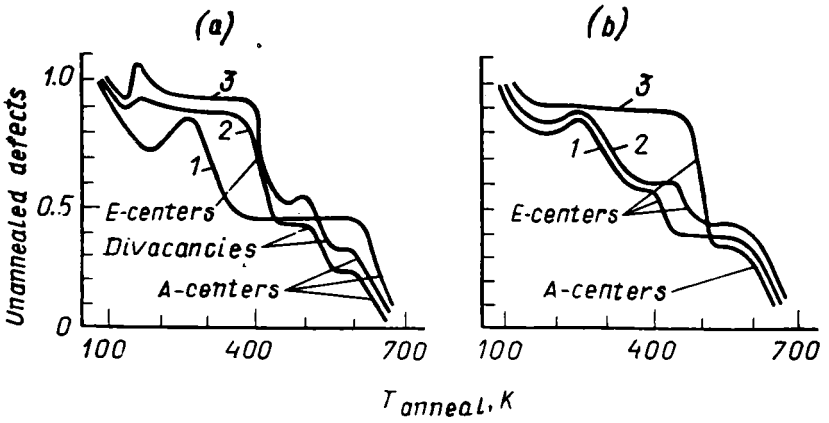

Fig. 2.9. Isochronal (15 min) annealing of silicon irradiated at 77 K [40]. *a*—$\Phi = 1.7 \cdot 10^{18}$ cm^{-2}, samples doped with phosphorus; *1*—silicon grown in quartz crucibles, $N_P = 5.25 \cdot 10^{14}$ cm^{-3}; *2*, *3*—silicon produced by crucibleless zone refining method I, $N_P = 5.25 \cdot 10^{14}$ cm^{-3}, and by crucibleless zone refining method II, $N_P = 4.8 \cdot 10^{14}$ cm^{-3}, respectively; *b*—$\Phi = 6.2 \cdot 10^{18}$ cm^{-2}, silicon samples grown in quartz crucibles and doped: *1*—with phosphorus at $N_P = 6.4 \cdot 10^{15}$ cm^{-3}; *2*—with arsenic at $N_{As} = 1.65 \cdot 10^{15}$ cm^{-3}; *3*—with antimony at $N_{Sb} = 2.1 \cdot 10^{15}$ cm^{-3}; $T_{meas} = 77$ K

[40]. Fig. 2.8 illustrates the dependence of the ratio of *E*- and *A*-center formation cross-sections on the covalence radius of the donor impurity

$$\sigma_E/\sigma_A = (N_O \cdot \eta_E)/(N_D \cdot \eta_A) = [N_O\,(dN_E/d\Phi)]/[N_D\,(dN_A/d\Phi)],$$

where σ_E, σ_A, η_E and η_A are the cross-sections and rates of formation of *E*- and *A*-centers, respectively; N_D, N_O, N_E, N_A are the concentrations of the donor, oxygen, *E*- and *A*-centers, respectively; Φ is the irradiation dose. It is also obvious from Fig. 2.7*b* that an increase in the covalent radius of the donor impurity is accompanied by a decrease in the rate and cross-section of formation of *A*-centers.

The oxygen content and type of donor impurity influence the annealing behaviour of defect centers (Fig. 2.9*a*, *b*). As the donor radius increases, the *E*-center annealing step shifts towards a higher temperature range, while the *A*-center annealing step remains unchanged (see Fig. 2.9*b*). In crystals with a greater oxygen content there are no registered annealing steps for *E*-centers and divacancies (see Fig. 2.9*a*).

Similar results (a shift towards a higher temperature range for *E*-center annealing steps with an increase in the covalence radius of the donor impurity) have been obtained by the authors of [41] for silicon doped with P, As, Sb or Bi (the concentrations of the donors of all types have been about 10^{14} cm^{-3}) after gamma irradiation from a Co^{60} source (Fig. 2.10).

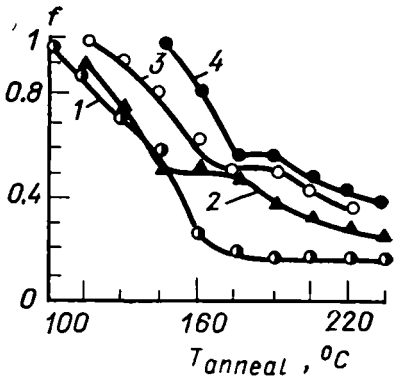

Fig. 2.10. Isochronal annealing of lifetime in silicon with a low oxygen content, irradiated with gamma-rays from a Co^{60} source [41].

The samples are doped with: *1*—phosphorus; *2*—arsenic; *3*—antimony; *4*—bismuth. Irradiation intensity, $2.75 \cdot 10^{11}$ cm$^{-2} \cdot$ s^{-1}; donor concentration, $1 \cdot 10^{14}$ cm^{-3}

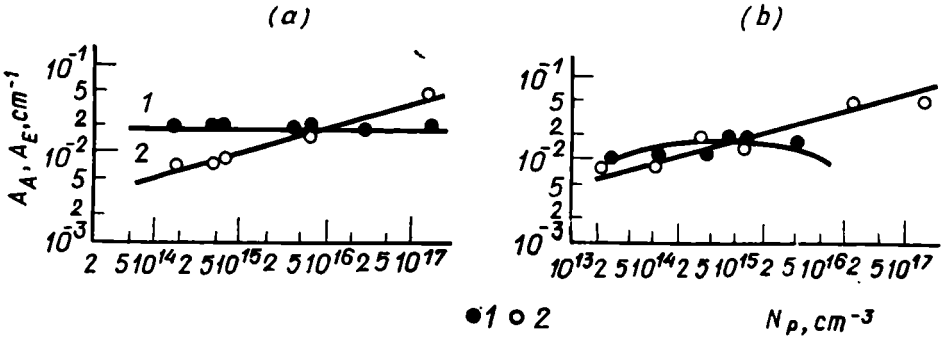

Fig. 2.11. *A*- and *E*-center formation rates vs concentration of phosphorus in silicon with (*a*) $N_O = (5\text{-}7) \cdot 10^{17}$ and (*b*) $N_O \leqslant 2 \cdot 10^{16}$ cm^{-3} [42].

According to [42], the rate of formation of *A*-centers in silicon by reactor neutron irradiation is slightly dependent on the concentration of the doping impurity atoms (phosphorus) while the rate of introduction of *E*-centers rises sublinearly with the donor concentration (Fig. 2.11*a*, *b*). In *n*-type silicon with a large oxygen content ($\approx 5 \cdot 10^{17}$ cm^{-3}), the *A*-center represents a dominating radiation defect as long as the concentration of the donor impurity does not exceed $\approx 10^{16}$ cm^{-3} (see Fig. 2.11*a*), while in silicon with a low oxygen content, the *E*-center is a dominating defect even with a donor concentration in excess of $\sim 10^{15}$ cm^{-3} (see Fig. 2.11*b*).

Fig. 2.11*a*, *b* shows that the rate of formation of *A*-centers depends but slightly on the oxygen content in the crystal. Similar results have been received in [13] for silicon with $N_P \leqslant 10^{16}$ cm^{-3}, gamma irradiated from a Co^{60} source. Table 2.3 gives the formation rates for *A*- and *E*-centers in gamma irradiated silicon, taken from [13]. The *A*-center also appears in *p*-type silicon, though at a rate which is lower than in *n*-type silicon [18].

The influence of an acceptor impurity on the *A*-center formation rate in silicon has been studied in [6]. An increase in the concentration of boron turned out to be a factor markedly increasing the

Table 2.3

***A*- and *E*-center formation rates in *n*-type silicon samples with different oxygen and donor impurity contents [13]**

Sample No.	N_O	$N_P \cdot 10^{-14}$	$(dN_A/d\Phi) \times 10^4$	$(dN_E/d\Phi) \times 10^4$	Sample No.	N_O	$N_P \cdot 10^{-14}$	$(dN_A/d\Phi) \times 10^4$	$(dN_E/d\Phi) \times 10^4$
	cm^{-3}		cm^{-1}			cm^{-3}		cm^{-1}	
1		0.8	7	0.14	8		14	4.2	14
2		1.1	8	0.17	9		16	9.5	10
3	$5 \cdot 10^{17}$	3.3	9.5	0.4	10		16	12	14
4		20	14	1.3	11		43	7	18
5		20	13	5	12	$< 2 \cdot 10^{16}$	53	4.3	22
					13		60	7	19
6		3	6	12	14		950	1.3	30
7		4.3	8	0.6					

Notes: 1. Samples 11 and 12 are doped with antimony and arsenic, respectively; other samples are phosphorus doped.
2. Before irradiation, samples 5 and 10 were heated for one week at 1000 °C.
3. Irradiation intensity, $4 \cdot 10^{12}$ $cm^{-2} \cdot s^{-1}$.

A-center content throughout the 1.8 MeV electron irradiation dose range under study (Fig. 2.12).

The formation of divacancies as secondary defects is an event which depends, sometimes, on the impurity content of silicon. The available experimental evidence on silicon indicates that the rate of production of divacancies in *n*-type silicon depends on the concentration of the doping impurity. Thus, in *p*-type silicon with a low oxygen content ($N_O < 10^{16}$ cm^{-3}), irradiated with reactor neutrons, the rate of production of divacancies changes from 5.7 to 6.4 cm^{-1} as the concentration of boron is increased from $5 \cdot 10^{14}$ to $2 \cdot 10^{17}$ cm^{-3} [18]. According to [14], in *n*-type silicon doped with boron and having a high oxygen content, the rate of production of divacancies during gamma irradiation is very low, while in silicon with a low oxygen content it amounts to $5 \cdot 10^{-5}$, $2 \cdot 10^{-5}$ and $2 \cdot 10^{-5}$ cm^{-1} for the samples with specific resistance values of 5, 15 and 50 ohm·cm, respectively.

The results of divacancy annealing depend on the oxygen content: in silicon with a high oxygen content, divacancies are annealed out at 290 °C, with a low oxygen content, at 350 °C [18].

Recently, intensive investigations have been focused on the influence of carbon impurity in silicon on the efficiency of introduction of defect centers. Carbon can be involved in complexes that change, for example, the IR absorption spectrum [43]. The authors

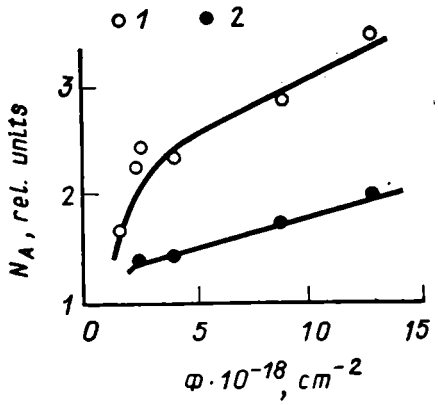

Fig. 2.12. Dose dependence of A-center concentration [6].
Concentration of boron, cm^{-3}; *1*—$4 \cdot 10^{15}$; *2*—$9 \cdot 10^{14}$

of [44] note the fact of competition between the atoms of oxygen and carbon for the vacancies introduced by irradiation with electrons of about 1 MeV.

The rate of formation of A-centers by 2 MeV electron irradiation of p-type silicon samples with high and low carbon contents ($N_C = 2 \cdot 10^{18}$ and $1.3 \cdot 10^{17}$ cm^{-3}) varies but insignificantly, i.e., the number of vacancies giving rise to interstitial oxygen slightly depends on the carbon content, whereas the rate of production of divacancies drops as the carbon content is decreased [45]. Such results have been obtained for silicon with a high oxygen content ($N_O = 2 \cdot 10^{18}$ cm^{-3}) [45]. It should be noted that the data [44, 45] on the influence of the carbon impurity on the A-center formation rate are somewhat contradictory. It seems that the importance of carbon in the radiation defect production process still requires some elucidating experiments.

It is a known fact that irradiation of germanium results in the emergence of a vacancy-donor (VD) complex analogous to the E-center in silicon. Unlike in silicon where the E-center level is well known ($E_C - 0.40$ eV), the level of the VD complex in germanium is a controversial issue. Some workers [4, 46] think that the VD complex has no level within the energy gap, while the others set this level at $E_C - 0.21$ and $E_V + 0.09$ eV [47].

The relationship between the radiation defect annealing curve and the tetrahedral covalent radius of the donor impurity in germanium was investigated in [15, 46, 48]. As is obvious from Fig. 2.13, the annealing temperature rises with different impurities placed as follows: P, As, Sb, Bi ($r = 1.10$, 1.225, 1.36, and 1.46 Å, respectively [49]).

Of considerable interest are the studies of the irradiation effect on the crystals which contain, except for the main doping impurity, other active impurities that balance out the action of the donors or acceptors, or impurities having little impact on the electrical behaviour of the non-irradiated crystals, but effectively interacting

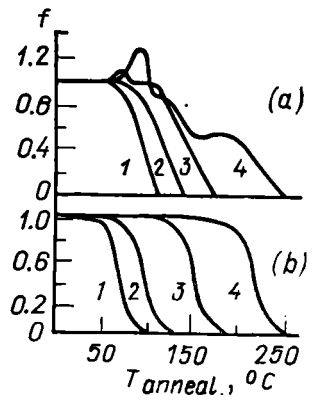

Fig. 2.13. Isochronal annealing of defects in germanium [46].
a—level E_C—0.20 eV: *1*—Ge(P), *2*—Ge(As), *3*—Ge(Sb), *4*—Ge(Bi); *b*—level E_V + 0.10 eV: *1*—Ge(P), *2*—Ge(As), *3*—E_V + 0.12 eV, Ge(Sb), *4*—E_V + 0.16 eV, Ge(Bi); *f* — a share of unannealed defects (the Hall emf was measured)

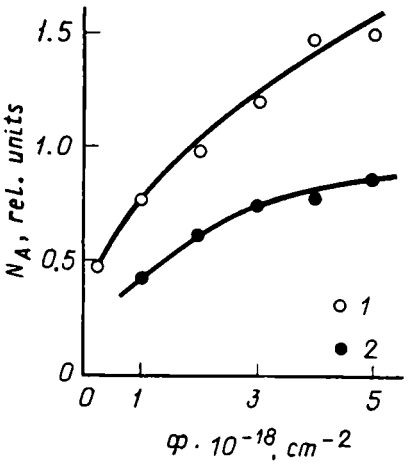

Fig. 2.14. A change in the concentration of *A*-centers in silicon of *p*-type (ρ = 10 ohm·cm) in accordance with the dose of 1.2 MeV electron irradiation [62].
1—silicon doped with boron; *2*—silicon doped with boron and gadolinium ($N_{Gd} \cong 10^{18}$ cm^{-3}). Concentration of oxygen in both materials s about 10^{18} cm^{-3}. Radiation intensity, $3 \cdot 10^{12}$ cm$^{-2} \cdot$s^{-1}

with the Frenkel pair components introduced by irradiation. The crystals with two or more impurities hold much promise as a means for enhancing radiation stability of semiconductors [4]. For example, introduction of compensating impurities, such as Ni, Co or Mn, into *n*-type silicon reduces the efficiency of formation of the *A*- and *E*-centers and divacancies during radiation from a Co^{60} source over a dose range of 10^{14} to $2 \cdot 10^{18}$ cm^{-2} [50]. A reduction in the defect production rate in gamma irradiated *n*-type germanium that contained impurities, Ca or Ba, was noted by the authors of [51]. In [62] it was shown that the presence of gadolinium in *p*-type silicon reduces the *A*-center formation rate (Fig. 2.14).

It is interesting to investigate the behaviour of some fast-diffusing impurities (Au, Cu, etc.) in silicon during irradiation. The irradiation may transfer them from the idle interstitial sites to the electrically active regular sites [52-54] and vice versa [4]. In other situations, the electrical activity of an impurity may remain unchanged [55]. It is apparent that the domination of a particular process may be due to presence of other impurities and irradiation conditions alike.

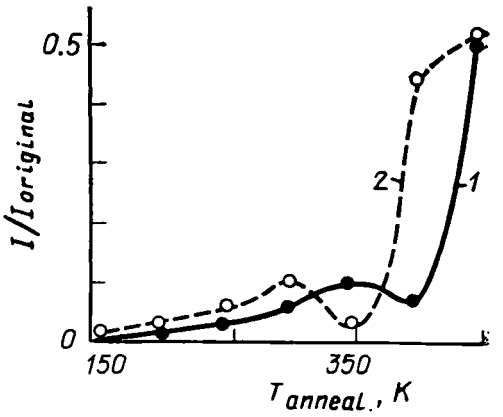

Fig. 2.15. Annealing of recombination radiation intensity in irradiated germanium [56].
1—*n*-type; *2*—*p*-type

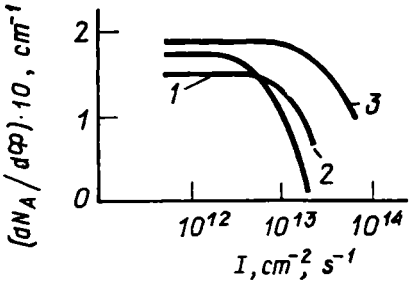

Fig. 2.16. *A*-center formation rate in silicon vs density of 2.2 MeV electron beam [57].
1—original sample (dislocation density, $3\cdot10^4$ cm^{-2}); *2*—after preliminary irradiation with 24.6 MeV protons; dose, $1.8\cdot10^{11}$ cm^{-2}; *3*—after deformation (dislocation density, $2\cdot10^6$ cm^{-2}). Material: *n*-type Si doped with phosphorus, $\rho = 60$ ohm·cm, $N_0 = 2\cdot10^{17}$ cm^{-3}

Dislocations in silicon and germanium take active part in the defect forming process during irradiation and annealing. This is conditioned not only by that the dislocations serve as sinks for the Frenkel pair components but that the impurity atmosphere around a dislocation enters upon an active interplay with defects. The *n*- and *p*-type germanium samples containing dislocations to a density of 10^5-10^6 cm^{-2}, introduced via plastic deformation, have been irradiated with 3.5 MeV electrons (the dose, $5\cdot10^{15}$ cm^{-2}) [56]. The recombination radiation spectrum associated with dislocations has been investigated in the 2.0 to 2.6 μm region. The recombination radiation spectrum completely suppressed by irradiation was beginning to recover at annealing temperatures of about 150 to 200 °C. However, complete annealing was not observed even at about 450 °C (Fig. 2.15) despite the fact that the nonradiative recombination centers are annealed out near 300 °C. To explain this phenomenon, the authors of [56] suppose that the Frenkel pair components originating from the nonradiative recombination centers dissociating during annealing enter the impurity atmospheres around dislocations thereby forming more stable complexes.

Introduction of dislocations in silicon changes the nature of the relation between the *A*-center formation rate and the irradiation intensity [57] (Fig. 2.16).

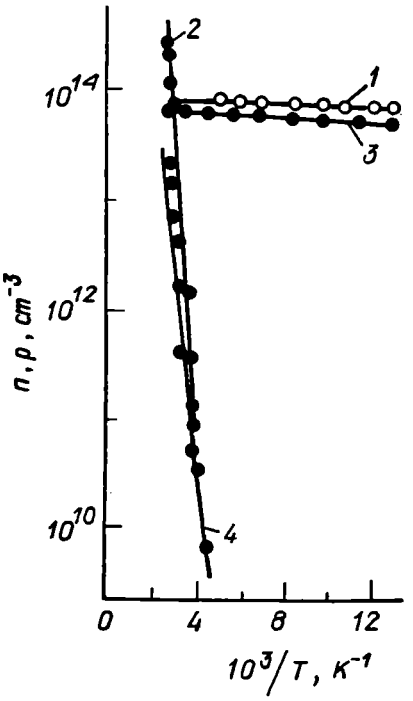

Fig. 2.17. Temperature dependence of carrier concentration in silicon [58]. *1*—before deformation, *n*-type; *2*—in deformed samples, *p*-type; *3*—in deformed and iron-saturated samples, *n*-type; *4*—after irradiation with $1 \cdot 10^{15}$ cm^{-2} electron dose; level $E_C - 0.29$ eV (an atom of iron in a regular lattice site)

A change of the impurity atmosphere around a dislocation often results in the formation of other radiation defects. The authors of [58] used 2.2-MeV electron irradiation on *n*-type silicon samples that have been previously treated as follows: first, dislocations have been introduced into the samples to a density of $\approx 10^8$ cm^{-2}, then the atoms of iron have been deposited on the dislocations (by heating the samples for half an hour at 1200 °C). The results thus obtained (Fig. 2.17) is a testimony to the appearance of iron regular sites after irradiation, the fact the authors attribute to the removal of iron from the Cottrell cloud by irradiation and the formation of a solid solution by substitution.

The preliminary irradiation, while changing the impurity-defect inventory of the crystal, affects the production of defect complexes during subsequent irradiation with various particles. Unfortunately this interesting problem is still not clearly understood. Some data exist on the interactions of disordered regions introduced by preliminary neutron irradiation with the defects emerging as a result of a subsequent irradiation (see Sec. 1.3). We shall therefore be content here with a mention of one paper [57] that shows that the introduction of disordered regions (by proton irradiation) in Si changes the manner in which the *A*-center formation rate is correlated to the electron irradiation intensity (see Fig. 2.16).

A heat treatment, i.e., heating to a high temperature with a subsequent rapid (hardening) or slow (annealing) cooling, appreciably affects the crystal prehistory, causing sharply defined changes in the basic parameters of the crystal. It is well known that in silicon the concentration of electrons in the conduction band increases after extended preheating. This fact is interpreted as having connection to the emergence of the so-called thermal donors, the defects such as the complexes of the SiO_n type ($n = 2, 3, 4$). The thermal donor formation rate is maximum at the heating temperatures of about

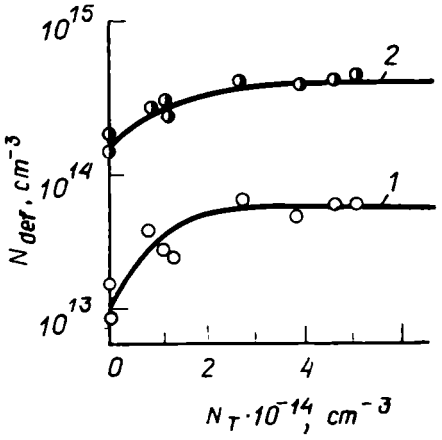

Fig. 2.18. A change in the nature of accumulation of radiation defects in accordance with concentration of thermal donors [60].
1—electrically active defects; *2*—*A*-centers. Material: silicon КЭФ-20, irradiated with 3.5 MeV electrons; dose, $1 \cdot 10^{15}$ cm^{-2}

450 to 470 °C [59]. Germanium, when hardened at 600 to 900 °C, experiences *n-p* conversion of its conductivity. A review of the properties of the thermal defects in silicon and germanium is provided in [49]. Let us consider some data on the change in the rates of production of particular defect complexes in thermally treated crystals.

An *n*-type silicon sample grown by the Czochralski method, with $\rho = 15$ and 40-75 ohm·cm, was irradiated with 2.2 MeV electrons [2]. Prior to irradiation, the sample was heat treated at 1350 °C. The results revealed an increase in the *A*-center formation rate in the sample first heated to 1350 °C and then rapidly cooled (Table 2.4).

Table 2.4

Dependence of *A*-center formation rate in silicon on heat treatment [2]

ρ_{orig}, ohm·cm	Material	$dN_A/d\Phi$, cm^{-1} (Hall effect measurements)	ρ_{orig}, ohm·cm	Material	$dN_A/d\Phi$, cm^{-1} (Hall effect measurements)
15	Original	$3.2 \cdot 10^{-2}$	40-75	Original	$1.7 \cdot 10^{-1}$
	Heated	$5.7 \cdot 10^{-2}$		Heated	$2.2 \cdot 10^{-1}$

With a slow cooling after a high-temperature heating, the *A*-center formation rate registered a drop. This was explained [2] by a redistribution of oxygen between the interstitial sites and during the SiO_2 phase.

There is a paper [60] that shows that the presence in silicon of thermal donors (introduced by heating with a subsequent slow cooling) leads to an increase in the concentration of irradiation-induced *A*-centers (Fig. 2.18). Some workers [13] observed a rise in the *E*-center formation rate in silicon with the oxygen content $N_O = 5 \cdot 10^{17}$ cm^{-3} and increased *A*- and *E*-center formation rates

in silicon with $N_O < 2 \cdot 10^{16}$ cm^{-3} on gamma-irradiation after heating the samples for a week at 1000 °C (see Table 2.3).

A heat treatment in one or another form is an integral part of the technological fabrication procedure of semiconductor devices. Therefore, a further investigation of the radiation behaviour of heat treated crystals is very important to prognostication of the likely changes in the parameters of semiconductor devices exposed to radiation and in the outer space.

The crystal boundary, as well as the interfaces between the semiconductor and the dielectric, semiconductor and the metal, etc. which serve as sinks for the radiation defects [4], have a marked effect on the characteristics of the defect centers. For example, the *A*-center located in the vicinity of the SiO_2-Si interface anneals out at a much lower temperature (200 to 220 °C) than in the crystal bulk (300 to 350 °C) [61].

Hence, by changing the crystal prehistory, we can introduce the desired complexes at preselected rates and obtain the crystals of the desired practical value. However, the entire complexity of the crystal prehistory, still remains to be unravelled. This is particularly true of the questions outlined in Items 5 through 7 of this section (refer to the beginning of the section). Further work in this field is likely to yield interesting results having practical significance.

Sec. 2.3. Importance of Radiation Intensity and Temperature

The importance of radiation intensity is explained by the following reasons [4]:

1. A high radiation intensity results in heating up of the irradiated samples.
2. The ionization arising from the irradiation changes the charge states of the defects sensitive to ionization and, as a consequence, the rates of production (and accumulation) of defect complexes.
3. The ionization changes the diffusion characteristics of the atoms of chemical impurities and other defects, which sometimes changes the rates of production of defect complexes.
4. The greater the density of the flux of the bombarding particles, the higher the rate of production of the Frenkel pairs. At high rates of production the defect formation processes develop features quite different from those peculiar to fluxes with low current densities: the vacancies and interstitials begin to enter upon effective interactions with each other, resulting in clusters and partial annihilation.
5. High ionization densities are likely to produce local liberation of energy by a defect complex during recombination of electron-

hole pairs on it (θ-flash) [63, 64]. As a consequence, the defect complex dissociates thus reducing the defect formation rate in general.

The effect of the crystal irradiation temperature on the defect production processes is determined by the following factors [4]:

1. A rise in temperature results in decreasing the threshold energy of production of the Frenkel pairs, which leads to a greater rate of production of free vacancies and interstitials. By increasing the irradiation temperature, one can introduce a desired number of the Frenkel pairs at a lower energy of the bombarding particles.

2. By changing the irradiation temperature one can change the probability of annihilation at the centers and sinking of the Frenkel pair components with the result that the number of free vacancies and interstitials (i.e., the atoms that can take part in the reactions) is changed as well.

3. The concentration of carriers and, hence, the charge states of the reacting defects are changed, which results in a sharp change in the reaction speeds.

4. The temperature dependence of the defect production and dissociation cross-sections leads to a faster production rate for more stable defects as the irradiation temperature increases.

5. A heating concurrent with the irradiation gives rise to various radiation-stimulated processes changing the inventory of the defects and their distribution in the crystal.

6. Due to the fact that most of the original materials are thermodynamically unbalanced, a high-temperature heating of the material places the crystal near the state of equilibrium, which changes the impurity-defect structure of the crystal (thermal donors, etc. appear). The irradiation accelerates this process (see below).

By varying the intensity and temperature of irradiation one can change the crystal properties over a wide range.

Let us address ourselves to some experimental evidence. The authors of [65] have received the data on the influence of the irradiation intensity on the A-center formation rate in n-type silicon with a specific resistance of 2 ohm·cm and an oxygen content of $2 \cdot 10^{17}$ cm^{-3}. The samples have been irradiated at room temperature with electrons of different energies. The plots of Fig. 2.19, using the data of [65], indicate that the accumulation of the A-centers shows an active growth towards the saturation at high current densities of the beam.

Quite a different situation has been obtained in [57] (see Fig. 2.16, *1*), where the A-center formation rate does not depend on the current density until a certain limit is reached following which it begins to drop. It seems that the correct interpretation of this inconsistency resides with a difference in the impurity-defect structures of the silicon samples [57, 65]. Specifically, it is worth noting that the silicon sample used in [57] contained less phosphorus ($\rho = 60$ ohm·cm)

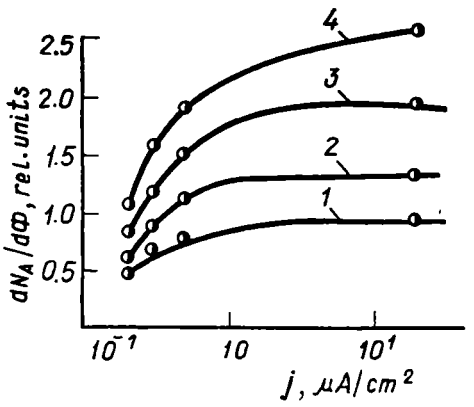

Fig. 2.19. *A*-center formation rate vs electron beam density (according to [65]).
Electron energy, MeV: *1*—0.6; *2*—0.8; *3*—1; *4*—1.2

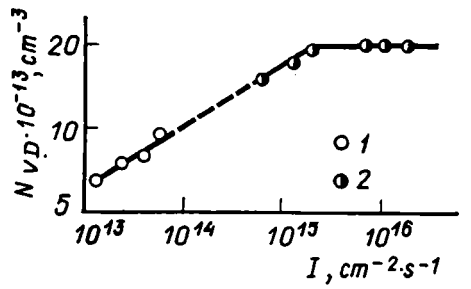

Fig. 2.20. Concentration of vacancy-donor complexes vs irradiation intensity [4].
1—Van de Graaf accelerator as a source of radiation (electron energy, 1 MeV); *2*—MICROTRON accelerator as a source of radiation (energy, 3.5 MeV). Plotted is the value of intensity corresponding to the density of the beam current in an impulse. The difference in electron energies is taken into account [4]. Material: germanium of *n*-type, ρ = 10 ohm·cm

than the sample used in [65] (ρ = 2 ohm·cm). A saturation of the electron irradiation intensity dependence of the defect production rate was also observed in germanium for a concentration of *VD* complexes (the donor is antimony) [66] (Fig. 2.20). This result was explained in [4]. Note here that the saturation curve of Fig. 2.20 has been obtained with irradiation by the MICROTRON pulse accelerator. The use of the Van de Graaf electrostatic accelerator turned out to be inadequate for obtaining the saturation point since the further increase in the electron current density resulted in a higher temperature of the samples. Thus, the employment of pulse radiation (1) helps avoid heating up of the sample and (2) provides for better reproducibility of the results because under high ionization during the pulse time, the irradiation intensity dependence of the defect production rate reaches the saturation point.

There are several papers that investigate the temperature dependence of the defect complex production rate. According to [40], the *E*-center formation rate drops with an increase in the irradiation temperature, while that of the *A*-centers varies non-monotonically (Fig. 2.21). One of the papers [42] notes an increase in the *A*-center formation rate concurrently with a drop in the *E*-center formation rate as the temperature of reactor neutron irradiation rises from 70 to 100 °C. A decrease in the *E*-center formation rate with a rise in the irradiation temperature was also observed in [67] (Fig. 2.22).

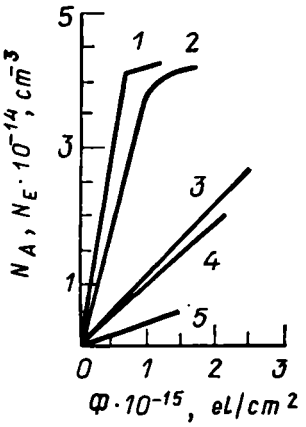

Fig. 2.21. Concentrations of A- and E-centers vs 1.5 MeV electron irradiation dose for silicon samples grown in quartz crucibles and doped with phosphorus with $N_P = 5.45 \cdot 10^{14}$ cm^{-3} [40].

T_{irrad}, K: *1*—380; *2*—273; *3*—500; *4*—273; *5*—380. $N_A(\Phi)$—for 1-3; $N_E(\Phi)$—for *4*, *5*

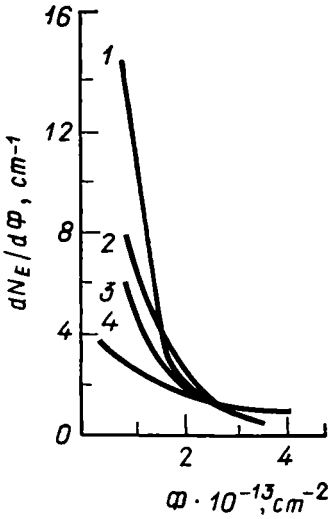

Fig. 2.22. Dose dependence of efficiency of E-center formation in n-type silicon ($N_O = (2\text{-}5) \cdot 10^{17}$ cm^{-3}) doped with phosphorus ($\rho = 40$ ohm·cm). Fast neutron irradiation temperature, °C: *1*—20; *2*—40; *3*—50; *4*—60

Some papers [68, 69] studied the dependence of the rates of formation of A-centers, divacancies and E-centers in n-type silicon ($\rho = 60$ ohm·cm, grown by zone refining in vacuum) on the temperature of 2.2 MeV electron irradiation. The non-monotonic dependence curves obtained (Fig. 2.23) are explained in [68, 69], on the one hand, by a change (with temperature) in the active center formation and dissociation rates and, on the other hand, by a change in the charge states of the vacancies and defect complexes as the Fermi level is shifted [70].

To compute the defect complex production rates at different irradiation temperatures, the authors of [68] suggest an optimum dose curve whereby to select, at a given temperature, the irradiation dose so that a change in the concentration of charge carriers δn_0 or δp_0 (proportional to the total number of the electrically active defects introduction) during irradiation is maintained at a constant level and is never in excess of the original concentration of free charge

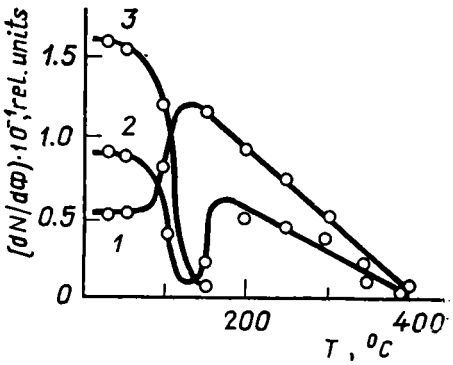

Fig. 2.23. Rates of introduction of *A*-centers (*1*), divacancies (*2*) and *E*-centers (*3*) in silicon vs 2.2 MeV electron irradiation temperature [69].

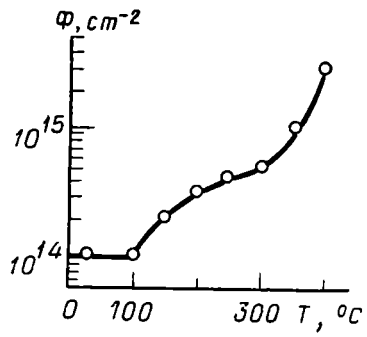

Fig. 2.24. A curve for selection of the optimum integral flux for different irradiation temperatures [68].

carriers. Fig. 2.24 shows such a curve for *n*-type silicon ($n_0 = 6 \cdot 10^{13}$ cm^{-3}) at $\delta n_0 = (3\text{-}4) \cdot 10^{13}$ cm^{-3}, irradiated with 2.2 MeV electrons. The effects of high temperature on the behaviour of silicon and germanium during irradiation is also analyzed in [2, 70-74].

Because a heat treatment of some kind is an indispensible operation at different stages of fabrication of semiconductor devices, we shall now dwell in greater detail on the nature of the processes involved in the production and rearrangement of defects when irradiation is concurrent with heating. The authors of this chapter understand that the considerations contained herein are largely controversial and need experimental confirmation.

When semiconductors are grown from a melt, the crystal is cooled from the temperature of the melt to room temperature. At high temperature, especially, near the melting temperature, the crystal develops a considerable concentration of point defects in equilibrium, vacancies in particular, which will interact with chemical impurities, dislocations, etc. As a result, the crystal reaches a thermodynamic equilibrium at a given temperature, a state with quite specific concentrations of free vacancies and interstitials and relationships between the numbers of impurity atoms in regular and interstitial sites, precipitates and dislocations, etc. The establishment and characteristics of the state of equilibrium are largely affected by the crystal electron subsystem.

As the crystal is cooled in the course of growing, the crystal-defect system tends to restore the equilibrium at each reduction of temperature, every time calling for a redistribution of the impurity and defect states and for a new concentration ratio thereof in the lattice. Stated another way, as the crystal is being cooled, the defects are continuously interacting with one another. To do this, they must diffuse in the crystal over rather long distances. In order for the cooling crystal to retain its state of equilibrium, the time it maintains a specific temperature should be long enough for all the reactions required to establish a thermodynamic equilibrium at this temperature to complete. However, the real rates of cooling during a monocrystal growth are relatively high with the result that the crystal has no time to fully change its impurity-defect inventory at a new equilibrium state. Hence, a crystal of silicon or germanium, grown from a melt at room temperature, is not in a state of equilibrium. There are papers [10, 11] that took a note of this fact.

It is a well known fact that complicated processes of rearrangement of defects occur in the crystals heated to above room temperature (see [75, 76]). Such processes involve precipitation of impurities, migration of the impurity atoms in the crystal, formation of various complexes of different impurity atoms with one another, etc. Should the crystal be in a state of equilibrium, such changes would be inexplicable: the crystal already had this temperature in the course of growing, had it not? It seems that the processes involving changes in the impurity defect inventory of the heated crystals (the emergence of "thermal donors" and "thermal acceptors", etc.) are the indications of the fact that the crystal, originally in the non-equilibrium state, is about to reach the state of thermodynamic equilibrium at a given heating temperature. One of the most probable mechanisms of interaction between the defects in the crystal nearing the equilibrium state is the diffusion of impurities and defects (vacancies, in particular). By subjecting the crystal to irradiation and subsequent annealing, we make its transfer to a state of equilibrium much easier, the process promoted both by radiation-enhanced diffusion of impurities (see Ch. 3) and by formation of a large number of vacancies and interstitials (for convenience of explanation, we consider the irradiation with such particles that produce only point defects). Thus we can presume that irradiation of the crystals produces two qualitatively different effects, such as (A) emergence of radiation defects (see Secs. 2.1 and 2.2) and (B) pushing the crystal state towards equilibrium at the given irradiation temperature, which manifests itself in reactivation of the reactions that have been "frozen" in the course of crystal growing. The process B generally occurs at any temperature, though at room and lower temperatures the process A seems to dominate. However, at sufficiently high doses of irradiation the crystal parameters show marked changes in the pro-

cess B, which are indicated by the "aftereffects" [77, 78] observed sometimes. At high-temperature irradiation, the process B seems to play an important role, like the process A, in production of more stable defect complexes. At extremely high temperatures, when the diffusion of most impurity atoms becomes appreciable and the concentration of self-vacancies considerable, the importance of irradiation factors decreases. From that it may be inferred that there must exist a temperature range within which the role of irradiation in the process B is most clearly defined. The lower boundary of this range is the temperature of complete annealing of point defects induced by radiation (about 300-350 °C in germanium and about 500-600 °C in silicon), the upper boundary, the temperature at which the impurities begin to diffuse (about 500-600 °C in germanium and about 700-800 °C in silicon). It is obvious that the same temperature range is most suitable for efficient radiation-enhanced diffusion.

References

1. Corbett, J. W., Watkins, G. D. Production of divacancies and vacancies by electron irradiation of silicon. *Phys. Rev.*, 1965, 138, 2A, pp. 555-560.
2. Milevsky, L. S., Tkacheva, T. M. Redistribution of primary Frenkel defects among impurity atoms in irradiated silicon monocrystals. In: *Study of Space Materials and Technology*, Moscow, Nauka, 1977, pp. 94-103 (in Russian).
3. Goryachev, V. G., Korotayeva, N. K., Mordkovich, V. N. On the influence of *E*-centers on a change in irradiated silicon conductivity. *Fizika i tekhnol. polupr.*, 1974, 8, 4, pp. 795-797 (in Russian).
4. *Physical Processes in Irradiated Semiconductors.* Ed. by L. S. Smirnov, Novosibirsk, Nauka, 1977, 254 pages (in Russian).
5. Akishin, A. I., Gorodetsky, S. M., Grigorieva, G. M., Kreinin, L. B., Nazarov, V. G. On selecting a combination of irradiations to simulate the action of space radiation on photoelectric converters. In: *Kosmicheskoye materialovedeniye i tekhnologiya*, Moscow, Nauka, 1977, pp. 149-157 (in Russian).
6. Bolotov, V. V., Vasilyev, A. V., Smirnov, L. S. Influence of acceptor impurity concentration on vacancy-oxygen complex formation rate in silicon. *Fizika i tekhnol. polupr.*, 1976, 10, 9, pp. 1787-1789 (in Russian).
7. Mordkovich, V. N., Temper, E. M. Influence of subthreshold energy electrons on electrical conductivity of *n*-type silicon. *Fizika i tekhnol. polupr.*, 1969, 3, 3, pp. 440-441.
8. Zaikovskaya, M. A., Kiv, A. E., Niyazova, O. R., Starodubtsev, S .V. Changes produced by subthreshold energy electron irradiation in silicon. *Fizika i technol. polupr.*, 1967, 1, 8, pp. 1131-1137 (in Russian).
9. Chen, J., McKay, J. W. Subthreshold electron damage in *n*-type germanium. *Phys. Rev.*, 1968, 167, 3, pp. 745-753.
10. Smirnov, L. S. On the reactions in crystals. In: *Structural Defects in Semiconductors.* Novosibirsk, Institute of Semiconductor Physics, Siberian Branch of USSR Academy of Sciences, 1973, pp. 201-207 (in Russian).
11. Medvedev, S. A. *Introduction into Technology of Semiconductor Materials.* Moscow, Vysshaya Shkola, 1970, p. 503 (in Russian).
12. Sonder, E., Templeton, L. C. Gamma irradiation of silicon. 1. Levels in *n*-type material containing oxygen. *J. Appl. Phys.*, 1960, 31, 7, pp. 1279-1286.

13. Sonder, E., Templeton, L. C. Gamma irradiation of silicon. II. Levels in *n*-type flote-zone material. *J. Appl. Phys.*, 1963, **34**, 11, pp. 3295-3301.
14. Sonder, E., Templeton, L. C. Gamma irradiation of silicon. III. Levels in *n*-type material. *J. Appl. Phys.*, 1965, **36**, 6, pp. 1811-1815.
15. Mashovets, T. V., Emtsev, V. V. Point defect in germanium. In: *Lattice Defects in Semiconductors. Conf. Ser. No. 23*, Inst. of Phys. London-Bristol, 1975, pp. 103-125.
16. Smirnov, L. S., Stas', V. F., Khainovskaya, V. V. Irradiation and annealing of germanium crystals with high density of dislocations. *Fizika i tekhnol. polupr.*, 1969, **3**, 12, pp. 1760-1765 (in Russian).
17. Vavilov, V. S., Ukhin, N. A. *Radiation Effects in Semiconductors and Semiconductor Devices.* Moscow, Atomizdat, 1964, 311 pages (in Russian).
18. Cheng, L. J., Lori, J. Characteristics of neutron damage in silicon. *Phys. Rev.*, 1968, **171**, 3, pp. 856-862.
19. Newman, R. C., Totterdell, D. H. J. An optical study of defects in silicon irradiated with fast neutrons. *J. Phys., C: Sol. St. Phys.*, 1975, **8**, 12, pp. 3944-3954.
20. Barnes, C. E. Absorption measurement in neutron irradiated silicon. In: *Radiation Effects in Semiconductors.* Ed. by J. W. Corbett, G. D. Watkins, London-N.Y.-Paris, Gordon and Breach Science Publishers, 1971.
21. Konozenko, I. D., Semenyuk, A. K., Khivrich, V. I. *Radiation Effects in Silicon.* Kiev, Naukova dumka, 1974, 199 pages (in Russian).
22. Gres'kov, I. M., Solovyev, S. P., Kharchenko, V. A. Influence of growth defects on change in conductivity of neutron irradiated silicon. *Fizika i tekhnol. polupr.* 1977, **11**, 8, pp. 1598-1601 (in Russian).
23. Didkovsky, A. P., Saakova, A. K., Khivrich, V. I. Some electrical characteristics of high-ohmic radiation-doped silicon. *Fizika i tekhnol. polupr.*, 1976, **10**, 3, pp. 543-545 (in Russian).
24. Lutgemeier, H., Schnitzke, K. Paramagnetic centers in proton irradiated silicon. *Phys. Letters*, 1967, **25A**, 3, pp. 232-233.
25. Botvin, V. A., Gorelkinsky, Yu. V., Sigle, V. O., Chubisov, M. A. Paramagnetic centers in silicon irradiated with heavy charged particles. *Fizika i tekhnol. polupr.*, 1972, **8**, 9, pp. 1683-1686 (in Russian).
26. Rubinova., E. E., Konopleva, R. F., Novikov, S. R. High-temperature annealing of 660-MeV proton irradiated silicon. *Fizika i tekhnol. polupr.*, 1975, **9**, 2, pp. 242-247 (in Russian).
27. Konopleva, R. F., Novikov, S. R., Rubinova, E. E. Electrical characteristics of 660 MeV proton irradiated silicon. *Fizika i tekhnol. polupr.*, 1975, **9**, 2, pp. 330-333 (in Russian).
28. Grigoryeva, G. M., Kolodin, L. G., Kreinin, L. B., Mukashev, B. N., Nusupov, K. Kh. Radiation defects in *p*-type silicon irradiated with 30 MeV protons. *Fizika i tekhnol. polupr.*, 1977, **11**, 11, pp. 2176-2180 (in Russian).
29. Konopleva, R. F., Ostroumov, V. N. *Interactions of High-Energy Charged Particles with Germanium and Silicon.* Moscow, Atomizdat, 1975, p. 126 (in Russian).
30. Mayer J., Eriksson L., Davies J. *Ion implantation in Semiconductors. Silicon and germanium.* New York-London. 1970, 280 pages.
31. Totterdell, D. H. J., Newman, R. C. The effect of irradiation induced lattice strain on the width of local mode absorption lines in Si. *J. Phys., C; Sol. St. Phys.*, 1975, **8**, 5, pp. 589-598.
32. Brower, K. L., Vook, F. L., Border, J. A. Depth distribution of EPR centers in 400 KeV O^+ ion-implanted silicon. *Appl. Phys. Lett.*, 1970, **16**, 3, pp. 108-110.
33. Vologdin, E. N., Zhukova, G. A., Mordkovich, V. N. Radiation damage in silicon surface layers. *Fizika i tekhnol. polupr.*, 1973, **7**, 4, pp. 835-836 (in Russian).

34. Browns, W. L., Augustiniak, W. M., Waite, T. R. Annealing of radiation defect in semiconductors. *J. Appl. Phys.*, 1959, **30**, 8, pp. 1258-1268.
35. Saito, H., Pigg, J. C., Crawford, J. R. Annealing of Co^{60}-gamma-irradiated germanium. *Phys. Rev.*, 1966, **144**, 2, pp. 725-733.
36. Vitovsky, N. A., Maksimov, M., Mashovets, T. V. A study of gamma-radiation-induced defects in high-purity germanium. *Fizika i tekhnol. polupr.*, 1970, **4**, 6, pp. 1030-1038 (in Russian).
37. Nakazawa, F., Ishino, S., Higashinakagawa, J., Hasiguti, R. R. Impurity dependence of annealing of gamma-ray irradiated *n*-type germanium. *J. Phys. Chem. Sol.* 1965, **26**, 12, pp. 1895-1907.
38. Tkachev, V. D., Urenev, V. I. Interactions of elementary defects of crystal lattice with donor impurity atoms in germanium. *Fizika i tekhnol. polupr.*, 1971, 5, 8, pp. 1516-1522 (in Russian).
39. Basman, A. R., Gerasimov, A. B., Gogotishvili, M. K., Dolidze, N. D., Kasparyan, K. I., Kakhidze, N. G., Konovalenko, B. M. Influence of donor impurities on kinetics of radiation defect annealing in germanium. *Fizika i tekhnol. polupr.*, 1973, 7, 7, pp. 1377-1381 (in Russian).
40. Vavilov, V. S., Glazman, V. B., Isaev, N. U., Mukashev, B. N., Spitsin, A. V. Influence of irradiation temperature and doping impurity type on processes of defect formation in electron irradiated *n*-type silicon. *Fizika i tekhnol. polupr.*, 1974, 8, 3, pp. 471-475 (in Russian).
41. Hirata, M., Hirata, M., Saito, H. *The interactions of point defects with impurities in silicon. J. Phys. Soc. Japan*, 1969, **27**, 2, pp. 405-414.
42. Vavilov, V. S., Uvarov, Ye. F., Chukichev, M. V. Dependence of radiation defect formation rate on concentration of phosphorus in silicon samples irradiated with factor neutrons. *Fizika i tekhnol. polupr.*, 1969, **3**, 12, pp. 1838-1843 (in Russian).
43. Dzhafarov, T. D. Neutron-irradiation-induced defects in silicon containing oxygen and carbon impurities. *Fizika i tekhnol. polupr.*, 1971, 5, 4, pp. 787-789 (in Russian).
44. Kholodar', G. A., Dankovsky, Yu. V., Konoplyanyi, V. V., Vinetsky, V. L. Non-direct recombination of vacancies and interstitials in irradiated silicon. *Fizika i tekhnol. polupr.*, 1976, **10**, 9, pp. 1712-1718 (in Russian).
45. Bean, A. R., Newman, R. C., Smith, R. S. Electron irradiation damage in silicon containing carbon and oxygen. *J. Phys. Chem. Sol.*, 1970, **31** 4, pp. 739-745.
46. Mashovets, T. V. Point defects in germanium: reliable and questionable. In: *Radiation Effects in Semiconductors. Conf. Ser. No. 31*, Inst. of Phys. Bristol-London, 1976, pp. 30-44.
47. Zhevno, A. N., Stelmakh, V. F., Tkachev, V. D., Urenev, V. I. On the vacancy-donor complexes in silicon and germanium. In: *Radiation Defects in Semiconductors.* Minsk, Belorussian State University, 1972, p. 55 (in Russian).
48. Abdurakhmanova, S. N., Dostkhodzhaev, T., Mashovets, T. V. On the influence of group V doping impurity type on annealing of gamma radiation damage in germanium. *Fizika i tekhnol. polupr.*, 1973, **7**, 9, pp. 1839-1841 (in Russian).
49. Boltaks, B. I. *Diffusion and Point Defects in Semiconductors.* Leningrad, Nauka, 1972, 384 pages (in Russian).
50. Bakhadyrkhanov, M. K., Zainobidinov, S., Teshabayev, A. T. Interactions of atoms of deep impurities with radiation defects in gamma irradiated silicon. *Fizika i tekhnol. polupr.*, 1977, **11**, 2, pp. 285-289 (in Russian).
51. Goncharov, L. A., Dosthodzhayev, T. N., Yemtsev, V. V., Mashovets, T. V., Ryvkin, C. M. Group II impurities in germanium and their participation and radiation defect formation. *Fizika i tekhnol. polupr.*, 1977, **11**, 5, pp. 945-950 (in Russian).

52. Tkachev, V. D., Plotnikov, A. F., Vavilov, V. S. On the photoconductivity spectra of *n*-type silicon irradiated with fast electrons. *Fiz. tverd. tela*, 1963, 5, 7, pp. 1827-1829 (in Russian).
53. Tkachev, V. D. A Study of formation of stable radiation damage in silicon. In: *Radiation Physics of Non-Metallic Crystals*. Kiev, Naukova dumka, 1967, pp. 112-118 (in Russian).
54. Woodbary, H. H., Ludwig, G. W. Vacancy interactions in silicon. *Phys. Rev. Letters*, 1960, 5, 3, pp. 96-97.
55. Berman, L. S., Shuman, V. B. A Study of the influence of gamma radiation on diffused silicon diodes containing gold. *Fizika i tekhnol. polupr.*, 1976, 10, 12, pp. 2389-2390 (in Russian).
56. Drigo, E. D., Safronov, L. N., Smirnov, L. S. A role of impurity atmospheres in radiative recombination at dislocations in germanium. *Fizika i tekhnol. polupr.*, 1972, 6, 9, pp. 1787-1790 (in Russian).
57. Zolotukhin, A. A., Kovalenko, A. K., Meshcheryakova, T. M., Milevsky, L. S., Pagava, T. A. On the influence of irradiation intensity on radiation damage in silicon. *Fizika i tekhnol. polupr.*, 1975, 9, 6, pp. 1201-1202 (in Russian).
58. Zolotukhin, A. A., Milevsky, L. S. Influence of fast electron irradiation on state of iron precipitates at dislocations in silicon. *Fizika i tekhnol. polupr.*, 1972, 6, 11, pp. 2240-2242 (in Russian).
59. Kaiser, W., Frish, H. L., Reiss, H. Mechanism of the formation of donor states in heat-treated silicon. *Phys. Rev.*, 1958, 112, 5, pp. 1546-1554.
60. Panov, V. I., Smirnov, L. S., Tishkovsky, E. G. On the interaction of heat- and radiation-induced defects in silicon. *Fizika i tekhnol. polupr.*, 1975, 9, 8, pp. 1580-1583 (in Russian).
61. Vologdin, E. N., Zhukova, G. A., Mordkovich, V. N. Low-energy charged particle irradiation of silicon coated with oxide film. *Fizika i tekhnol. polupr.*, 1972, 6, 7, pp. 1306-1310 (in Russian).
62. Akhmetov, V. D., Bolotov, V. V., Vasilyev, A. V., Karpov, Yu. A., Shakhovtsov, V. I., Shindich, V. L. On the formation of radiation defects in silicon containing gadolinium. *Fizika i tekhnol. polupr.*, 1977, 11, 11, pp. 2243-2245 (in Russian).
63. Lenchenko, V. M. On the activation of displacements at relaxation of electronic excited states in solids. *Fiz. tverd. tela*, 1969, 11, 3, pp. 799-801 (in Russian).
64. Lenchenko, V. M. Activation of quasi-chemical processes in solids by nuclear irradiation. In: *Physico-chemical Problems of Solids*, Krasnoyarsk, 1975, pp. 3-32 (in Russian).
65. Gerasimenko, N. N., Dvurechensky, A. V., Panov, V. I., Smirnov, L. S. On the threshold energy of radiation defect formation in semiconductors. *Fizika i tekhnol. polupr.*, 1971, 5, 8, pp. 1644-1646 (in Russian).
66. Bolotov, V. V., Vasilyev, A. V., Smirnov, L. S. On the migration energy of elementary defects in germanium and silicon. *Fizika i tekhnol. polupr.*, 1974, 8, 3, pp. 518-521 (in Russian).
67. Makarevich, A. I., Raines, L. Yu., Kurilovich, N. F. A study of introduction of deep states in *n*-type silicon at intra-reactor irradiation. In: *Radiation Physics of Non-metallic Crystals*, Kiev, Naukova dumka, 1967, pp. 122-126 (in Russian).
68. Milevsky, L. S., Pagava, T. A. Influence of irradiation temperature on kinetics of formation and annealing of radiation defects. In: *Study of Space Materials and Technology*, Moscow, Nauka, 1977, pp. 103-111 (in Russian).
69. Milevsky, L. S., Pagava, T. A. Influence of Fermi energy on efficiency of radiation defect formation in electron irradiated silicon. *Fizika i tekhnol. polupr.*, 1976, 10, 7, pp. 1287-1291 (in Russian).

70. Bolotov, V. V., Vasilyev, A. V., Kashnikov, B. P., Smirnov, L. S. A role of temperature in changing complex formation rate in irradiated crystals. *Fizika i tekhnol. polupr.*, 1975, **9**, 4, pp. 813-814 (in Russian).
71. Gres'kov, I. M., Solovyev, S. P., Kharchenko, V. A. A dependence of some changes of electrophysical properties and microstructure of silicon on irradiation conditions and properties of original crystal. In: *Radiation Effects in Silicon*. Kiev, 1976, pp. 26-27 (in Russian).
72. Bolotov, V. V., Vasilyev, A. V., Smirnov, L. S. Formation of defects in silicon at increased irradiation temperatures. *Fizika i tekhnol. polupr.*, 1976, **10**, 9, pp. 1670-1674 (in Russian).
73. Bolotov, V. V., Vasilyev, A. V., Kashnikov, B. P., Smagulova, S. A., Smirnov, L. S. Formation of defects in germanium increased irradiation temperatures. *Fizika i tekhnol. polupr.*, 1976, **10**, 1, pp. 81-88 (in Russian).
74. Pchelyakov, O. P., Aseev, A. L., Smirnov, L. S., Stenin, S. I. High-temperature radiation effects in germanium irradiated in high-voltage electronic microscope. *Fizika i tekhnol. polupr.*, 1976, **10**, 8, pp. 1472-1479 (in Russian).
75. Hrostowski, H. J., Kaiser, R. H. Infrared spectra of heat treatment centers in silicon. *Phys. Rev. Lett.*, 1958, **1**, 6, pp. 199-200 (in Russian).
76. Bullough R., Newman, R. Kinetics of point defects migration to dislocations. Rep. Prog. Phys., 33, **2**, 101, 1970.
77. Smirnov, L. S., Stas', V. F., Khainovskaya, V. V. Irradiation and annealing of germanium crystals with high dislocation density. *Fizika i tekhnol. polupr.*, 1969, **3**, 12, pp. 1760-1765 (in Russian).
78. Bolotov, V. V., Vasilyev, A. V., Smagulova, S. A. Electron irradiation and annealing of Ge ⟨Si⟩ alloy. *Fizika i tekhnol. polupr.*, 1976, **10**, 10, pp. 1981-1983 (in Russian).
79. Reznikov, R. S., Seldyakov, Yu. P. *Industrial Semiconductor Detectors*. Moscow, Atomizdat, 1975, 87 pages (in Russian).
80. Nemets, O. F., Gofman, Yu. V. *Nuclear Physics Handbook*. Kiev, Naukova dumka, 1975, 414 pages (in Russian).

CHAPTER 3

RADIATION-ENHANCED DIFFUSION (RED)

Sec. 3.1. General Information

The problems of impurity diffusion control with the aid of particle irradiation attract attention of many researchers. The study of the radiation-enhanced diffusion (RED) helps us to have a better insight into the real crystals and physical processes occurring therein and is important for solution of many a practical task. The experimental evidence on RED shows that in comparison with the "ordinary" thermal diffusion it possesses a number of important features that include:

(1) a significant decrease in the temperature of introduction of impurities, the main operation in fabrication of any semiconductor device;

(2) feasibility of obtaining "unusual" impurity distribution profiles in one step, i.e., of obtaining reverse distribution gradients, extra sharp profiles, distribution profiles with two peaks, etc.;

(3) conducting diffusion in localized areas of the crystal.

The RED effects (acceleration or deceleration of diffusion, change of the impurity distribution profile, etc.) result from a change in the speed of interactions between the impurities and defects during ionization and production of defects. Such effects are discovered in experiments, such as:

(1) implantation of an impurity at room temperature, followed by a high-temperature annealing;

(2) implantation at high temperatures;

(3) creation of the doping impurity profile (by thermal diffusion or implantation with subsequent annealing), followed by irradiation with elementary particles (protons, non-doping impurity ions, electrons, neutrons, gamma-rays, etc.) at room temperature with subsequent annealing, or irradiation concurrent with heating;

(4) bombardment with non-doping impurity ions (formation of a disordered or amorphous layer at a sufficient depth in the crystal) with a subsequent diffusion of the doping impurity (oxide, polycrystal, sputtered or implanted layer);

(5) irradiation with elementary particles of a crystal having a doping impurity layer on the surface and a subsequent heating.

The diversity of the data yielded by the above experiments has given rise to a great variety of models of the physical processes

attendant with RED. Such models may be grouped into two classes), namely, the models of the processes involved (1) in the defect-forming irradiation and (2) in the non-defect-forming irradiation. In the latter case, the radiation effects are attributed to an ionization occurring in the crystal, particularly, to the influence of the charge state on the migration energy of the impurity atom or defect (see, for example, [1-4]). A fairly large material [5-13] is dedicated to studying the influence of an ionizing radiation (light, X-rays, etc.) on the diffusion of various impurities in the crystals. At present, however, there is still no widely accepted theory explaining the conditions under which the ionization effects involved in RED completely reveal themselves. The experimental evidence is often irreproducible (see, for example, [5-11] and [14-16]) and we shall not discuss it in this book which is devoted to the technological problems. Extensive reviews of the field, including the suggested mechanisms explaining the dominating influence of ionization upon diffusion are found in [14, 17, 45].

In contrast to the above, outstanding (and reproducible at that) results have been achieved from investigation of the diffusion in the presence of radiation defects. The influence of the defect-generating beam on the diffusion of impurities is normally attribut d to either an increased concentration of vacancies [30, 31, 36, 37] or to the migration of the impurity atoms from one interstitial site to another [61, 64]. Yet, some investigators argue (see Sec. 3.2) that the diversity of the results obtained from experiments on RED often cannot fit such simple ideas. At present, there is no consensus among the investigators on RED and on diffusion in general [18, 19, 20].

Earlier the RED of phosphorus and other impurities in silicon was interpreted [24] to involve vacancies which were presumed to stick to the atoms of oxygen before approaching the atom of phosphorus. This allowed the author of [24] to avoid contradictions in explaining the results of his experiments (see Sec. 3.2). This work did not receive, however, further development, since little information seemed to exist at that time (1963) on formation of defect complexes and presence of uncontrollable impurities. In 1974, the general theory of the RED-dependent diffusion in the crystals was developed proceeding from the assumption that the formation of defect complexes was vital to real semiconductors.

Proceeding from the radiation physics data available, particularly, from the fact of a high mobility of the vacancies and interstitials [2, 22], the authors of [21] have assumed the migration energy of impurities and other defects to be low, and the low values of the observed diffusion coefficients to be associated with the capture of the diffusing particles by the traps always present in the real crystals. Any defects, both point and more complex ones, may act as traps for such particles. Specifically, the traps may be furnished by the

atoms of inactive impurities present in large quantities in the original crystals (see Ch. 1, Tables 1.3 and 1.4) and by their association with one another and with other defects. Thus, the migration speed is mainly limited by the formation of the complexes of the diffusing impurity with the traps and by the eventual dissociation of the complexes. The transition of an impurity or a host crystal atom from the interstitial to the regular site and vice versa is an example of formation or dissociation of the complex. In the model under consideration, the impurity atoms migrate either via the interstitial sites of the lattice (in this case, the vacancy is one of the most efficient traps) or via vacancies (then the diffusion speed depends on the trapping of vacancies and their subsequent liberation). The processes involved in the complexing are characterized by the energy and associated parameters (the complexing barrier and bond energy) depending on the charge state of the reacting defects (for details, see [18, 21]). Hence the effect of ionization. From [21] it transpires that with great concentrations of traps of several types, the effective coefficient of diffusion of an impurity via, say, interstitial sites is given by

$$D^{\text{eff}} = D_J/(1+\sum_{i=1}^{n} \varkappa_i N_{ti}) \tag{3.1}$$

where $D_j = D_0 \exp(-E_m/kT)$; $\varkappa_i = \beta_i \exp[(E_{bi} - E_{ci} - E_m)/kT]$; $\beta_i = a_{0i}\sigma_{0i}$ $(i = 1, 2, \ldots, n)$; N_{ti} is a concentration of traps of the ith type; E_m is the migration energy of the atom of a diffusion impurity (without adhesion); E_{ci} is the barrier energy of formation of a complex of the diffusing atom with a trap of the ith type; E_{bi} is the kinetic energy (see [21]) that binds the defects together in a complex (i.e., bond energy).

If we present (3.1) in the form of the well known Arrhenius equation

$$D^{\text{eff}} = D_0^{\text{eff}} \exp(-E_A/kT), \tag{3.2}$$

then from juxtaposition of (3.2) with (3.1), we can derive expressions for E_A and D_0^{eff}:

$$E_A = E_m + \left\{\sum_{i=1}^{n} (E_{bi} - E_{ci} - E_m) A_i\right\} \Big/ (1+\sum_{i=1}^{n} A_i) \tag{3.3}$$

$$D_0^{\text{eff}} = [D_0/(1+\sum_{i=1}^{n} A_i)] \exp\left\{(1+ \right.$$

$$\left. +\sum_{i=1}^{n} A_i)^{-1} \sum_{i=1}^{n} A_i (E_{bi} - E_{ci} - E_m)/kT\right\} \tag{3.4}$$

where

$$A_i \equiv \beta_i N_{ti} \exp[(E_{bi} - E_{ci} - E_m)/kT],$$

from which it becomes obvious that both the diffusion activation energy, E_A, and the preexponential factor, $D_0^{ef_1}$, have a complex relationship to the concentrations and energy parameters of the diffusing impurity traps.

Still earlier [23] it was thought that the diffusion activation energy had the form

$$E_A = E_m^{\text{eff}} + E_b^{\text{eff}} + E_c^{\text{eff}} \tag{3.5}$$

Juxtaposition of (3.5) and (3.3) gives

$$E_m^{\text{eff}} = E_m/(1 + \sum_{i=1}^{n} A_i)\,; \tag{3.6}$$

$$E_b^{\text{eff}} = (1 + \sum_{i=1}^{n} A_i)^{-1} \sum_{i=1}^{n} A_i E_{bi} \tag{3.7}$$

$$E_c^{\text{eff}} = -(1 + \sum_{i=1}^{n} A_i)^{-1} \sum_{i=1}^{n} A_i E_{ci} \tag{3.8}$$

In the specific case of adhesion of the diffusing impurity to the traps of one type, expressions (3.3) and (3.4) are considerably simplified. With a strong adhesion ($A \gg 1$), the diffusion factor takes the form

$$D = (D_0/\beta N_t) \exp\,[-(E_b - E_c)/kT], \tag{3.9}$$

from which it is evident that the diffusion activation energy depends on the complex formation parameters only, while the pre-exponential factor depends on the number (N_t) and properties (β) of the traps. For strong adhesion ($A = \beta N_t \exp\,[(E_b - E_c - E_m)]/kT \gg 1$), it is required that the concentration of traps be increased and the temperature decreased, and the bond energy of the diffusing impurity at the trap be decreased as well. On the contrary, weak adhesion ($A \ll 1$) does not seem to find its realization in practice. Indeed, assuming that $N_t \simeq 10^{18}$ cm^{-3} (which corresponds to the amount of "uncontrollable" impurities in the initial material, say, in silicon, and is way below the concentration of defects in the implanted layer), $a_0 \simeq 10^{-8}$ cm, $\sigma_0 \simeq 10^{-15}$ cm^2, we arrive at $A > 1$, if

$$E_b - E_c - E_m > 10\ kT \tag{3.10}$$

Under the real assumption of $E_b - E_c - E_m \gtrsim 1$ eV [18], condition (3.10) is satisfied practically for all temperatures used in studies of RED.

The above described situation with impurities diffusing via interstitial sites uses the model suggested in [21]. A similar approach may be used for treatment of the diffusion of vacancies, whereby the vacancies are assumed to adhere to the traps, or some other situations (see [21] for details) occurring in RED experimental studies.

The presented theories offer a satisfactory explanation of many peculiarities involved in the diffusion of impurities and defects and may be successfully applied to radiation-assisted diffusion control. On the one hand, new traps are generated, in the course of irradiation, for the diffusing impurity and on the other hand, the old traps that existed in the initial crystal or implanted layer get "clogged up". This latter effect is caused either by formation of complexes of radiation defects with traps, which results in the emergence of associations exhibiting low efficiency in trapping the atoms of diffusing impurities, or by a decrease in the efficiency of the traps due to a change in their energy parameters on ionization. The competition between said processes results, depending on the conditions of the experiment (the type of the original profile, energy and kind of irradiation, etc.), in a total increase or decrease in the efficiency of adhesion and, consequently, acceleration or deceleration of the diffusion.

Let us note that the diffusion coefficient, given by (3.1), represents in the general case a complex function of the distance between the surface and any point deep inside the crystal. This complexity is attributed to the irregularity of the depth distribution of impurities and defects (traps) in, say, an implanted layer and to the irregularity of generation of defects during irradiation.

A change in the irradiation or annealing temperature results in changing the type of traps dominating the adhesion process, while a change in the irradiation intensity brings about a change in the efficiency of the traps (the values of E_b and E_c). When the temperatures are not very high, the adhesion is strong even with a small concentration of traps. As a consequence, it has been experimentally proved that no RED is observed below a certain "threshold" temperature and dose of irradiation. The combined action of many types of traps may result in little dependence of RED on the irradiation temperature, which has also been observed by some experimenters (see Sec. 3.2).

A similar approach may be used for explanation of many other peculiarities involved in RED experiments. So far no sufficient information has been accumulated to allow a detailed interpretation of the available experimental evidence. We shall, therefore, be content with the summary of the most prominent effects (see Sec. 3.2) yielded by RED investigations and will present the interpretations thereof given by the authors, although they do not always give adequate explanations of the results of the experiments.

We believe that the model described in [21] supplies a reliable basis to further the understanding of the processes involved in the diffusion of impurities and interactions of these with the defects generated by irradiation. In our opinion, this model can serve as a prototype for creation of diffusion control techniques with the help of the ionizing and defect forming irradiation (see Sec. 3.3).

Sec. 3.2. Experimental Studies of RED in Semiconductors

One of the first analyses of the RED mechanisms is described in [25]. A *p-n* junction was formed at a depth of 6 μm by diffusion of Ga in *n*-Si. A subsequent 275-keV proton irradiation ($R_p = 3$ μm) over a temperature range of 900 to 1100 °C gave rise to a significant displacement of the *p-n* junction in irradiated sections of the sample. In [25], this effect is attributed to an increase in the number of vacancies upon irradiation.

The authors of [26] investigated an acceleration of boron diffusion in Si irradiated with a proton beam over a temperature range of 500 to 700 °C. As a preliminary step, a *p-n* junction has been created on the substrate at a depth of 0.06 μm via a thermal diffusion of boron. An intriguing relationship between the boron profile and the energy of protons has been discovered (see Fig. 3.1): at $E = 10$ keV, the line suddenly stops at a certain depth, while at $E = 50$ keV, the profiles appear with "tails". Diffusion acceleration does not depend on T_{irrad} over the range under study. For interpretation of the results, the authors of [26] used the theory which explains RED as a process occurring via vacancies.

The authors of [27] used an isotope technique to observe an acceleration of Sb diffusion in *n*- and *p*-type silicon samples under the action of ions of He ($E = 55$ keV, $\Phi = 1.25 \cdot 10^{17}$ cm^{-2}).

It happened that the profile of an Sb concentration in the samples irradiated and annealed at 950 or 1100 °C extended further than in non-irradiated samples and had a typical "tail". The effect was more pronounced for *p*-Si. At an annealing temperature of 950 °C, the effect of irradiation shows more clearly than at 1100 °C. The authors of [27] have attributed the results thus obtained to Sb diffusion via interstitial sites.

Some papers [28, 29] have been devoted to a study of RED of the atoms of antimony and phosphorus in silicon under the action of proton irradiation at 900 °C, the proton energy being 150 to 450 keV

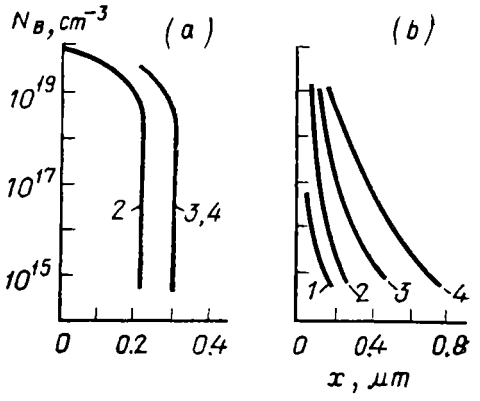

Fig. 3.1. Boron profiles in proton irradiated silicon [26].
Proton energy, keV: *a*—10 ($R_p = 0.15$ μm); *b*—50 ($R_p = 0.5$ μm). Irradiation time, min: *1*—15; *2*—30; *3*—60; *4*—120; T_{irrad} = 700 °C; $I = (3\text{-}7) \cdot 10^{11}$ cm$^{-2} \cdot$s^{-1}

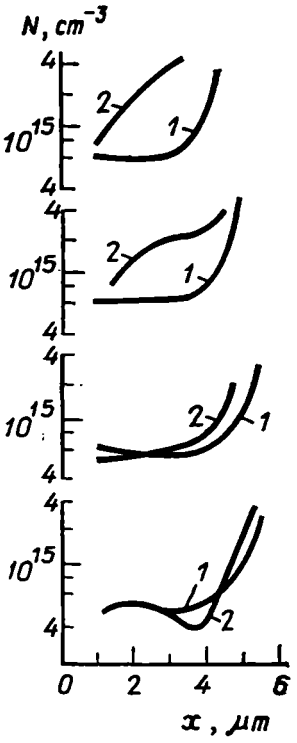

Fig. 3.2. Phosphorus profiles in silicon epitaxial films having different thickness [29].

1—before irradiation; *2*—after irradiation. The irradiation is by protons at 450 keV; current density, about 30 μA/cm²; irradiation time, 40 min; T_{irrad} = 900 °C

and current density, 6 to 30 μA/cm². The experiments have been conducted on diffusion-preshaped impurity profiles and on epitaxial structures (an *n*-epitaxial layer built up of arsenic to a concentration of $5\text{-}7 \cdot 10^{14}$ cm^{-3} on a substrate heavily doped by phosphorus or antimony with about 10^{17} cm^{-3} of phosphorus and about 10^{19} cm^{-3} of antimony). In the latter case, the experimenters registered an effect of pulling the doping impurity from the substrate into the proton-damaged area of the epitaxial layer. The concentration profiles have been determined using the Schottky barrier *C-V* characteristics. The obtained results have been analyzed on the basis of the vacancy model under the assumption that the diffusion coefficient changes with depth along a Gaussian curve, depending on the generation of radiation defects. The shape of the impurity profile at RED was determined from the values of R_p, the thickness of the epitaxial layer or the depth of the initial profile (Fig. 3.2). Some workers observed a slight increase in the diffusion coefficient of phosphorus at RED, depending on the intensity of proton irradiation (Fig. 3.3). For antimony, the calculations [28] have shown clearly defined distinctions between the diffusion parameters under study for the diffusion profiles and epitaxial structures. All this information has prompted a conclusion [28] that with an impurity diffusion enhanced with proton irradiation the usual diffusion theory that takes into account surplus vacancies does not provide a satisfactory interpretation of the experimental data.

Some workers [30] investigated the RED of atoms of phosphorus in germanium and boron in silicon when irradiated with protons or molecules of H_2 at 500 to 800 °C. The initial profiles of boron and phosphorus have been shaped by thermal diffusion (boron in *n*-Si; layer thickness, 0.05 to 0.12 μm) and by ion bombardment (phosphorus in *p*-Ge, $E = 25$ keV, $T_{irrad} = 580$ °C, $\Phi = 4 \cdot 10^{14}$ cm^{-2}). The profiles of distribution of an electrically

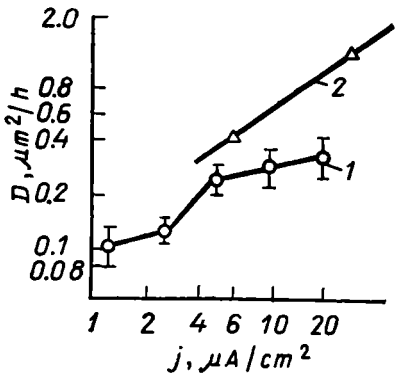

Fig. 3.3. Phosphorus diffusion coefficient vs proton irradiation intensity [29].
1—diffusion layers; proton energy, 150 keV; T_{irrad} = 900 °C; *2*—epitaxial films; proton energy, 450 keV; T_{irrad} = 900 °C. The irradiation dose is constant

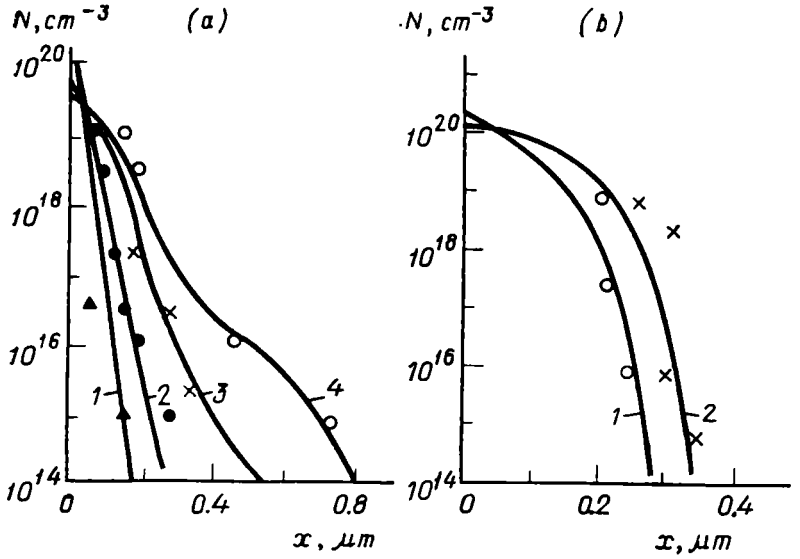

Fig. 3.4. Boron concentration profile in silicon [30].
a—50-keV proton bombardment; proton current density j = 80 mA/cm²; T_{irrad} = 600 °C. The original profile has been produced by thermal diffusion, Xj = 0.05 μm. Irradiation time, min: *1*—15, *2*—30, *3*—60, *4*—120; *b*—15-keV proton bombardment; proton current density j = 38 mA/cm²; T_{irrad} = 600 °C, R_p = 0.27 μm. Irradiation time, min: *1*—30, *2*—60. The dots denote the experimental results, the solid curves, the theoretical assumptions

active impurity and the depth of the *p-n* junction, X_j, were measured.

In [30], like in [28, 29, 31, 32 and 37], it was shown that the shape of the resultant profile depended on several parameters, such as the vacancy diffusion path, L_D, the value of R_p, and the initial profile depth, (x). When $R_p \leqslant x$, the profile has a stepped shape, while with $R_p > x$, the depth distribution of the impurity registers "tails" (Fig. 3.4*a*, *b*-Fig. 3.5). The values of diffusion coefficients at RED were 3.5 orders of magnitude as great as the value of thermal diffusion coefficient of phosphorus in germanium and 5 orders of magnitude as great as the value of the thermal diffusion coefficient of boron in silicon.

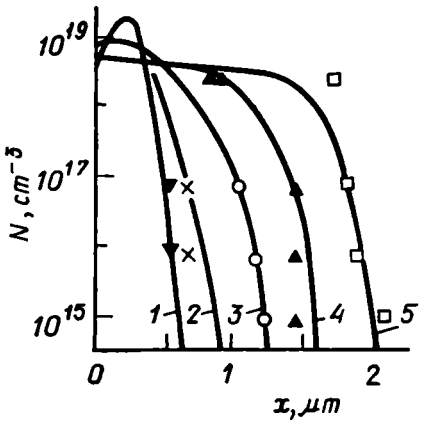

Fig. 3.5. Phosphorus concentration profile in germanium [30].
Irradiation time, min: *1*—0, *2*—1, *3*—6, *4*—30, *5*—150. Bombardment is by 70-keV protons; proton current density $j = 40$ mA/cm², $T_{irrad} = 580$ °C. The original profile has been produced by phosphorus ion implantation ($E = 25$ keV, $\Phi = 4 \cdot 10^{14}$ cm^{-2}, $T_{irrad} = 580$ °C). The dots denote the results of experiment, the solid curves, the theoretical assumptions

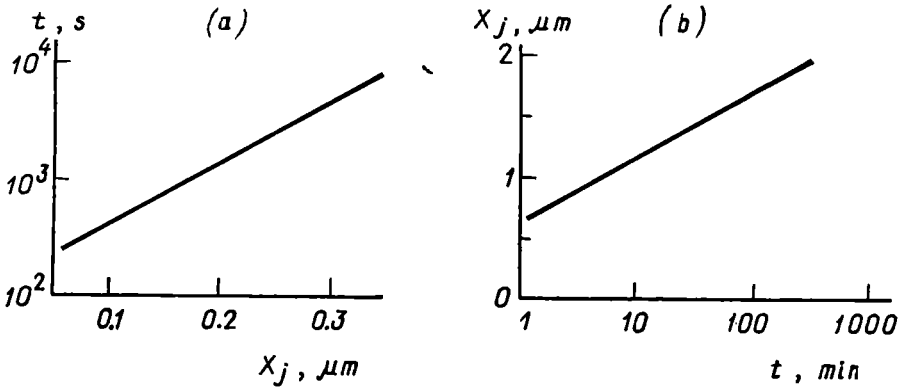

Fig. 3.6. Depth of *p-n* junction in (a) silicon and (b) germanium vs proton irradiation time [30].
The irradiation parameters are the same as indicated in Fig. 3.5

Comparison of the experimental data with the theory based on the assumption of a vacancy-enhanced diffusion of impurities and space-dependent diffusion coefficient, $D(x)$, allowed an experimental evaluation of L_D that proved to be equal to 0.086 μm in Si (independent of T_{irrad} over a range of 500 to 700 °C) and 0.24 to 0.3 μm in Ge. A disagreement between the magnitude of L_D and data obtained by the authors of [32] is explained by the authors of [30] by a different range of the proton beam intensities employed. It should be noted that the quantity L_D that forms part of the vacancy-type RED models is an effective one. It depends on the irradiation conditions, material prehistory (i.e., the prehistory of the material where diffusion has occurred) and on the kind of diffusing impurity. The experiments revealed a dependence of the diffusion enhancement rate upon the irradiation dose (see Fig. 3.6*a*, *b*).

There is an extensive review [32] that analyzes the RED results in semiconductors. The authors proceed from the traditional model in which the vacancies are treated as an agent enhancing impurity diffusion, particularly, in silicon irradiated with a proton beam.

According to this model, it has been established [31, 32] that at $R_p < x$ the form of the profile is dictated by the space-dependent variable $D(x)$ which has the maximum value at $x = R_p$; with an increase in x ($x > R_p$), the number of surplus defects drastically decreases thereby decreasing $D(x)$.

In case $R_p > x$, the number of non-equilibrium vacancies slightly changes with depth, while $D(x)$ remains practically constant (it is assumed that D is independent of the impurity content). In such an event, the impurity profile has the shape typical for the thermal diffusion but with a high diffusion coefficient. Likewise, the impurity distribution should change as the diffusion is accelerated by an irradiation producing a regular distribution of defects in depth, say, by electron irradiation. In [32], it is noted that the values of L_D obtained by various workers from RED experiments reside within 0.1 to 3 μm, which may be attributed to both different defect inventories of the samples and to different techniques of experiment and interpretation of the results.

The RED effects have been observed in Si for the atoms of boron, phosphorus, gallium, and antimony at T_{irrad} of about 700 to 1000 °C [32], beginning from a certain crytical temperature, T_{irrad} of about 800 °C (depending on the proton irradiation density), the irradiation temperature no longer affecting the RED. The diffusion coefficients for boron, gallium, phosphorus and antimony at RED in Si ranged from 10^{-11} to 10^{-12} cm^2/s [32].

An exacting investigation of boron profiles in silicon by the mass spectroscopy of secondary ions [31, 32] resulting from RED induced by proton beam irradiation ($R_p < x$) has revealed a dip in the B concentration in the region of R_p and its rise beyond R_p. The authors of the above papers give a calculated model interpreting the obtained results to involve an assumed displacement of boron into interstitial sites by interstitial atoms of silicon (at $x \simeq R_p$), their fast migration from the area of damage and subsequent dissolution of boron at regular lattice sites (see Fig. 3.7).

The results presented in [31] and [32] are indicative of the participation in RED of vacancies, host crystal atoms, impurity-interstitials, and defect complexes, which attests to the diversity and complexity of the RED mechanisms. An attempt at establishing the area of domination of a particular mechanism is given in [31, 32], which singles out, depending on the intensity and temperature of proton irradiation, the following areas: (1) the area with a strong beam intensity and low T_{irrad} where the interstitial content is great and the mechanism associated with migration of impurity interstitials from the damage region is the dominating one, (2) the area with a low beam intensity and high T_{irrad} where the vacancy mechanism dominates and (3) the area with medium beam intensity and T_{irrad}, where both mechanisms are effective.

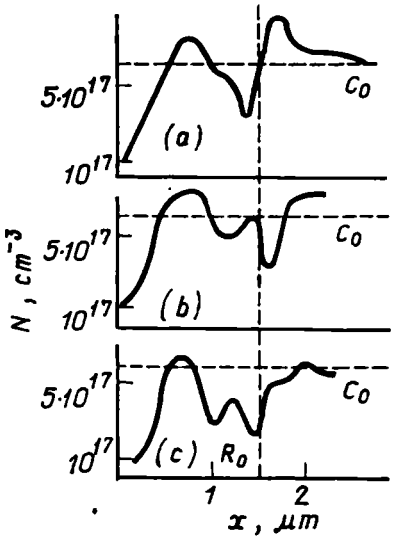

Fig. 3.7. Boron distribution profile after 150-keV proton irradiation at 850 °C [31, 32].

Proton irradiation dose, cm^{-2}: *a*—$1 \cdot 10^{17}$; *b*—$2 \cdot 10^{17}$; *c*—$4 \cdot 10^{17}$. The original boron concentration $N_B = 6 \cdot 10^{17}$ cm^{-3} (homogeneous throughout the sample)

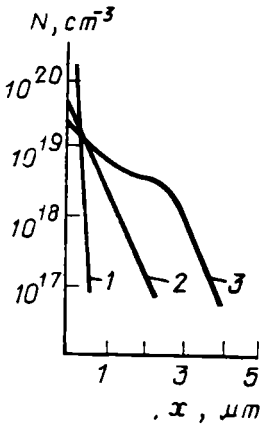

Fig. 3.8. Carrier concentration profiles with proton-enhanced diffusion of P in Si [33].

1—annealing for one hour at 900 °C (without irradiation). H_2^+ ion irradiation (T_{irrad} = 900 °C, $j = 4$ μA/cm², T_{irrad} = 1 h) with energy E, MeV: *2*—1 ($R_p \approx 6$ μm), *3*—0.5 ($R_p \approx 2.5$ μm)

The authors of [33] used H ions for high-temperature irradiation of *p*-type silicon samples (КДБ-10) first doped with ions of phosphorus ($E = 100$ keV, $\Phi = 5 \cdot 10^{15}$ cm^{-2}). The results thus obtained they interpret (Fig. 3.8) as involving an acceleration of diffusion of the impurity due to its interaction with radiation defects. One also has to make an assumption of a considerable amount of point defects produced by hydrogen ion bombardment even far off the region with the maximum number of elastic collisions.

The enhanced diffusion of the atoms of antimony in *p*-type germanium, caused by a beam of protons having an energy of 400 keV to 1.5 MeV, has been described in [34]. The experiments conducted over a temperature range of 500 to 700°C have revealed a rise in the RED effect with an increase in the irradiation temperature ($T_{irrad} <$ < 600 °C). According to the author of [34], the length of the vacancy diffusion path, the diffusion activation energy and the concentration of sinks for the vacancies are about 0.3 μm, about 1 eV and 10^{15} cm^{-3}, respectively. Like [72], [34] contains an assumption of a difference

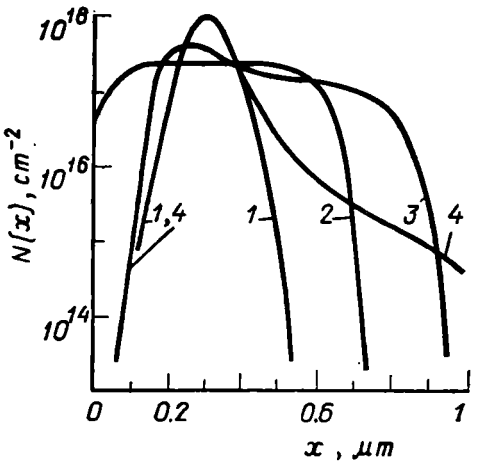

Fig. 3.9. Calculated concentration profiles of As in Si with proton-enhanced diffusion (after [37]).
Irradiation time, min: *1*—0; *2-4*—60. Proton energy, keV: *2*—20; *3*—40; *4*—60. Implantation of As ions at E=580 keV, then irradiation with protons (T_{irrad} = 600 °C, j = 1 μA/cm²)

between the processes involved in the generation of the secondary defects at RED in the high and low irradiation temperatures and, with some reservations, of a possible interaction between diffusing vacancies and various impurities.

The diffusion enhancement theory utilizing the vacancy mechanism, as in [30, 31, 32] and [66], is also described in [37]. For comparison, an experiment was conducted (implantation of As ions in silicon at E = 580 keV, followed by proton bombardment at 600 °C at E = 15 keV and j = 0.64 μA/cm²) that yielded a value of L_D equal to 0.053 μm. Simulation of the vacancy-dependent diffusion enhancement mechanism with the aid of a computer has shown that the form of the profile registers a marked change with a change in the proton energy (Fig. 3.9).

The radiation enhanced diffusion of an impurity in semiconductors is also observed at a uniform rate of generation of radiation defects, particularly, during electron, neutron or gamma irradiation (see, for example, [23, 33, 46]). The effect of electron irradiation upon the diffusion of boron in silicon has been studied in [35]. In КЭФ-7,5 samples, boron was diffused at 1000 to 1200 °C with the result that *p-n*-junctions 0.3 to 110 μm deep were produced, following which the samples were irradiated with 3.2 MeV (pulsed beam) or 1.8 MeV electrons (steady beam) at room temperature. Upon irradiation, the samples were annealed at 700 °C during 30 min. The electrical measurements taken at successive removal of the sample layers were used in determining the concentration of boron in the regular sites (depth distribution).

The results of the work done by the authors of [35] can be summarized as follows.

1. The diffusion is only promoted when the electron beam is directed to decrease the boron concentration.

2. The enhancement is the greater, the deeper the original *p-n*-junction is located (j = 1 μA/cm², $\Phi = 10^{17}$ cm^{-2}), μm:

X_j	ΔX_j	X_j	ΔX_j
105	11 ± 1	6	0.16 ± 0.02
85	8 ± 1	1.1	0.037 ± 0.003
		0.3	0 ± 0.003

3. There was no difference observed in the nature of action of the pulsed and steady beams.

The results were interpreted [35] to involve an increase, upon irradiation, of the interstitial boron that is carried along the beam by the "wind" of lattice vibrations excited by the electrons.

The authors of [48] observed a RED of rhodium and gold when they investigated the Schottky diodes gamma irradiated from a Co^{60} source. The diffusion coefficient of these impurities under RED conditions amounted to about $2.3 \cdot 10^{-14}$ cm^2/s. No RED of the atoms of indium was ever observed in similar experiments.

The RED effects have also been observed in annealed layers upon ion implantation [38 through 47, 49, 50]. These effects are normally related both to presence of a great number of defects and, very often, to an abnormal position of the implanted impurity in the lattice.

F. N. Schwettmann [38] investigated the depth distribution of electrically active arsenic in silicon upon implantation at room temperature and subsequent annealing. The results obtained are presented in Fig. 3.10. They can be interpreted as follows.

1. The profiles exhibit exponential "tails". The slope of the exponential curve does not depend on the irradiation dose (the doses used ranged from 10^{13} to 10^{16} cm^{-2} and included the amorphization dose of $2 \cdot 10^{14}$ cm^{-2}). Neither it depends on the energy of the ions (the energy ranged from 60 to 210 keV). The slope does not change even with the implantation performed through an oxide film of 200 to 600 Å thick.

2. The profile form does not change with the annealing temperature ranging from 725 to 1000 °C.

3. If the layer containing the maximum amount of implanted impurity has been removed prior to annealing, the annealing (performed under the same conditions) gives rise to a "tail" resembling the one observed during annealing in the presence of the high concentration region. From this fact it was inferred that the "tails" were formed in the course of implantation, not annealing.

The data thus obtained the author of the above work interpreted to involve an As interstitial diffusion mechanism.

In some instances a diffusion of the impurity from the implanted layer towards the surface is observed. Thus, in [39] the back-scattering method was used in investigation of the distribution profiles of impurities I (Rb, Cs), II (Zn, Cd, Hg, Ca), III (In), V (Sb) and VI (Se, Te) of groups of elements in Si. The ion energy was 400 keV for Sb and In ($T_{\text{irrad}} = 20$ °C) and 50 keV for other elements

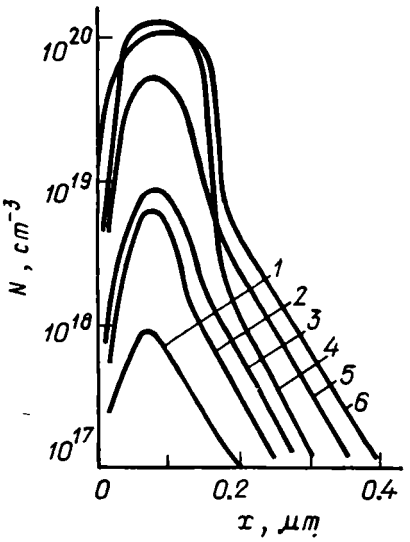

Fig. 3.10. Influence of irradiation dose on profile of electrically active As in Si [38].
Irradiation dose, cm^{-2}: *1*—10^{13}; *2*—$5\cdot10^{13}$; *3*—10^{14}; *4*—10^{15}; *5*—$5\cdot10^{15}$; *6*—10^{16} (amorphization dose, $2\cdot10^{14}$ cm^{-2}). *p*-Type silicon, ρ = 5-10 ohm·cm. Irradiation with As ions at E = 120 keV, $j = 6.25\cdot10^{12}$ cm$^{-2}\cdot$s^{-1}, 60-min annealing at 725 °C

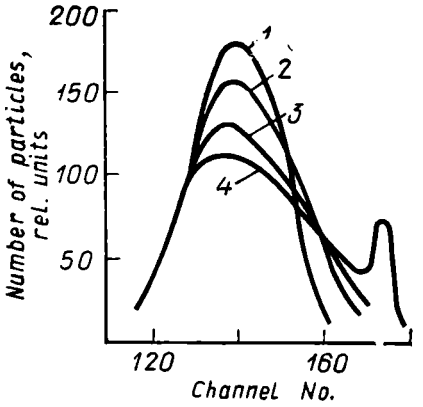

Fig. 3.11. Energy spectra of He ions (E = 1 MeV) back-scattered from Sb atoms implanted in Si (after [39]).
1—original distribution; t_{anneal}, min: *2*—40, *3*—100, *4*—300; T_{irrad} = 20 °C, E =400 keV, $\Phi = 8\cdot10^{14}$ cm^{-2}, T_{anneal} = =900 °C; 10 channels correspond to a depth of 0.056 μm

(T_{irrad} = 20 and 350 °C); the irradiation dose was changed from $5\cdot10^{13}$ to $2\cdot10^{-15}$ cm^{-2}. The samples were cut from a zone-molten silicon of the *n*- and *p*-types with the resistivity ranging from 10^2 to $3\cdot10^5$ ohm·cm. Upon implantation, an isothermal or isochronal (15 min) annealing was performed. Fig. 3.11 shows the results for Sb, which indicates a diffusion of Sb towards the surface only (i.e., no diffusion occurs inside the bulk of the crystal). For the atoms of Cd and Se, during an isochronal annealing at $T_{anneal} \geqslant 600$ °C for Se and 600°C $\leqslant T_{anneal} \leqslant$ 900 °C for Cd, the distribution maximum was observed to displace towards the surface (T_{irrad} = 20°C). Under similar conditions, the same effect was not observed for the atoms of Cs, Rb, Zn and Hg.

The diffusion of the atoms of Be towards the surface during annealing of the implanted layer was observed with the method of mass spectroscopy of secondary ions used [40]. The authors associate

the obtained results with a diffusion of Be through the defect-containing areas.

A study of the distribution profiles of the electrically active aluminium in silicon upon ion implantation at room temperature and subsequent annealing [41, 42] has indicated a presence of enhanced diffusion of aluminium for annealing temperatures of 600 to 800 °C. In this case it was found that the main influence on the value of RED is produced by the defects (vacancies, in the opinion of the authors) liberated from the clusters present in the disordered crystal behind the amorphous layer (ionization doses $2 \cdot 10^{15}$ cm^{-2}, i.e., higher than the amorphization dose). According to the authors of [41], the typical lifetime of an excessive concentration of free vacancies affecting the diffusion of aluminium did not exceed 1 min at 800 °C.

In [43], the mass spectroscopy of secondary ions was used in study of the distribution profiles of aluminium in silicon upon implantation at a dose of 10^{13} to 10^{15} cm^{-2} ($E = 60$ keV, $T_{\text{irrad}} = 20$ °C) and subsequent annealings at 380 to 800 °C. In contrast to [41, 42] where the profiles of electrically active aluminium were measured, it was discovered in [43] that an amorphous layer appearing at high doses of aluminium ions has a marked effect on the formation of the typical (with two maxima) profile of aluminium during annealing at temperatures ranging from 480 to 600 °C (Fig. 3.12*a*). A similar depth distribution of aluminium atoms has been obtained in the samples irradiated with a low dose of Al^+ (below the amorphization dose) and, then, turned to an amorphous state by irradiation with ions of neon (Fig. 3.12*b*). Two maxima in the depth distribution profile of an implanted impurity were also revealed upon irradiation of silicon with the ions of gallium ($E = 80$ keV, $\Phi = 3.5 \cdot 10^{14}$ cm^{-2}, $T_{\text{anneal}} = 700$ °C) though were not registered when irradiation was effected with ions of boron. The authors of [43] associate the results thus obtained with a redistribution of the impurity atoms during recrystallization of the amorphous layer.

The authors of [44] give an analysis of the experimental evidence on diffusion of impurities from the ion-implanted layers. It is shown that a considerable fraction of the implanted impurity atoms diffused via interstices with the result that the impurity distribution profiles developed characteristic exponential "tail". At the same time, it is supposed that the impurity atoms present in the crystal's regions that are heavily damaged do not diffuse as they interact with this damage. Taking into account the results of the experiments showing that the "tails" in the impurity depth profiles appear right in the course of irradiation and their formation is independent of temperature within 77 to 800 K, and an evidence on an increase in the characteristic length of the exponential "tails" with a growth of the ionization losses, the authors of [44] presume that the diffusion

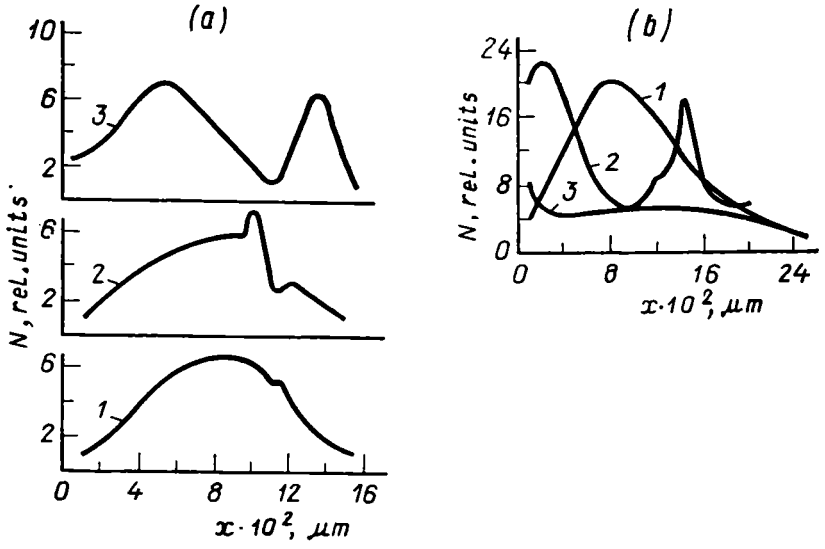

Fig. 3.12. Depth distribution profiles of Al in Si after 60-keV Al ion implantation at 20 °C [43].
a—$\Phi = 2 \cdot 10^{15}$ cm^{-2}, T_{anneal}, °C: *1*—380, *2*—480, *3*—600, t_{anneal} = 30 min; *b*—Φ = $= 5 \cdot 10^{13}$ cm^{-2}, *1*—without annealing, *2*—T_{anneal} = 800 °C, t_{anneal} = 30 min additional irradiation with Ne ions (E = 45 keV, $\Phi = 3 \cdot 10^{15}$ cm^{-2}), *3*—T_{anneal} = 800 °C, t_{anneal} = = 30 min, without additional irradiation

of an interstitial impurity atoms occurs by one of the RED ionization mechanisms [45]. It should be noted that the influence of the energy losses on the formation of the "tails" has not been proved in [38] as yet.

The data on RED of antimony, gallium, indium in silicon versus the temperature of the target material in ion implantation and intensity of the ion beam (the activation analysis method) are presented in [51 through 54]. A marked enhancement of diffusion of the atoms of indium was observed at $T_{irrad} > 300$ °C, those of gallium at $T_{irrad} > 200$ °C, and those of antimony at $T_{irrad} \geqslant 500$ °C. (Figs. 3.13 through 3.16). An increase in the irradiation temperature above the specified ones did not result in a marked rise in the RED effect. An increase in the intensity of the ion beam promoted the diffusion of antimony (see Fig. 3.16), while there were no significant changes in the diffusion of indium and gallium. It is worth noting that the time of irradiation with different intensities of the beam was the same, i.e., the samples received different irradiation doses. The authors supposed that an enhancement of the diffusion of Sb depended on the extra radiation-induced vacancies, while the effects of promotion of diffusion of In and Ga were attributed to the interstitial content of the diffusion of these impurities.

In the case of RED of antimony the calculations are provided and the diffusion coefficients obtained from the comparison with the

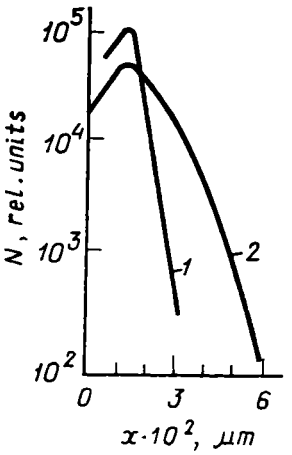

Fig. 3.13. Antimony concentration profiles in silicon [51].
Temperature during implantation, °C: *1*—20; *2*—500, 600, 700 and 800. *n*-Type silicon (B), $\rho \simeq 5$ ohm·cm; ion energy, 20 keV; $I = 1.2 \cdot 10^{12}$ cm$^{-2} \cdot$s^{-1}, $t_{irrad} = 20$ min

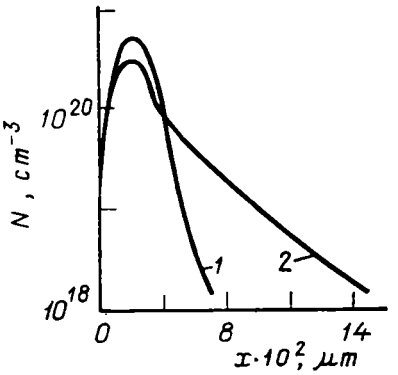

Fig. 3.14. Indium concentration profiles in silicon [51].
Temperature during ion implantation, °C: *1*—20, 1000, 200; *2*—300, 400, 500, 600, 700. *n*-Type silicon (B), $\rho \simeq 5$ ohm·cm; ion energy, 45 keV; $I = 3 \cdot 10^{11}$ cm$^{-2} \cdot$s^{-1}; $t_{irrad} = 1$ h

experimental data for the atoms of antimony: $D = 1.1 \cdot 10^{15}$ and $6.6 \cdot 10^{-15}$ cm^2/s with irradiation intensities of $1.2 \cdot 10^{12}$ and $7.2 \cdot 10^{12}$ cm^{-2}.s^{-1}, respectively (the thermal diffusion coefficients vary from 10^{-25} to 10^{-19} cm^2/s over a temperature range of 500 to 800 °C).

The authors of [55] investigated the RED of boron, phosphorus and antimony in silicon first irradiated with various doses of 50-keV neon and 100-keV argon ions. After the irradiation, the impurities were allowed to diffuse in silicon at 700 to 1200 °C. The concentration profiles were studied by electrical and radioactive tracer methods using layer-by-layer etching. The main result was the enhancement of the diffusion for all the impurities under test at a depth not exceeding the thickness of the damaged layer and retardation of the diffusion at a depth in excess of the said thickness. To explain this result, the authors proceed from the assumption that there is a competition between the enhancement of the impurity diffusion due to saturation of the crystals with vacancies after a preliminary ion bombardment and a retardation associated with the formation, in the regions damaged by the bombardment, of centers that immobilize the diffusing impurity. The authors of [55] presume that at low temperatures and with short diffusion anneal times the vacancies are the agent

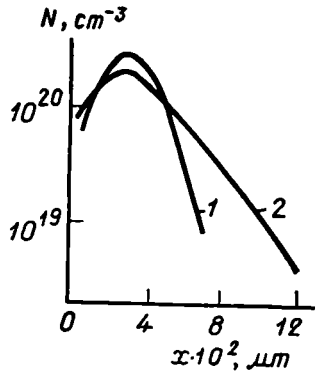

Fig. 3.15. Gallium concentration profiles in silicon [51].
Ion implantation temperature, °C: *1*—20, 100; *2*—150, 200, 300, 400, 500, 600, 700. Other parameters are the same as in Fig. 3.14

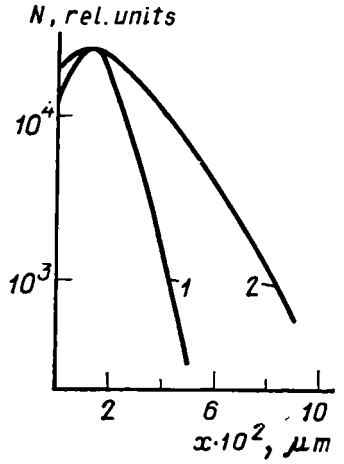

Fig. 3.16. Antimony concentration profiles in silicon [51].
Ion irradiation intensity, $cm^{-2} \cdot s^{-1}$: *1*—$1.2 \cdot 10^{12}$, $T_{irrad} = 500$ and 700 °C; *2*—$7.2 \cdot 10^{12}$, $T_{irrad} = 500$ and 700 °C. *p*-Type silicon (B), $\rho = 5$ ohm·cm; ion energy, 20 keV; $t_{irrad} = 20$ min

of impurity diffusion enhancement, while at high temperatures and with long diffusion anneal times the sinks are the dominating factor. Like the case in [55], in [56] it is noted that the preliminary bombardment of silicon with ions of inert gases (e.g., argon) has a double effect on the subsequent diffusion of the atoms of phosphorus. However, with the diffusion source (red phosphorus) changed to P_2O_5, the diffusion retardation effects disappeared, which allowed the authors of [56] to assume a neutralization of the diffusing phosphorus trapping centers as a result of their interaction with the atoms of oxygen.

According to [57], the preliminary amorphization (with ions of Si, $E = 140$ keV, $\Phi = 3 \cdot 10^{15}$ cm^{-2}, $R_p = 0.21$ μm) at 800 °C retards the diffusion of boron in silicon from the implanted layer ($E_B^+ = 40$ keV, $\Phi = 6 \cdot 10^{14}$ cm^{-2}, $R_p = 0.13$ μm). The authors argue that during the implantation a considerable number of atoms of boron occupy irregular positions, such as interstitial sites or complexes with vacancies. In a heavily damaged (by ions) Si layer, a large number of host-crystal interstitial atoms gives rise to annihilation

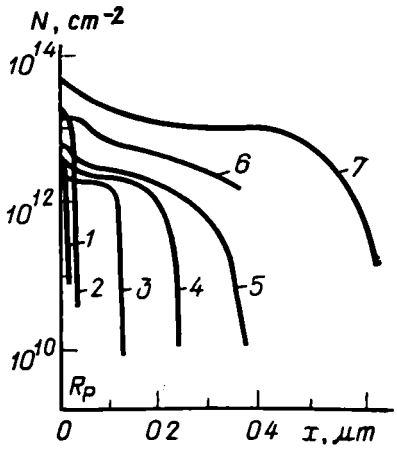

Fig. 3.17. Integral depth distributions of electrons in gallium arsenide layers produced by diffusion of tin (T = = 800 °C, $t = 10^3$ s) [59].

Ar ion pre-irradiation parameters ($E = 40$ keV): T_{irrad} = 100 °C; Φ, cm⁻²: *1*—$3 \cdot 10^{14}$, *4*—$1.5 \cdot 10^{15}$, *5*—$5 \cdot 10^{15}$; T_{irrad} = 20 °C; Φ, cm⁻²; *3*—$6.3 \cdot 10^{13}$, *7*—$2 \cdot 10^{14}$; *2*—non-irradiated sample; *6*—proton irradiation, E = = 30 keV, $\Phi = 10^{16}$ cm⁻², T_{irrad} = 500-600 °C; R_p—projection of mean free path of Ar ions with $E = 40$ keV in GaAs

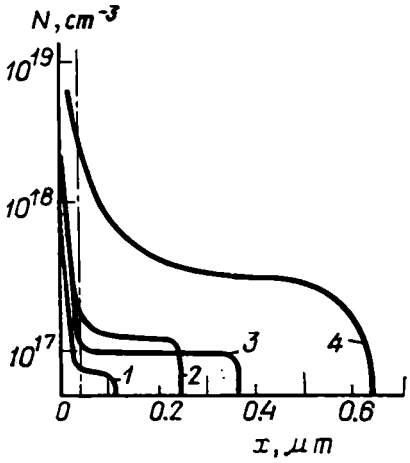

Fig. 3.18. Concentration profiles of electrically active atoms of tin in GaAs layers produced by enhanced diffusion [59].

Dose (cm⁻²) and temperature (°C) of Ar ion pre-irradiation ($E = 40$ keV), respectively: *1*—$6.3 \cdot 10^{13}$ and 20; *2*—$1.5 \cdot 10^{15}$ and 100; *3*—$5 \cdot 10^{15}$ and 100; *4*—$2 \cdot 10^{14}$ and 20

of the boron-vacancy complexes and acts as a retarder for an anomalous diffusion.

The influence of preamorphization with ions of inert gases on the diffusion of implanted boron in Si has been investigated in [58].

Of considerable scientific and practical interest is the study of the RED of impurities in semiconductor compounds ([59] through [66]) where the use of ordinary thermal diffusion meets with difficulty because of the instability of the compounds or high temperatures.

The authors of [59] investigated the possibility of enhanced diffusion of Sn in GaAs by preliminary irradiation of the surface to be doped with ions of inert gases. The samples of semi-insulating GaAs were irradiated with 40 and 300 keV Ar ions. Upon irradiation, a layer of Sn about 0.5 μm thick was built by sputtering on the surfaces of the samples, following which, an annealing was performed at 800°C for 10^3 s. Then tin was removed from the surface and the impurity depth distribution profiles were investigated by measuring the electrical conductivity and Hall effect in combination with

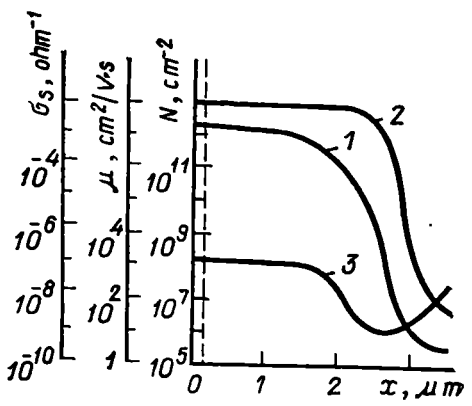

Fig. 3.19. Distribution of (*1*) conductivity, (*2*) concentration of free carriers and (*3*) mobility in GaAs layers produced by enhanced diffusion of Sn after preliminary bombardment with Ar ions with $E = 300$ keV and dose of 10^{16} cm^{-2} at room temperature [59]. The dashed line shows the values of R_p

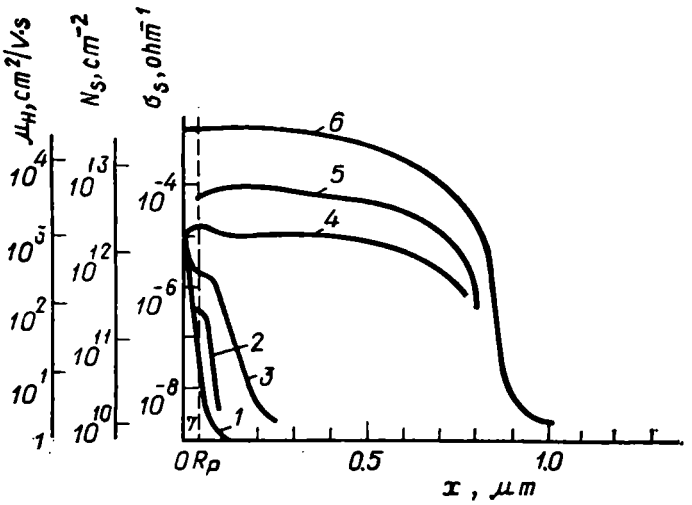

Fig. 3.20. Depth distribution of conductivity (*1*, *3*, *6*), concentration of free electrons (*2*, *5*) and effective Hall mobility (*4*) in GaAs layers produced by radiation-enhanced diffusion of Sn ($T_{anneal} = 600$ °C, $t_{anneal} = 10^3$ s) upon preliminary irradiation with As ions with $E = 100$ keV [60].
Φ, cm^{-2}: *1*—10^{15}; *2*, *3*—$5 \cdot 10^{15}$; *4*, *5*, *6*—$(4\text{-}6) \cdot 10^{16}$; *7*—distribution of conductivity in a layer produced by radiation-enhanced diffusion of Sn in GaAs ($T_{anneal} = 600$ °C, $t_{anneal} = 10^3$ s) upon a preliminary irradiation with Ar ions ($E = 40$ keV, $\Phi = 2 \cdot 10^{14}$ cm^{-2}). The dash-and-dot line shows the values of R_p for As+

the layer-by-layer etching. It was discovered that an Ar ion bombardment resulted in an abnormally deep penetration of Sn during a subsequent diffusion. A study of the width of doped layers versus the energy, temperature and dose of preirradiation with Ar ions has allowed obtaining the following results (Figs. 3.17-3.19).

1. Bombardment at room temperature gives rise to layers whose depth is maximum 20 times as great as the projection of the ion path and maximum 100 times as great as the depth of the layers produced by conventional diffusion at a respective temperature.

2. A high-dose bombardment at fixed temperature and energy results in a wider profile.

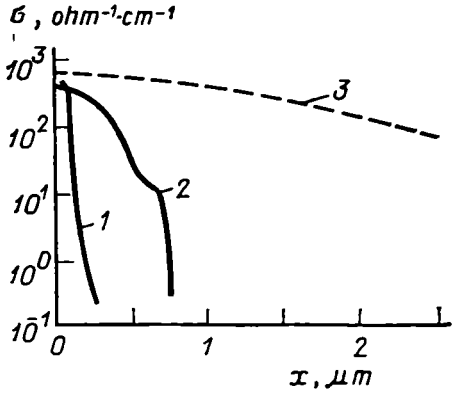

Fig. 3.21. Depth distribution of conductivity in GaAs layers produced by Zn ion implantation ($E = 35$ keV, $\Phi = 3 \cdot 10^{15}$ cm^{-2}) [63].

1—with preliminary As ion implantation ($E = 100$ keV, $\Phi = 10^{16}$ cm^{-2}); *2*—without preliminary As ion implantation; *3*—calculated diffusion profile ($D = 5 \cdot 10^{-12}$ cm^2/s). Annealing was performed in vacuum at 750 °C during 10^3 s

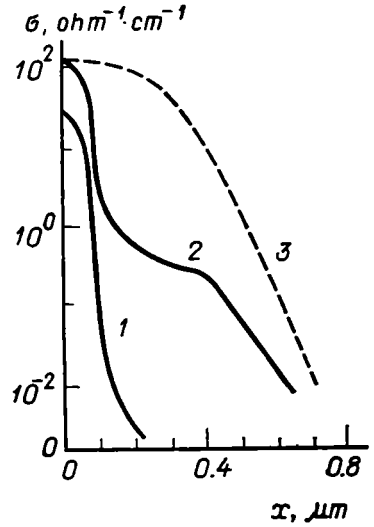

Fig. 3.22. Depth distribution of conductivity in GaAs layers produced by Cd ion implantation ($E = 35$ keV, $\Phi = 10^{15}$ cm^{-2}) [63].

1—with preliminary As ion implantation ($E = 100$ keV, $\Phi = 5 \cdot 10^{15}$ cm^{-2}); *2*—without preliminary As ion implantation; *3*—calculated diffusion profile ($D = 1.5 \cdot 10^{-13}$ cm$^2 \cdot$s^{-1}). Annealing was performed in vacuum at 800 °C during 10^3 s

3. A higher irradiation temperature with a fixed dose decreases the depth of the subsequent penetration of the atoms of tin.

For interpretation of these results, the authors of [59] use a model according to which an increase in the depth of penetration of the impurity depends on the generation of vacancies during annealing of layers damaged by ion bombardment.

Enhanced diffusion of Sn in CaAs after a preliminary irradiation with As ions was observed by the authors of [60] (Fig. 3.20). The authors assume that this effect is associated with the formation of a stream of gallium vacancies caused by a deviation of the irradiated crystal from the normal stoichiometric characteristics. In [61, 62] it is shown that a large number of gallium vacancies retards the diffusion of zinc and cadmium into GaAs from the implanted layer. A preliminary bombardment of GaAs samples with ions of arsenic adds to this effect (Figs. 3.21 and 3.22) [63]. The authors of [63] suppose that the diffusion of Zn and Cd occurs via interstices. A recrystallization attendant upon annealing of layers containing surplus

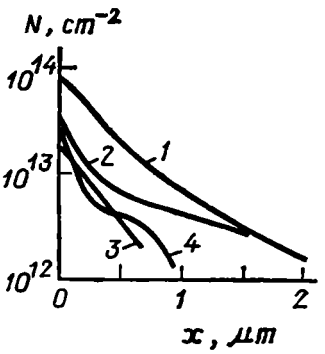

Fig. 3.23. Distribution of layer concentration of electrons upon annealing of implanted layers [64].
T_{anneal}, °C: *1*, *3*—980; *2*, *4*—910 (t_{anneal} = = 550 s); T_{irrad}, °C: *1*, *2*—20; *3*, *4*—200; GaAs with Te implants (E = 35 keV, Φ = = 10^{15} cm ^{2})

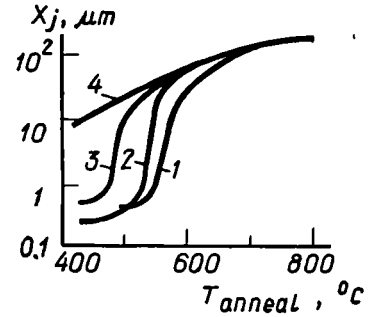

Fig. 3.24. The depth of p-n junctions, X_j, produced in silicon by Na ion implantation (E = 50 keV, j = = 0.8 μA/cm², $\Phi = 1.25 \cdot 10^{15}$ cm^{-2}) vs annealing temperature (t_{anneal} = = 30 min) [71].
T_{irrad}, °C: *1*—23; *2*—300; *3*—425; *4*—500. p-Type silicon grown by crucibleless zone refining, $\rho \simeq 1$ kilohm·cm, $N_d < 5 \cdot 10^{4}$ cm^{-2}

As is accompanied by the production of an increased concentration of gallium vacancies this promoting the diffusion retardment.

A change in the irradiation conditions changes the nature of interaction of the diffusing impurity with the radiation defects and, as a consequence, the speed of diffusion. The authors of [64] studied the diffusion of Te implanted in GaAs (E = 35 keV, $\Phi = 10^{15}$ cm^{-2}) during annealing at 900 to 1000 °C. It has been found (Fig. 3.23) that the speed of diffusion depends on irradiation temperature. The authors believe that irradiation temperature sets the initial ("starting") position of Te implants. At T_{irrad} = 20 °C, most Te atoms are in sites other than regular ones, while at T_{irrad} = 200 °C, all Te atoms immediately occupy the regular lattice sites. The emergence of "tails" on the profiles (see curves *1* and *2* in Fig. 3.23) point to the effect of Te diffusion via interstices.

Up to the present time, there have been several attempts at using RED in production of semiconductor devices [30, 66-70]. The authors of [67 and 68] used RED caused by a proton beam to obtain unusual profiles of impurity distribution in fabrication of silicon transistors.

It is clear from the above experimental data that, depending on the environment (defect inventory of the target material, energy and intensity of irradiation, dose, position of the impurity in the crystal lattice, etc.), RED promotes various interactions between the impurity and the defects with the result that the diffusion of the impurity may be either enhanced or retarded. The need for using the idea of an interaction between the defects in interpretation of

RED experimental evidence has been emphasized by a number of authors [14, 56, 71-75]. Thus, despite the general negative attitude to feasibility of low-temperature diffusion of gold in silicon, caused by irradiation with 15, 100 keV and 1.5.-MeV electrons, the authors of [14] note that in samples previously subjected to heat treatment at 1000 °C for 2-3 h (either in preliminary diffusion of non-radioactive gold or in air-heating) an enhanced diffusion of radioactive gold Au^{195} is observed at 200-400 °C. This result points to a significant influence of the defect inventory of the material, changing upon heat treatment, on the diffusion speed of gold. This can account for the difference in the evidence on RED of gold in silicon, obtained by various experimenters.

A considerable dependence of RED on the defect inventory of the material [18] is indicated in [28] and [29] where the authors have discovered large discrepancies in RED of antimony in epitaxial silicon structures (impurity pulling from the substrate) and in silicon samples with a prearranged antimony profile.

The authors of [71] observed a retardment of diffusion of Na in Si during interactions with radiation defects. Upon implantation of Na ions, *p*-Si samples were annealed at 400 to 750 °C. The depth of the *p-n* junction was determined. It was found that with an increase in the temperature of the target during implantation, the speed of Na diffusion increased (Fig. 3.24). The authors associate this result with the interactions of diffusing atoms of Na with complexes of radiation defects produced during the implantation.

The suggested importance of formation of defect complexes to diffusion processes (see [18, 21]) in a particular RED case was taken into account in one of the earlier papers [24], which contains the results of RED studies of phosphorus, gallium and boron in silicon (the *p-n* junction colouring technique). The diffusion was promoted either with 200 keV to 1 MeV protons or with 1 MeV electrons (current densities, 3 and 30 $\mu A/cm^2$, respectively). In the case of protons, the value of R_p was comparable to the depth of the *p-n* junction. The irradiation temperature was maintained within 600 to 1200 °C. The main results obtained in [24] are as follows: (1) the lifetime of the defect (vacancy) taking part in RED is about 100 s at $T_{irrad} = 850$ to 900 °C; (2) the diffusion length of the defect (vacancy) depends on the quality of the crystal (i.e., on how perfect it is). In most crystals, the vacancy diffusion length is about 3 μm. The RED experiments using electron irradiation at T_{irrad} of about 900-1000°C yielded diffusion lengths of about 4-5 μm [72].

According to the author of [24], the high values of activation energies (1.6. to 2.3 eV) are associated with the interactions of the diffusing defect (vacancy) with the atoms of oxygen, resulting in the formation of an *A*-center. The effective capture of the vacancies during the diffusion reduces the impurity diffusion coefficient on the

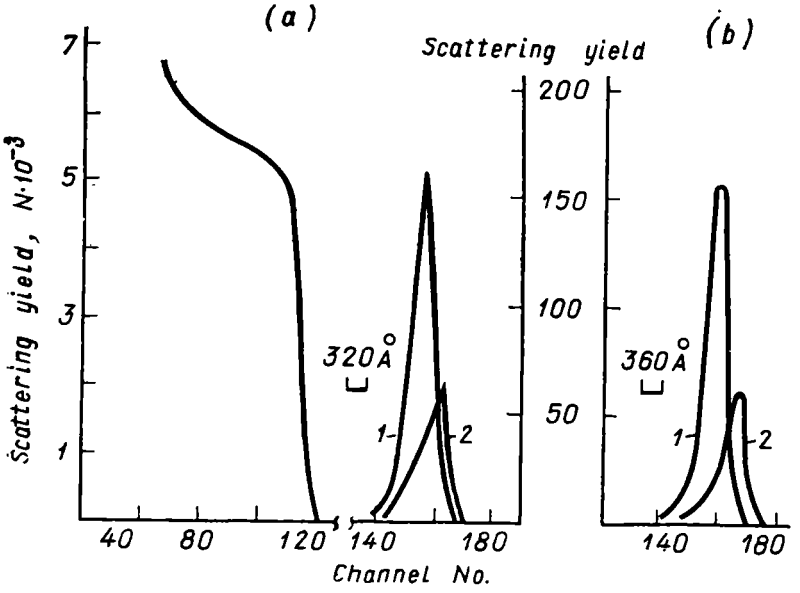

Fig. 3.25. Spectra of He ions with initial energy E_0, back-scattered from ⟨110⟩ oriented and Zn ion implanted silicon wafers [72].
a—E_0 = 1 MeV (a sample without the oxynitride film): *1*—before LA, N_{Zn} = 2.1·10¹⁵ cm⁻²; *2*—after LA, N_{Zn}=1·10¹⁵ cm⁻²; *b*—E_0=1.5 MeV (a sample with the oxynitride film applied): *1*—before LA, N_{Zn} = 2.1·10¹⁵ cm⁻²; *2*—after LA, N_{Zn} = 1.1·10¹⁵ cm⁻²

one hand, and changes the diffusion activation energy, with a change in the experiment temperature, on the other.

Although the author of [24] has considered a particular RED case, the model of the process, suggested by him, which includes an interaction of the vacancy with the atoms of oxygen has been, in our opinion, very fruitful. Yet it did not receive further development in papers on RED [32, 34]. At a later stage, a more general and complete model of impurity diffusion, based on a suggested dominating role of defect complexing in impurity diffusion, has been developed [21] (see 3.1). Specifically, this model has been used for interpretation of the results obtained in [72] where redistribution of Zn in Si under the influence of laser pulses was investigated. The КЭФ-7,5 samples with orientations ⟨111⟩, ⟨110⟩ and ⟨100⟩ were implanted with Zn ions (E = 35 keV, T_{irrad} = 125 °C, Φ = (1.5-2)·10¹⁵ cm⁻²) prior to being subjected to laser annealing (λ = 0.53 μm; pulse duration, 10⁻⁸ s; pulse energy, 0.6 to 0.8 μJ). Redistribution of Zn was measured by the method of back-scattering of He ions. The following results have been achieved (see Figs. 3.25 and 3.26).

1. With laser annealing (LA) of silicon doped with ions of Zn at Φ = 2·10¹⁵ cm⁻², the diffusion of Zn both towards the surface and inside the bulk of the crystal over at least 1 μm distance is observed.

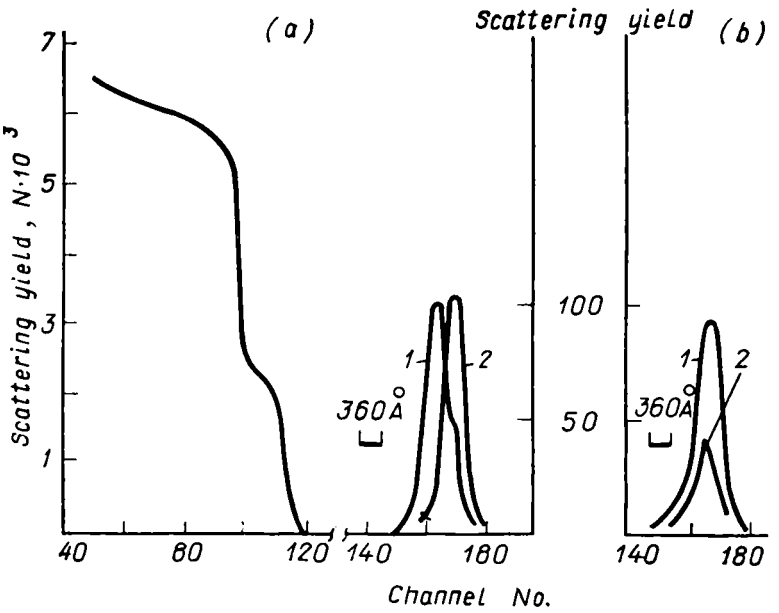

Fig. 3.26. Spectra of He ions with original energy of 1.5 MeV, backscattered from ⟨100⟩ oriented, nitrogen, then zinc ion irradiated silicon wafers [72]. *a*—test sample (without LA): *1*—before LA, $N_{Zn} = 1.4 \cdot 10^{15}$ cm^{-2}, *2*—after LA, $N_{Zn} = 1 \cdot 10^{15}$ cm^{-2}; *b*—after TA (15 min, 700 °C): *1*—before LA, $N_{Zn} = 1.3 \cdot 10^{15}$ cm^{-2}, *2*—after LA, $N_{Zn} = 0.56 \cdot 10^{15}$ cm^{-2}

2. Irradiation with N ions ($E = 65$ keV, $\Phi = 10^{15}$ cm^{-2}, $T_{irrad} = 20$ °C, $R_p = 0.15$ μm) prior to Zn implantation results in inhibition of Zn diffusion on the volume and in an increased number of atoms diffusing towards the surface at LA. The degree of inhibition depends on the crystallographic orientation and decreases in the order: ⟨111⟩, ⟨110⟩, ⟨100⟩.

3. Thermal annealing (TA) for 15 min at 700 °C recrystallizes the region damaged by the implantation of N and Zn. In this case, the atoms of Zn stay in the near-the-surface layer, but their diffusion increases on subsequent LA.

Interpretation of the above data the authors of [72] proceed from the model of diffusion, provided in [21] (see Sec. 3.1). They believe that the atoms of Zn diffuse interstitially, adhering to the traps. The estimated diffusion coefficient at LA amounts to about 1 cm^2/s, i.e., by 6-7 orders of magnitude greater than the thermal diffusion coefficient. According to [18], the diffusion at TA is controlled not only by the energy of migration of interstitial atoms but also, and mainly, by the energies that bind the atom to the traps, sections (barriers) of interaction (complexing) and with the concentrations of traps. At LA accomplished in short pulses (about 10^{-8} s), the interstitial atoms seem to move freely (with a low migration energy) during the pulse time and get trapped as soon as the pulse ceases.

Slight migration at LA may be conditioned (according to [72]) either by a high (over 700°C) temperature in the absorbing layer during the laser irradiation, or by the fact that a high ionization level reduces the energy that binds the atoms of Zn to defects and decreases the cross-sections of capture of interstitial atoms with traps. A change in the number and efficiency of the traps, effected by additional means (N implantation, TA) results in a changed diffusivity of Zn, observed in the experiment.

Sec. 3.3. Principles and Techniques of Radiation Control of Diffusion in Semiconductors

The experimental data given in Sec. 3.2 attest to strong possibilities opened up by the employment of RED for technological purposes. An analysis of these possibilities, made on the basis of the models provided in [21] (see Sec. 3.1) allows one to formulate some general principles and efficient techniques of RED:

(1) creation of directional streams of uncompensated defects (vacancies or interstitials) by, say, irradiation of an atomic semiconductor with the ions of the basic material, by disturbance of the stoichiometry in semiconductor compounds, by injection into the crystal of elastic stress fields (production of oxide films on the crystal surface, injection of dislocations, compression and extension of the crystal);

(2) a change in the efficiency of the adhesion centers of diffusing impurities as a result of interaction of the centers with the radiation defects on irradiation and annealing;

(3) a change in the initial positions of the atoms of the diffusing impurity: (a) during interactions with the vacancies and interstitials of the host material (for instance, a known effect whereby the impurity atoms are dislodged from the regular lattice sites by host-crystal interstitial atoms); (b) when the target temperature changes upon ion bombardment, which results in a redistribution of the concentration of the implanted impurity both in regular and interstitial sites and different efficiency of the channeling processes (a rise in temperature decreases the probability of blocking the channels with defect complexes and, at the same time, leads to dechanneling);

(4) introduction of impurity into the crystal in excess of the dissoluble amount (for instance, by ion bombardment), which should generally result in a strong interstitial content;

(5) a change in the dissolubility of the impurity within the defect-populated area created by an additional operation (e.g., by irradiation with protons or other ions) at moderate annealing. In this case, significant is not only the difference in mobility of the vacancies and interstitials but also the fact that the successively repetitive acts of

annihilation of the Frenkel pair components at the impurity promote chaotic jumping of the latter.

Some of the above techniques have already been tested and now yield interesting results. However, in general, for practical employment, wide-scale and detailed experimental studies of particular diffusant-crystal (or device) systems are required. One has also to select the type and conditions of irradiation, and to change the chemical composition of the crystal. The RED capabilities will be further extended if we manage to achieve strong and regularly repetitive effects of enhancement of diffusion due to ionization.

References

1. Kiv, A. E., Umarova, F. T. A study on the microscopic theory of diffusion in semiconductors. *Fizika i tekhnol. polupr.*, 1970, **4**, 3, pp. 571-573 (in Russian).
2. Watkins, G. D. ESR studies of the lattice vacancy and low-temperature damage processes in silicon. In: *Lattice Defects in Semiconductors. Conf. Ser. No. 23*, Inst. of Phys. London-Bristol, 1975, pp. 1-22.
3. Gerasimov, A. B., Gerasimov, B. A., Tsertsvadze, A. A. An influence of impurity charge state on diffusion of impurities in semiconductors. *Soobshcheniya AN GruzSSR*, 1975, **77**, 1, pp. 53-56 (in Russian).
4. Gerasimov, A. B., Djandieri, M. Sh., Tsertsvadze, A. A. A model of radiation-enhanced diffusion with a dissociative mechanism. *Fizika i tekhnol. polupr.*, 1978, **12**, 5, pp. 1000-1003 (in Russian).
5. Zaikovskaya, M., Takhirov, K., Yunusov, M. Radiation effects in X-rayed silicon. *Fizika i tekhnol. polupr.*, 1976, **10**, 1, pp. 37-40 (in Russian).
6. Klimkova, O. A., Niyazova, O. R. Radiation-enhanced diffusion of gold in silicon. *Fizika tverd. tela.*, 1970, **12**, 7, pp. 2199-2200 (in Russian).
7. Mannanova, Kh. Kh., Niyazov, Kh. R. A study of mechanism of radiation enhanced diffusion of sulphur in cadmium sulfide. *Fizika i tekhnol. polupr.*, 1971, 5, 4, pp. 785-787 (in Russian).
8. Kiv, A. E., Umarova, F. T. Radiation-enhanced migration processes in solids. *Fiz. tverd. tela*, 1967, 9, 8, pp. 2225-2229 (in Russian).
9. Kaneev, M. A. Experimental determination of radiation-enhanced diffusion coefficient for CdS. *Fiz. tverd. tela*, 1968, **10**, 3, pp. 922-923 (in Russian).
10. Starodubtsev, S. V., Niyazova, O. R., Kaneev, M. A. Radiation-enhanced diffusion in cadmium sulfide. *Fiz. tverd. tela*, 1967, **9**, 3, pp. 872-874 (in Russian).
11. Niyazova, O., Kaneev, M. On Radiation-induced distortions in crystals of cadmium sulfide. *Fiz. tverd. tela*, 1963, 5, 9, pp. 2731-2733 (in Russian).
12. Koifman, A. I., Narkulov, A. N., Oksengendler, B. L., Yunusov, M. S. The Low-temperature doping of silicon by radiation-induced diffusion *Phys. Stat. Sol.* (*a*), 1976, **38**, 2, pp. 439-446.
13. Koifman, A. I., Narkulov, N. A., Yunusov M. S. Influence of structure defects on the radiation-enhanced gold diffusion in silicon. *Phys. Stat. Sol* (*a*), 1975, **31**, 2, pp. K169-K173.
14. Cheng, L. J., Süli, M., Kowall, J. P., Wallace P. W., Corbett, J. W. Effects of radiation on gold diffusion in silicon. *Phys. Stat. Sol.* (*a*), 1976, **38**, 1, pp. 321-330.
15. Malkovich, R. Sh., Nistiryuk, I. V., Savin, E. P. An attempt at detection of gamma radiation-induced migration of gold in silicon. *Phys. tverd. tela.*, 1975, **17**, 8. pp. 2415-2416 (in Russian).
16. Konorova, L. F., Malkovich, R. Sh. On photoexcited migration of lithium in germanium. *Fiz. tverd. tela.*, 1975, **17**, 9, pp. 2805-2806 (in Russian).

17. *Radiation-Enhanced Processes in Silicon.* Ed. by Sh. A. Vakhidov, Tashkent, Fan, 1977, 166 pages (in Russian).
18. *Physical Processes in Irradiated Semiconductors.* Ed. by L. S. Smirnov. Novcsibirsk, Nauka, 1977, 256 pages (in Russian).
19. *Radiation-Enhanced Diffusion in Semiconductors.* Preprint of Institute of Semiconductor Physics, Siberian Branch of USSR Academy of Sciences. Ed. by L. S. Smirnov. Novosibirsk, 1975, 26 pages (in Russian).
20. Smirnov, L. S. On reactions in crystals. In: *Defects in Semiconductors Structure.* Novosibirsk, 1973, pp. 201-208 (in Russian).
21. Bolotov, V. V., Vasilyev, A. V., Smirnov, L. S. Reactions in crystals as factor governing diffusion processes. *Fizika i tekhnol. polupr.*, 1974, 8, 6 pp. 1175-1181 (in Russian).
22. Gwozdz, P. S., Kochler, J. S. Changes in AC conductivity of silicon with electron irradiation at 0.5 K. *Phys. Rev., B*, 1972 6, 12, pp. 4571-4574.
23. Smirnov, L. S. Development and problems of germanium radiation physics. In: *Proceedings of All-Union Meeting on Structural Defects in Semiconductors.* Part 1. Novosibirsk, 1969, pp. 143-159 (in Russian).
24. Pfister J. C. Radiation-enhanced diffusion in silicon. In: *Radiation Damage in Semiconductors.* Paris-Royaunmont, Dunod, 1965, pp. 281-285.
25. Baruch, P., Constantin, C., Pfister, J. C., Saintesprit, R. Vacancy-enhanced diffusion in silicon. *Discuss. Faraday Soc.* 1961, 31, pp. 86-99.
26. Nelson, D. G., Gibbons, J. F., Johnson, W. S. Radiation-enhanced diffusion of boron in silicon. *Appl. Phys. Lett.*, 1969, 15, 8, pp. 246-248.
27. Panteleev, V. A., Isavtseva, L. N. Diffusion of antimony from ion bombarded silicon layer. *Izv. vuzov. Fizika*, 1969, 8, pp. 27-30 (in Russian).
28. Abe, T., Ohmura, Y., Konaka, M., Mimura, S., Kanazawa, M., Ohtsubo, H., Shibaura, T. Enhanced diffusion of Sb in Si by hot proton irradiation. In: *Ion Implantation in Semiconductors.* Ed. by S. Namba. Japan Soc. for the Promotion of Science, 1972, pp. 57-62.
29. Ohmura, Y., Mimura, S., Kanazawa, M., Abe T., Konaka, M. Enhanced diffusion and the dose rate dependence of Sb and P in Si by proton irradiation. *Rad. Eff.*, 1972, 15, 3-4, pp. 167-174.
30. Minear, R. L., Nelson, D. G., Gibbons J. F. Enhanced diffusion in Si and Ge by light ion implantation. *J. Appl. Phys.*, 1972, 43, 8, pp. 3468-3480.
31. Baruch, P., Monnier, J., Blanchard, B., Castaing, C. Redistribution of boron in silicon through high-temperature proton irradiation. In: *Lattice Defects in Semiconductors. Conf. Ser. No. 23*, Inst. of Phys. London-Bristol, 1975, pp. 453-460.
32. Baruch, P. Radiation defects and impurity diffusion in silicon. In: *Radiation Effects in Semiconductors. Conf. Ser. No. 31*, Inst. of Phys. London-Bristol 1977, pp. 126-143.
33. Gerasimenko, N. N., Obodnikov, V. I., Smirnov, L. S., Sokolov, S. A. Diffusion of phosphorus in silicon by hydrogen ion irradiation at high temperature. *Fizika i tekhnol. polupr.*, 1975, 9, 11, pp. 2220-2221 (in Russian).
34. Brelot, A. Enhanced diffusion in germanium. In: *Radiation Effects in Semiconductors.* Ed. by F. L. Vook, N. Y., Plenum Press, 1968, pp. 460-465.
35. Seryapin, V. G., Seryapina, N. V., Smirnov, L. S., Romanov, S. I., Obodnikov, V. I. Redistribution of boron in silicon on fast electron irradiation. *Fizika i tekhnol. polupr.*, 1973, 7, 1, pp. 183-185 (in Russian).
36. Kurata, M., Morikawa, Y., Nagami, K., Kuroda, H. Remarks on the vacancy mechanisms in ion implantation. *Japan J. Appl. Phys.*, 1973 12, 3, pp. 472-473.
37. Maby, E. W. Bombardment-enhanced diffusion of arsenic in silicon. *J. Appl. Phys.*, 1976, 47, 3, pp. 830-836.
38. Schwettmann, F. N., Enhanced diffusion during the implantation of arsenic in silicon. *Appl. Phys. Lett.*, 1973, 22, 11, pp. 570-572.

39. Meyer, O., Mayer, J. W. Enhanced outdiffusion in ion implanted silicon. *Phys. Lett.*, 1970, **31A**, 7, pp. 387-388.
40. Hurrle, A., Schulz, M. Anomalous outdiffusion of berillium implanted into silicon. In: *Lattice Defects in Semiconductors. 1974. Conf. Ser. No. 23*, Inst. of Phys. London-Bristol, pp. 474-480.
41. Itoh, T., Ohdomari, I. Experiments on enhanced diffusion of aluminium implanted in silicon. In: *Ion Implantation in Semiconductors.* Ed. by S. Namba, Japan Soc. for the Promotion of Science, Kyoto, 1972, pp. 43-48.
42. Itoh, T., Ohdomari, I. Analysis of radiation-enhanced diffusion of aluminium in silicon. In: *J. Appl. Phys.*, 1970, **41**, 1, pp. 434-436.
43. Dietrich, H. B., Weisenberger, W. H., Comas, J. Anomalous migration of ion implanted Al in Si. *Appl. Phys. Lett.*, 1976, **28**, 4, pp. 182-184.
44. Bourgoin, J., Peak, D., Corbett, J. W. Ionization-enhanced diffusion: ion implantation in semiconductors. *J. Appl. Phys.*, 1973, **44**, 7, pp. 3022-3027.
45. Bourgoin, J. C., Corbett, J. W. Ionization effects on impurity and defect migration in semiconductors. In: *Lattice Defects in Semiconductors, Conf. Ser. No. 23*, Inst. of Phys. London-Bristol, 1975, pp. 149-163.
46. Kutukova, O. G., Streltsov, L. N. Influence of irradiation dose on diffusion processes in ion-implanted layers. *Fizika i tekhnol. polupr.*, 1976 **10**, 4, pp. 796-798 (in Russian).
47. Okabayashi, H., Shinoda, D. Lateral spread of P^{31} and B^{11} ions implanted in silicon. *J. Appl. Phys.*, 1973, **44**, pp. 4220-4221.
48. Kotov, B. A., Yunusov, M. S., Shakirov, U. A. Co^{60} Gamma radiation enhanced diffusion of impurities in silicon. *Fizika i tekhnol. polupr.*, 1976, **10**, 11, pp. 2047-2052 (in Russian).
49. Pavlov, P. V., Pashkov, V. I., Tulovchikov, V. S., Chigirinskaya, T. Yu. Influence of radiation damage on diffusion of impurities from implanted layer in silicon. *Fizika i tekhnol. polupr.*, 1977, **11**, 2, pp. 314-318 (in Russian).
50. Gerasimenko, N. N., Romanov, S. I., Stas', V. F., Tseitlin, G. M. Diffusion of phosphorus in silicon from heavily ion-implanted layer. *Fizika i tekhnol. polupr.*, 1975, **9**, 11, pp. 2117-2120 (in Russian).
51. Namba, S., Masuda, K., Gamo, K., Iwaki, M. Enhanced diffusion in ion-implanted silicon. In: *Ion Implantation in Semiconductors.* Ed. by S. Namba, Japan Soc. for the Promotion of Science, Kyoto, 1972, pp. 49-56.
52. Gamo, K., Doi, A., Masuda, K., Namba, S., Ishihara, S., Kimura, J. Enhanced diffusion of ion implanted Sb in silicon. *Japan J. Appl. Phys.*, 1970, **9**, 3, pp. 333-334.
53. Gamo, K., Masuda, K., Namba, S., Ishihara, S., Kimura, J. Enhanced diffusion of high-temperature ion implanted antimony into silicon. *Appl. Phys. Lett.*, 1970, **17**, 9, pp. 391-393.
54. Gamo, K., Iwaki, M., Namba, S., Ishihara, S., Kimura, I., Mitchell, I. V., Ilic, G., Whitton, J. L., Davies, J. A. Enhanced diffusion and lattice location of indium and gallium implanted in silicon. *Japan J. Appl. Phys.*, 1973, **12**, 5, pp. 735-741.
55. Karmanov, V. T., Khokhlov, A. F., Pavlov, P. V., Zorin, E. I. Influence of radiation defects on impurity diffusion in silicon. *Fizika i tekhnol. polupr.*, 1977, **11**, 10, pp. 1871-1873 (in Russian).
56. Karmanov, V. T., Pavlov, P. V., Zorin, E. I., Tetelbaum, D. I. Influence of argon ion bombardment on diffusion and electrical activity of phosphorus in silicon. *Mikroelektronika*, 1977, **6**, 1, pp. 84-87 (in Russian).
57. Barcz, A., Rosinski, W., Turos, A., Wielunski, Wojtowicz-Natanson, B. Influence of preamorphization on concentration profiles of boron implanted into silicon. *Phys. Stat. Sol.* (*a*), 1975, **27**, 2, pp. K65-K68.
58. Pistryak, V. M., Tetelbaum, D. I., Kozlov, V. F., Vasilyev, V. K., Zorin, E. I., Pavlov, V. P., Fogel, Ya. M. Influence of amorphization on distribu-

tion of boron in silicon during ion bombardment. *Fizika i tekhnol. polupr.*, 1973, **7**, 10, pp. 1987-1990 (in Russian).
59. Zelevinskaya, V. M., Kachurin, G. A., Pridachin, N. B. Enhancement of impurity diffusion by preliminary ion bombardment. *Fizika i tekhnol. polupr.*, 1974, 8, 2, pp. 394-396 (in Russian).
60. Pridachin, N. B., Kachurin, G. A., Smirnov, L. S. On the mechanism of radiation-enhanced diffusion in gallium arsenide irradiated with ions. *Fizika i tekhnol. polupr.*, 1974, 8, 10, pp. 1996-1997 (in Russian).
61. Zelevinskaya, V. M., Kachurin, G. A., Pridachin, N. B., Smirnov, L. S. Doping of gallium arsenide by zinc ion implantation. *Fizika i tekhnol. polupr.*, 1970, 4, 9, pp. 1784-1788 (in Russian).
62. Zelevinskaya, V. M., Kachurin, G. A., Bogomyakov, N. P., Azikov, B. S., Shirokov, L. L. Capture of impurity atoms by vacancies in implanted layers. *Fizika i tekhnol. polupr.*, 1974, 8, 2, pp. 254-257 (in Russian).
63. Gavrilov, A. A., Kachurin, G. A., Pridachin, N. B., Smirnov, L. S. On diffusion of zinc and cadmium in gallium arsenide preirradiated with arsenic ions. *Fizika i tekhnol. polupr.*, 1974, 8, 11, pp. 2236-2238 (in Russian).
64. Zelevinskaya, V. M., Kachurin, G. A., Smirnov, L. S. On interstitial diffusion of impurity from implanted layers. *Fizika i tekhnol. polupr.*, 1975, **9**, 8, pp. 1627-1629 (in Russian).
65. Kachurin, G. A., Pridachin, N. B., Smirnov, L. S. Enhancement and retardment of diffusion by defects in GaAs. In: *Lattice Defects in Semiconductors. Conf. Ser. No. 23*, Inst. of Phys. London-Bristol, 1975, pp. 461-466.
66. Zuk, W., Bazuluk, D. The influence of radiation damage on the diffusion of P and Kr atoms implanted in GaAs monocrystals. In: *Radiation Effects in Semiconductors. Conf. Ser. No. 31*, London-Bristol, 1977, pp. 511-512.
67. Tarui, Y., Komija, Y., Teshima, H., Takahashi, T. Application of ion implantation and RED to lateral transistor. In: *Ion Implantation in Semiconductors.* Ed. by S. Namba, Japan Soc. for the Promotion of Science, Kyoto, 1972, pp. 99-106.
68. Abe, T., Yamamoto, S., Sakamoto, T., Zhota, Y. Application of radiation enhanced diffusion to microwave transistor fabrication and its design optimizations. In: *Ion Implantation in Semiconductors*, Ed. by S. Namba, Japan Soc. for the Promotion of Science, Kyoto, 1972, pp. 121-128.
69. Verkhodanov, S. P., Gashtold, V. P., Gerasimenko, N. N., Pridachin, N. B. Influence of radiation-enhanced diffusion on breakdown voltages of diodes fabricated by ion implantation. *Elektronnaya tekhnika. Ser. 2. Poluprovodnikovye pribory*, 1974, 6 (88), pp. 35-37 (in Russian).
70. Baranov, A. S., Tetelbaum, D. I., Zorin, E. I., Pavlov, P. V., Dobrokhotov, E. V., Kuritsyna, A. K. On distribution of impurity atoms and current carriers in silicon during recoil atom doping and use of this doping method for improvement of ohmic characteristics of contacts. *Fizika i tekhnol. polupr.*, 1973, **7**, 9, pp. 1722-1726 (in Russian).
71. Belikova, M. N., Zastavny, A. V., Korol, P. M. On retarding action of radiation defects during sodium diffusion in silicon. *Fizika i tekhnol. polupr.*, 1976, **10**, 3, pp. 535-537 (in Russian).
72. Mustafin, T., Kachurin, G., Popov, V., Pridachin, N., Seryapin, V., Smirnov, L. Diffusion of zinc during laser annealing of implanted silicon layers. *Fizika i tekhnol. polupr.* 1978, **12**, 7, pp. 1312-1317 (in Russian).
73. Boltaks, B. I., Malkovich, R. Sh., Pokoeva, V. A., Sokolov, V. P. Influence of copper on diffusion of phosphorus in silicon. *Fizika i tekhnol. polupr.*, 1976, **10**, 4, pp. 755-756 (in Russian).
74. Akio, Y. A. Method to diffuse impurities into solid materials. An austrian patent, book 2.54 (HOll), No. 419637.
75. Bolotov, V. V., Vasilyev, A. V., Kashnikov, B. P., Smagulova, S. A., Smirnov, L. S. High-temperature annealing of irradiated germanium. *Fizika i tekhnol. polupr.*, 1976, **10**, 1, pp. 154-156 (in Russian).

CHAPTER 4

POSSIBILITIES OF TECHNOLOGICAL EMPLOYMENT OF RADIATION DEFECTS

A knowledge of the extents of the changes caused to the electrophysical and other properties of semiconductors by radiation is indispensible for solution of a number of practical problems, such as control of parameters of a semiconductor by irradiating it with particles, prediction of degradation of the device and material properties in the radiation fields, hardening them against the influence of radiation, simulating one kind of radiation through another, etc. The present chapter gives the experimental evidence on the influence of irradiation with light and heavy particles on the parameters of the basic semiconductor materials. It also considers the main data on determination of degradation constants, properties of the local levels of defects as well as on the properties and possibilities of technological employment of disordered layers.

Sec. 4.1. Control of Electrophysical Parameters

A concentration of free charge carriers (for example, electrons) changes if irradiated with a dose $\Delta\Phi$ according to the following relation [1, 6]:

$$n = n_0 \pm \Delta\Phi \sum_{i=1}^{m} K_i \{1 + g_i \exp[(E_i - E_F)/kT]\}^{-1}, \qquad (4.1)$$

where n_0 and n are the concentrations of electrons before and after the irradiation, respectively; K_i is the rate of formation of defects of the ith type; E_F is position of the Fermi level; E_i is the energy level of the defect of the ith type; g_i is spin factor of degeneration; k is the Boltzmann constant; T is the absolute temperature. A similar expression exists for irradiation of a p-type material. With low irradiation doses when a change in the position of the Fermi level may be ignored, the dependence of $\Delta n = n_0 - n$ or $\Delta p = p_0 - p$ on the dose is linear (4.1): $\Delta n\ (\Delta p) = \pm K_{n(p)}\Delta\Phi$, where $K_{n(p)}$ is the coefficient of degradation of free charge carriers, characterizing the total number of radiation-induced electrically active defects.

Radiation-induced changes in the lifetime of non-equilibrium charge carriers, τ, are characterized by the degradation coefficient,

K_τ [2, 6]

$$1/\tau = 1/\tau_0 + K_\tau \Phi \tag{4.2}$$

where τ_0 and τ are the lifetimes before and after the irradiation, respectively; Φ is the irradiation dose. Relation (4.2) is true of low irradiation doses and its validity is supported by numerous experiments on materials and devices. The coefficient, K_τ, is determined by a set of produced disturbances, rates of their formation, depth and filling of the defect levels, capture cross-sections of electrons and holes.

As a general case, the following relation may be written for the coefficient K_τ [2]:

$$K_\tau = [N_A \sigma_d (E)\, \bar{\nu}(E)] \sum_{i=1}^{m} \eta_i (\sigma_{pi} \bar{\nu}_p f_{ni} + \sigma_{ni} \bar{\nu}_n f_{pi}) \tag{4.3}$$

where N_A is the concentration of atoms, cm^{-3}; $\sigma_d (E)$ is the cross-section for production of primary displacements; $\bar{\nu}(E)$ is the average number of atoms displaced by the primary recoil atoms; η_i is the rate of formation of the ith recombination center; σ_{pi} and σ_{ni} are the cross-sections of the capture of a hole or electron at the ith center; $\bar{\nu}_p$ and $\bar{\nu}_n$ are the average thermal movement speeds of the hole and electron; f_{ni} and f_{pi} are the functions of filling the centers with electrons and holes, independent of the position of the Fermi level relative to the energy level of the ith centers. The product taken in the square brackets characterizes the rate of formation of defects per unit flux of the incident radiation and depends both on the species and the energy of the bombarding particles. The product under the summation sign characterizes the recombination properties of radiation defects.

In the experiment, the values of $K_{n(p)}$ and K_τ are determined from the initial sections of the dose dependences, Δn $(\Delta p)/\Delta\Phi$ cm^{-1} and $[\Delta (1/\tau)]/\Delta\Phi$ $s^{-1} \cdot cm^2$, respectively.

Silicon. Figs. 4.1 through 4.23 and Tables 4.1 through 4.4 give the experimental evidence on changes in the concentration, mobility and lifetime of charge carriers in silicon samples of the n- and p-types irradiated with gamma-quanta, electrons, neutrons, protons and then annealed [1] through [27]. The figures and tables to this section use the following symbols: T—silicon grown by the Czochralski method; Z—silicon produced by zone refining; $\Delta (1/\tau)$—change in the value of the reciprocal of the lifetime of non-equilibrium charge carriers (proportional to the change in the concentration of recombination centers); I—intensity of the incident radiation flux; f—the share of defects that remain after annealing. For example, in investigation of the changes in the concentration of electrons on annealing $f = (n_0 - n_{\text{anneal}})/(n_0 - n_{\text{irrad}})$, where n_0, n_{irrad} and

Fig. 4.1. Electron concentration in *n*-type silicon (P) vs Co^{60} gamma irradiation dose [3].

Resistivity, ohm·cm: *1*—56; *2*—53; *3*—30; *4*—12; *5*—21. A silicon sample grown by Czochralski method (T), $T_{irrad} \cong 20$ °C; irradiation intensity $I = 1 \cdot 10^{12}$ $cm^{-2} \cdot s^{-1}$ (for curve *5*, the scale figures on the axes should be multiplied by 5)

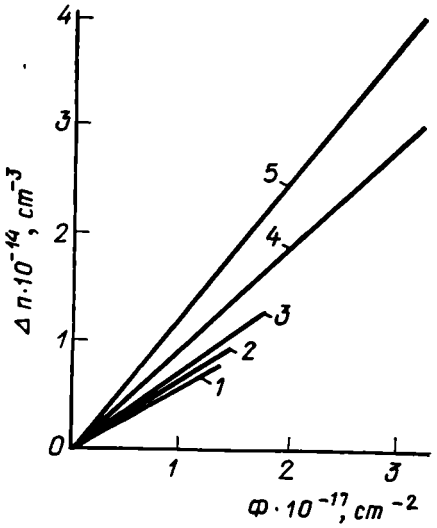

Fig. 4.2. Temperature dependence of electron mobility in silicon [3].

Irradiation dose, cm^{-2}: *1*—before irradiation; *2*—$6 \cdot 10^{17}$; *3*—$1.24 \cdot 10^{18}$; *4*—$1.66 \cdot 10^{18}$; *5*—$2.36 \cdot 10^{18}$. Silicon (T), phosphorus doped, $n_0 = 2.4 \cdot 10^{15}$, irradiated at $T_{irrad} \cong 20$ °C with gamma radiation from Co^{60}, $I = 1 \cdot 10^{12}$ $cm^{-2} \cdot s^{-1}$

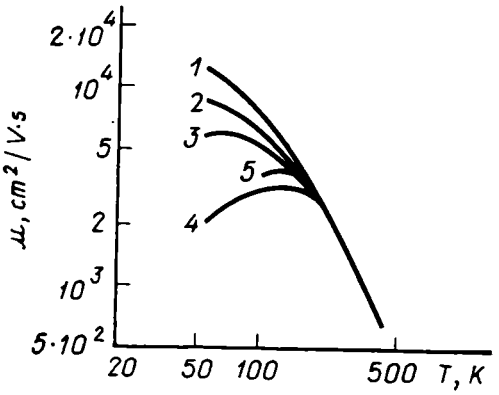

Fig. 4.3. Dose dependence of increments in the quantity reciprocal of lifetime [Δ (1τ)] in *n*-Si with different concentration of phosphorus and oxygen [4].

Resistivity (ohm·cm) and oxygen concentration (cm^{-3}), respectively: *1*—440 and $5 \cdot 10^{16}$; *2*—60 and $3 \cdot 10^{17}$; *3*—100 and $1 \cdot 10^{17}$; *4*—150 and $5 \cdot 10^{16}$; *5*—5000 and 10^{15}; *6*—2000 and 10^{15}; *7*—400 and 10^{16}; *8*—16 and 10^{16}. The samples were irradiated with gamma radiation from a Co^{60} source

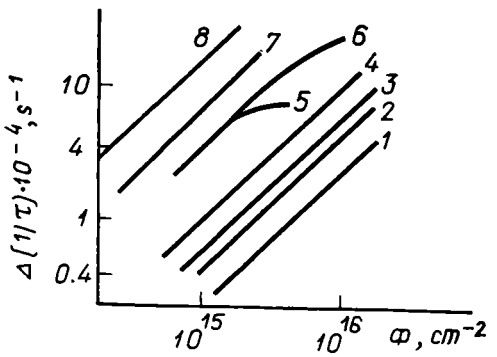

Fig. 4.4. Dose dependence of Δ (1/τ) increments in *n*-type silicon [5].

1 through *3*—silicon (T), phosphorus doped, ρ = 80 ohm·cm, dislocation density $N_d = 1.6 \cdot 10^3$ cm^{-2}, oxygen concentration $N_O = 6 \cdot 10^{17}$ cm^{-3}; *4*, *5*—silicon (Z), phosphorus doped, ρ = 80 ohm·cm, $N_d = 8.8 \cdot 10^3$ cm^{-2}. Irradiation intensity, $cm^{-2} \cdot s^{-1}$: *1*—$1.1 \cdot 10^{12}$; *2*—$2.7 \cdot 10^{11}$; *3*—$4.9 \cdot 10^{10}$; *4*—$1.1 \cdot 10^{12}$; *5*—$4.9 \cdot 10^{10}$. The samples were irradiated with gamma radiation from a Co^{60} source at $T_{irrad} = 20$ °C

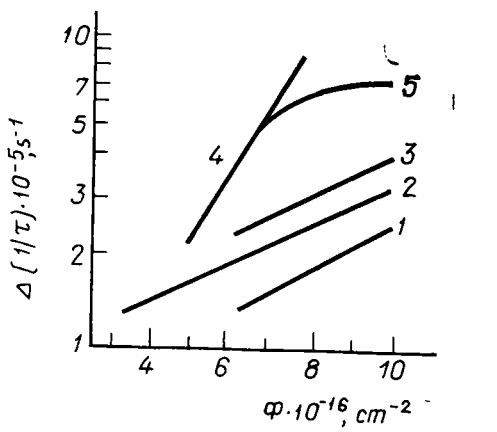

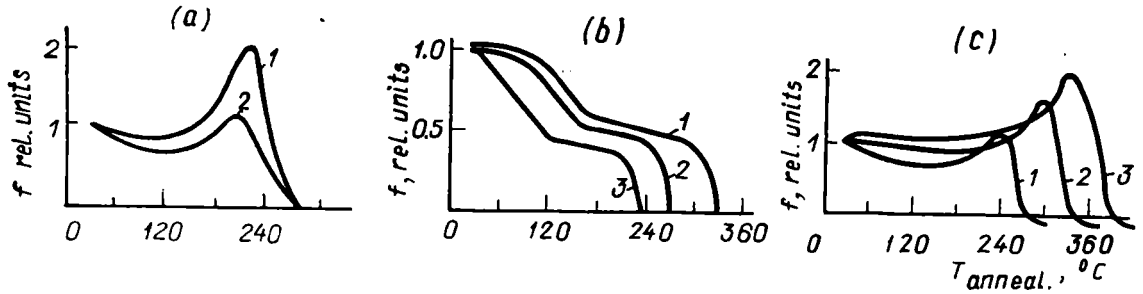

Fig. 4.5. Isochronal (10 min) annealing of $\Delta(1/\tau)$ in n-type silicon gamma radiated from Co^{60} source at $T_{irrad} \cong 20$ °C [5].

a—I, $cm^{-2} \cdot s^{-1}$: 1—$4.9 \cdot 10^{10}$, 2—$1.1 \cdot 10^{11}$; $\Phi = 4.8 \cdot 10^{16}$ cm^{-2}; silicon (T); b—I, $cm^{-2} \cdot s^{-1}$: 1, 3—$2.7 \cdot 10^{11}$, 2—$4.7 \cdot 10^{10}$; Φ, cm^{-2}: 1, 2—$3.84 \cdot 10^{16}$, 3—$1.4 \cdot 10^{17}$; silicon (Z), phosphorus doped, $\rho = 80$ ohm·cm, $N_d = 8.8 \cdot 10^{3}$ cm^{-2}; c—Φ, cm^{-2}: 1—$4.8 \cdot 10^{16}$, 2—$9.3 \cdot 10^{16}$, 3—$1.4 \cdot 10^{17}$; $I = 2.7 \cdot 10^{11}$ $cm^{-2} \cdot s^{-1}$; silicon (T)

Fig. 4.6. Hole removal rate vs carrier concentration in silicon [4].

Irradiation dose, cm^{-2}: 1—$2.3 \cdot 10^{17}$; 2—$2.3 \cdot 10^{18}$. Co^{60} gamma irradiation at $T_{irrad} = 20$ °C

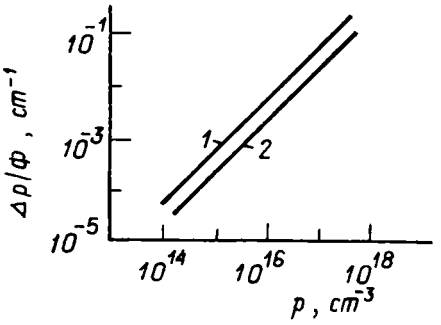

Fig. 4.7. Dose dependence of $\Delta(1/\tau)$ in p-type silicon with low oxygen content [4].

Resistivity, ohm·cm: 1—190; 2—230; 3—$4 \cdot 10^{4}$; 4—$2.6 \cdot 10^{4}$. Co^{60} gamma irradiation; irradiation intensity, $6 \cdot 10^{12}$ $cm^{-2} \cdot s^{-1}$

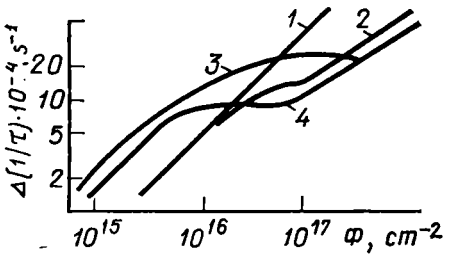

Fig. 4.8. Isochronal annealing of $\Delta(1/\tau)$ in p-type silicon [8].

Resistivity, ohm·cm: 1—17, dislocation density, $\approx 10^{4}$ cm^{-2}; 2—20, without dislocations. Irradiation dose, $1.6 \cdot 10^{16}$ cm^{-2}, Co^{60} gamma radiation

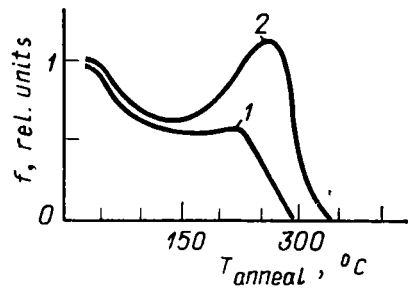

Fig. 4.9. Isochronal annealing of changes of concentration of holes in silicon with low oxygen content [4].

Concentration of holes, cm^{-3}: *1*—$5.4 \cdot 10^{13}$ (left-hand scale); *2*—$2.7 \cdot 10^{14}$ (right-hand scale). Irradiation dose, 10^{19} cm^{-2}. Co^{60} gamma irradiation

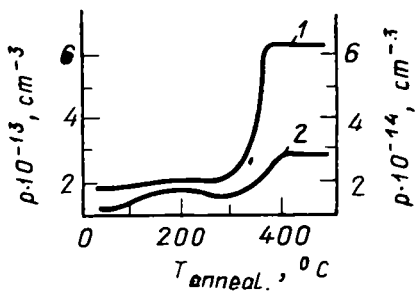

Fig. 4.10. Initial rates for carrier removal in *n*- and *p*-type silicon samples.

Irradiation with 4.5 MeV electrons at $T_{irrad} = 0$ °C: *1*—*p*-type silicon; *2*—*n*-type silicon. Plotted on the horizontal axis is the position of the Fermi level in the material: $E_C - E_F$ and $E_V + E_F$ for *n*- and *p*-type silicon samples, respectively. The chart uses the data of [12]

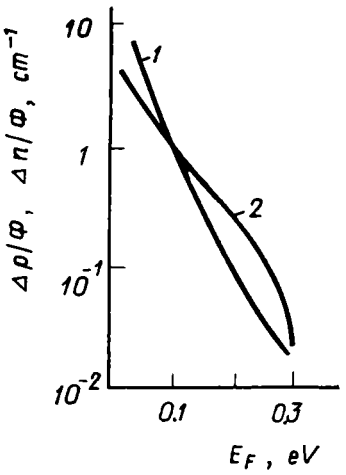

Fig. 4.11. Initial rates for carrier removal in *n*- and *p*-type silicon samples [10].

Energy of irradiation electrons, MeV: 2.5 (*1*, *1'*), 10 (*2*, *2'*), 30 (*3*, *3'*) and 100 (*4*, *4'*); *1'* through *4'*—*n*- and *p*-type silicon samples (T), $N_O \geqslant 6 \cdot 10^{17}$ cm^{-3}; *1* through *4*—same (Z), $N_O \leqslant 10^{16}$ cm^{-3}; *a*—*n*-type silicon; *b*—*p*-type silicon

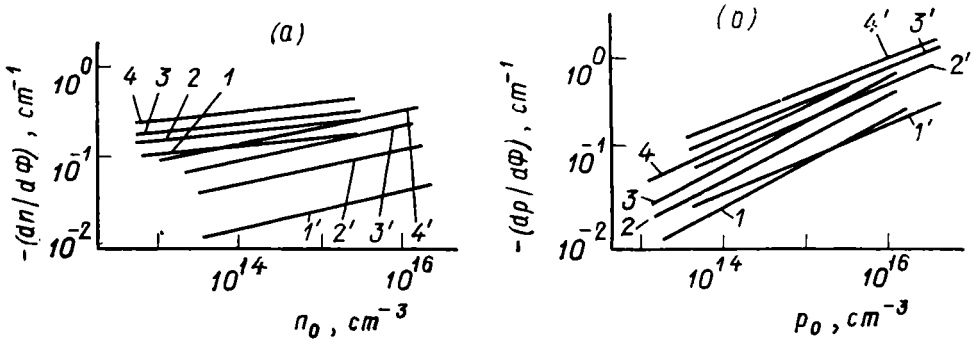

Fig. 4.12. Dose dependence of $\Delta(1/\tau)$ (*a*) and dependence of K_τ on resistivity (*b*) in *n*-type silicon (P) [11].

Resistivity, ohm·cm: *1*—0.3 to 5.5; *3*—15. Samples were irradiated with 4 MeV electrons

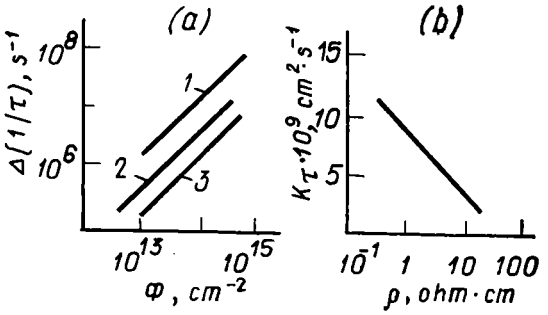

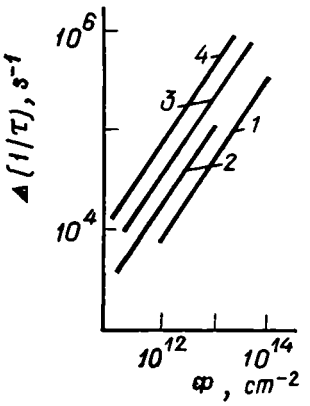

Fig. 4.13. Dose dependence of $\Delta(1/\tau)$ in n-type silicon [12].

Electron irradiation energy, MeV: *1*—2.5; *2*—10; *3*—30; *4*—100. Silicon (Z, T), phosphorus doped, $n_O = 7 \cdot 10^{13}$ cm^{-3}; oxygen concentration, $N_O \leqslant 10^{16}$ (Z) and $N_O = 4 \cdot 10^{17}$ (T); $T_{irrad} = 50$ °C

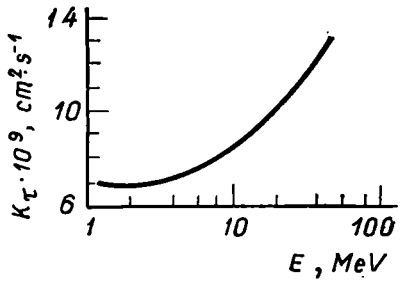

Fig. 4.14. Energy dependence of K_τ in n-type silicon [17].

Silicon (T), phosphorus doped, $\rho = 30$ ohm·cm

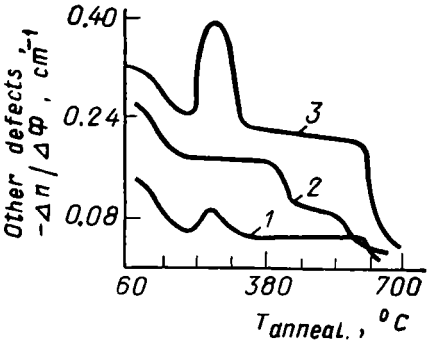

Fig. 4.15. Isochronal annealing of changes of electron concentration in silicon [16].

Irradiation temperature (K) and material: *1*—80, n-type silicon (T); *2*—80, n-type silicon (Z); *3*—97, n-type silicon (T). Resistivity $\rho = 10$ ohm·cm (300 K), phosphorus doped silicon. Temperature of measurement, 80 K. Samples were irradiated with 1.8 MeV electrons

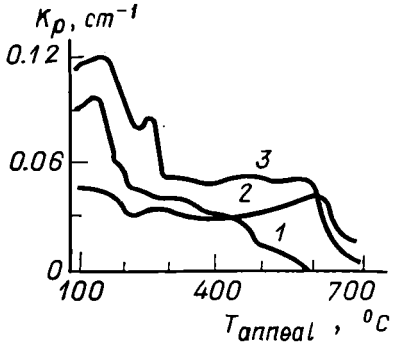

Fig. 4.16. Isochronal annealing of changes of hole concentration in p-Si (B) [16].

1—Si (for Lopex see [18]); *2*—Si (T); *3*—Si (Z). Measurement temperature, 80 K. Samples were 1.8 MeV electron irradiated at $T_{irrad} = 80$ K, $\rho = 10$ ohm·cm

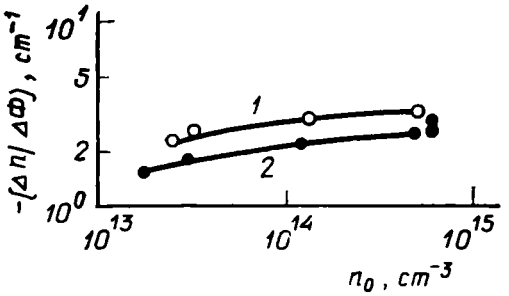

Fig. 4.17. Dependence of K_n in silicon on original electron concentration [22].

1—14.5 MeV; *2*—reactor ($\bar{E}$ = 1.7 MeV). *n*-type silicon, phosphorus doped (T), neutron irradiated at T_{irrad} = about 20 °C. The chart uses the data of [25]

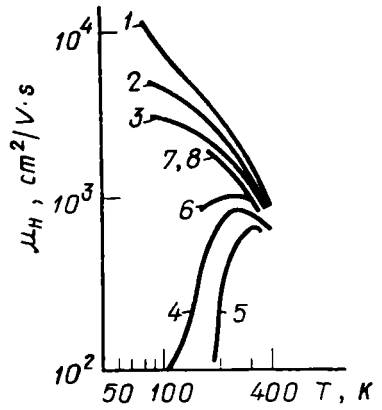

Fig. 4.18. Dependence of hall mobility on temperature for different irradiation fluxes [23].

Irradiation dose, $\Phi \cdot 10^{-14}$, cm^{-2}: *1*—0; *2*—2; *3*—3; *4*—6; *5*—7; *6*—9; *7*—12; *8*—37. Irradiation is by fast neutrons, T_{irrad} = 50 to 70 °C. Material: silicon БКЭФ-1

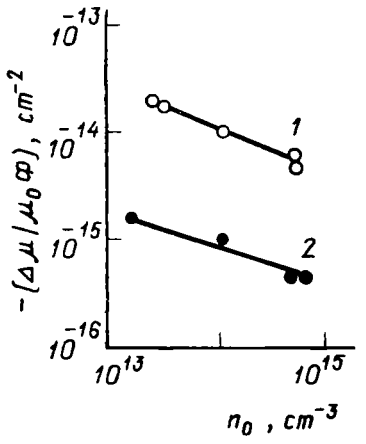

Fig. 4.19. A change in hall mobility of electrons upon irradiation vs initial electron concentration [22].

1—14.5 MeV; *2*—reactor ($\bar{E}$ = 1.7 MeV). *n*-type silicon, phosphorus doped (T), neutron irradiated at room temperature. The chart uses the data of [25]

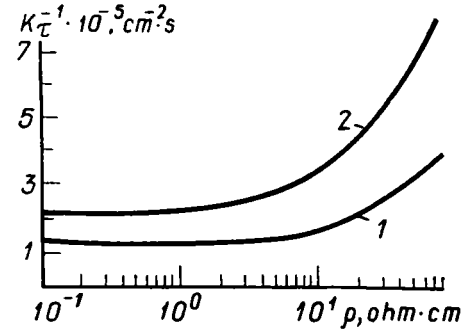

Fig. 4.20. Dependence of K_τ in *n*- and *p*-type silicon samples on resistivity [2].

1—*n*-Si; *2*—*p*-Si. Irradiation is by neutrons

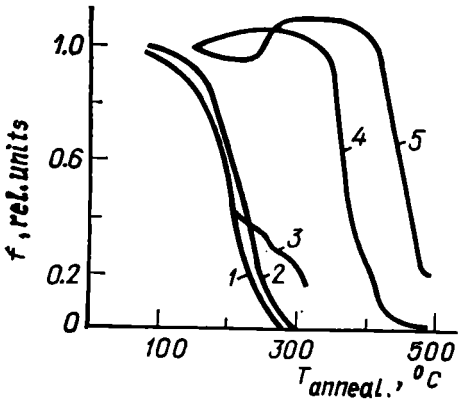

Fig. 4.21. Isochronal annealing of $\Delta(1/\tau)$ in silicon [21].

1, *2*—*n*-Si (Z) and (T), respectively; $\rho = 50$ ohm·cm, phosphorus doped, $\Phi = 2 \cdot 10^{10}$ cm^{-2}; *3*—*p*-Si (T), $\rho = 200$ [ohm·cm, boron doped, $\Phi = 2 \cdot 10^{10}$ cm^{-2}; *4*—*p*-Si (Z), $\rho = 150$ ohm·cm, boron doped, dislocation density $N_d = 1.8 \cdot 10^4$ cm^{-2}, $\Phi = 2.6 \cdot 10^{13}$ cm^{-2}; *5*—*p*-Si (T), $\rho = 200$ ohm·cm, boron doped at $N_d < 10^1$, $\Phi = 2.6 \cdot 10^{12}$ cm^{-2}. Irradiation is by fast neutrons at $I = 2 \cdot 10^{11}$ cm$^{-2} \cdot$s^{-1}, $T_{irrad} = 20$ °C

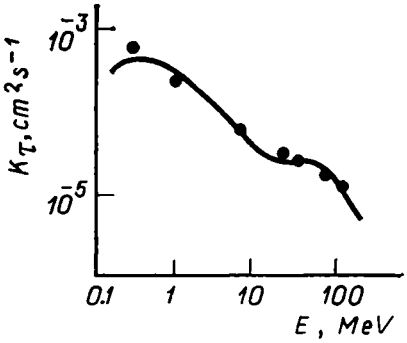

Fig. 4.22. Dependence of K_τ in *p*-type silicon on proton energy [24].

The dots show the experimental results, and the continuous curve, the theoretical assumptions

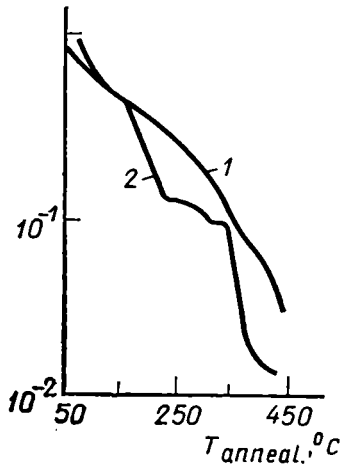

Fig. 4.23. Isochronal annealing of lifetime changes in *p*-type silicon [24].

Irradiation: *1*—protons, $E = 30$ MeV, $\Phi = 3 \cdot 10^{11}$ cm^{-2}; *2*—neutrons, $E = 14$ MeV, $\Phi = 10^{13}$ cm^{-2} (the reading on the ordinate axis is in relative units (f))

n_{anneal} are the concentrations of electrons before irradiation, after irradiation and after annealing, respectively. In a similar way you may write f for changes in the concentration of holes. For the lifetime of non-equilibrium carriers (τ), $f = (\tau^{-1}_{anneal} - \tau_0^{-1})/(\tau^{-1}_{irrad} - \tau_0^{-1})$, where τ_0, τ_{irrad} and τ_{annel} are the lifetimes before irradiation, after irradiation and after annealing, respectively.

From the above data it is obvious that the rates of change of the electrophysical parameters on irradiation are determined by the

Table 4.1

Degradation constants of carrier concentrations in silicon

Material	Carrier concentration N, cm^{-3}; resistivity ρ, ohm·cm	Irradiation technique	Irradiation (particle; energy E, MeV; intensity I, $cm^{-2} \cdot s^{-1}$; dose Φ, cm^{-2})	$K_{n(p)}$, cm^{-1}	References
n-Si (P)	$N = 2.4 \cdot 10^{15}$	T	γ (Co^{60}), $I = 1 \cdot 10^{12}$, $T_{irrad} = 300K$, $\Phi = 6 \cdot 10^{17}$-$2.36 \cdot 10^{18}$	(1.35-1.10) 10^{-2}	[3]
n-Si (P)	$4.3 \cdot 10^{14}$	T	Same, $\Phi = 1.1 \cdot 10^{17}$-$3.6 \cdot 10^{17}$	(9.5-9.2) 10^{-4}	[3]
n-Si (P)	$2.4 \cdot 10^{14}$	T	Same, $\Phi = 4.64 \cdot 10^{16}$-$6.6 \cdot 10^{17}$	(7.5-6.4) 10^{-4}	[3]
n-Si (P)	$1.4 \cdot 10^{14}$	T	Same, $\Phi = 2.81 \cdot 10^{16}$-$1.06 \cdot 10^{17}$	(7.1-6.4) 10^{-4}	[3]
n-Si (Sb)	$\rho = 13.7$	Z	γ (Co^{60})	$6 \cdot 10^{-4}$	[6]
n-Si (Sb)	2.5	Z	γ (Co^{60})	10^{-3}	[6]
n-Si (As)	1.01	Z	γ (Co^{60})	$2.3 \cdot 10^{-3}$	[6]
n-Si (As)	0.86	Z	γ (Co^{60})	$1.8 \cdot 10^{-3}$	[6]
p-Si (B)	7	T	γ (Co^{60}), $I = 1.0 \cdot 10^{12}$, $T_{irrad} = 300K$, $\Phi = 2.6 \cdot 10^{19}$	$\sim 10^{-4}$	[7]
p-Si (B)	16	T	Same, $\Phi = 1.5 \cdot 10^{19}$	$\sim 8.5 \cdot 10^{-5}$	[7]
p-Si (B)	180	T	Same, $\Phi = 9 \cdot 10^{17}$	$\sim 10^{-4}$	[7]
p-Si (B)	5	Z	Same, $\Phi = 5.8 \cdot 10^{19}$	$\sim 5 \cdot 10^{-5}$	[7]
p-Si (B)	15	Z	Same, $\Phi = 2.5 \cdot 10^{19}$	$\sim 2 \cdot 10^{-5}$	[7]
p-Si (B)	50	Z	Same, $\Phi = 7.1 \cdot 10^{18}$	$\sim 2 \cdot 10^{-5}$	[7]
p-Si (B)	500	Z	γ (Co^{60})	$8 \cdot 10^{-3}$	[6]
p-Si (B)	80	Z	γ (Co^{60})	$6 \cdot 10^{-3}$	[6]
p-Si (B)	12	Z	γ (Co^{60})	$1 \cdot 10^{-3}$	[6]
n-Si (P)	15	T	$\bar{e}$, $E = 0.7$	$1.1 \cdot 10^{-1}$	[6]
n-Si (P)	0.4	T	$\bar{e}$, $E = 0.7$	$3.5 \cdot 10^{-1}$	[6]
n-Si (P)	6.8	Z	$\bar{e}$, $E = 1.0$	$6 \cdot 10^{-1}$	[6]
n-Si (P)	16	—	$\bar{e}$, $E = 4.5$	$4 \cdot 10^{-1}$	[6]
n-Si (P)	0.5	—	$\bar{e}$, $E = 4.5$	$2.2 \cdot 10^{-1}$	[6]
p-Si	1.0	T	$\bar{e}$, $E = 0.7$	$8 \cdot 10^{-3}$	[6]
p-Si	0.1	T	$\bar{e}$, $E = 0.7$	$5.7 \cdot 10^{-1}$	[6]
p-Si (B)	10	T	$\bar{e}$, $E = 1.0$	$2.5 \cdot 10^{-2}$	[6]
p-Si (Al)	10	T	$\bar{e}$, $E = 1.0$	$2.5 \cdot 10^{-2}$	[6]
p-Si (Ga)	12	—	$\bar{e}$, $E = 1.0$	$1.4 \cdot 10^{-2}$	[6]
p-Si	10	—	$\bar{e}$, $E = 1.5$	$4 \cdot 10^{-2}$	[26]
p-Si	10	—	$\bar{e}$, $E = 1.7$	$7 \cdot 10^{-2}$	[26]

Table 4.1 Cont'd

Material	Carrier concentration N, cm^{-3}: resistivity ρ, ohm·cm	Irradiation technique	Irradiation (particle; energy E, MeV; intensity I, $cm^{-2} \cdot s^{-1}$; dose Φ, cm^{-2})	$K_{n(p)}$, cm^{-1}	References
p-Si	10	—	$\bar{e}$, $E=2.3$	5.10^{-2}	[26]
p-Si	10	—	$\bar{e}$, $E=4.5$	10^{-1}	[26]
p-Si	10	—	$\bar{e}$, $E=5$	$9 \cdot 10^{-2}$	[26]
p-Si	10	—	$\bar{e}$, $E=30$	$2.3 \cdot 10^{-1}$	[26]
p-Si (B)	100	T	n^0, fast, $I=2 \cdot 10^{11}$, $T_{irrad}=20°C$, $\Phi=2 \cdot 10^{12}$	12.5	[21]
p-Si (Al)	16	Z	n^0, fast, $\Phi=5 \cdot 10^{13}$	5-6	[21]
p-Si (Ga)	50	Z	Same	4	[21]
p-Si (B)	100	Z	n^0, fast, $\Phi=2 \cdot 10^{13}$	3	[21]
p-Si (B)	50	T	n^0, reactor, $E=1$	1.5	[6]
p-Si (B)	3.0	—	Same	5.6	[6]
p-Si (B, Ga)	43	T	Same	5.7	[6]
p-Si (Ga)	2.0	T	Same	2.95	[6]
p-Si (Al)	2.0	T	Same	3.19	[6]
n-Si (P)	100	Z	Same	2.6	[6]
n-Si (P)	10	Z	Same	4.0	[6]
n-Si (P)	1.0	T	Same	2.0	[6]
n-Si (P)	10	—	Same	9.1	[6]
n-Si (P)	500	Z	Same	11	[6]
n-Si (Sb)	2.0	Z	Same	1.98	[6]
n-Si (P)	100	Z	n^0, $E=14$	7.6 ± 0.2	[6]
n-Si (P)	10	Z	n^0, $E=14$	11.2 ± 0.1	[6]
p-Si (B)	30	T	p^+, $E=660$	17	[6]
p-Si (B)	8	T	p^+, $E=660$	42	[6]
n-Si (P)	192	T	p^+, $E=660$	9	[6]
n-Si (P)	24	T	p^+, $E=660$	44	[6]
p-Si	10	—	p^+, $E=30$	7	[26]

Note. $\bar{e}$–electrons; p–protons, n^0–neutrons; γ–gamma radiation.

impurity and defect inventory of the material, and by irradiation conditions (species of the particles, their energy, temperature and intensity of the irradiation). Specifically, one can conclude from the data on gamma irradiation [3-5] that the degradation constant, K_τ in n-Si increases with an increase in the concentration of phosphorus and decreases with a decrease in the concentration of oxygen (see Fig. 4.3 and Table 4.2). Sometimes, accumulation and annealing

Table 4.2

Degradation constants of non-equilibrium carrier lifetime in silicon

Material	Resistivity ρ, ohm·cm	Production technique; impurity content, cm^{-3}	Irradiation (particle; energy E, MeV)	K_τ, $cm^2 \cdot s^{-1}$	References
n-Si (P)	440	$N_O = 5 \cdot 10^{16}$	γ (Co^{60})	$2.3 \cdot 10^{-12}$	[4]
n-Si (P)	150	$N_O = 5 \cdot 10^{16}$	γ (Co^{60})	10^{-11}	[4]
n-Si (P)	100	T, $N_O = 1 \cdot 10^{17}$	γ (Co^{60})	$6 \cdot 10^{-12}$	[4]
n-Si (P)	60	T, $N_O = 3 \cdot 10^{17}$	γ (Co^{60})	$5 \cdot 10^{-12}$	[4]
n-Si (P)	$5 \cdot 10^3$	Z, $N_O = 10^{15}$	γ (Co^{60})	$4 \cdot 10^{-11}$	[4]
n-Si (P)	$2 \cdot 10^3$	Z, $N_O = 10^{15}$	γ (Co^{60})	$4 \cdot 10^{-11}$	[4]
n-Si (P)	400	Z, $N_O = 10^{16}$	γ (Co^{60})	$8 \cdot 10^{-11}$	[4]
n-Si (P)	16	Z, $N_O = 10^{16}$	γ (Co^{60})	$1.8 \cdot 10^{-10}$	[4]
p-Si (B)	20	T	γ (Co^{60})	$6 \cdot 10^{-12}$	[4]
p-Si (B)	80	Z	γ (Co^{60})	$5.5 \cdot 10^{-12}$	[4]
p-Si (B)	$5 \cdot 10^3$	Z	γ (Co^{60})	$1.3 \cdot 10^{-11}$	[4]
p-Si (B)	190	Extra pure	γ (Co^{60})	$5.2 \cdot 10^{-12}$	[4]
p-Si (B)	320	Same	γ (Co^{60})	$5.2 \cdot 10^{-12}$	[4]
p-Si (B)	$2.6 \cdot 10^3$	Same	γ (Co^{60})	$1.4 \cdot 10^{-11}$	[4]
p-Si (B)	$4 \cdot 10^4$	Same	γ (Co^{60})	$2.1 \cdot 10^{-11}$	[4]
n-Si	1	Z	$\bar{e}$, 3	$6 \cdot 10^{-8}$	[15]
n-Si	1	Z	$\bar{e}$, 3	$3 \cdot 10^{-7}$	[15]
n-Si	1	T	$\bar{e}$, 3	$1.5 \cdot 10^{-7}$	[15]
n-Si	10	Z	$\bar{e}$, 3	$2 \cdot 10^{-8}$	[15]
n-Si	10	T	$\bar{e}$, 3	$1 \cdot 10^{-9}$	[15]
p-Si	10	—	$\bar{e}$, 1,5	$3 \cdot 10^{-9}$	[26]
p-Si	10	—	$\bar{e}$, 1.7	$3.5 \cdot 10^{-9}$	[26]
p-Si	10	—	$\bar{e}$, 2.3	$4.5 \cdot 10^{-9}$	[26]
p-Si	10	—	$\bar{e}$, 5.0	$1.5 \cdot 10^{-8}$	[26]
p-Si	10	—	$\bar{e}$, 30	$5.5 \cdot 10^{-8}$	[26]
p-Si	1	Z	$\bar{e}$, 3	$1 \cdot 10^{-8}$	[15]
p-Si	1	T	$\bar{e}$, 3	$(2\text{-}8) \cdot 10^{-8}$	[15]
p-Si	10	T	$\bar{e}$, 3	$0.5 \cdot 10^{-8}$	[15]
p-Si	10	Z	$\bar{e}$, 3	$2 \cdot 10^{-8}$	[15]
p-Si	100	Z	$\bar{e}$, 3	$(3\text{-}8) \cdot 10^{-9}$	[15]
n-Si (P)	6	—	n^0, reactor	$5.8 \cdot 10^{-6}$	[2]
n-Si (P)	16	T	Same	$1.3 \cdot 10^{-6}$	[4]
n-Si (P)	250	T	Same	$5 \cdot 10^{-7}$	[4]
n-Si (P)	$2 \cdot 10^3$	T	Same	$4.2 \cdot 10^{-7}$	[4]
n-Si (P)	$5 \cdot 10^3$	T	Same	$3.2 \cdot 10^{-7}$	[4]

Table 4.2 Cont'd

Material	Resistivity ρ, ohm·cm	Production technique; impurity content, cm^{-3}	Irradiation (particle; energy E, MeV)	K_τ, $cm^2 \cdot s^{-1}$	References
n-Si (P)	1.0	—	n^0, reactor, ~1.0	$1 \cdot 10^{-5}$	[15]
n-Si (P)	10	—	Same	$6 \cdot 10^{-6}$	[15]
n-Si (P)	100	—	Same	$1 \cdot 10^{-5}$	[15]
n-Si	1.0	—	p^+, 20	$5 \cdot 10^{-6}$	[15]
n-Si	10.0	Z	p^+, 20	$5 \cdot 10^{-6}$	[15]
n-Si	10.0	T	p^+, 20	10^{-6}	[15]
p-Si	1.0	—	p^+, 20	$(1-3) \cdot 10^{-5}$	[15]
p-Si	10	—	p^+, 20	$5 \cdot 10^{-6}$	[15]
n-Si (P)	123	T	p^+, 3000	$1.7 \cdot 10^{-6}$	[6]
n-Si (P)	190	T	p^+, 3000	10^{-6}	[6]
p-Si	10	—	p^+, 30	$5 \cdot 10^{-6}$	[26]

Note. For explanation of symbols, see Table 4.1.

[5] of radiation-induced recombination centers in *n*-type silicon on gamma irradiation depends on the intensity of the irradiation (see Figs. 4.4, 4.5*a*, *b*). The annealing of the changes, τ, (see Figs. 2.10 and 4.5*a*, *b*, *c*) in *n*-Si has indicated an increase in the activation energies of the anneal stages with a growth of the covalent radius of the doping impurity and a rise in the annealing temperature with an increase in the gamma radiation dose [3-5]. The rate of decrease in the concentration of electrons, K_n, drops with a decrease in the concentration of the doping impurity (see Fig. 4.1 and Table 4.1) [3].

Irradiation of *p*-type boron doped silicon with gamma-quanta (Co^{60}) and its subsequent annealing have shown an increase in the concentration of holes above the initial (before irradiation) value (see Table 4.3). The authors of [4] associate this fact with dissolu-

Table 4.3

Hole concentration increment (cm^{-3}), Δp, in boron doped silicon after irradiation and annealing versus initial carrier concentration p_0 [4]

p_0	p_1	Δp
$7 \cdot 10^{12}$	$6.1 \cdot 10^{13}$	$5.4 \cdot 10^{13}$
$1.5 \cdot 10^{13}$	$2.85 \cdot 10^{14}$	$2.7 \cdot 10^{14}$
$2 \cdot 10^{13}$	$9 \cdot 10^{14}$	$8.8 \cdot 10^{14}$

Note. p_0, p_1 – hole concentrations before irradiation, after irradiation and annealing, respectively; $\Delta p = p_1 - p_0$.

tion of the interstitial boron in the vacancies liberated during annealing out of the radiation defects, which confirms the view according to which the irradiation stimulates the processes "frozen" during the crystal growing (see Sec. 2.3).

A decrease in the concentration of holes in p-Si with an increase in the dose of gamma radiation is of non-linear nature and depends on the initial concentration of charge carriers [4]. The value of constant K_p grows with an increase in the degree of material doping and drops with an increase in the irradiation dose [4] (see Fig. 4.6). The authors of [4] also note a small dependence of K_τ in p-Si on the crystal growing technique (see Table 4.2). Nevertheless, the annealing of $\Delta(1/\tau)$ (see Fig. 4.8) has shown that the value of τ in the samples with great density of dislocations recovers more rapidly [4, 8].

Fig. 4.7 shows a dose dependence of $\Delta(1/\tau)$ in p-Si with a low oxygen content [4, 9]. It is a characteristic feature of this material that irradiation thereof with gamma rays resulted in disappearance of the resistivity gradients and in a stable (with respect to annealing) increase in mobility [9].

Fairly extensive reviews of changes on the concentration and mobility of the majority carriers, lifetime of non-equilibrium carriers in n- and p-type silicon samples [10 through 16] are available. The results of the investigations are presented in Fig. 1.3*a*, *b*; 1.4; 4.7 through 4.13 and in Tables 4.1, 4.2 and 4.3. The authors of [10] used a wide range of n- and p-type materials that proved to be helpful in determining the initial rate of removal of charge carriers over an electron energy range of 2.5 to 100 MeV:

$$-(dn/d\Phi)_0 = K_n n_0 = n_0^{1-\gamma}/C$$

$$-(dp/d\Phi)_0 = K_p p_0 = p_0^{1-\gamma}/C.$$

The values of C and γ were obtained from comparison with the experimental data (see Fig. 4.13 and Table 4.4). Any changes in

Table 4.4

Calculated values of coefficients γ and C [10]

Growing method	Electron energy, MeV	n-Si		p-Si		Growing method	Electron energy, MeV	n-Si		p-Si	
		γ	C	γ	C			γ	C	γ	C
Z	2.5	0.75	$1.6\cdot10^5$	0.60	$1.4\cdot10^7$	Z	30	0.75	$1.8\cdot10^4$	0.60	$2.8\cdot10^6$
T		0.90	$8.8\cdot10^1$	0.51	$3.1\cdot10^8$	T		0.90	$4.8\cdot10^1$	0.51	$1.2\cdot10^8$
Z	10	0.75	$3.9\cdot10^4$	0.60	$4.5\cdot10^6$	Z	100	0.80	$2.5\cdot10^3$	0.65	$3.4\cdot10^5$
T		0.90	$5.9\cdot10^1$	0.51	$1.8\cdot10^8$	T		0.93	$2.1\cdot10^1$	0.51	$6.6\cdot10^7$

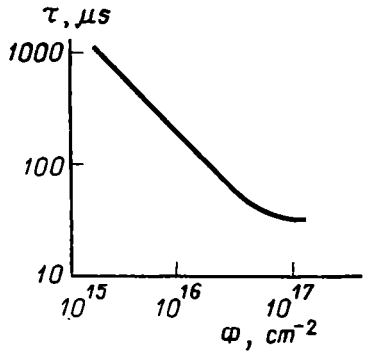

Fig. 4.24. Changes in lifetime of non-equilibrium carriers vs irradiation dose [35].
Co^{60} gamma irradiation, $T_{irrad} = 77$ K. Material: germanium of n-type, antimony doped, $\rho = 16$ ohm·cm, $T_{meas} \cong 300$ K

mobility (at $T_{irrad} = 300$ K) begin to tell for high irradiation doses of electrons [1]. From the investigation of τ when using electron irradiations of varying energies, the authors of [12] have deduced that the A-center is a dominating recombination center in oxygen-containing and oxygen-free n-type silicon samples (see Fig. 4.11). A rise of electron energy above 10 MeV sharply increases the value of $K\tau$ in n-Si (see Fig. 4.14), the fact attributed to the emergence of DR-type defects [13].

The results of electron irradiation of silicon depend on the intensity of the irradiation [14]. Isochronal annealing (see Figs. 1.4, 2.9, 4.15, 4.16) has shown that the changes in the lifetime and concentration of the charge carriers on electron irradiation are determined by defect complexes, such as V-O, V-P, V-V, and V-B (see Secs. 1.2 and 2.2).

Irradiation of silicon with neutrons and high-energy protons results in greater changes in the concentration and mobility of electrons and holes, as well as in the lifetime, τ (see Figs. 4.17 through 4.23 and Tables 4.1 and 4.2) [17-25], which is caused by emergence in the crystal, along with point defects, of large defect complexes such as DRs (see Sec. 1.3). Presence of DRs leads to an anomalous temperature dependence of the charge carrier mobility (see Fig. 4.18) [6, 17, 18]. The annealing of changes in the electrophysical parameters after neutron or proton irradiation has a complex nature and depends on the dose and energy of irradiation, and defect inventory of the material (see Fig. 1.4, 4.21, 4.23) [17, 18, 24, 25]. The typical feature is the temperatures used for complete annealing out of defects. These temperatures are normally higher than those used in electron and gamma irradiations. Sometimes the annealing has a stepless nature (see Sec. 1.3).

The influence of high-energy proton irradiation on the properties of germanium and silicon is investigated in detail in [6].

Germanium. The changes in the electrophysical parameters of germanium on irradiation with various particles have been investigated in numerous papers [29 through 37]; the results have been summerized in some reviews [6, 17, 27, 28].

Table 4.5

Degradation constants of carrier concentration in germanium

Material	Concentration of electrons or holes, N, P, cm^{-3}; resistivity ρ, ohm·cm	Irradiation (particle; energy E, MeV; T_{irrad}, K)	$K_{n\,(p)}$, cm^{-1}	References
n-Ge	$N = 6 \cdot 10^{13}$-$8 \cdot 10^{15}$	γ (Co^{60}); $T_{irrad} = 293$	$-(0.52\text{-}2) \cdot 10^{-3}$	[6]
n-Ge	$N = 10^{14}$-10^{15}	γ (Co^{60}), $T_{irrad} = 310$	$-5 \cdot 10^{-4}$	[6]
p-Ge	$P = 2 \cdot 10^{2}$	γ (Co^{60}), $T_{irrad} = 293$	$+10^{-4}$	[6]
n-Ge	$N = 3 \cdot 10^{13}$-$1.5 \cdot 10^{14}$	$\bar{e}$, $E = 1$, $T_{irrad} = 293$	-0.13	[6]
p-Ge	$P = 1.5 \cdot 10^{15}$	$\bar{e}$, $E = 1$, $T_{irrad} = 80$	$+0.07$	[6]
p-Ge	$P = 1 \cdot 10^{13}$	$\bar{e}$, $E = 1$, $T_{irrad} = 293$	$+10^{-2}$	[6]
n-Ge	$N = 2 \cdot 10^{15}$	$\bar{e}$, $E = 2.5$, $T_{irrad} = 293$	-0.07	[6]
n-Ge	$N = 5 \cdot 10^{13}$-$3 \cdot 10^{17}$	$\bar{e}$, $E = 28$, $T_{irrad} = 293$	-0.4	[6]
n-Ge	$N = 10^{14}$-10^{16}	n^0, reactor, $E = 1$	-3.2	[2]
p-Ge	$P = 10^{13}$-10^{15}	Same	$+0.13$	[2]
n-Ge	$N = 10^{13}$	n^0, $E = 4\text{-}5$, $T_{irrad} = 300$	-10	[2]
n-Ge	$N = 10^{13}$	n^0, $E = 14$, $T_{irrad} = 300$	-12	[2]
n-Ge	$\rho = 1.0$	n^0, reactor	-3.3	[2]
n-Ge	2.0	Same	-8.0	[2]
n-Ge	1.6	Same	-3.6	[2]
n-Ge	5.0	Same	-3.2	[2]
p-Ge	1.0	Same	$+0.13$	[2]
p-Ge	7.0	Same	$+0.15$	[2]
p-Ge	33.0	Same	$+0.13$	[2]
n-Ge	$N = 10^{15}$	p^+, $E = 660$, $T_{irrad} = 300$	-10^{2}	[6]
p-Ge	$P = 10^{15}$	p^+, $E = 660$, $T_{irrad} = 300$	$+10^{2}$	[6]

Note. For explanation of symbols, see Table 4.1.

Table 4.6

Values of K_τ in n-type germanium (Sb) irradiated with 3000 MeV protons [6]

Resistivity, ρ ohm·cm	K_τ, $cm^2 \cdot s^{-1}$	Resistivity ρ, ohm·cm	K_τ, $cm^2 \cdot s^{-1}$
6.0	$1.08 \cdot 10^{-7}$	27.0	$2.12 \cdot 10^{-8}$
15.0	$3.42 \cdot 10^{-8}$	65.0	$1.08 \cdot 10^{-8}$

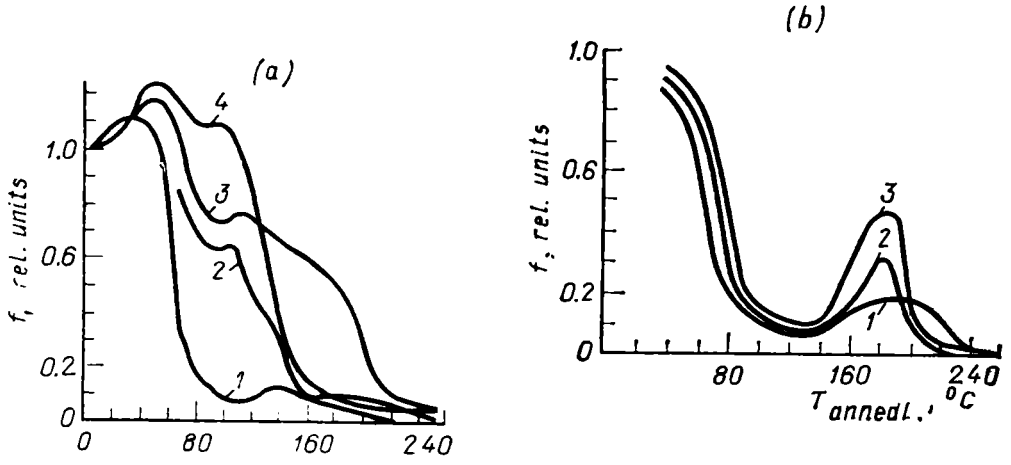

Fig. 4.25. Isochronal annealing of $\Delta(1/\tau)$ in Co^{60} gamma irradiated germanium ($T_{irrad} = 77$ K) [35].
a—ρ, ohm·cm: *1*—1.6; *2*—10.2; *3*—16; *4*—6.05; antimony doped germanium; *b*—ρ, ohm·cm; *1*—2.6; *2*—11.1; *3*—4.9; arsenic doped germanium. Measurement temperature, 300 K

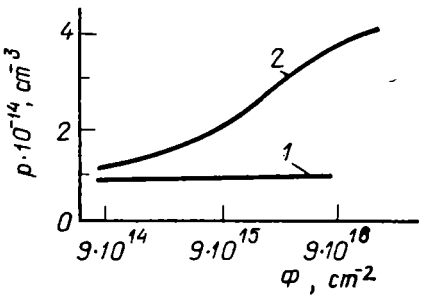

Fig. 4.26. A change in hole concentration in gallium doped germanium vs irradiation dose [27].
1—ingot 1; *2*—ingot 2. Resistivity, about 25 ohm·cm. Irradiation is by 3.5 MeV electrons at $T_{irrad} \simeq 20$ °C

The behaviour of germanium on irradiation is much similar to that of silicon. As with silicon, with germanium the irradiation conditions (intensity, temperature, species and energy of the particles) and defect inventory of the crystals determine the changes in the parameters (Figs. 4.24 through 4.27 and Tables 4.5 and 4.6). Irradiation of *n*-type germanium reduces the concentration of electrons; at a certain dose, *n-p* conversion is observed. In *p*-type germanium irradiated with electrons and gamma rays, the concentration of holes may either stay unchanged or even increase (see Fig. 4.26) [27]. The changes in the concentration of free charge carriers in *p*-type germanium are not so intensive as in *n*-type germanium (irradiation with electrons and gamma rays). The annealing out of the changes in the lifetime of charge carriers in germanium is shown in Fig. 4.25*a*, *b* [36]. For germanium of *n*-type, irradiated with electrons or gamma rays at room temperature, the concentration is recovered in three stages: about 80, 140 and 270 °C [27] (see also Fig. 2.13). Irradiation of germanium with neutrons and protons is characterized with high

values of K_τ and $K_{n(p)}$ (see Fig. 4.27 and Tables 4.5 and 4.6) [6, 17, 18].

Of practical interest is the behaviour of the A_3B_5 compounds, such as gallium arsenide and indium antimonide. A large number of papers are dedicated to the investigation of the properties of irradiated GaAs and InSb [38 through 55]. Let us discuss the results achieved by some of the authors (Figs. 4.28 through 4.34, Table 4.7).

Table 4.7

Parameters of GaAs samples versus kind of irradiation [40] (to Fig. 4.30)

n_0, cm^{-3}	Master alloy	Mobility, cm^2/V·s	Kind of irradiation
$1 \cdot 10^{18}$	Te	1 600	γ, n^0, 2.5; 12; 100
$8 \cdot 10^{18}$	Sn	1 800	γ, n^0, 12
$6.2 \cdot 10^{18}$	Te	2 000	γ, 2.5
$4 \cdot 10^{18}$	Te	2 200	γ, n^0, 2.5; 12; 100
$3.7 \cdot 10^{18}$	Te	2 310	12
$3 \cdot 10^{18}$	S	1 520	γ, n^0, 2.5
$2.6 \cdot 10^{18}$	Te	2 600	γ, n^0, 2.5; 10; 12; 14; 17; 20; 23; 29; 100
$1.95 \cdot 10^{18}$	Sn	2 300	γ, n^0, 2.5; 12; 100
$1.8 \cdot 10^{18}$	Se	2 290	γ, 2.5
$1.45 \cdot 10^{18}$	Si	2 300	γ, 2.5; 100
$1.3 \cdot 10^{18}$	Si	2 500	γ, n^0, 2.5; 100
$8 \cdot 10^{17}$	Si	26 500	γ, n^0, 2.5; 100
$6 \cdot 10^{17}$	Ge	1 400	γ, n^0, 2.5; 10; 12; 14; 17; 20; 23; 29; 100
$5 \cdot 10^{17}$	Sn	3 300	γ, n^0, 2.5; 12; 100
$3.2 \cdot 10^{17}$	S	3 500	γ, 2.5; 12
$2.6 \cdot 10^{17}$	Se	3 800	γ, n^0, 2.5; 12
$1.8 \cdot 10^{17}$	Non-doped	4 650	γ, n^0, 2.5; 12; 100
$1.0 \cdot 10^{17}$	Same	4 900	2.5

Note. $T_{meas} = 300$ K; n^0 — neutrons; Co^{60} gamma irradiation. The figures in the last column indicate the electron energy (MeV).

Gallium arsenide. A substantial difficulty that complicates a detailed study of the radiation processes in gallium arsenide is its contamination with impurities, which is higher than in germanium and silicon. Irradiation of GaAs with gamma rays, electrons and protons results in a compensation of conductivity (see Figs. 4.28,

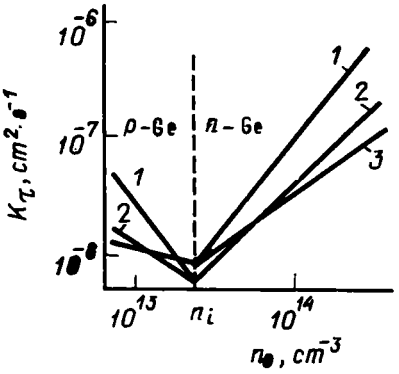

Fig. 4.27. Dependence of K_τ on concentration of original impurities in germanium [6].
Irradiation is by 207 (*1*), 590 (*2*) and 3000 (*3*) M V protons

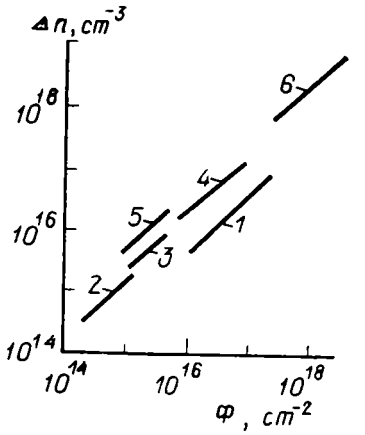

Fig. 4.28. Dose dependence of changes in concentration of electrons in gallium arsenide [38].
Electron concentrations in samples, n_0, cm^{-3}: *1*—$4 \cdot 10^{16}$ to $5 \cdot 10^{17}$; *2*—$7 \cdot 10^{15}$; *3*—$9 \cdot 10^{15}$; *4*—$2 \cdot 10^{17}$; *5*—$2.5 \cdot 10^{16}$; *6*—$6 \cdot 10^{18}$. Irradiation is by 1-MeV electrons. Carrier removal rate, K_n = 0.5 to 5 cm^{-1}

4.32 and 4.33). However, with higher doses of neutrons and protons, the experimenter observes an increase in the material conductivity, which is associated with various mechanisms arising from overlapping of defects of the DR type [39, 43, 56]. A study of the degradation of the non-equilibrium carrier lifetime [38, 40, 47] has revealed no marked influence of the kind and concentration of the doping impurity on the results of irradiation [38, 40]. Nevertheless, the energy spectrum of the levels after the irradiation is discernible in the material of *n*- or *p*-type (see Table 4.12). To elucidate the role of chemical impurities in the radiation-induced complexing of GaAs, further investigations are required.

A comparison of the values of the degradation constants of the charge carrier lifetimes in proton irradiated GaAs and Si has shown that in GaAs this value is about 27 times that of silicon [47].

A great width of the energy gap in GaAs should promote a higher intensity of the processes involving non-equilibrium electrons and holes arising in the course of irradiation. In [45], the authors note that a pulsed nature of electron irradiation to a density of 30 A/cm^2 drastically changed the inventory of the radiation-induced defects.

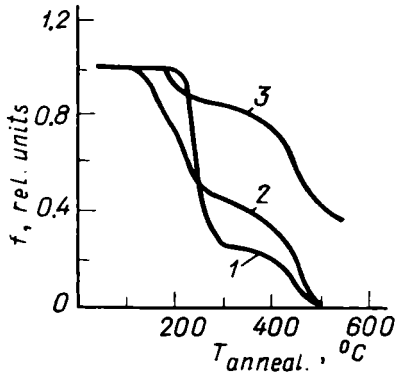

Fig. 4.29. Annealing stages in irradiated Gallium Arsenide [38].
1, *3*—*n*-GaAs; *2*—*p*-GaAs. Irradiation is by 1 MeV electrons, $\Phi = 10^{17}$ cm^{-2} (*1*, *2*) and by fast neutrons, $\Phi = 10^{15}$ cm^{-2} (*3*)

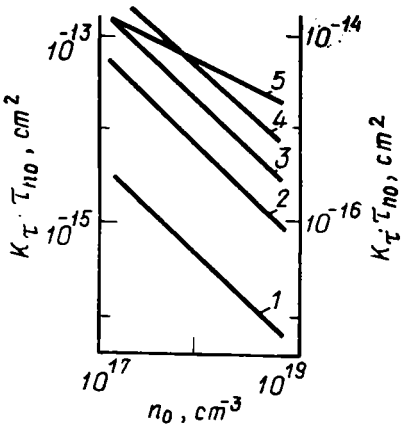

Fig. 4.30. Dependence of $K_\tau \tau_{n0}$ on concentration of electrons, n_0, in gallium arsenide samples [40].
Irradiation: *1*—Co^{60} gamma irradiation (the scale is to the right; *2-4*—2.5, 12- and 100-MeV electrons, respectively; *5*—fast neutrons. For irradiation parameters, see Table 4.7

Specifically, the rate of removal of the charge carriers proved to be 1.5-2 orders of magnitude lower than in irradiation with a continuous beam of low intensity, while the defects introduced were unstable at room temperature.

The steps in annealing out the defects are shown in Fig. 4.29 [38]. The annealing stages for GaAs have been set at about 150, 250, and 470 °C when electron irradiated and at about 230 and 450 °C when neutron irradiated [38]. The annealing of the changes in the lifetime of the non-equilibrium charge carriers after the proton irradiation in *p*-GaAs is practically stepless and is completed at 400 °C; the annealing temperature becomes somewhat higher as the proton dose is increased [47].

Indium antimonide. At present, the purity of the crystals of InSb available is as high as that of Ge and Si. However, the radiation effects in indium antimonide have become the subject of investigation very recently [44, 49-55].

The authors of [49] have investigated the influence of fast neutron irradiation on *n*- and *p*-InSb with a concentration of charge carriers equal to 10^{12}-10^{15} cm^{-3} at 78 K. The irradiation was performed at 78,

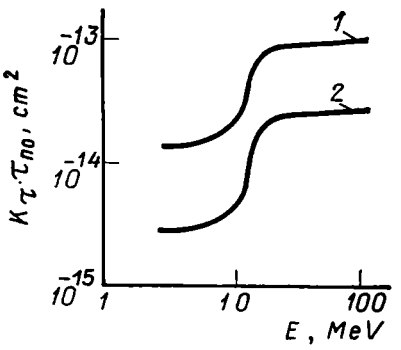

Fig. 4.31. Dependence of $K_\tau \tau_{n0}$ in GaAs on electron energy [40].
Electron concentration in samples, n_0, cm^{-3}: *1*—$6 \cdot 10^{17}$ (Ge); *2*—$2.6 \cdot 10^{18}$ (Te)

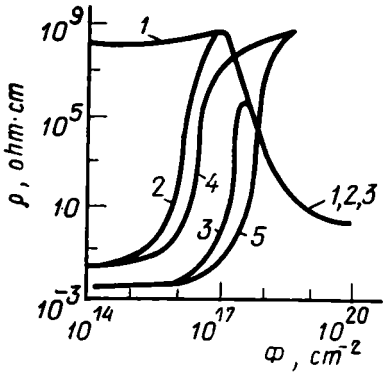

Fig. 4.32. Dependence of gallium arsenide resistivity on irradiation dose [39].
1-3—fast neutron irradiation; *4*, *5*—2 MeV electron irradiation

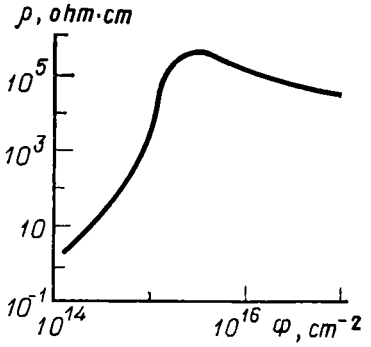

Fig. 4.33. Dependence of *p*-type gallium arsenide resistivity on proton irradiation dose [43].
Proton energy, 300 keV; hole concentration in original sample, $2 \cdot 10^{19}$ cm^{-3}

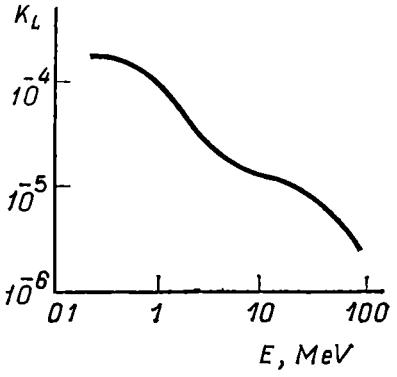

Fig. 4.34. Dependence of minority carrier diffusion length degradation constant on proton energy (*p*-GaAs) [47].

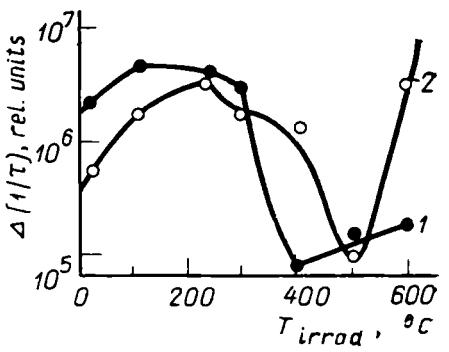

Fig. 4.35. Dependence of $\Delta(1/\tau)$ in silicon on irradiation temperature [59].
1—КЭФ-4,5 (Т); *2*—КДБ-4,5 (Т). Irradiation dose, 10^{15} cm^{-2}; electron energy, 1.7 MeV

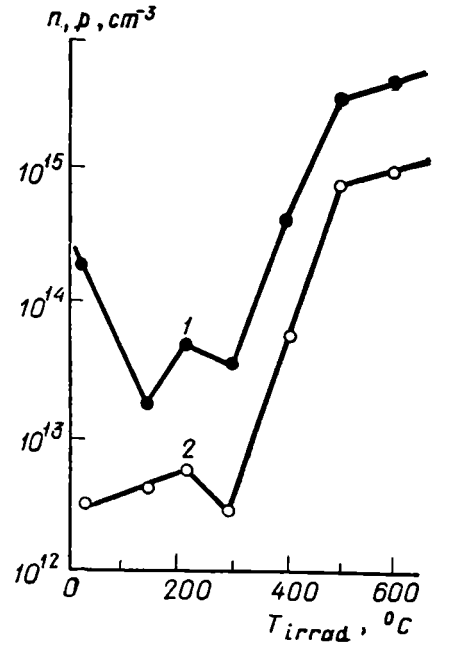

Fig. 4.36. Change of carrier concentration with irradiation temperature in *n*- and *p*-type silicon samples [59].
1—КЭФ-4,5 (Т); *2*—КДБ-4,5 (Т). Irradiation dose, 10^{17} cm^{-2}; electron energy, 1.7 MeV

300, and 330 K. Then the results of the isochronal annealing were studied. The subsequent measurements revealed *n-p* conversion. It proved impossible, however, to fully recover the original properties by annealing.

The authors of [50, 51] electron irradiated *n*- and *p*-InSb samples at 7 and 50 MeV. The results of the experiments have indicated that both decrease and recovery of the concentration of carriers were not associated with introduction and annealing out of balancing defects and were stemming from a loss, during the formation of the defect complexes, of electrical activity of the impurity centers. It was noted that irradiation of *p*-InSb with 50 MeV electrons resulted in conductivity conversion [51]. During the recovery of the concentration of carriers the annealing revealed steps of about 300, 380 and 480 K after neutron irradiation [49] and 160, 270 and 380 K after electron irradiation [50, 51].

Silicon carbide is another promising semiconductor where further studies of the radiation processes are required. Because of its high thermal and radiation stability, silicon carbide is used at present as a suitable material for radiators and high-temperature counters of nuclear particles [57]. The basic evidence on the influence of the irradiation on the properties of SiC has been received by optical, luminescent and electrophysical methods [57, 58].

In Ch. 2 it was shown that by changing the irradiation conditions one could control the defect formation rates. A detailed analysis of the changes in the electrical and photoelectrical parameters on high-temperature irradiation of germanium and silicon is given in [27, 59] and [60]. Figs. 4.35, 4.36 and Tables 4.8 and 4.9 present, as examples, the changes in the lifetime and concentration of carriers in silicon and germanium versus electron irradiation temperature. Let us note that an increase in the temperature enhances the stability of the radiation-induced changes in the electrophysical parameters, and a decrease in the threshold energy value, caused by a tempera-

Table 4.8

Degradation constant of non-equilibrium carrier lifetime, K_τ, in silicon versus irradiation temperature

T_{irrad}, °C	$K_\tau \cdot 10^9$, $cm^2 \cdot s^{-1}$			
	КДБ-1	КДБ-7,5	КЭФ-1	КЭФ-25
20	1.0	3.0	11.0	10.5
50	3.2	3.0	13.0	4.0
80	3.6	1.6	8.0	6.0
100	5.3	2.2	15.0	6.2
150	4.0	4.0	6.5	5.1

Table 4.9

Degradation constant of carrier concentration, K_n (K_p), in silicon versus irradiation temperature

T_{irrad}, °C	K_p, cm^{-1}		K_n, cm^{-1}	
	КДБ-1	КДБ-7,5	КЭФ-1	КЭФ-25
20	9.6	24.0	0.08	0.01
50	53.0	8.4	0.06	0.01
80	48.0	10.0	—	0.03
100	22.0	8.4	0.073	0.02
150	9.2	5.0	0.125	0.013

ture rise (see Sec. 2.3), allows for accumulation of sufficient number of defects from, say, electron irradiation at lower energies.

The authors of [61] studied the electrical properties of silicon on electron irradiation within a temperature range of 150 to 550 °C. They observed a conductivity conversion of *n*-silicon on high-temperature irradiation, the irradiation dose causing the conversion decreasing with an increase in temperature. Recovery of the initial conductivity completed at an irradiation temperature of about 1100 °C. Irradiation of dislocation-free silicon with fast electrons at $T_{irrad} > 500$ °C has revealed structural defects in the form of the dislocation loops with impurity precipitates and flat-bottom etching holes [61]. The results confirming the basic regularities of the high-temperature irradiation [27, 59, 60] have been received for gallium arsenide [66].

A preliminary heat treatment (annealing, hardening) induces considerable changes in the crystal defect inventory, which leads to changes in the production rates of various defects (see Sec. 2.2) and in the respective degradation constants [62 through 65].

When irradiation with particles is used for technological purposes a question arises about a limit in the changes of the crystal parameters on irradiation. This problem has been treated in a number of papers (see, for example, [4, 67, 68]). From the extensive information given in this section, it is obvious that defect production rates decrease with an increase in the radiation dose. This is associated either with depletion of the impurity forming part of the complex or with annihilation of V and I at the impurity centers (it is assumed that the radiation defect retains its stability at T_{irrad}). That is why, we can affirm that the limiting changes in the parameters (concentration, lifetime of carriers) will be determined, in a given material, by the inventory and rates of production of the defects that depend, as they do, on many conditions (see Ch. 2). The changes in the parameters of irradiated crystals bring about the changes in the limiting characteristics obtained through irradiation. As the amounts of impurities (both controllable and otherwise) in the crystals are great (see Tables 1.3 and 1.4), the most probable cause of saturation of the characteristics, depending on the irradiation dose, is annihilation at the defect centers. The limiting lifetimes of carriers in germanium and silicon on electron irradiation are from 10^{-7} to 10^{-8} s (see, for example, Fig. 1.3); on extended irradiation, silicon practically turns to the intrinsic state with either electrons or holes slightly dominating [4, 67, 68]. It should be emphasized that the calculated values of the decrease in the lifetime, induced by introduction into the semiconductors of some deep-level (about 10^{-9} to 10^{-10} s) impurities, were never achieved in practice [69] with the exception of doping silicon with gold. Since the rate of annihilation depends on many conditions [27], it is possible to

obtain the desired limiting changes in the characteristics of the crystals by changing the irradiation parameters.

In actual practice, of importance is a problem of decreasing the values of the degradation constants of carrier concentration and lifetime (enhancement of radiation stability of semiconductor materials). The basic approaches to this problem solution are outlined in [27]. Unfortunately, the experimental studies of this problem are far from complete. Note such papers as [70] through [77] that show how promising the methods of introduction into the crystals of the centers of annihilation for vacancies and interstitials are, as well as [70, 71, 72, 78, 79] and [80] whose authors have found an enhancement of radiation stability of some parameters of silicon and germanium samples containing special impurities (Co, Gd, etc.), the phenomenon which seems to involve an action of the impurity centers (or defects that incorporate such centers) as the centers of annihilation or sinks for the active components of the Frenkel pairs (capture centers).

Sec. 4.2. Local Levels

In most instances, a change in the electrophysical parameters of semiconductors upon irradiation is associated with the emergence, in the forbidden zone, of new localized states (or energy levels) which act as traps for electrons and holes or as recombination centers.

The problem of level identification, that is, correlation of a level to a particular defect, is the one whose complexity remains to be unravelled. The present section provides a review of the basic properties of radiation energy levels in the most technologically important semiconductors, such as silicon, germanium and gallium arsenide.

Many authors have investigated the energy level spectrum in semiconductors irradiated with various particles [6, 7, 10, 38, 81 through 112]. To locate an energy level within the energy gap, use is made of the Hall effect [114, 115], photoconductivity spectra [113], temperature dependence of the lifetime (τ) of the non-equilibrium carriers [113], etc. Recently, wide acceptance has been gained by the capacitance methods of semiconductor investigation, which allows one to obtain an extensive information about the parameters of localized levels [116, 117]. Tables 4.10, 4.11 and 4.12 give the energy positions of the localized levels observed in irradiated Si, Ge and GaAs. Even a short glance at the tables reveals a great variety of levels appearing after the irradiation. The levels "cover", for all practical purposes, the entire forbidden zone at a spacing of 0.02 to 0.05 eV. If you compare this picture to the system of levels known for chemical impurities [118], you will see that each impurity has its own "radiation analog". This analogy stems from the fact that not all radiation-induced levels represent defect complexes containing

Table 4.10

Energy levels observed in irradiated silicon

Position of level, eV	Kind of irradiation (energy, MeV)	Measurement technique	Type of conduction of original material	References
E_C—0.03	γ, n^0, e^- (1)	H,	n	[92, 98]
—0.05	p^+ (660)	H	n	[6]
—0.10	p^+ (660)	PC	p	[6]
—0.17	γ, n^0, e^- (1; 2.5; 9; 10; 30; 100), p^+ (660), d (6.3)	H, PC, IR, τ, E	n, p	[6; 10, 92, 97-101, 110, 121]
—0.22	γ, n^0, e^- (1; 2.5; 10; 30; 100)	H, PC, IR	n, p	[6, 92, 99, 10]
—0.24	p^+ (660)	τ	n	[6]
—0.26	γ, n^0, e^- (1)	PC	n, p	[92, 100]
—0.27	e^- (1), d (6.3)	E, PC	p	[107, 121]
—0.28	γ, n^0, e^- (1), p^+ (660)	PC, τ	n, p	[6, 92, 100]
—0.30	γ, n^0, e^- (1, 9)	H, PC	n, p	[92, 101]
—0.33	γ, n^0, e^- (1)	PC	n, p	[92, 100]
—0.36	γ, n^0, e^- (1), d (6.3)	PC	n, p	[92, 100, 121]
—0.38	γ, n^0, e^- (1, 9)	H, PC	n, p	[92, 101]
—0.40	γ, n^0, e^- (1; 2.5; 10; 30; 100), d (6.3)	H, PC	n, p	[10, 92, 94, 98, 100, 121]
—0.44	n^0	PC	n	[94]
—0.46	e^- (1, 9)	H, PC	n	[94, 101]
—0.50	γ, n^0, e^- (1)	PC, E	n, p	[92, 94, 110]
—0.55	γ, n^0, e^- (1, 9), d (6.3)	H, PC	n, p	[92, 101, 121]
—0.62	e^- (1)	PC	n	[94]
—0.71	n^0	PC	n	[94]
—0.78	e^- (1)	PC	n	[94]
E_V+0.57	γ, p^+ (660), d (6.3)	PC, E	n, p	[6, 110, 121]
+0.55	γ, n^0, e^- (1, 9), p^+ (660)	H, PC, IR	n, p	[6, 92, 98, 100, 101]
+0.49	γ, n^0, e^- (1; 10; 30), p^+ (660)	PC, E	n, p	[6, 92, 105, 107]
+0.45	γ, n^0, e^- (1), d (6.3)	PC	n, p	[92, 97, 98, 100, 121]
+0.42	γ, n^0, e^- (1)	PC, IR	n, p	[92]
+0.40	p^+ (660)	τ	p	[6]
+0.38	γ, n^0, e^- (1; 10; 30)	PC, E	n, p	[92, 97, 98, 105, 107]
+0.35	γ, n^0, e^- (1; 2.5; 10; 30; 100)	H, PC, IR	n, p	[92, 97, 98, 10]
+0.33	γ, n^0, e^- (1), p^+ (660)	PC	n, p	[6, 92]

Table 4.10 Cont'd

Position of level, eV	Kind of irradiation (energy, MeV)	Measurement technique	Type of conduction of original material	References
+0.30	γ, n^0, e^- (1; 10; 30), p^+ (660), d (6.3)	H, PC, IR, τ, E	n, p	[6, 92, 97, 98, 105, 107, 121]
+0.28	γ, n^0, e^-, (1; 2.5; 10; 30; 100), d (6.3)	H, PC, E	n, p	[92, 110, 10, 121]
+0.24	γ, n^0, e^- (1)	PC, IR, E	n, p	[92, 98, 99, 107]
+0.21	γ, n^0, e^- (1; 2.5; 10; 30; 100)	H, PC, IR	n, p	[6, 92, 98, 10]
+0.18	γ, n^0, e^-, (1; 2.5; 10; 30; 100)	H, PC, IR, E	n, p	[10, 92, 100, 107]
+0.16	γ, d (6.3)	PC, τ, E	n, p	[93, 110, 121]
+0.12	γ, n^0, e^- (1), p^+ (660)	PC, τ	n, p	[6, 92, 98]
+0.10	γ, n^0, e^- (1), p^+ (660)	H, PC, τ	n, p	[6, 92, 93]
+0.07	n^0, p^+ (660)	IR, τ	n, p	[6, 92]
+0.05	γ, n^0, e^- (1), d (6.3)	H, PC	n, p	[92, 98, 121]

Note. 1. Kind of irradiation: γ — Co^{60} gamma radiation; n^0 — reactor neutrons; e^- — electrons; p^+ — protons; d — deutrons. Measurement technique: H — temperature dependence of electrical conductance or Hall effect; PC — photoconductivity spectrum; IR — IR absorption spectrum; τ — temperature dependence of non-equilibrium carrier lifetime; E — transient capacitance spectroscopy. 2. The table gives tentative data for irradiation near room temperature. The exception is the neutron irradiation data obtained at $T_{irrad} \simeq 70$ °C.

Table 4.11

Energy levels observed in irradiated germanium

Position of level, eV	Kind of irradiation (energy, MeV)	Measurement technique	Type of conduction of original material	References
E_C—0.09	n^0, e^- (1), p^+ (660)	H, PC	n, p	[6, 82, 96]
—0.12	e^- (3.5), p^+ (660)	PC	n, p	[6, 111, 120]
—0.20	γ, n^0, e^- (2; 3.5; 15), p^+ (660)	H, PC	n, p	[6, 81, 83, 87, 96, 106, 109, 120]
—0.27	p^+ (660)	PC, τ	n	[6, 120]
—0.30	e^- (15)	H, PC	n	[109]
—0.32	n^0	H, PC	n	[86, 96]

Table 4.11 Cont'd

Position of level, eV	Kind of irradiation (energy, MeV)	Measurement technique	Type of conduction of original material	References
—0.36	n^0, p^+ (660)	H, PC	n, p	[6, 87, 120]
—0.40	e^- (3.5; 15)	PC, τ	n	[109, 112]
E_V+0.52	γ, e^- (2.5; 28)	H, PC	n, p	[88, 89, 90, 91]
+0.48	γ, e^- (2.5; 28)	H, PC	n, p	[88-91]
+0.44	γ, e^- (3.5)	PC	n, p	[88, 91, 106]
+0.42	γ, e^- (1; 2.5; 28)	PC	n, p	[85, 88, 89, 91]
+0.36	γ, e^- (1; 2.5; 28), p^+ (660)	PC	n, p	[6, 85, 88, 99, 91]
+0.33	γ, e^- (2.5; 3.5; 28)	H, PC	n, p	[88, 89, 90, 106]
+0.30	γ, n^0, p^+ (660)	H, PC, τ	n, p	[6, 86, 88, 91, 96, 120]
+0.26	γ, e^- (2; 2.5; 28), p^+ (660)	H, PC	n, p	[6, 84, 88, 89, 90, 91]
+0.22	γ, e^- (2.5; 28)	H, PC	n	[89-91]
+0.20	γ, e^- (2.5; 28), p^+ (660)	H, PC	n, p	[6, 81, 89, 120]
+0.18	n^0, e^- (2.5; 28)	PC	n	[86, 89, 96]
+0.16	γ, n^0, e^- (2.5; 28)	H, PC	n	[81, 87, 89, 91]
+0.12	p^+ (660)	H, PC	n, p	[6, 120]
+0.10	e^- (2.5; 28)	H, PC	n	[89, 90]
+0.08	n^0, p^+ (660)	H, PC	n, p	[6, 86, 87, 96]
+0.01	n^0, e^- (28), p^+ (660)	H	n, p	[6, 87, 90]

Note. For explanation of symbols, refer, to Table 4.10.

Table 4.12

Energy levels observed in gallium arsenide

Position of level, eV	Kind of irradiation (energy, MeV)	Measurement technique	Type of conduction of original material	References
E_C—0.13	γ, e^- (1)	H, K, T, E	n, p	[38, 104]
—0.20	e^- (1), N	H, K, T, E	n, p	[38, 104]
—0.23	n^0	PC	n	[95]
—0.27	n^0	PC	n	[95]
—0.31	γ, n^0, e^- (1)	PC,E	n	[38, 95]
—0.34	n^0	PC	n	[95]
—0.36	n^0, e^- (1)	H, PC, K	n	[95, 104]
—0.43	n^0	PC	n	[95]

Table 4.12 Cont'd

Position of level, eV	Kind of irradiation (energy, MeV)	Measurement technique	Type of conduction of original material	References
—0.50	n^0	PC	n	[95]
—0.53	n^0, e^- (1)	PC	n, p	[95, 104]
—0.62	n^0	PC	n	[95]
—0.72	n^0, e^- (1), N	PC	n, p	[95, 104]
—0.82	n^0	PC	n	[95]
E_V+0.59	e^- (1), N	PC, K	n, p	[104]
+0.45	e^- (1.6-1.8)	H	p	[103]
+0.43	n^0	PC	n	[95]
+0.40	e^- (1), N	PC, K	p	[104]
+0.37	n^0	PC	n	[95]
+0.35	e^- (1), N	PC, K, T	n	[104]
+0.32	γ, n^0, e^- (1)	PC, E	n	[38, 95]
+0.22	e^- (1.6-1.8)	H	p	[103]
+0.20	e^- (1)	T	n	[104]
+0.10	γ, e^- (1; 1.6-1.8), N	H, T, E	n, p	[38, 103, 104]
+0.04	N	T	n	[104]

Note. Irradiation: γ — Co^{60} gamma radiation; n^0 — reactor neutrons; e^- — electrons; N—non-irradiated material. Measurement techniques: H — Hall effect; PC — photoconductivity spectrum; K — kinetics of impurity conductance; T — temperature dependence of photoconductivity; E — transient capacitance spectroscopy.

one of the components of the Frenkel pair. Indeed, some levels are due to the atoms of chemical impurities. This fact was noted, say, in [92] and [106]. One of the reasons why these levels are found only in irradiated crystals (while they are seemingly absent in the original samples) resides in an increase of the concentration of the impurity in the regular lattice sites [92]. Another reason is a more sensitive technique of locating the levels after the crystal has been irradiated with the result that the impurity existing in the original material now "reveals" itself [106].

The emergence of localized levels upon irradiation shifts the photoconductivity (PC) spectrum to a region with longer waves. It was shown [106] that changing the irradiation dose and annealing temperature allows an arbitrary displacement (with a certain range) [106] of the red PC boundary in germanium (Figs. 4.37, 4.38). A change in the form of the PC spectrum upon irradiation and annealing was observed in silicon as well [98].

A suppression of PC in irradiated semiconductors was observed by several workers (see, for example, [83, 84, 91, 94, 95]). A result

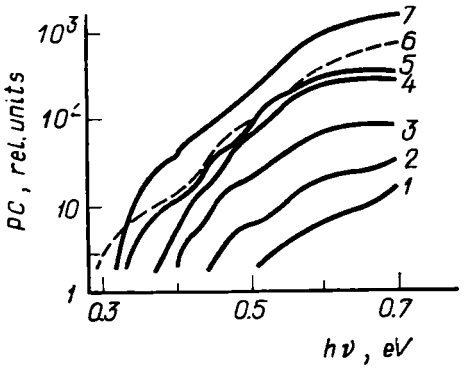

Fig. 4.37. Change in PC spectra with irradiation dose [106].

1—before irradiation. Irradiation is by 3.5 MeV electrons at 20 °C. Dose, cm^{-2}: *2*—$1.5 \cdot 10^{14}$; *3*—$3 \cdot 10^{14}$; *4*—10^{15}; *5*—$2 \cdot 10^{15}$; *6*—$1.5 \cdot 10^{16}$; *7*—$5 \cdot 10^{15}$. Material: *n*-type germanium (Sb), $\rho \approx 0.65$ ohm·cm, $N_d \approx 10^3$ cm^{-2}

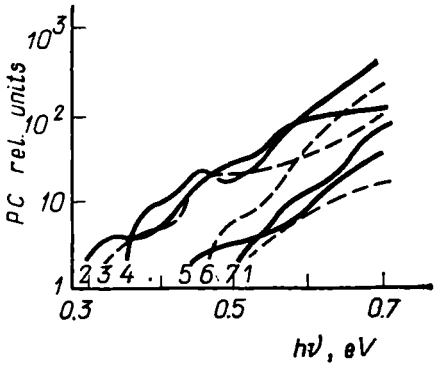

Fig. 4.38. Change in PC spectra during isochronal (10 min) annealing [106].

1—before and after annealing; *2*—before annealing and after 3.5 MeV electron irradiation at 20 °C; dose, 10^{16} cm^{-2}; annealing at *T*, °C: *3*—149, *4*—160, *5*—181, *6*—212, *7*—289. Material: *n*-type germanium (Sb), $\rho \approx 0.65$ ohm·cm, $N_d \approx 10^3$ cm^{-2}

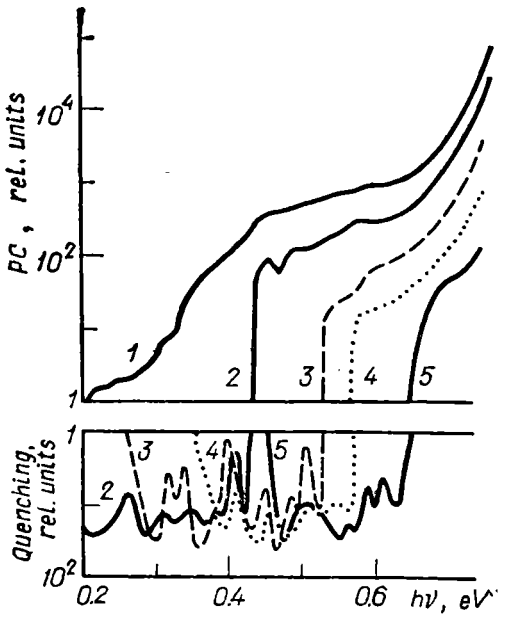

Fig. 4.39. PC and quenching spectra in *n*-type germanium (N_{Sb} = $= 1.6 \cdot 10^{14}$ cm^{-3}) after Co^{60} gamma irradiation at 20 °C [91].

1—without brightening. Brightening intensity ($h\nu = 0.74$ eV), rel. units: *2*—0.006; *3*—0.02; *4*—0.15; *5*—1. Measurement temperature, 77 K

interesting from the viewpoint of possible practical application has been received on *n*-type germanium compensated with gamma radiation [91], namely, a PC signal in the suppression region, i.e., the one excited with two light beams, exceeds, in its value, that excited with long-wave light only (Fig. 4.39).

The authors of [107] used the junction capacitance spectroscopy to investigate the defect levels in *p*-type silicon doped with boron and having resistivities of 0.3, 2 and 8 ohm·cm. The samples were irradiated with 1 MeV electrons at 25-30 °C. The experiments yielded data on the defect energy levels introduced by irradiation, the rates of their production, their stability to annealing and cross-sections for capture of electrons and/or holes (Table 4.13 and Figs. 4.40 and 4.41*a*, *b*). The rate of formation of the level $E_V + 0.23$ eV does not depend on N_B and constitutes about 0.002 cm^{-1} in various samples. The rates of formation of the levels $E_V + 0.18$, $+0.31$ and 0.48 eV were set at 0.001, 0.002 and 0.002 cm^{-1}, respectively. The behaviour of the level $E_V + 0.38$ eV was found to be anomalous: it had two hole capture cross-sections (see Table 4.13). This level seems to be associated with two kinds of defect. From Fig. 4.41, it is apparent that some levels form immediately upon irradiation, while the others only after an additional annealing. All the levels are annealed out at $T_{anneal} \leqslant 400$ °C.

Table 4.13

Carrier capture cross-sections versus level positions in *p*-type silicon irradiated with 1 MeV electrons [107]

Energy level, eV	Cross-section, $\sigma \cdot 10^{16}$, cm^2
	After irradiation
$E_V+0.18$	$\sigma_p > 0.2$
$E_V+0.23$	$\sigma_p = 3$
$E_V+0.31$	$\sigma_p > 0.2$
$E_V+0.38$	$\sigma_{p1} = 2$
	$\sigma_{p2} = 0.002$ (after annealing)
	$\sigma_{p2} = 0.05$ (after annealing at 350 °C)
	$\sigma_{p2} = 0.01$ (after annealing at 400 °C)
	After annealing (see Fig. 4.41)
$E_V+0.48$	$\sigma_p > 0.2$
$E_C-0.27$	$\sigma_n = 2000$
$E_V+0.30$	$\sigma_p = 2$
$E_V+0.26$	—
$E_V+0.20$	—
$E_V+0.47$	$\sigma_p = 4$

Fig. 4.40. $E_V + 0.38$ (*1*) and $E_C - 0.27$ eV (*2*) level formation rates vs boron concentration in *p*-type silicon irradiated with 1 MeV electrons [107].

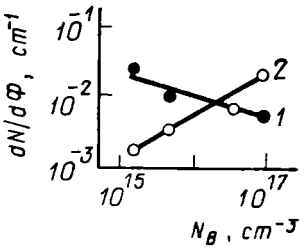

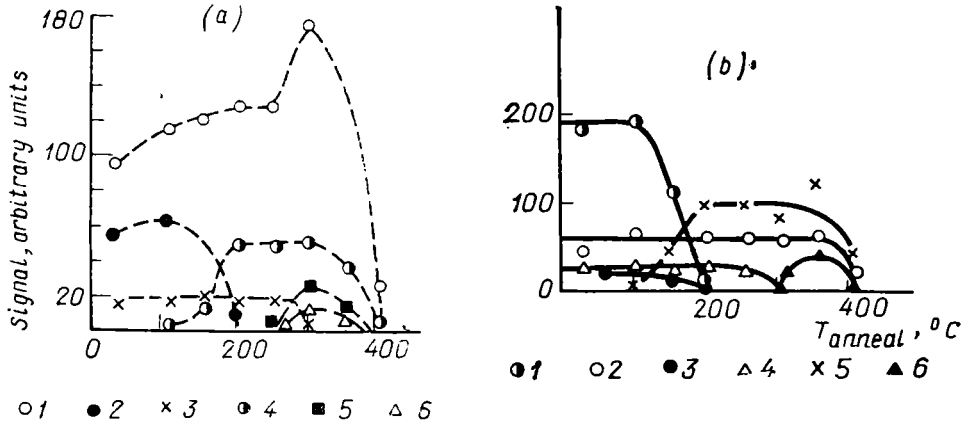

Fig. 4.41. Isochronal annealing of levels in *p*-type silicon irradiated with 1 MeV electrons [107].

a—levels, eV: *1*—$E_V + 0.38$; *2*—$E_C - 0.27$; *3*—$E_V + 0.24$; *4*—$E_V + 0.30$; *5*—$E_V +$ $+ 0.26$; *6*—$E + 0.20$. Silicon resistivity, 2 ohm·cm; *b*—levels, eV: *1*—$E_C - 0.27$; *2*—$E_V + 0.38$; *3*—$E_V + 0.48$; *4*—$E_V + 0.23$; *5* — $E_V + 0.30$; *6*—$E_V + 0.26$. Silicon resistivity, 0.3 ohm·cm

Fig. 4.42. Level formation rate vs phosphorus concentration in *n*-type silicon [101].

I—material produced by zone refining; II—material produced by Czochralski method. Levels: *1*—$E_C - 0.17$; *2*—$E_C - 0.30$; *3*—$E_C - 0.47$; *4*—$E_C - 0.39$; *5*—$E_C - 0.54$; *6*—$E_V + 0.55$ eV. Irradiation is by 9 MeV electrons, $\Phi \simeq 10^{18}$ cm^{-2}

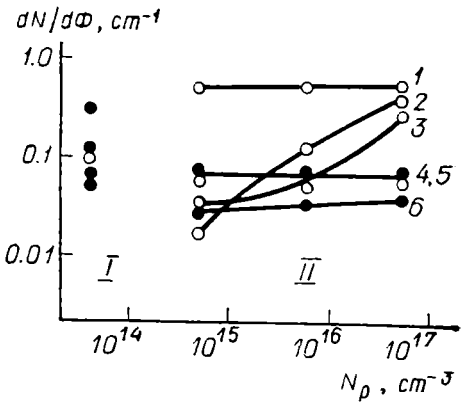

Fig. 4.43. Level formation rates vs electron energy in *n*-type silicon [101].

Energy levels, eV: *1*—$E_C - 0.17$; *2*—$E_C - 0.40$; *3*—$E_C - 0.47$; *4*—$E_V + 0.55$; *5*—$E_C - 0.30$. $N_P = 5 \cdot 10^{14}$ cm^{-3}, $N_0 =$ 10^{17}-10^{18} cm^{-3}

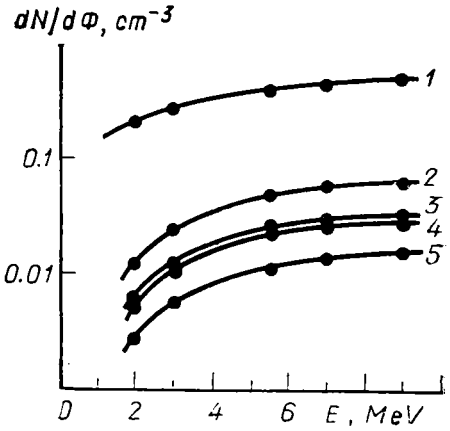

Table 4.14

Parameters of levels in gamma irradiated *n*-type silicon [102]

Level, eV	$N_O = (3\text{-}5)\cdot 10^{17}$ cm^{-3}		$N_O = (1\text{-}3)\cdot 10^{16}$ cm^{-3}	
	$N\cdot 10^{-12}$, cm^{-3}	σ_n or $\sigma_p\cdot 10^{15}$, cm^2	$N\cdot 10^{-12}$, cm^{-3}	σ_n or $\sigma_p\cdot 10^{15}$, cm^2
$E_C-0.16$	80	$\sigma_n=5$	80	$\sigma_n=20$
$E_C-0.37$	3.7	$\sigma_n=4$	2.8	$\sigma_n=3$
$E_V+0.35$	30	$\sigma_p=1$	30	$\sigma_p=1$
$E_C-0.24$	1.5	$\sigma_n=2$	1.1	$\sigma_n=1$
$E_C-0.50$	1.4	$\sigma_n=140$	1.3	$\sigma_n=70$

Table 4.15

Parameters of levels in electron irradiated *p*-type silicon [119]

Sample	Level 1			Level 2			Level 3			Level 4		
	E_V+E_1, eV	$N\cdot 10^{-13}$, cm^{-3}	$\sigma_p\cdot 10^{16}$, cm^2	E_V+E_2, eV	$N\cdot 10^{-12}$, cm^{-3}	$\sigma_p\cdot 10^{18}$, cm^2	E_V+E_3, eV	$N\cdot 10^{-12}$, cm^{-3}	$\sigma_p\cdot 10^{17}$, cm^2	E_C-E_4, eV	$N\cdot 10^{-13}$, cm^{-3}	$\sigma_n\cdot 10^{15}$, cm^2
1	0.33	4.5	5	0.21	3.4	0.3	0.17	7.2	1	0.24	1.4	1
2	0.34	5.6	7	0.22	3.4	1.3	0.16	8.7	0.2	0.23	1.7	1
3	0.33	2.5	4	—	0.5	—	0.17	5.2	0.5	0.24	4.3	1
4	0.35	2.1	6	—	0.5	—	0.17	6.1	2	0.25	4.8	6

Note. $N_O = (6\text{-}8)\cdot 10^{16}$ cm^{-3}, *p*-Si (Al), $\rho = 50$ ohm·cm (samples 1, 2); *p*-Si (B), $\rho = 30$ ohm·cm (samples 3, 4). Dose, $2\cdot 10^{15}$ cm^{-2}; 1.3 MeV electrons, $T_{irrad} = 20$ °C.

Table 4.16

Recombination properties of levels in 660-MeV proton irradiated germanium and silicon samples [6]

Material	$N_D(N_A)\cdot10^{-13}$, cm^{-3}	$\Phi\cdot10^{-12}$, cm^{-2}	$M\cdot10^{-13}$, cm^{-3}	Level, eV	$\sigma_p\cdot10^{15}$, cm^2	$\sigma_n\cdot10^{15}$, cm^2
	6.4	2.0	0.82	$E_C-0.26$	26	0.024
n-Ge	7.0	3.2	1.2	$E_V+0.31$	470	0.12
	6.4	2.1	0.8	$E_V+0.20$	1.2	0.2
	1.1	0.44	1.0	$E_C-0.29$	210	—
	0.19	0.44	1.0	$E_C-0.24$	1.5	—
n-Si	2.1	0.11	2.8	$E_C-0.16$	1600	—
	21	3.2	7.4	$E_C-0.18$	2900	—
	0.9	0.44	1.0	$E_V+0.40$	—	—
	0.09	0.44	1.0	$E_V+0.30$	—	—
p-Si	200	1.1	2.8	$E_V+0.40$	—	85
	—	—	—	$E_V+0.08$	—	230
	270	1.1	2.8	$E_V+0.12$	—	5
	—	—	—	$E_V+0.08$	—	430

Note. M and $N_D(N_A)$ — level and donor (acceptor) concentration; σ_n (σ_p) — electron (hole) capture cross-section.

Table 4.17

Injection of donors into *n*-Si by Co^{60} gamma irradiation [7]

σ_{orig}, ohm·cm	Impurity	Dose $\Phi \cdot 10^{-19}$, cm^{-2}	Energy level, eV		Formation rate, $\eta \cdot 10^5$, cm^{-1}	σ_{orig}, ohm·cm	Impurity	Dose $\Phi \cdot 10^{-19}$, cm^{-2}	Energy level, eV		Formation rate, $\eta \cdot 10^5$, cm^{-1}
			Hall effect measurement results	mean value					Hall effect measurement results	mean value	
7	B, O	2.6	0.358	0.35	10	15	B	2.5	0.204	0.21	2
16	B, O	1.5	0.355	0.35	8.5	50	B	7.1	0.206	0.21	2
180	Ga, O	0.09	0.350	0.35	10	50	B	1.0	0.281	0.28	$\leqslant 1$
5	B	5.8	0.217	0.21	5	50	B	1.5	0.290	0.28	$\leqslant 1$

Table 4.18

Defect production rate in silicon [10]

Growing technique	Electron energy, MeV	Initial defect formation rates, cm^{-1}, with levels, eV						
		$E_C-0.17$	$E_C-0.22$	$E_C-0.40$	$E_V+0.35$	$E_V+0.18$	$E_V+0.21$	$E_V+0.27$
		n-type				*p*-type		
Z	2.5	$(1.2\pm0.4)\,10^{-1}$	$(8\pm3)\,10^{-2}$	$(1.4\pm0.6)\,10^{-2}$	$(1.0\pm0.4)\,10^{-1}$	$(4\pm2)\,10^{-1}$	—	—
T		$(1.2\pm0.4)\,10^{-1}$	—	$(1.4\pm0.6)\,10^{-1}$	—	—	$(5.5\pm2)\,10^{-2}$	$(4.5\pm1.5)\,10^{-2}$
Z	10	$(1.8\pm0.3)\,10^{-1}$	$(1.2\pm0.4)\,10^{-1}$	$(2.5\pm1.0)\,10^{-2}$	$(4\pm2)\,10^{-1}$	$(9\pm3)\,10^{-2}$	—	—
T		$(1.7\pm0.4)\,10^{-1}$	—	$(1.8\pm0.4)\,10^{-1}$	—	—	$(2.3\pm0.7)\,10^{-1}$	$(1.0\pm0.3)\,10^{-1}$
Z	30	$(2.0\pm0.5)\,10^{-1}$	$(1.5\pm0.4)\,10^{-1}$	$(5.0\pm1.5)\,10^{-2}$	$(6\pm2)\,10^{-1}$	$(1.0\pm0.3)\,10^{-1}$	—	—
T		$(1.9\pm0.6)\,10^{-1}$	—	$(2.2\pm0.7)\,10^{-1}$	—	—	$(3\pm1)\,10^{-1}$	$(1.4\pm0.4)\,10^{-1}$
Z	100	$(3.5\pm0.5)\,10^{-1}$	$(2.5\pm0.7)\,10^{-1}$	$(6.5\pm2.5)\,10^{-2}$	$(8\pm1)\,10^{-1}$	$(1.1\pm0.3)\,10^{-1}$	—	—
T		$(3.2\pm0.7)\,10^{-1}$	—	$(3.4\pm0.8)\,10^{-1}$	—	—	$(4\pm1.5)\,10^{-1}$	$(2.4\pm0.6)\,10^{-1}$

Note. Z–crystals grown by zone melting; T–crystals grown by Czochralski method.

Table 4.19

Energy levels and their formation rates in 1 MeV electron or gamma irradiated gallium arsenide [38]

Measurement technique* and level parameters	Level, eV						
	*E*1	*E*2	*E*3	*E*4	*E*5	*H*1	*H*2
E	0.08	0.19	0.45	0.76	0.96	0.09	0.32
*H***	0.12	0.20	0.38	—	—	0.10	—
	0.13	0.17	0.31	—	—	0.10	—
PC***	—	—	0.38	0.52	0.72	—	—
	—	—	—	0.54	—	0.10	—
Optimum energy level [38]	0.13	0.20	0.31	—	—	0.10	0.29
Formation rate, $N/1$; 1 MeV electrons, 300 K, cm^{-1}****	1.8	2.8	0.7	0.08	0.1	—	0.7

* See Note to Table 4.12.
** Data obtained by different authors (see [38]).
*** *E*1-*E*5 — electron traps (the level is referred to the conduction band; *H*1-*H*2 — hole traps (the level is referred to the valence band).
**** The formation rates have been obtained for electron current densities of 0.1 μA/cm².

The radiation defects generated in silicon p^+-n junctions by Co^{60} gamma radiation were studied in [102]. The authors studied phosphorus doped ($N_P = 2 \cdot 10^{14}$ cm^{-3}) n-type silicon samples grown by the Czochralski method ($N_O = (3\text{-}5) \cdot 10^{17}$ cm^{-3}) and by the crucibleless method ($N_O = (1\text{-}3) \cdot 10^{16}$ cm^{-3}). The irradiation dose was 1.6·

Table 4.20

Level formation and annealing temperatures in neutron irradiated *p*-type silicon [108]

Energy level, eV	Material (Z — zone refined; C — crucible-grown)	T_{form}, °C	T_{anneal}, °C	Energy level, eV	Material (Z — zone refined; C — crucible-grown)	T_{form}, °C	T_{anneal}, °C
E_V+0.11	C	—	150	+0.43	Z, C	—	375
+0.16	Z	225	300	+0.48	C	—	—
+0.22	Z	425	525	+0.55	Z, C	—	300
+0.26	C	—	500	E_C—0.51	C	—	200
+0.29	C	—	425	—0.49	Z	375	525
+0.30	Z	—	375	—0.49	C	300	525
+0.30	C	—	300	—0.39	Z	375	525
Peak 3.9 μm	Z	—	375	—0.39	C	425	525
Peak 3.9 μm+	C	—	300	—0.16	C	—	450
+0.36	C	—	475				

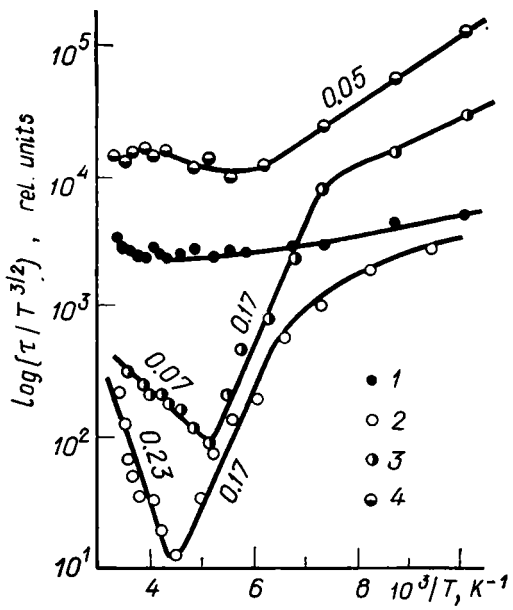

Fig. 4.44. Temperature dependence of τ in p-type germanium.
1—original sample; *2*—sample irradiated for 2 h at 20 °C; *3*—same at 300 °C; *4*—sample heated for 2 h at 300 °C. The numbers on the curves indicate the energy level positions (eV)

$\cdot 10^{17}$ cm^{-2}. The experimenters determined the concentrations of some levels and their cross-sections of capture of electrons or holes (Table 4.14). The other data on the parameters of the localized levels are presented in Figs. 4.42, 4.43 and in Tables 4.15 through 4.19.

The authors of [108] investigated the stability of radiation defect levels in n-type silicon with $N_O > 5 \cdot 10^{17}$ cm^{-3} (grown in crucibles) and $N_O < 5 \cdot 10^{16}$ cm^{-3} (grown by zone melting). The resistivity was $\rho_{initial} = 1$ to 50 ohm·cm, reactor neutron irradiation dose $\Phi = 10^{15}$ and 10^{16} cm^{-2}, and T_{irrad}, about 70 °C. Table 4.20 gives the temperatures of generation (T_{gen}) and annealing (T_{annel}) of the levels observed by the authors.

The system of introduced localized levels depends on irradiation temperature. Thus, in n-type germanium doped with antimony ($\rho \sim 5$ ohm·cm), 3.5 MeV electron irradiation (dose, $4.5 \cdot 10^{16}$ cm^{-2}; current density, 1 μA/cm^2) at 20 °C gives rise to a 0.40 eV level, and at 300 °C, a 0.17 eV level [112]. Similar experiments on p-type germanium were conducted by the authors of [111]. The samples containing $1.5 \cdot 10^{14}$ cm^{-3} of gallium were given a 10^{16} cm^{-2} irradiation dose of 3.5 MeV electrons at temperatures of 26, 140, 225 and 290 °C and, then, were subjected to an isochronal annealing (10 min) to a temperature of about 480 °C. Like in [112], here the temperature dependences of lifetime (τ) were measured. The results have indicated that the level $E_C - 0.12$ eV radiation-induced at 20 °C disappeared with a rise in the irradiation temperature, giving way to $E_C - 0.07$ eV at $T_{irrad} \simeq 225$ °C. The level $E_C - 0.12$ eV is annealed out over a temperature range of 120 to 220 °C, and $E_C - 0.07$ eV, at a step of 320-440 °C. During the same step, a new level, $E_C - 0.13$ eV, appears.

Let us consider the results of our studies of defect energy levels in germanium samples having different prehistory. These levels had been introduced by 3.5 MeV electron irradiation at temperatures of 20 and 300 °C. *n*- and *p*-Type samples (Sb and Ga) with $\rho \simeq 5$ ohm·cm were separated into three groups: dislocation-free ones ($N_d \sim$ $\sim$ 0-10^1 cm^{-2}), with a dislocation density of about 10^3 cm^{-2} (grown) and about 10^7 cm^{-2} (introduced by plastic bend). Irradiation was conducted with a current (electron) density of 1 μA/cm^2 for 2 hours

Table 4.21

Energy levels arising from irradiation and heating of germanium samples with different dislocation densities, eV

Type of connection	Treatment	Kinds of dislocations and their density, cm^{-2}		
		dislocation-free crystal, $N_d \sim 0\text{-}10^1$	grown crystals, $N_d \sim 10^3$	introduced by plastic deformation, $N_d \sim 10^7$
	Irradiation at 20 °C	0.63 A, 0.17 R, 0.06 A	0.40 A	0.63 A, 0.12 R
n	Same at 300 °C	0.17 A	0.17 A	0.06 A
	Heating for 2 h at 300 °C	0.29 A	0.29 R, 0.05 A	0.21 A
	Irradiation at 20°C	0.23 R, 0.07 A	0.23 R, 0.17 A	0.17 A
p	Same at 300 °C	0.05 A	0.07 R, 0.17 A	0.36 A, 0.12 R, 0.29 A
	Heating for 2 h at 300 °C	0.10 A	0.05 A	0.10 A

Note. R — recombination level; A — adhesion level (see Fig. 4.44).

Table 4.22

Energy levels produced by 25 MeV electron irradiation of *n*-GaAs at different irradiation temperatures [66]

Level, eV	Original material	Irradiation temperature, °C					
		20	80	140	200	250	300
$E_C-0.57$		+	+	+	+		
-0.62		+	+	+	+		
-0.65		+	+	+	+	+	+
-0.71		+	+	+			
-0.82	+	+	+	+	+	+	+
-0.90					+	+	+
$E_V+0.16$	+	+	+	+	+	+	+

Note. The + sign marks the conditions of level observation.

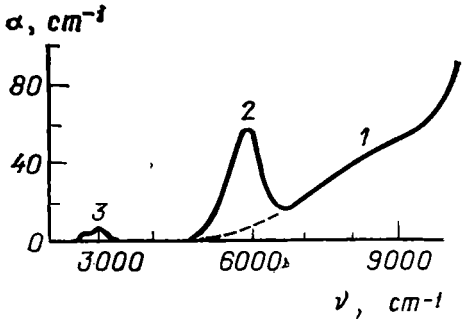

Fig. 4.45. Pure silicon absorption spectrum at 80 K after neutron irradiation ($\Phi = 10^{18}$ cm^{-2}, $T_{irrad} \simeq$ $\simeq$ 20 °C) [123].
1—near-edge absorption; *2*, *3*—peaks of divacancies at 1.7 and 3.6 μm

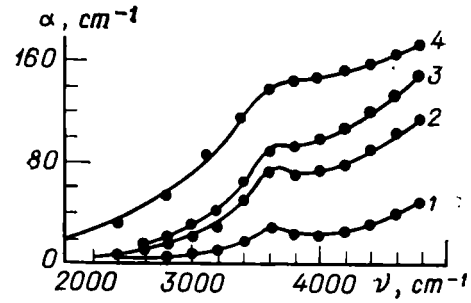

Fig. 4.46. Absorption in antimony doped germanium ($N_{Sb} = 6 \cdot 10^{18}$ cm^{-3}) after neutron irradiation [37].
$\Phi \cdot 10^{18}$, cm^{-2}: *1*—0.7; *2*—0.9; *3*—1.3; *4*—3

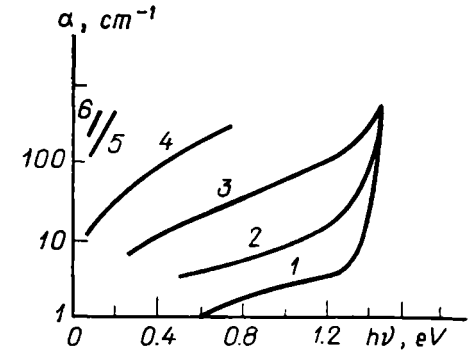

Fig. 4.47. Optical absorption in neutron irradiated gallium arsenide (300 K) [39].
Dose, cm^{-2}: *1*—0; *2*—$4.3 \cdot 10^{15}$; *3*—$3.6 \cdot 10^{16}$; *4*—$4.2 \cdot 10^{17}$; *5*—$9 \cdot 10^{18}$ *6*—$1.5 \cdot 10^{20}$

(dose, $4.5 \cdot 10^{16}$ cm^{-2}). The test samples were heated (without irradiation) for 2 hours at 300 °C. The temperature dependence of the lifetime, τ, was measured. Fig. 4.44 shows, by way of example, the results obtained for one of the samples. A summary list of detected levels is given in Table 4.21.

An influence of the irradiation temperature on the energy level spectrum in GaAs was studied in [66]. The samples (undoped, $n_0 =$ $= 5 \cdot 10^{16}$ cm^{-2}, $\mu_n = 3000$ cm^2/V·s, $\rho = 8$ to 10 ohm·cm) were electron irradiated at 25 MeV ($I = 10^{12}$ cm$^{-2} \cdot$s^{-1}; after irradiation, $\rho = 45$ to 50 ohm·cm) at temperatures of 20, 80, 140, 200, 250 and 300 °C. The photoconductivity spectra were taken. The results are presented in Table 4.22.

The introduction of localized levels near the conduction band or the valence band constitutes one of the causes of displacement of the

absorption edge towards the longer waves. This effect was observed in Si, Ge and in other crystals when irradiated with various particles (see, for example, [37, 39, 122, 123]). The space considerations prevent our dwelling on the subject. We shall therefore be content with giving, as an example, the typical absorption spectra behind the edge of the intrinsic conductivity bands for Si, Ge and GaAs (Figs. 4.45, 4.46 and 4.47).

We see that the experimental evidence shows that the existing information on the properties of the localized levels in irradiated semiconductors is not yet complete. This is one of the areas where further work is obviously required, particularly with regard to the characteristics of the defect energy levels introduced by irradiation.

Sec. 4.3. Employment of Disordered Layers

Non-crystalline semiconductors (e.g., glass-like or amorphous) are of considerable interest not only from the scientific viewpoint but from the practical one as well. The main advantages that make such semiconductors of value to a scientist or engineer are their comparative ease of fabrication, low sensitivity to radiation and the possibility of obtaining various volt-ampere characteristics (VAC) with such semiconductors. One semiconductor structure can perform different functions. For example, the amorphous semiconductor-crystal system operates as a threshold switch, heterojunction and a storage element.

Production of disordered layers by irradiation of semiconductor crystals with fast particles has certain advantages over other methods. Among the advantages are good reproducibility, possibility of making structures of a complex geometrical shape (e.g., with the aid of a well focused ion beam), and a low temperature of the sample during the bombardment.

The amorphous layers forming upon ion irradiation of semiconductors are in many respects similar to the amorphous films produced by other methods [124]. It seems that the only significant distinction is non-uniformity of depth distribution of the implanted layers (see Ch. 1). Nevertheless, by varying the dose and energy of the ions, these layers can be made uniform enough. It is also probable that the non-uniformity of the layers made amorphous by ion implantation may prove useful in some device structures.

At present, extensive work is being done to produce functional devices incorporating non-crystalline semiconductors fabricated by various methods, including the ion bombardment of the crystals. Let us discuss some examples of such functional elements.

Threshold switch and storage element. The VAC of the conductor-amorphous semiconductor-conductor system—may be of several kinds. Some of them are symmetrical and are distinguished for

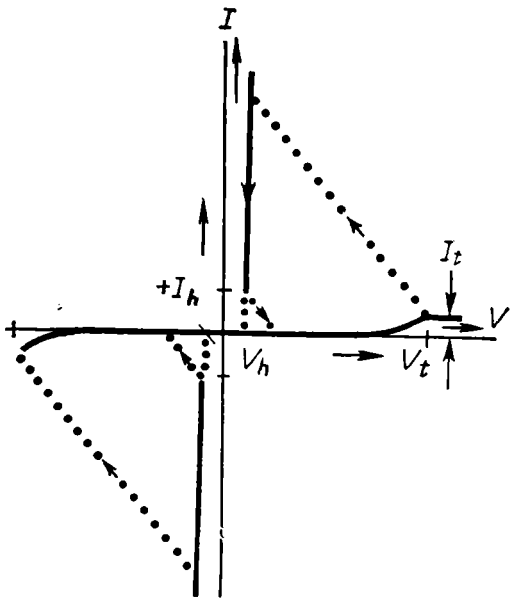

Fig. 4.48. A schematic representation of volt-ampere characteristic of threshold switch.

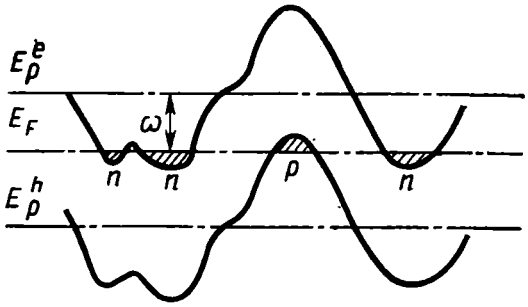

Fig. 4.49. Variation of potential if traced n a random direction.
Hatched areas are occupied by electrons (*n*) and holes (*p*) [149]

a sudden change from the high- to the low-conductivity state [125 through 128]. The resistance of such a structure changes by 3 to 8 orders of magnitude. The VAC of such an element is schematically represented in Fig. 4.48. Initially, at a voltage below V_t, a low current is flowing. At V_t, for at least 1 ns, there occurs a breakdown along the dotted line, preset by a resistance placed in series with the sample under study. The sample is not destroyed during the breakdown. The other parameters that describe the given element called the threshold switch are the holding voltage, V_h, and a respective current, I_h. When the current drops below I_h, the system switches to the initial high-ohmic state.

A number of suggested mechanisms of switch-over of the elements to the "on" (conducting) state are explained proceeding from the amorphous semiconductor model based on the assumption of random potential fluctuations with an amplitude commensurate with the semiconductor energy gap [129, 130]. According to the model, the

amorphous semiconductor is essentially an aggregate of randomly positioned *p*- and *n*-areas, i.e., a set of chaotically sited *p-n* junctions [131, 132]. Under conditions of a complex charge pattern, there is a barrier for current flow in the form of an energy gap between the Fermi level and the "passage" level. The passage level is the minimum energy level for charge carriers, whereat it is still possible to find a connected region extending to infinity in all directions. Fig. 4.49 shows variation of the potential in an arbitrary direction. Here, E_F is the Fermi level and $E_p^{e,h}$ are the passage levels for electrons and holes, i.e., the values of energy which, if provided, will allow the carrier to pass from one electrode to the other without tunnelling through the potential humps but bypassing them. It follows from this model that conductivity is of the activation nature, the activation energy, ε, equalling in the high-temperature region the difference between the passage and Fermi levels. In the low-temperature region, the tunnel mechanism should dominate as regards the states close to the Fermi level. The activation energy ε in the given model continuously decreases with a decrease in the temperature T according to the Mott's law, $\varepsilon \simeq T^{3/4}$, or $\ln \sigma \simeq T^{1/4}$ [133].

Transition of an amorphous semiconductor to a high-conductivity state can be governed by the following mechanisms [128, 131, 132]:

(1) heating the carriers and transferring them to an energy level higher than the passage level;

(2) lowering, by injection of carriers, the barriers in multilayer *n-p-n-p-n...* structures;

(3) phased transition of the material to an ordered state.

The first two mechanisms are based on the above amorphous semiconductor model. Let us discuss the second mechanism because the first one is easily explained by the model.

A system of series-connected *n-p* junctions has an S-shaped volt-ampere characteristic, i.e., features a switching effect (for current). Indeed, for *n-p-n-p* structures, this is a well known fact. An analysis of the VAC for the structures containing more than four alternating *n*- and *p*-regions has revealed that they retain their S-shaped characteristics [134].

The third of the above mechanisms of transition to the conducting state is self-explanatory.

Under certain conditions, the conductor-amorphous semiconductor-conductor structure stores (memorizes) the switching state with the result that a switching device with memory is obtained. This is typical of some amorphous semiconductors when a heavy current is maintained through them for 10^{-6} to 10^{-1} s. A study of microstructures [135] shows that a process of transition to a storing state may be interpreted as the formation of a crystalline channel extending from the anode to the cathode. The rate of formation (growth) of this channel depends on the composition of the amorphous semiconductor

and varies from 10^{-2} to 10^{2} cm/s. The "erasure" of the stored information is either by a reverse-polarity pulse or by a short pulse of the forward polarity.

The employment of the ion bombardment method for production of thin amorphous layers and switches looks promising because of good reproducibility and high efficiency. The authors of [136] and [137] have discovered and studied the switching effect in the layers amorphized by ion bombardment. The experimenters [136] used p-type silicon with $p \simeq 1.5$ ohm·cm. The samples were irradiated with Ar^+ ions with the energy successively changed from 70 to 220 keV. The total dose amounted to $4 \cdot 10^{14}$-$1.5 \cdot 10^{17}$ cm^{-2}. After the irradiation, an aluminium film was applied to the surface by sputtering. This film served as a contact to the amorphized layer.

The switching effect was only observed in the layers irradiated with a dose of $1.5 \cdot 10^{17}$ cm^{-2} and exposed to a pulse of 30 V with a current density of 0.1 mA/cm^2.

The authors of [137] conducted the investigation on p-type silicon, $\rho \simeq 0.02$ ohm·cm, irradiated with Ar^+ ions at $E = 40$ keV to a fluence $\Phi = 6.2 \cdot 10^{15}$ cm^{-2}. The samples used were multilayer structures (aluminium-monocrystal silicon-amorphized silicon-aluminium).

No reversible switching was observed in the samples after their fabrication. A stable threshold switching was only noted after the samples have been annealed at 200-250 °C. Before being irreversibly set to the low-ohmic state, the structures withstood 10^3 to 10^5 switchings when a sinewave voltage of 10^3 to 10^4 Hz and a current not in excess of 3-5 mA were used. In a static condition, the switchover proved irreversible.

The threshold voltage for the structures under study varied within 5 to 11 V and rose with an increase in the ion irradiation dose, which seemed to be associated with the growth of the thickness of the amorphous layer. The critical value of the electric field, at which the switching occurs, is $(6\text{-}9) \cdot 10^5$ V/cm. The authors of [137] believe that the observed threshold switching is associated with electronic, not thermal, processes.

Amorphous layer-crystal structure. An interest in the electrical characteristics of such elements is prompted, among other reasons, by the possibility of obtaining a heterojunction between the amorphous and crystalline semiconductors [138 through 143].

The formation of heterojunctions in the structures of the above type is explained by the fact that in amorphous semiconductors the electron energy spectrum preserves its zonal character although specific: unlike the case in the crystals, the zone widths change here due to emergence of the localized state "tails" in the energy gap. The optical absorption studies have revealed, in addition, that under appropriate conditions the production of amorphous silicon

shows an increase in the width of the energy gap to 1.8 eV, i.e., by a value greater than in the crystal [144].

The VAC studies were mainly conducted on structures with the amorphous layer (AL) produced by precipitation of an evaporating material on a semiconductor substrate. The elements with the AL formed by ion bombardment have not been investigated so far, which points to a lack of data on the AL-crystal junctions.

The most comprehensive information exists on the properties of the amorphous Si-crystalline Si (a-Si-c-Si) and a-Ge-c-Ge junctions [140, 141]. As to the passage of current through such structures, these were thought to be analogous to the metal-semiconductor junctions in the following main respects: (1) the dominating jump-like conduction by localized states in the amorphous material due to the presence of carriers near the Fermi level; (2) a steep barrier within the junction and (3) the VAC described by the emission of the majority carriers through the barrier. With these assumptions, the equation for the current, I, flowing through barrier V^b is given by

$$I(U) = I_0(U) f(U) \exp(-V^b/kT) [\exp(eU/kT) - 1]. \quad (4.4)$$

This equation differs from the ideal one describing the passage of current through the barrier at the metal-semiconductor interface (the Shottkey diode [145]) by the factor $f(U)$ depending on the voltage and parameters of the semiconductors (amorphous and crystalline). Specifically, $f(U)$ depends on the concentration of impurity in the crystal and density of states near the Fermi level, N_F, in an amorphous semiconductor.

Experimental studies of the a-Si-c-Si and a-Ge-c-Ge structures have allowed determination of the barrier height and N_F in such junctions. The experiments have been conducted on Si monocrystals of both n- and p-types with $\rho \simeq 0.1$ ohm·cm. An amorphous Si film 0.5 μm thick was applied in a vacuum of $\simeq 5 \cdot 10^{-6}$ mm Hg. The resistivity of the amorphous layer was 800 ohm·cm. Sputtered aluminium films were used as contacts for the crystal and the amorphous layer. The resistance of the a-Si-Al contact proved below that of the a-Si-c-Si junction and amounted to 3 ohm·cm^2.

The height of the barrier in said structures was calculated from the straight branches of the VAC and amounted to 0.73 eV for the contact between a-Si and p-type Si, and to 0.39 eV when the amorphous film was brought in contact with n-type Si. The density of states near the Fermi level in Si was calculated proceeding from the comparison of the experimental results with the theoretical assumptions [see Eq. (4.4)] and amounted to $1.2 \cdot 10^{20}$ eV^{-1}·cm^{-3} for the conditions selected for producing the amorphous phase.

For the a-Ge-c-Ge structure fabricated with the use of n-type Ge with a donor concentration of 10^{17} cm^{-3}, the a-Ge film was applied in

a vacuum of 10^{-6} mm Hg, the barrier height was 0.31 eV and N_F, $9 \cdot 10^{19}$ $eV^{-1} \cdot cm^{-3}$.

It transpires from the above that the employment of the AL-crystal structures in the semiconductor device technology is quite feasible. For example, a-Si and Si monocrystal can be used as a basis for obtaining a junction with a characteristic resembling that of the Schottky diode. It should be stressed that production of AL by ion bombardment of the crystals will clear away the problems involved in the fabrication and cleaning of the crystal surface before application of the amorphous semiconductor. This method, however, has its disadvantages, namely, the presence of defects behind the AL for between the AC and the crystal matrix there is an intermediate crystalline region with an increased damage content. To obviate this difficulty, an annealing of the structures at a temperature not in excess of the AL crystallization temperature is likely to be of help.

Recording optical information on disordered layers. The optical storage (memory) effects are associated with changes in the structural, optical and electrophysical characteristics of the material upon irradiation. The introduced changes are preserved after the irradiation ceases either for an infinitely long or finite time, the phenomenon called the optical storage.

Let us consider two types of optical storage. In the first type, the structure of the amorphous material is rearranged as a result of the action of a light impulse, whereas in the second type no such rearrangement was ever observed.

1. Light impulses with a power in excess of a certain threshold value are capable of inducing crystallization of amorphous layers. This process is attendant with a significant increase in their conductivity, reflection and absorption coefficients (particularly, in the IR region) [146, 147 and Ch. 8] of this book.

The authors of [148] used amorphous films of GeTe and InSb, applied in a vacuum by sputtering to NaCl and glass substrates, as the material for recording the optical signals on. Interference gratings have been obtained with a spatial frequency of 1000 lines (max) per millimeter. These gratings are essentially alternating sections with different spectral and structural properties. The samples have been subjected to pulsed ruby ($\lambda = 0.69$ μm) and neodimium ($\lambda = 1.06$ μm) irradiation derived from lasers run free.

Depending on the constant of the grating under study, two kinds of structural change in the films have been registered [148]. For the grating with 100-200 lines per millimeter, the slits represent strips of polycrystalline material, separated by amorphous sections. With 1000 lines per millimeter, the grains have been observed to grow larger for the entire irradiated area of the film, though the optical density of the slits and sections separating them is varying.

Similar results have been obtained for holographic grating records

on ion irradiated silicon layers [147]. Here, silicon amorphization was accomplished by P^+ ion bombardment at $E = 100$ keV and $\Phi = 6 \cdot 10^{15}$ cm^{-2}. The recording was made with the aid of a neodimium laser. The result was an interference grating with a spatial frequency of 1250 lines per millimeter.

2. Where no structural rearrangement is registered, the optical storage effect resides in, say, extremely slow rate of decrease in the photo current (with a time constant of the order of many minutes or hours [131]) after the exciting illumination has been removed. The sample can be restored to its initial condition only after application of a break-down voltage pulse. Specifically, such an effect is observed with a heavily compensated *n*-type Ge (the degree of compensation is equal to the ratio of concentrations of the compensating to the main doping impurity and nears 1). The compensation of *n*-type Ge can be achieved by fast neutron irradiation [149].

In this case, the optical storage effect can be explained proceeding from the amorphous semiconductor model based on the assumption of presence therein of random fluctuations of the potential [129, 130]. Since according to this model, the amorphous semiconductor represents an aggregate of arbitrarily sited *p-n* junctions, the irradiation brings about separation of non-equilibrium carriers across these junctions. As this happens, electrons are attracted to wells, and holes, to the humps of the potential relief. The recombination of such carriers can occur either by a thermally excited rise of carriers over the recombination barrier, or by the tunnel effect [131]. As has been stated above, the flowing current has to overcome a barrier representing an energy gap between the Fermi level and the passage level. As a result of attraction of an additional number of carriers to the wells (or humps, for the holes), the barrier for the current to overcome diminishes, i.e., the material conductivity becomes better. This accounts for the presence of a long tail in the photo current decrease kinetics after the illumination is removed.

References

1. Hill, D. E. Electron bombardment of silicon. *Phys. Rev.*, 1959, 114, 6, pp. 1414-1420.
2. Vavilov, V. S., Ukhin, N. A. *Radiation Effects in Semiconductors and Semiconductor Devices.* Moscow, Atomizdat, 1969, 311 pages (in Russian).
3. Sonder, E., Templeton, L. C. Gamma irradiation of silicon. I. Levels in *n*-type material containing oxygen. *J. Appl. Phys.*, 1960, 31, 7, pp. 1279-1286.
4. Konozenko, I. D., Semenyuk, A. K., Khivrich, V. I. *Radiation Effects in Silicon.* Kiev, Naukova dumka, 1974, 199 pages (in Russian).
5. Nakano, T., Inuishi, J. Effects of dosage and impurities on radiation damage of carrier lifetime in silicon. *J. Phys. Soc. Japan.*, 1964, 19, 6, pp. 851-858.
6. Konopleva, R. F., Ostroumov, V. N. *Interaction of High-Energy Charged Particles with Germanium and Silicon.* Moscow, Atomizdat, 1975, 128 pages (in Russian).

7. Sonder, E., Templeton, L. C. Gamma irradiation of silicon. III. Levels in *p*-type material. *J. Appl. Phys.*, 1965, 36, 6, pp. 1811-1815.
8. Khivrich, V. I. On the nature of recombination centers and negative annealing in gamma irradiated industrial silicon. In: *Radiation Defects in Semiconductors.* Minsk, Belorussian State University, 1972, pp. 107-109 (in Russian).
9. Konozenko, I. D., Levchuk, L. V., Galushka, A. P., Khivrich, V. I. Influence of neutron and gamma radiation on properties of high-ohmic silicon grown in hydrogen environment. *Fizika i tekhnol. polupr.*, 1971, 5, 4, pp. 747-750 (in Russian).
10. Kozlov, I. P., Logvinenko, T. A., Lugakov, P. F., Tkachev, V. D. Change in concentration of carriers in fast electron irradiated silicon. *Fizika i tekhnol. polupr.*, 1974, 8, 8, pp. 1431-1435 (in Russian).
11. Gass, V. F., Nikolayevskii, I. F., Shurenkov, V. V. Measurement of minority carrier lifetime in electron irradiated silicon. In: *Radiation Defects in Semiconductors.* Minsk, Belorussian State University, 1972, pp. 34-36 (in Russian).
12. Lugakov, P. F., Mishchuk, S. V., Nozdrina, V. V., Tkachev, V. D. Recombination of carriers in *n*-type silicon irradiated with fast electrons. In: *Radiation Defects in Semiconductors.* Minsk, Belorussian State University, 1972, pp. 85-86 (in Russian).
13. Ivanov, G. M., Sirota, N. N. On the relative role of disordered regions in damage of electron irradiated silicon. In: *Radiation Defects in Semiconductors.* Minsk, Belorussian State University, 1972, pp. 56-57 (in Russian).
14. Panov, V. I., Smirnov, L. S. Influence of irradiation intensity on processes of accumulation of radiation defects in silicon. *Fizika i tekhnol. polupr.*, 1917, 5, 2, pp. 346-348 (in Russian).
15. Van Lint, V. A., Gigas, G., Barengoltz, J. Correlation of displacement effects produced by electrons, protons and neutrons in silicon. *IEEE Trans. on Nucl. Science*, 1975, NS-22, 6, pp. 2663-2668.
16. Stein, H. J. Defects in silicon: concept and correlations. In: *Radiation Damage in Semiconductors.* Proc. of Intern. Conf. Ed. by J. Corbett and G. D. Watkins, London-N. Y.-Paris, Gordon and Breach, 1971, pp. 125-140.
17. Konopleva, R. F., Litvinov, V. L., Ukhin, N. A. *Peculiarities of Radiation Damage of Semiconductors by High-Energy Particles.* Moscow, Atomizdat, 1971, 175 pages (in Russian).
18. Ukhin, N. A. Influence of complex structural damage on properties of semiconductors. In: *Radiation Physics of Non-Metallic Crystals*, 3, part 1. Kiev, Naukova dumka, 1971, pp. 66-93 (in Russian).
19. Vavilov, V. S., Uvarov, E. F., Chukichev, M. V. Dependence of radiation defect production rate on concentration of phosphorus in silicon samples irradiated with reactor neutrons. *Fizika i tekhnol. polupr.*, 1969, 3, 12, pp. 1838-1843 (in Russian).
20. Goryachev, V. G., Korotaeya, N. K., Mordkovich, V. N. Influence of monoenergetic neutron irradiation of electrical properties of *n*-Si. In: *Radiation Defects in Semiconductors.* Minsk, Belorussian State University, 1972, p. 43 (in Russian).
21. Nakashima, K., Inuishi, J. The effects of neutron irradiation in *p*-type silicon. *J. Phys, Soc. Japan*, 1969, 27, 2, pp. 397-405.
22. Koba, B. V., Kramer-Ageev, E. A., Mironov, Yu. A., Yaryna, V. P. Comparative changes in electrical behaviour of silicon when irradiated with reactor neutrons and 14.5 MeV electrons. *Fizika i tekhnol. polupr.*, 1975, 9, 12, pp. 2362-2364 (in Russian).
23. Litvinenko, A. G., Murin, L. I., Tkachev, V. D. Peculiarities of change in mobility in neutron irradiated *n*-type silicon. *Fizika i tekhnol. polupr.*, 1977, 11, 8, pp. 1586-1589 (in Russian).
24. Akishin, A. I., Gorodetsky, S. M., Grigoryeva, G. M., Kreinin L. B., Nazarov, V. G. On selection of combination of irradiations to simulate effects

of space radiation on photoelectrical photoconverters. In: *Space Materials and Technology*. Moscow, Nauka, 1977, pp. 149-157 (in Russian).
25. Grigoryeva, G. M., Kolodin, L. G., Kreinin, L. B., Mukashev B. N., Nusupov, K. Kh. Radiation defects in *p*-type silicon irradiated with 30 MeV protons. *Fizika i tekhnol. polupr.*, 1977, **11**, 11, pp. 2176-2180 (in Russian).
26. Van Lint, V. A., Leadon, R. E. Implication of cluster model of neutron effects in silicon. In: *Lattice Defects in Semiconductors. Conf. Ser. No. 23*, Inst. of Phys. London-Bristol, 1975, pp. 103-125.
27. *Physical Processes in Irradiated Semiconductors*. Ed. by L. S. Smirnov. Novosibirsk, Nauka, 1977, 256 pages (in Russian).
28. Mashovets, T. V. Point defects in germanium: reliable and questionable. In: *Radiation Effects in Semiconductors. Conf. Ser. No. 31*, Inst. of Phys. London-Bristol, 1977, pp. 30-44.
29. Gerasimov, A. B., Dolidze, N. D., Kakhidze, N. G., Konovalenko, B. M., Chelidze, N. V. On kinetics of radiation defect annealing in germanium irradiated with fast electrons at 77 K. In: *Radiation Physics of Crystals and p-n Junctions*. Minsk, Nauka i tekhnika, 1972, p. 55 (in Russian).
30. Mashovets, T. V., Emtsev, V. V. Point defects in germanium. In: *Lattice Defects in Semiconductors. Conf. Ser. No. 23*, Inst. of Phys. London-Bristol, 1975, pp. 103-125.
31. Gerasimov, A. B., Gogotishvili, M. K., Dolidze, N. D. Radiation defects in *n*-type germanium irradiated with fast electrons at low temperatures. In: *Radiation Effects in Germanium*. Kiev, 1976, pp. 44-45 (in Russian).
32. Zhevno, A. N., Stelmakh, B. F., Tkachev, V. D., Urenev, V. I. On the vacancy-donor complexes in silicon and germanium. In: *Radiation Defects in Semiconductors*. Minsk, Belorussian State University, 1972, p. 55 (in Russian).
33. Gerasimov, A. B., Dolidze, N. D., Kakhidze, N. G., Konovalenko, B. M., Mtskhvetadze, M. G. On kinetics of light-sensitive defect annealing in germanium irradiated at 77 K. In: *Radiation Defects in Semiconductors*. Minsk, Belorussian State University, 1972, pp. 117-119 (in Russian).
34. Zhevno, A. N., Stelmakh, V. F., Tkachev, V. D., Urenev, V. I. On kinetics of accumulation, energy spectra of levels and charge states of vacancy-donor complexes in germanium. In: *Radiation Defects in Semiconductors*. Minsk, Belorussian State University, 1972, pp. 125-127 (in Russian).
35. Streetman, V. G. Recombination and trapping in Co^{60} gamma irradiated *n*-type germanium. *J. Appl. Phys.*, 1966, **37**, 8, pp. 3145-3152.
36. Fukuoka, N., Tatsumi, J., Saito, M., Cleland, J. The E_C—0.2 eV level in irradiated *n*-type germanium. *J. Phys. Soc. Japan*, 1972, **32**, 2, pp. 283-284.
37. Newman, R. C., Totterdell, D. H. J. Electronic absorption near the band edge in neutron irradiated germanium. In: *Lattice Defects in Semiconductors. Conf. Ser. No. 23*, Inst. of Phys. London-Bristol, 1975, pp. 172-177.
38. Lang, D. V. Review of radiation-induced defects in III-V compounds. In: *Radiation Effects in Semiconductors. Conf. Ser. No. 31*, Inst. of Phys. Bristol-London, 1977, pp. 70-94.
39. Coates, R., Mitshell, E. W. A model for damage produced by fast neutrons in gallium arsenide. In: *Radiation Damage and Defects in Semiconductors. Conf. Ser. No. 16*, Inst. of Phys. London-Bristol, 1972, pp. 96-102.
40. Lomako, V. M., Novoselov, A. M. Radiation-induced changes in lifetime of carriers in gallium arsenide. *Fizika i tekhnol. polupr.*, 1976, **10**, 5, pp. 900-904 (in Russian).
41. Brailovskii, E. Yu., Broudnyi, N. N., Groza, A. A. Annealing of defects and formation of clusters in *n*-type GaAs upon electron irradiation. In: *Radiation Defects in Semiconductors. Conf. Ser. No. 16*, Inst. of Phys. London-Bristol, 1972, pp. 121-128.
42. Broudnyi, V. N., Brailovskii, E. Yu., Krivov, M. A., Red'ko, V. P. Infrared absorption caused by deep defect levels in gallium arsenide. In: *Izv. vuzov. Fizika*, 1974, 10, pp. 118-121 (in Russian).

43. Dyment, J. C., North, J. C., d'Asaro, L. A. Optical and electrical properties of proton-bombarded *p*-type GaAs. *J. Appl. Phys.*, 1973, 44, pp. 207-212.
44. Mashovets, T. V. The status and perspectives of radiation physics of A_3B_5 group semiconductors. In: *Radiation Physics of Non-Metallic Crystals*. V. 3, Part 1. Kiev, Naukova dumka, 1971, pp. 5-28 (in Russian).
45. Bogdankevich, O. V., Kalendin, V. V., Kryukova, I. V. Influence of fast electron intensive beam irradiation on electrophysical and optical properties of gallium arsenide. In: *Radiation Defects in Semiconductors*. Minsk, Belorussian State University, 1972, p. 138 (in Russian).
46. Brailovsky, E. Yu., Broudnyi, V. N. Production and annealing of defects in electron irradiated *n*-GaAs. In: *Radiation Defects in Semiconductors*. Minsk, Belorussian State University, 1972, pp. 141-143 (in Russian).
47. Grigoryeva, G. M., Kagan, M. B., Kreinin, L. B., Landeman, A. P., Meshcheryakova, T. M. Experimental studies of influence of proton irradiation and subsequent annealing on recombination in GaAs. In: *Radiation Defects in Semiconductors*. Minsk, Belorussian State University, 1972, pp. 155-156 (in Russian).
48. Kolchenko, T. I., Lomako, V. M. Influence of electron and fast neutron irradiation on electrical properties of gallium arsenide. In: *Radiation Defects in Semiconductors*. Minsk, Belorussian State University, 1972, pp. 161-162 (in Russian).
49. Vikhlii, G. A., Karpenko, A. Ya., Konozenko, I. D., Oganesyan, O. V., Tarabrova, L. I. Influence of fast neutron irradiation and annealing on electrical properties of InSb. In: *Radiation Effects in Semiconductor Compounds*. Kiev, Naukova dumka, 1976, pp. 48-49 (in Russian).
50. Vikhlii, G. A., Konozenko, I. D., Oganesyan, O. V. Influence of 7 MeV electron irradiation on electrical properties of InSb. In: *Radiation Effects in Semiconductor Compounds*. Kiev, 1976, pp. 50-51 (in Russian).
51. Vikhlii, G. A., Karpenko, A. Ya., Konozenko, I. D., Oganesyan, O. V., Tarabrova, L. I. Influence of 50 MeV electron irradiation on electrical properties of InSb. In: *Radiation Effects in Semiconductor Compounds*. Kiev, 1976, pp. 52-53 (in Russian).
52. Zaitov, F. A., Mukhina, O. V., Polyakov, A. Ya., Ovanesov, V. N. Influence of disordered regions on electrophysical and photoelectrical parameters of indium antimonide. In: *Radiation Effects in Semiconductor Compounds*. Kiev, 1976, pp. 54-55 (in Russian).
53. Kurdiani, N. I. Annealing of radiation defects and mobility in neutron irradiated InSb. *Fizika i tekhnol. polupr.*, 1969, 3, 11, pp. 1683-1686 (in Russian).
54. Mashovets, T. V. Point defects in germanium and indium antimonide. In: *Radiation Effects in Solids*. Kiev, Naukova dumka, 1977, pp. 11-24 (in Russian).
55. Abdullayev, A., Vitovsky, I. A., Mashovets, T. V., Mustafakulov, D. Structural defects production process in gamma irradiated indium antimonide. *Fizika i tekhnol. polupr.*, 1975, 9, 2, pp, 282-286 (in Russian).
56. Lezheiko, L. V., Pridachin, N. B., Smirnov, L. S. On semiconductor conductivity via disorder produced by heavy particle bombardment. *Fizika i tekhnol. polupr.*, 1972, 6, 5, pp. 899-901 (in Russian).
57. Choyke, W. J. Review of radiation damage in SiC. In: *Radiation Effects in Semiconductors. Conf. Ser. No. 31*, Inst. of Phys. Bristol-London, 1977, pp. 58-60.
58. Geitsi, I. I., Gorin, S. I., Nesterov, A. A., Pletyushkin, A. A. On the nature of the "red" cathodoluminescence band in irradiated beta-SiC. In: *Radiation Physics of Non-Metallic Crystals*, V. 3, Part 2, Kiev, Naukova dumka, 1971, pp. 97-110 (in Russian).
59. Bolotov, V. V., Vasilyev, A. V., Smirnov, L. S. Production of defects in silicon at increased irradiation temperatures. *Fizika i tekhnol. polupr.*, 1976, 10, 9, pp. 1670-1674 (in Russian).

60. Bolotov, V. V., Vasilyev, A. V., Kashnikov, B. P., Smagulova, S. A., Smirnov, L. S. Production of defects in germanium at increased irradiation temperatures. *Fizika i tekhnol. polupr.*, 1976, 10, 1, pp. 81-82 (in Russian).
61. Gres'kov, I. M., Solovyev, S. P., Kharchenko, V. A. Dependence of some changes in electrophysical properties and microstructure of silicon on irradiation conditions and properties of original material. In: *Radiation Effects in Silicon.* Kiev, 1976, pp. 26-27 (in Russian).
62. Bortnik, M. V., Novokreshchennaya, T. I., Yukhnevich, A. V. Radiation damage in heat-treated silicon crystals irradiated with Co^{60} gamma rays. In: *Radiation Physics of Non-metallic Crystals.* 3, Part 1. Kiev, Naukova dumka, 1971, pp. 264-269 (in Russian).
63. Gartseva, L. Ye., Levchuk, L. V., Mordkovich, V. N., Starchik, M. I. Behaviour of oxygen containing silicon at concurrent heat treatment and irradiation. In: *Radiation Physics of Non-metallic Crystals.* 3, Part 1. Kiev, Naukova dumka, 1971, pp. 284-288 (in Russian).
64. Groza, A. A., Tomchuk, L. V. Influence of high-temperature and radiation treatments on silicon properties. In: *Radiation Effects in Silicon.* Kiev, 1976, pp. 55-56 (in Russian).
65. Panov, V. I., Smirnov, L. S., Tishkovsky, E. G. On interactions of thermal and radiation-induced defects in silicon. *Fizika i tekhnol. polupr.*, 1975, 9, 8, pp. 1580-1583 (in Russian).
66. Sirota, N. N., Kurilovich, N. F., Gatalskii, G. V. Influence of temperature on accumulation and properties of radiation damage in electron irradiated gallium arsenide. In: *Dokl. AN SSSR*, 1977, 232, 5, pp. 1062-1065 (in Russian).
67. Vinetski, V. L., Smirnov, L. S. On compensation of conductivity by radiation defects in semiconductors. *Fizika i tekhnol. polupr.*, 1971, 5, 1, pp. 176-178 (in Russian).
68. Litvinenko, A. G., Murin, L. I., Tkachev, V. D. Vacancy and interstitial mechanisms of formation of radiation damage in silicon. In: *Radiation Effects in Silicon.* Kiev, 1976, pp. 18-19 (in Russian).
69. Boltaks, B. I., Bakhadyrkhanov, M. K., Gorodetsky, S. M., Kulikov, G. S. *Complex-Containing Silicon.* Nauka, 1972, 121 pages (in Russian).
70. Akhmetov, V. D., Bolotov, V. V., Vasilyev, A. V., Karpov, Yu. A., Shakhovtsov, V. I., Shindich, V. L. On formation of radiation defects in gadolinium-containing silicon. *Fizika i tekhnol. polupr.*, 1977, 11, 11, pp. 2243-2245 (in Russian).
71. Bolotov, V. V., Vasilyev, A. V., Smagulova, S. A. *Electron Irradiation and Annealing of* Ge ⟨Si⟩ *Alloy* (in Russian).
72. Bolotov, V. V., Vasilyev, A. V., Smirnov, L. S. Influence of acceptor impurity concentration on rate of formation of vacancy-oxygen complexes in silicon. *Fizika i tekhnol. polupr.*, 1976, 10, 9, pp. 1787-1789 (in Russian).
73. Bolotov, V. V., Vasilyev, A. V., Rudinskaya, D. E., Smagulova, S. A., Smirnov, L. S. On the role of radiation defect annihilation centers in semiconductors. *Fizika i tekhnol. polupr.*, 1975, 9, 1, pp. 186-187 (in Russian).
74. Vasilyev, A. V., Rybakova, L. A., Smirnov, L. S. On radiation defect annihilation centers. *Fizika i tekhnol. polupr.*, 1972, 6, 4, pp. 733-734 (in Russian).
75. Vasilyev, A. V. On kinetics of formation and annealing of radiation defects in crystals. *Fizika i tekhnol. polupr.*, 1972, 6, 4, pp. 603-608 (in Russian).
76. Bolotov, V. V., Vasilyev, A. V., Smirnov, L. S. The annihilation processes of radiation produced vacancies and interstitials. In: *Radiation Effects in Semiconductors*, 1976, *Conf. Ser., No. 31*, Inst. of Phys. Bristol-London, 1977, pp. 472-477.
77. Smirnov, L. S. On the problems of the radiation physics of semiconductors. In: *Radiation Effects in Solids.* Kiev, Naukova dumka, 1977, pp. 5-11 (in Russian).

78. Shakhovtsov, V. I., Shindich, V. L. The peculiarities of behaviour of rare-earth metal doped silicon in nuclear radiation fields. In: *Radiation Effects in Solids*. Kiev, Naukova dumka, 1977, pp. 88-102 (in Russian).
79. Bakhadyrkhanov, M. K., Zainobidinov, S., Teshabaev, A. T. Interactions of deep-impurity atoms with radiation defects in gamma irradiated silicon. *Fizika i tekhnol. polupr.*, 1977, 11, 2, pp. 285-289 (in Russian).
80. Goncharov, L. A., Dostkhodzhaev, T. N., Emtsov, V. V., Mashovets, T. V., Ryvkin, S. M., The II group impurities in germanium and their role in the processes of radiation defect formation. In: *Fizika i tekhnol. polupr.*, 1977, 11, 5, pp. 945-950 (in Russian).
81. Tkachev, V. D., Urenev, V. I. Interaction of elementary lattice defects with donor impurity atoms in germanium. *Fizika i tekhnol. polupr.*, 1971, 5, 8, pp. 1516-1522 (in Russian).
82. Akimchenko, I. P., Vavilov, V. S., Plotnikov, A. F. Photoconductivity spectra of germanium crystals doped with oxygen and irradiated with fast electrons. *Fizika i tekhnol. polupr.*, 1966, 8, 7, pp.1981-1984 (in Russian).
83. Khansevarov, R. Yu. A study of impurity photoconductivity in fast electron irradiated germanium. *Fiz. tverd. tela*, 1966, 8, 7, pp.1981-1984 (in Russian).
84. Ryvkin, S. M., Khansevarov, R. Yu., Yaroshetsky, I. D. A study of impurity conductivity in gamma irradiated germanium. *Fiz. tverd. tela*, 1961, 3, 10, pp. 3211-3219 (in Russian).
85. Akimchenko, I. P., Vavilov, V. S., Plotnikov, A. F. The spectra and kinetics of photoconductivity associated with elementary structural defects in germanium monocrystals. *Fiz. tverd. tela*, 1963, 5, 5, pp. 1417-1422 (in Russian).
86. Novikov, S. R., Rubinova, E. E., Ryvkin, S. M. Photoconductivity in fast neutron irradiated germanium. *Fiz. tverd. tela*, 1964, 6, 3, pp. 896-898 (in Russian).
87. Konopleva, R. F., Novikov, S. R., Ryvkin, S. M. Energy levels produced by fast neutron bombardment of germanium. *Fiz. tverd. tela*, 1963, 5, 7, pp. 1842-1851 (in Russian).
88. Gerasimov, A. B., Konovalenko, B. M., Yaroshetsky, I. D., Barkalaya, A.A. On impurity conductivity produced by gamma irradiation of germanium. *Fiz. tverd. tela*, 1964, 6, 10, pp. 3166-3168 (in Russian).
89. Gerasimov, A. B., Ryvkin, S. M., Yaroshetsky, I. D. A study of impurity conductivity in fast neutron irradiated germanium. *Fiz. tverd. tela*, 1964, 6, 3, pp. 695-8705 (in Russian).
90. Konovalenko, T. M., Ryvkin, S. M., Yaroshetsky, I. D. A study of radiation defects produced in germanium by 28 MeV fast electron irradiation. *Fiz. tverd. tela*, 1963, 5, 8, pp. 2075-2086 (in Russian).
91. Vasilyev, A. V., Smirnov, L. S. On photoconductivity in gamma irradiated *n*-type germanium samples. In: *Radiation Physics of Non-Metallic Crystals*, Kiev, Naukova dumka, 1967, pp. 183-188 (in Russian).
92. Tkachev, V. D. A study of the stable radiation damage formation processes in silicon. In: *Radiation Physics of Non-Metallic Crystals*. Kiev, Naukova dumka, 1967, pp. 112-118 (in Russian).
93. Konozenko, I. D., Eritsyan, G. N., Khivrich, V. I. Influence of gamma irradiation on lifetime of minority carriers in *n*-type silicon. In: *Radiation Physics of Non-Metallic Crystals*. Kiev, Naukova dumka, 1967, pp. 133-136 (in Russian).
94. Lugakov, P. F., Tkachev, V. D. Fotoconductivity of *n*-type silicon irradiated with fast electrons and neutrons. In: *Radiation Physics of Non-Metallic Crystals*. Kiev, Naukova dumka, 1967, pp. 157-161 (in Russian).
95. Stelmakh, V. F., Tkachev, V. D. A photoconductivity study of radiation damage in gallium arsenide. In: *Radiation Physics of Non-Metallic Crystals*. Kiev, Naukova dumka, 1967, pp. 212-216 (in Russian).

96. Novikov, S. R., Rubinova, E. E. The kinetics of impurity conductivity in neutron irradiated germanium. *Fizika i tekhnol. polupr.*, 1968, 2, 10, pp. 1500-1505 (in Russian).
97. Plotnikov, A. F., Vavilov, V. S., Smirnov, L. S. The kinetics of photoconductivity in neutron irradiated *n*-type silicon. *Fizika i tekhnol. polupr.*, 1961, 3, 11, pp. 3253-3259 (in Russian).
98. Vavilov, V. S., Plotnikov, A. F., Tkachev, V. D. A photoconductivity study of structural defects in silicon monocrystals. *Fiz. tverd. tela*, 1962, 6, 12, pp. 3446-3454 (in Russian).
99. Fan, H. Y., Ramdas, A. K. Infrared absorption and photoconductivity in irradiated silicon. *J. Appl. Phys.*, 1959, 30, 8, pp, 1127-1134.
100. Tkachev, V. D., Plotnikov, A. F., Vavilov, V. S. On the photoconductivity spectra in *n*-type silicon irradiated with fast electrons. *Fiz. tverd. tela*, 1963, 5, 7, pp. 1826-1829 (in Russian).
101. Wada, T., Yasuda, K., Ikuta, S., Takeda, M., Masuda, H. Complex defects introduced into silicon by high-energy electron irradiation: production rates of defects in *n*-Si. *J. Appl. Phys.*, 1977, 48, 6, pp. 2145-2152.
102. Berman, L. S., Vitman, R. F., Shuman, V. B. A study of radiation defects in silicon p^+-*n*-junctions irradiated with gamma rays. *Fizika i tekhnol., polupr.*, 1975, 9, 2, pp. 311-315 (in Russian).
103. Brailovsky, E. Yu., Broudnyi, V. N. Radiation defects in heavily irradiated *p*-GaAs crystals. *Fizika i tekhnol. polupr.*, 1974, 8, 5, pp. 963-965 (in Russian).
104. Vitovsky, N. A., Mashovets, T. V., Ryvkin, S. M., Khansevarov, R. Yu. A change in electrical and photoelectrical properties of gallium arsenide irradiated with 1 MeV electrons. *Fiz. tverd. tela*, 1963, 5, 12, pp. 3510-3523 (in Russian).
105. Petrov, V. V., Tkachev, V. D. Influence of adhesion effects on spectra of photoconductivity in *n*-type silicon irradiated with fast electrons. *Fizika i tekhnol. polupr.*, 1974, 8, 7, pp. 1402-1404 (in Russian).
106. Vasilyev, A. V., Rybakova, L. A., Smirnov, L. S. On photoconductivity spectra in irradiated and plastically deformed germanium crystals. *Fizika i tekhnol. polupr.*, 1968, 2, 12, pp. 1720-1723 (in Russian).
107. Mooney, P. M., Cheng, L. J., Suli, M., Gerson, J. D., Corbett, J. W. Defect energy levels in boron doped silicon irradiated with 1 MeV electrons. *Phys. Rev., B*, 1977, 15, 8, pp. 3836-3843.
108. Petrov, V. V., Tkachev, V. D. Energy spectrum and thermal stability of radiation defects in *p*-Si. *Fizika i tekhnol. polupr.*, 1976, 10, 5, pp. 966-969 (in Russian).
109. Kolesnikov, N. V., Rozanov, Yu. N. Impurity conductivity in *n*-type germanium irradiated with fast electrons. *Fizika i tekhnol. polupr.*, 1976, 10, 6, pp. 1196-1197 (in Russian).
110. Berman, L. S., Akhmedova, M. M., Vitman, R. F., Zvyagina, K. N., Kreinin, L. B. On gamma radiation defects in crucibleless high-ohmic silicon. *Fizika i tekhnol. polupr.*, 1976, 10, 10, p. 2015 (in Russian).
111. Bolotov, V. V., Vasilyev, A. V., Smagulova, S. A., Smirnov, L. S. On radiation defects in *p*-type germanium produced by high-temperature irradiation. *Fizika i tekhnol. polupr.*, 1976, 10, 11, pp. 2162-2164 (in Russian).
112. Vasilyev, A. V., Rybakova, L. A., Smirnov, L. S. On influence of temperature on change of electrical and photoelectrical properties of electron irradiated germanium. *Fizika i tekhnol. polupr.*, 1971, 5, 12, pp. 2297-2300 (in Russian).
113. Ryvkin, S. M. *Photoelectrical Effects in Semiconductors.* Moscow, Fizmatgiz, 1963, 494 pages (in Russian).
114. Kuchis, E. V. *Hall-Effect Measurement Methods.* Moscow, Sov. radio, 1974, 328 pages (in Russian).

115. Vitovsky, N. A., Mashovets, T. V. On one possibility of accurately determining activation energy of impurity and defect energy levels in semiconductors. *Fiz. tverd. tela*, 1964, 6, 6, pp. 1654-1656 (in Russian).
116. Berman, L. S. *Capacitance Methods of Semiconductor Studies*. Leningrad, Nauka, 1972, 104 pages (in Russian).
117. Lang, D. V. Fast capacitance transient apparatus: Application to ZnO and O-centers in GaP *p-n* junction. *J. Appl. Phys.*, 1974, 45, 7, pp. 3014-3022.
118. Boltaks, B. I. *Diffusion and Point Defects in Semiconductors*. Leningrad, Nauka, 1972, 384 pages (in Russian).
119. Berman, L. S., Kreinin, L. B., Nasredinov, F. S. A study of capacitance properties of silicon n^+-p diodes irradiated with fast electrons. *Fizika i techknol. polupr.*, 1972, 6, 2, pp. 294-299 (in Russian).
120. Konopleva, R. F., Rubinova, E. E., Sadikov, V. P., Ukhin, N. A., Zaporozhchenko, Yu. A. High-temperature annealing of germanium irradiated with 660 MeV protons. In: *Radiation Physics of Non-Metallic-Crystals*. 3, Part 1, Kiev, Naukova dumka, 1971, pp. 171-177 (in Russian).
121. Bulgakov, Yu. V., Kolomenskaya, T. I. Radiation defects in silicon irradiated with heavy charged particles. In: *Radiation Physics of Non-Metallic Crystals*. 3, Part 1, Kiev, Naukova dumka, 1971, pp. 292-297 (in Russian).
122. Gerasimov, A. B., Rogachev, A. A., Eristavi, G. L. Absorption edge in fast electron irradiated germanium. *Fizika i tekhnol. polupr.*, 1971, 1, 10, pp. 1582-1584 (in Russian).
123. Newman, R. C., Toterdell, D. H. An optical study of defects in silicon irradiated with fast neutrons. *J. Phys., C: Solid State Phys.*, 1975, 8, pp. 3944-3954.
124. Crowder, B. L., Title, R.S., Brodsky M. H., Pettit, G. D. ESR and optical absorption studies of ion-implanted silicon. *Appl. Phys. Lett.*, 1970, 16, 5, pp. 205-208.
125. Ovshinsky, S. R. Reversible electrical switching phenomenon in disordered structures. *Phys. Rev. Lett.*, 1968, 21, 20, pp. 1450-1453.
126. Milov, A. A. Switching devices based on amorphous semiconductor materials. *Electronnaya tekhnika*, Ser. VI. *Mikroelektronika*, 1971, 3, pp. 3-13 (in Russian).
127. Grigorovichi, R. Amorphous semiconducting films: Physical background of applications. *Thin Sol. Films*, 1972, 12, 2, pp. 153-166.
128. Lyamichev, I. Ya., Litvak, I. I., Oshchepkov, N. A. Devices based on amorphous semiconductors. Moscow, *Sov. radio*, 1976, 128 pages (in Russian).
129. Shklovsky, B. I., Efros, A. L. Impurity zone and conductivity of compensated semiconductors. *ZhETF*, 1971, 60, 2, pp. 867-878 (in Russian).
130. Shklovsky, B. I., Efros, A. L. A transition from metal conductivity to activation conductivity in compensated semiconductors. *ZhETF*, 1971, 61, 2, pp. 816-825 (in Russian).
131. Ionov, A. N., Ryvkin, S. M., Shlimak, I. S. Simulation of "storage" effects in amorphous semiconductors. *Fizika i tekhnol. polupr.*, 1972, 6, 11, pp. 2308-2311 (in Russian).
132. Ryvkin, S. M. On switching mechanism in amorphous semiconductors. *Pisma v ZhETF*, 1972, 15, 10, pp. 632-635 (in Russian).
133. Shlimak, I. S., Nikulin, E. I. Conductivity of doped germanium at extra-low temperatures. *Pisma v ZhETF*, 1972, 15, 1, pp. 30-33 (in Russian).
134. Grekhov, I. V., Kostina, L. S. Static volt-ampere characteristic of multicollector thyristor in turned-on condition. *Fizika i tekhnol. polupr.*, 1970, 4, 8, pp. 1462-1466 (in Russian).
135. Uttecht, R., Stevenson, U., Sie, C. H., Griener, J. D., Raghovon, C. H. Electric field-induced filament formation in As-Te-Ge glass *J. Non-Cryst. Sol.*, 1970, 2, pp, 358-370.

136. Götz, G., Endter, R. Switching effects in amorphized silicon layers. *J. Non-Cryst. Sol.*, 1974, **13**, 2, pp. 286-294.
137. Usov, N. N., Yudin, V. V., Karatsyuba, A. P., Kurinyi, V. I. Switching effects in amorphized silicon layers. *Fizika i tekhnol. polupr.*, 1976, **10**, 3, pp. 560-562 (in Russian).
138. Grigorovichi, R., Croitoru, N., Marina, M., Nâstase, L. Heterojunctions between amorphous Si and Si single crystals. *Rev. Roum. Phys.*, 1968, **13**, 4, pp. 317-325.
139. Osipov, K. A., Folmanis, G. E., Lozinsky, Yu. N. Film structures with amorphous heterojunctions. *Dokl. AN SSSR*, 1973, **212**, 2, pp. 354-356 (in Russian).
140. Brodsky, M. N., Döhler, G. H., Steinhardt, P. J. On the measurements of the conductivity density of states of evaporated amorphous silicon films. *Phys. Stat. Sol.* (*b*), 1975, **72**, pp. 761-769.
141. Yoshida, A., Ido, T., Arizumi, T. Heterojunctions composed of amorphous and crystalline Ge. In: *Electronic Effects in Non-Crystalline Semiconductors.* Leningrad, Nauka, 1976, pp. 407-410 (*Proc. of VI Intern. Conf. on Amorph. and Liquid semiconductors*).
142. Fush, W., Heder, G., Niemann, K., Stuke, J. Properties of junctions between amorphous and crystalline silicon. In: *Electronic Effects in Non-Crystalline Semiconductors.* Leningrad, Nauka, 1976 (*Proc. of VI Intern. Conf. on Amorphous and Liquid Semiconductors*).
143. Chung, C. H., Dunn, B. Construction of energy-band diagrams for amorphous/crystalline heterojunctions. *J. Appl. Phys.*, 1977, **48**, 4, pp. 1751-1752.
144. Brodsky, M. H., Kaplan, D. M., Ziegler, J. E. The optical absorption of amorphous silicon as a function of decreasing spin concentration. In: *Proc. II Intern. Conf. on Phys. Semicond.* Warsaw, Polish Scientific Publishers, 1972, pp. 529-535.
145. Milnes, A., Feucht, D. *Heterojunctions and Metal-Semiconductor Junctions.* New York, 1972, 432 pages.
146. Zakharov, V. P., Gerasimenko, V. P. *Structural Peculiarities of Amorphous Semiconductors.* Kiev, Naukova dumka, 1976 (in Russian).
147. Khaibulin, I. B., Shtyrkov, E. I., Zaripov, M. M., Galyautdinov, M. F., Bayazitov, R. M. Annealing of ion doped layers by laser radiation. Dep. No. 2661-74, *VINITI*, 32 pages (in Russian).
148. Belokrinitsky, N. S., Gnatovsky, A. V., Danileiko, M. V., Zakharov, V. P., Kozlov, A. V., Shpak, M. T. Optical information recording on amorphous films of semiconductor compounds. *Pisma v ZhETF*, 1972, **15**, 4, pp. 198-200 (in Russian).
149. Gadzhiev, A. R., Ryvkin, S. M., Shlimak, I. S. Fast neutron compensated *n*-type germanium as a model of amorphous semiconductors. *Pisma v ZhETF*, 1972, **15**, 10, pp. 605-608 (in Russian).

CHAPTER 5

STATUS AND PROSPECTS OF ION IMPLANTATION IN SEMICONDUCTORS

By the present time, a sufficient wealth of material has been accumulated on semiconductor doping by accelerated ion implantation. This material has been largely generalized in a number of books [1 through 5]. Many original works and reviews have appeared in the proceedings of the international conferences on ion implantation and radiation physics of semiconductors [6-19].

In this chapter we shall make an attempt at determining the status of the ion implantation physics and point out some new and promising trends in this field. From the technological viewpoint, the most important are the relationships between the implanted impurity and defect profiles and the implantation and annealing conditions, relations between the concentrations of implanted ions and electrically active centers, the influence of the target temperature on the ion implantation results, the role of defects at various stages of annealing, etc.

At first, let us discuss the results which we regard to be rather fully ascertained.

1. The paths of ions with a mass of 10 to 100 in amorphous targets are given by the theoretical formulae of Lindhard-Scharff-Schiott (LSS) for the entire practically used range of initial ion energies (10 to 1000 keV).

2. Distribution of ion paths in monocrystalline substrates differs from the profiles given by the LSS formulae mainly by the presence of "tail" caused by the channelling effect. So far, nobody has succeeded in deriving simple mathematical relations to calculate the profiles with allowance made for the channelling effect. For the most part it is explained by the fact that the fraction of the channelled ions has a strong dependence on the mass of the implanted particle, target material, ion energy, irradiation temperature, and relative orientation of the beam and substrate. Besides, the channelling conditions continuously vary with growth of the dose due to an increase in the concentration of defects and implanted impurity.

Nevertheless, the LSS theory is successfully applied to calculations of ion path profiles in monocrystals, since in most instances (unless special conditions favourable for channelling are provided) the fraction of the channelled ions does not go in excess of 1% and, as

such, does not bear a significant effect on the position of the impurity distribution maximum.

3. The radiation defect profiles are more close to the surface than the implanted ions. This is credited to the fact that all ions take part in increasing the concentration of defects in the near-the-surface layers. At the same time, in the layers deeper than the projection of the ion mean free path, defects are produced by only those particles that penetrate most deeply. Due to a high mobility of the defects, their actual profiles differ from the calculated ones. Specifically, the surface serves as a good sink for the defects where the latter can accumulate even to form an additional near-the-surface amorphous layer.

4. When a light particle is implanted in a material having a low atomic weight, the track of this particle represents a branched cascade of displacements. In this case, the formation of an amorphous region within an individual track is unlikely, and the amorphization of the implanted layer, observed after a high-dose irradiation, results from accumulation of defects. The availability of sinks for the defects promotes the accumulation process. As a heavy particle slows down due to collisions, the energy losses per unit path grow and the cascade of displacements turns out to be strongly localized.

The probability of amorphization caused by an individual ion increases. As a result, the overlapping of individual amorphous microregions becomes a dominating mechanism of amorphization of the implanted layer. There is an evidence that in some cases the overheated matter inside a localized cascade of displacements may harden to form crystallites misoriented with respect to the matrix.

5. Increasing the target temperature during irradiation proves an effective technique for preventing amorphization of the implanted layer. In most cases (e.g., silicon, germanium, gallium arsenide) no amorphization occurs even at an irradiation temperature of 200 °C for all doses of practical interest.

6. Annealing is essential to electrical activation of the implanted impurity. The annealing involves several processes: the impurity atoms are dissolved at the lattice sites, the complexes dissociate if they comprise defects and impurity atoms, and the compensating centers are removed.

7. After annealing, the concentration of free carriers is far from being always in agreement with the implanted dose. At the initial stage of investigation of the possibilities offered by ion implantation, it seemed that this method could be used for implantation of any impurity into the crystal in the amount exceeding the dissolubility limit. However, numerous works have shown that whenever the dissolution of impurity atoms at the lattice sites is concerned, the dissolubility limit can be exceeded with moderate annealing only. Further increase in temperature and duration of heat treatment

inevitably results in ejection of the surplus impurity from the lattice sites (so-called "negative annealing"). The use of pulsed heating (e.g., laser heating) allows one to increase the impurity concentration in the lattice sites due to a momentary temperature rise almost to the melting point and subsequent rapid cooling.

8. If the crystalline structure is not disturbed by ion implantation (due to a low dose, increased irradiation temperature), then in silicon a major fraction of group V impurity atoms occupy the lattice sites immediately and the concentration of interstitial atoms is not high. A considerable fraction of substitutional atoms is also observed for the IV and VI group elements implanted in silicon. It should be emphasized that the reliable information on the positions of impurity atoms in the silicon crystal lattice is available only for the heavy elements. Unfortunately, the most widely used donor element, phosphorus, has hot been sufficiently studied in this respect, since the back-scattering, the basic technique for location of impurity atoms in the lattice, shows low sensitivity to the atoms whose mass is close to or less than that of the substrate.

9. When group III elements are implanted in silicon, the percentage of substitutional atoms in them is lower than in group V impurities. A major fraction of group III impurity atoms occupy the tetrahedral interstitial positions. At the implantation temperature of 350-450 °C, the interstitial content is, in the main, nearly equal to the substitutional one. The group II elements implanted in silicon at 350 °C do not, for all practical purposes, yield any substitutional impurity. For the majority of well known impurities, their behaviour in germanium and silicon is almost identical as far as their distribution in the lattice after implantation is concerned.

10. The distribution of implanted impurity atoms in type $A_{III}\,B_V$ compounds is not as clear as in silicon. This is in part due to availability of a wide range of the major semiconductor materials of the given type, such as gallium arsenide, triplex solutions based on GaAs and on InSb. In all likelihood, group II elements occupy the sites in the gallium sublattice even before the annealing. Group VI elements implanted in gallium arsenide at room temperature are mostly found in the interstices. If the implantation occurred at a temperature in excess of 200 °C, then, as was shown by the experiment involving tellurium, almost all impurity atoms immediately occupy the lattice sites. The atoms of group IV elements show a tendency to fill the gallium sublattice in gallium arsenide.

11. The nature of the post-implantation annealing depends on whether the amorphization has been achieved after ion bombardment. In implanted silicon layers, the restoration of the crystalline structure and electrical activation of the impurity are observed near 600 °C if the layers have been amorphized. If no amorphization occurred after ion bombardment, the annealing causes the concentration

of free carriers to gradually increase till the temperature becomes 1000 °C. In boron doped silicon, the amorphization tangibly increases the utilization factor of the implanted impurity. For this purpose, the boron-implanted layers are additionally irradiated with ions of inert gases or silicon. In ion implantation of gallium arsenide, the amorphization is particularly important for implantation of group VI ions. The amorphized layers are annealed at 800 °C and higher temperatures. The annealing of non-amorphized layers begins at 500-600 °C and includes a subsequent "negative" section followed with a repeated rise in the concentration of free electrons.

12. The post-annealing behaviour of impurities in implanted layers of silicon, germanium and gallium arsenide agrees with their behaviour during diffusion doping although the ionization energies of the impurity atoms may be somewhat different due to the effects of unannealed lattice imperfections. As was already noted, amphoteric impurities of group IV in gallium arsenide have a tendency to fit into the gallium sublattice. The bombardment with inert gas ions and subsequent annealing of *p*-GaAs containing a high concentration of silicon atoms result in the conversion of the material due to the redistribution of the impurity among the sublattices.

13. The distribution of impurity atoms after annealing differs sometimes from the distribution of the ion paths. This is caused by the diffusion of impurities during annealing. With a high temperature and long-time annealing, the diffusion acceleration obeys ordinary laws of diffusion with normal coefficients. In the event of short-time annealings at relativily low temperatures, an enhanced diffusion is often observed. The diffusion enhancement is determined by two reasons. On the one hand, an increased concentration of vacancies in the implanted layers favours a faster migration of impurity atoms along the lattice sites. On the other hand, a fraction of the implanted atoms stuck in the interstices can now diffuse at a high speed along the interstices to the pinning points, e.g., to vacancies. The vacancy mechanism of diffusion enhancement dominates near the damage maximum, the interstitial mechanism, at a great depth. The relation between the vacancy and interstitial fluxes depends on the nature of the substrate and impurity as well as on the implantation conditions, since these determine the initial ("starting") position of the impurity atoms prior to annealing. If the impurity in the substrate can diffuse by both vacancies and interstitials with the interstitial migration proceeding at a faster rate, the surplus vacancies in the implanted layer cause a retardment of the diffusion.

14. Complete annealing out of defects is attained only with low-dose (about 10^{13} cm^{-2}) implantations. With medium (about 10^{14} to 10^{15} cm^{-2}) and high (about 10^{16} cm^{-2} and higher) doses of implants, it is not possible to fully prevent the radiation damage even by prolonged heating at 1000 °C and higher temperatures. The residual defects

represent dislocation loops resulting from coagulation of vacancies or interstitials, or a dislocation network. Another important factor is the presence of high concentrations of foreign atoms giving rise to stresses in the implanted layer. These stresses can be relaxed by forming misfit dislocation networks.

15. Implantation of super-high doses, when the concentration of implanted impurity atoms becomes commensurate with that of the target atoms, results in emergence of new phases and in synthesis of new compounds. Sometimes, super-high dose implantations are attended with the recovery of the crystalline structure in disordered layers. The process does not require an additional heating though reveals itself in high densities of ion current. Evidently, the structural transformations are conditioned by the irradiation-induced activation of solid-phase reactions involving production and dissociation of the compounds in the material of the substrate and implanted impurity. It is quite probable that the activation mechanism is associated with the emergence of increased pressure centers in the layer that has been amorphised so far.

We have listed the major characteristics of the ion implantation technique. To a considerable degree, they determine the present and future fields of application of ion implantation for production of circuits and components of semiconductor micro- and optoelectronics. The same characteristics impose certain limitations on the employment of the said method.

In the first place, it is advisable to apply ion implantation to fabrication of semiconductor device components if thickness is less than 1 μm thick. It is extremely difficult to have a controlled diffusion at a depth less than 1 μm. In addition, increasing the thickness of an implanted layer through increasing the ion energy also meets with serious technical difficulties when the enhancement potential exceeds 0.5 to 1 MV. Employment of multiply charged ions is not always practicable, but even when the operating conditions of the ion source allow separation of multiply charged ions, the current density of such ions is too low and prolonged exposures are required to attain medium and high doses.

A greater thickness of the implanted layer can also be achieved by accelerated diffusion of the impurity implanted into a thin near-the-surface layer. Where the effect of the enhanced diffusion is used, the annealing temperature may be comparatively low, e.g., 600 to 900 °C for silicon or gallium arsenide. However, both with the vacancy and interstitial enhancement mechanisms, the effect is observed only about 1 μm deeper than the implanted layer. Outside this region, the diffusion occurs in the usual manner and high temperatures are required for the impurity to penetrate to greater depths. Very often an enhanced diffusion in the implanted layer, driving the impurity 2-3 μm deep, is considered good practice, since the implan-

tation allows injection, in a controlled way, of the desired amount of a homogeneous impurity into the thin near-the-surface layer, while a momentary diffusion sets the boundary of the implanted region beyond the radiation damage zone. Still, the application of ion implantation and enhanced diffusion for fabrication of layers more than 5-10 μm thick is hardly technically feasible.

Another area where ion implantation is obviously more attractive than the traditional impurity injection techniques is the production of complex doping profiles. With diffusion doping, the distribution of impurity atoms is strictly determined by the laws of diffusion which make it practically impossible to obtain a concentration profile of a complex configuration. In principle, ion implantation allows obtaining any impurity profile by selecting a suitable energy and dose of implants. In this case, the postimplantation annealing temperature should be low since an overheating will result in equalizing the doping profiles. The basic difficulty encountered in the production of complex impurity profiles resides in elaboration of a program for timing the processes of irradiation and annealing, since one has to reckon with the effects of the preceding irradiation on the subsequent one. Most likely, the employment of computers will solve this problem.

Finally, it is worthwhile to consider the application of ion implantation for controlled injection of low-dose impurities into the near-the-surface layers. The main advantages offered by the ion-beam technique in the given case are a high degree of homogeneity of the impurity and but a slight dependence of the implanted layer properties on the sample prehistory and imperfections present in the near-the-surface region. At present, the minimum doses that find practical application amount to 10^{11} cm^{-2}. With the implanted layer 0.5 μm thick, the volume concentration will be of the order of $2 \cdot 10^{15}$ cm^{-3}. It is rather difficult to obtain such a concentration in a thin layer by diffusion with reproducibility. This doping level is not, however, the lowest one and when it is required to inject a small but strictly preset number of impurity atoms in a small volume, the ion beam is the best choice. Of special interest is the doping effected without masking. In this method, the doping is accomplished by scanning sharply focused beams over the surface of the semiconductor water. At present, this method undergoes a stage of laboratory investigations, while its implementation would allow discarding, in a number of instances, some operations involving photolithography.

At the same time, the ion implantation method has some limitations. The main one is likely to be the need for annealing out the radiation defects, which prevents ion implantation from being a true low-temperature process. Although more often than not the defect annealing temperature is considerably less than the temperatures specific to diffusion, the post-implantation annealing is not always

desirable and possible. In this connection, of particular interest is a pulsed heating. For instance, when a semiconductor surface is exposed to powerful laser pulses lasting for a nanosecond or so, only a layer several microns thick is heat-treated. Similarly, the heat has no time to spread across the layer also, which makes possible the localized annealing of the semiconductor wafer microregions. Light pulses of a millisecond duration heat the material to a depth of hundreds of microns, yet the temperature rise so transient presents no serious danger for the substrate and adjacent microcircuit components. This applies not only to light pulses but equally to pulsed irradiation with electrons, *X*- and gamma-rays, ions, protons, etc. Each kind of irradiation has its peculiarities, disadvantages and advantages. It is probable that application of doping impurity ions in short powerful pulses will enable one to combine the actions of implantation and annealing of defects. Until the present time no publications have appeared on pulsed ion bombardment.

It could be possible to inject impurity atoms to great depths and, at the same time, to avoid formation of complex radiation defects if the ion implantation occurred concurrently with the growth of the semiconductor film. The development of the molecular beam epitaxy in vacuum has made this process possible. There is an experimental evidence according to which the ionization of the impurity beam substantially improves the doping efficiency during molecular beam epitaxy in vacuum. Another limitation of the ion implantation method resides in a relatively complicated procedure of readjustment of the ion-beam apparatus when changing from one kind of impurity to another. Often one needs to have two or three ion guns each permanently using only one ion species for its operation. Though recent years have seen the emergence of equipments with simple selection of ion beams, the number of ion species is limited and exploration of new doping elements meets some difficulties. It would be very desirable to have one versatile apparatus using one ion species and capable of injecting different doping elements into the crystal. This problem can be solved in part, and there exist two options.

The first option is based on the employment of the RED effect. The doping elements are deposited as thin layers on the appropriate sections of the semiconductor wafer, following which, the entire structure is irradiated with inert gas ions at elevated temperature. The ion energy selected should permit penetration of ions through the impurity layer and cause the maximum damage in the region near the substrate surface. As a result, an increased concentration of defects brings about an enhanced diffusion of the impurity to a depth determined by the ion path and diffusion length of the defects.

In the second option, the impurity is injected into the semiconductor in the form of recoil atoms. Like in the first case, the doping

element is applied as a thin layer to the substrate and then irradiated. In this technique, however, it is required that the region of maximum energy losses due to elastic collisions be within the impurity film. The bombarding ions communicate some energy, on impact, to the impurity atoms thus driving them inside the substrate. The advantages of the method include, apart from simplicity and versatility, the fact that each primary bombarding ion gives rise to a cascade of displacements with the result that the share of implanted atoms becomes several times that of the primary ions.

When the displacement peak represents an overheated region near the surface (heavy target, great ion mass, low energy), the atoms adsorbed at the surface are apt to be pulled into this region. This phenomenon is also of some interest for practical development of a universal doping method.

To conclude, we can state that over the last 15 years of intensive studies of the ion implantation technique considerable advances have been made in the understanding of the physical processes involved in ion bombardment of crystalline targets and subsequent annealing. The main efforts have been directed to the study of ion implantation in silicon. The number of works on this subject is well over 1000 and we believe that it is in this field that a need for new original ideas is acute. To some extent, this also applies to ion implantation in gallium arsenide. Other semiconductors are known much less, as far as ion implantation is concerned. It seems that the maximum interest has been aroused in some compounds of the A_{II} B_{VI} type which, due to self-compensation, have only one type of conductivity, and multicomponent compounds of the III and V group elements. The earlier reports stating the instrumental role of ion implantation in overcoming the self-compensation in cadmium sulfide and production of the *p*-type material cannot be considered sufficiently reliable. The ion implantation of compounds containing three and more components so far undergoes the stage of the initial laboratory investigations. Now as before, the main problem of ion implantation is the avoidance of radiation damage. So, the efforts are focused here on the study of the implantation conditions providing for minimum concentration of defects and on the development of the defect annealing techniques preventing detrimental effects of heating on the semiconductor material. Even a partial progress in the solution of this problem will drastically expand the area of possible application of the ion implantation method.

Incidentally, it is interesting to consider a possibility of crystallization of amorphous layers by ion bombardment. Assume there is an amorphous semiconductor layer on a monocrystal substrate, which is irradiated with ions whose energy allows them to travel a path approximately equal to the thickness of the amorphous layer. At the end of the path, the ions form an excitation region, i.e., a ther-

mal spike characterized by high temperatures and pressures, if the spike coincides with the interface between the amorphous layer and the monocrystal and, also, takes up some atoms from the substrate and from the layer, then, on cooling down, the whole region will crystallize on the orienting matrix into a single piece. A bombardment, if sufficiently long, will bring about a complete crystallization of the amorphous layer. To preclude amorphization of the substrate, it is necessary to irradiate the structure at elevated temperature. Such a technique will allow crystallization not only of the macrolayers but, also, of the microvolumes commensurable with the thermal spike. A similar mechanism applies for explaining the super-high dose effects if we assume that with high densities of ionic current the substrate temperature registers a marked increase as the irradiation nears an end.

References

1. *Semiconductor Doping by Ion Implantation.* Ed. by V. S. Vavilov and V. M. Gusev. Moscow, Mir Publishers, 1971, 523 pages (in Russian).
2. Mayer, J., Eriksson, L., Davies, J. *Ion Implantation in Semiconductors. Silicon and Germanium.* New York-London. 1970, 280 pages.
3. *Ion Implantation in Semiconductors.* Translation from Japanese. Ed. by Pavlov P. V. Mir Publishers, 1973, 296 pages (in Russian).
4. Zorin, E. I., Pavlov, P. V., Tetelbaum, D. I. *Ion Implantation in Semiconductors.* Moscow, Energiya, 1975, 128 pages (in Russian).
5. *Physical Processes in Irradiated Semiconductors.* Ed. by L. S. Smirnov, Novosibirsk, Nauka, 1977, 256 pages (in Russian).
6. *Ion Implantation.* Ed. by F. H. Eisen, L. T. Chadderton. London-N.Y., Gordon and Breach, 1971, 695 pages.
7. Radiation damage and defects in semiconductors. *Conf. Ser. No. 16*, Inst. of Phys. London-Bristol, 1973, 371 pages.
8. *Ion Implantation in Semiconductors.* Ed. by I. Ruge, J. Graul. Berlin, Springer-Verlag, 1971, 480 pages.
9. *Ion Implantation in Semiconductors and Other Materials.* Ed. by B. L. Crowder, N.Y.-London, Plenum Press, 1973, 611 pages.
10. *Proceedings of U. S.* Japan seminar on ion implantation in semiconductors. Kyoto, Japan, Soc. for Promotion of Science, 1972, 305 pages.
11. *Radiation Effects in Semiconductors.* Ed. by J. W. Corbett, G. D. Watkins. London. Gordon and Breach. 1971, 477 pages.
12. *Proceedings of the international conference on ion implantation in semiconductors.* Lublin, Publ. by Inst. Nucl. Research, Swierk, 1974, 1, pp. 1-289; 2, pp. 290-579.
13. International conference on ion implantation in semiconductors. Budapest, *KFKI*, 1975, 662 pages.
14. International working meeting on ion implantation equipment. Swierk, Publ. by Inst. Nucl. Research, 1973, 183 pages.
15. Lattice defects in semiconductors, 1974. *Conf. Ser. No. 23*, Inst. of Phys. London-Bristol, 1975, 599 pages.
16. Radiation effects in semiconductors, 1976, *Conf. Ser. No. 31*, Inst. of Phys. Bristol-London, 1977, 534 pages.
17. *Ion Implantation in Semiconductors. Science and Technology.* Ed. by S. Namba. N.Y.-London, Plenum Press, 1975, 742 pages.
18. *Ion Implantation in Semiconductors.* Ed. by F. Chernov, J. A. Borders, D. K. Brice. N.Y.-London, Plenum Press, 1977, 754 pages.
19. *Application of Ion Beams to Materials.* Ed. by G. Garter, J. S. Colligon, W. A. Crant. London-Bristol, Inst. of Phys., 1976, 364 pages.

CHAPTER 6

ION IMPLANTATION IN INDIUM ANTIMONIDE

Sec. 6.1. Basic Characteristics and Prospects of Employment of Indium Antimonide

Indium antimonide is one of the first compounds of the A_{III} B_V type to be studied systematically and in detail. This can be explained, on the one hand, by ease of its production and, on the other hand, by the possibility of utilization of this material for fabrication of various semiconductor devices. Low melting temperature and relatively low pressure of the vapours of the components make it possible to produce highly purified monocrystalline ingots by zone refining. This, in turn, makes indium antimonide an attractive material for laboratory studies of the physical regularities and constants in pure crystals. In a large measure, the practical and theoretical interest in indium antimonide is prompted by the peculiarities of its band pattern, particularly, by an exceptionally high mobility of electrons at low temperatures (to 10^6 $cm^2 \cdot V/s$). At present, the properties of indium antimonide are known fairly well. Let us recall the basic parameters of this material.

Crystalline structure	zinc blende
Lattice parameter	6.4788 Å
Molecular weight	236.58
Specific weight	5.775 g/cm^3
Melting temperature	525 °C
Index of refraction	3.75
Magnetic susceptibility (290 K)	$(-33.2 \cdot 10^{-6})$ cm·g·s
Microhardness	220 ± 20 kg/cm^2
Energy gap (300 K)	0.17 eV
Same (77 K)	0.23 eV
Carrier concentration (300 K)	$1.5 \cdot 10^{14}$ cm^{-3}
Electron mobility (300 K)	78 000 $cm^2 \cdot V/s$
Same (77 K)	10^6 $cm^2 \cdot V/s$
Hole mobility (300 K)	750 $cm^2 \cdot V/s$
Same (77 K)	10^4 $cm^2 \cdot V/s$
Electron diffusion length	10 μm
Hole diffusion length	50-100 μm
Dielectric constant	17
Absorption coefficient ($h\nu = 1$ eV)	$3 \cdot 10^4$ cm^{-1}
Heat conductivity (300 K)	0.04 cal/cm·s·deg
Heat capacity	5.87 cal/g-atom·deg
Coefficient of linear expansion	$5.5 \cdot 10^{-6}$ deg^{-1}
Debye temperature	228 K
Covalent radius (In)	1.44 Å
Same (Sb)	1.36 Å
Self-diffusion coefficient (In)	$D = 0.05 \exp(-1.81 \text{ eV/kT})$
Same (Sb)	$D = 0.05 \exp(-1.94 \text{ eV/kT})$

The high electron mobility in indium antimonide allows its employment in sensitive meters and multipliers based on the Hall effect. The best sensing elements based on the Hall effect are capable of detecting magnetic fields of the order of 100 Oe. Also of some interest are the Hall converters, amplifiers power factor meters, analog multipliers, modulators, radio signal spectrum analyzers. The use of the magnetoresistance effect makes it possible to fabricate current switches and regulators. Indium antimonide can be also used in fabrication of power diodes in the microwave region.

However, indium antimonide finds its most extensive application in fabrication of optical and photoelectrical devices in the infrared region, such as filters, photoresistors, photo and light emitting diodes, and lasers. It is in the production of one of the major types of such instruments, namely, the infrared photodetector, that the advantages offered by the ion-beam technique have been shown in full. An analysis of the respective works is given in the closing section of this chapter. Before we proceed to this analysis, let us dwell on the radiation effects in indium antimonide and on the peculiarities of the behaviour of defects and injected impurity atoms in implanted layers.

Sec. 6.2. Radiation Effects Caused by Corpuscular and Electromagnetic Irradiations

Radiation defects in semiconductors are in fact either elementary point-like disorders (interstitials and vacancies) or structural damage complexes consisting of the lattice imperfections and impurity atoms. Generally, the defects have a wide spectrum of energy levels some of which are lying within the energy gap and exert a deciding influence on the electrophysical properties of the irradiated material.

Even at the nitrogen temperature, the width of the energy gap in indium antimonide is but 0.23 eV. This means that up to the middle of the energy gap all the energy levels are comparatively shallow, i.e. they are capable of supplying carriers both to the conduction and valence bands. Hence, in principle, radiation defects in InSb can be as effective donors and acceptors as chemical impurities.

In both germanium and silicon, the defects that dominate after electron or neutron irradiation affect equally the electrical properties of the samples. If, for example, neutron irradiation of germanium changes the conductivity from *n*-type to *p*-type, electron irradiation causes a similar effect. In indium antimonide, such a correlation is not observed. Reference [1] shows that fast neutron irradiation of InSb crystals at 300 K results in conductivity conversion for *p*-type samples and in a decreased conduction for *n*-type samples. When electron irradiation occurs at 80 K, the reverse situation takes place, i.e., the conversion is observed in *n*-type samples and decreased con-

duction in *p*-type samples [2, 3]. The authors of reference [4] made it a point to examine the behaviour of the material after neutron irradiation at low temperature and after electron irradiation at room temperature. It turned out that after neutron irradiation the *p*-type samples converted to *n*-type, while the *p*-type samples registered a drop in conduction, i.e. a tendency to saturation. The electrical properties of *p*-type samples showed little change after being irradiated with 1 MeV electrons at room temperature. The conduction of the *n*-type material decreased with increase in the radiation dose. Experiments show that the change in neutron irradiation temperature has little effect on the final properties of indium antimonide. At the same time, the target temperature plays an important role during electron irradiation.

In all probability, point defects in InSb are mobile and extremely unstable even at low temperatures. Hence, the properties of the irradiated material will be determined by secondary formations, such as complexes of point defects with other lattice imperfections, rather than by the point defects themselves. According to [5], defects arising from low-temperature gamma irradiation anneal out at 77 K for one or two months. After gamma irradiation at 77 K, as well as after electron irradiation, an *n*-type material has turned to *p*-type. At the same time, a concentration of holes has increased in the *p*-type material.

These examples show that experimental studies of point defects in indium antimonide meet with considerable difficulties caused by the instability of the primary damage. According to the authors of [6], radiation defects can appear in indium antimonide even under the action of light. It was shown earlier [7] that irradiation of *p*-InSb with *X*-rays having a subthreshold energy changed its electrical properties analogous to those observed as a result of gamma and electron irradiations. The authors of [6] have discovered a change in resistivity of *p*-InSb as a result of a low-temperature (77 K) irradiation with a light of lamp ДКсШ-1000 within the intensity range of $(5 \cdot 10^6\text{-}5 \cdot 10^{18})$ eV/cm^2·s. Such changes were also observed upon irradiation with light rays with a maximum energy of quanta equal to 0.7 eV. No changes were discovered in *n*-type indium antimonide after irradiation with light and *X*-rays. No defects were produced by illuminating the samples dipped in liquid helium [8]. The most likely cause of the defects is the generation and subsequent recombination of carriers at loosely bound atoms near the surface [8]. As a whole, the effect described is extremely small and is observed only in *p*-type material with a volume concentration of free carriers of about 10^{13} cm^{-3}. Even under such conditions the increase in the hole concentration does not exceed percentages of several tens.

A different situation arises when indium antimonide is irradiated with powerful laser pulses. The authors of [4] were the first to inves-

tigate this situation. They suggested that the conversion of the *p*-type material after neutron irradiation was due to the fact that the displacement peaks were essentially remelted microregions with electron conductivity. The authors of reference [4] made an attempt at simulating the displacement peak by irradiating InSb with a powerful pulse of a focused ruby laser beam. Measurements with a thermal probe have shown that the regions remelted with the laser pulse are indeed of the *n*-type. The properties of *n*-layers formed under the effect of laser pulses are given a more rigorous treatment in [9].

The relationship between the electron layer concentration and energy of the laser beam during irradiation of samples with single pulses of a ruby laser is given in Fig. 6.1. The value of the threshold energy of *n*-layer formation is in the vicinity of 5 J/cm^2. The curve reveals a tendency towards saturation for energies near 30 J/cm^2.

Integral depth distributions of free electrons are shown in Fig. 6.2. Let us note the following peculiarities involved in the formation of *n*-layers. We see that with a rise in the pulse energy, the thickness of the converted layer (curves *2* and *4*) increases. After the samples have been irradiated with highly powerful laser pulses, a slight increase in the concentration of free holes (curve *2*) has been observed behind the *n*-layer produced. Protection of the irradiated surface with a transparent film 700 Å thick previously applied by cathode sputtering of silicon in the atmosphere of residual gases enhances the conversion effect (curves *3* and *4*). Such a result is likely to be conditioned by the brightening action of the film. Finally, irradiation of *p*-InSb with a series of neodimium laser pulses of 12.5 Hz for 20-30 min not only resulted in the formation of the *n*-layer but increased appreciably the concentration of acceptors in the substrate region next to the layer (curve *1*).

Differentiation of the integral electron distribution curves has shown that the main result of an increase in the energy of millisecond pulses is a greater thickness of the converted layer (Fig. 6.3). In this situation, the surface concentration of donors is small. The use of nanosecond pulses makes it possible to substantially increase the concentration of free electrons. Donor centers arising from pulsed laser action turn out to be sufficiently stable to subsequent heating. Isochronal annealing ($t_{\text{anneal}} \simeq 10^3$ s) in vacuum has shown the recovery of hole conduction occurs within 375-400 °C (Fig. 6.4). The annealing at temperatures above 300 °C was effected with the use of a protective film.

Now, let us consider a probable character of the donor centers appearing in InSb after pulsed laser irradiation. In the first place, such centers are not caused by heating, as heat treatment mostly introduces acceptors into InSb [10, 11]. The time during which the surface layer remains in a heated state is about the same order of magnitude as that of the laser pulse. This enables us to neglect the

Fig. 6.1. Electron layer concentration vs ruby laser pulse energy.

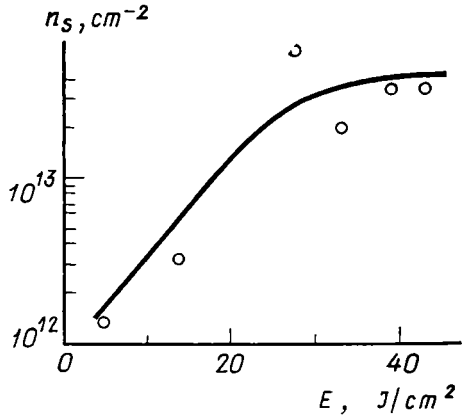

Fig. 6.2. Electron layer concentration profile after laser irradiation under different conditions.

1—neodimium laser, *2-4*—ruby laser. Ruby laser pulse energy, J/cm²: *2*—40; *3*—5 (the sample was irradiated through a protective film); *4*—5

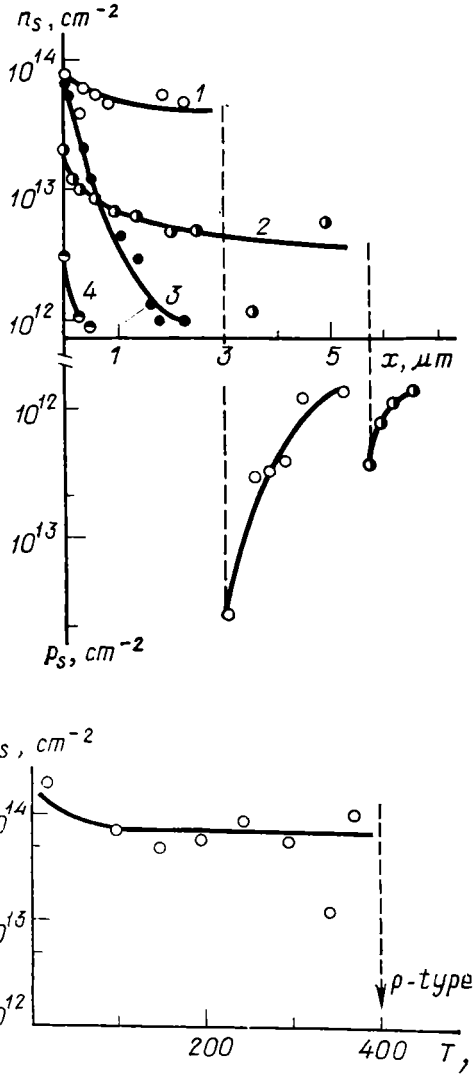

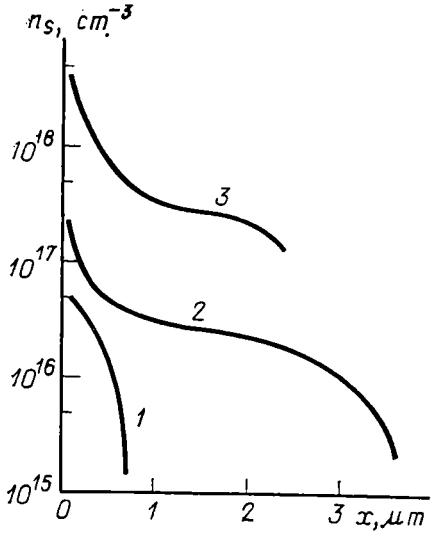

Fig. 6.3. Depth distribution of volume concentration of electrons.

1, *2*—ruby laser; neodimium laser. Ruby laser pulse energy, J/cm²: *1*—5; *2*—40

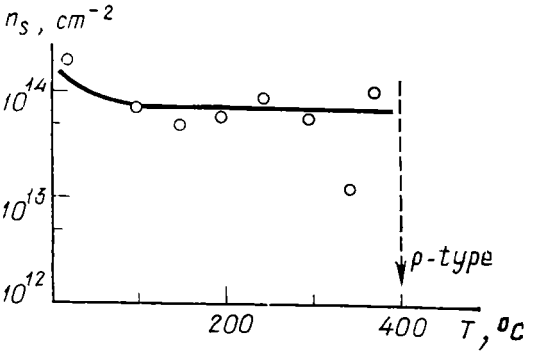

Fig. 6.4. Isochronal annealing of *n*-layer ($t_{anneal} = 10^3$ s).

diffusion of the impurity from the surface, since the diffusion coefficients of the majority donors are too low for doping a layer 3 μm thick to a level of 10^{18} cm^{-3}. Likewise, one should not associate the emergence of donor centers with decomposition (evaporation of antimony) of the irradiated layers since the application of protective films did not diminish the effect. Besides, the self-diffusion coefficients of In and Sb atoms amount to 10^{-14} cm^2/s [12], which means that for the time of the pulse they could have moved a maximum distance of 10^{-8} cm. In evaluation of the diffusion length it was assumed that the layer next to the surface remained in a solid state. At the same time, with high powers of the pulses, a surface fusion occurred. Nevertheless, the fusion of the near-the-surface layer cannot be accepted as an essential condition for the formation of donor centers, as these have been observed to form with powers well below the noticed fusion threshold [13].

It could be well to assume that the laser pulse action brings about an electrical activation of the donor impurity present till this moment in the crystals in the form of neutral segregations. Experiments were carried out on various crystals of *p*-InSb and on pure *n*-InSb ($n_0 = 2 \cdot 10^{14}$ cm^{-3}, $\mu_n = 2 \cdot 10^5$ $sm^3/V \cdot s$) previously converted to *p*-type by ordinary heating in vacuum. No differences were found in the properties of the formed *n*-layers, the fact which argues against the impurity activation hypothesis.

Most likely the formation of donor centers after pulsed laser irradiation is associated with structural changes due to hardening. This seems to be sufficient to account for a greater efficiency of nanosecond pulses as compared with that of millisecond pulses.

Sec. 6.3. Behaviour and Properties of Radiation Defects Caused by Ion Bombardment

The processes involved in amorphization and recrystallization of implanted layers have a significant bearing upon the state of the implanted impurity. Even though in some instances the ion implantation has been successfully applied in fabrication of InSb-based devices, the structural transformations in implanted layers of this material are still not properly understood. According to [14], amorphization is observed after implantation of $2.5 \cdot 10^{14}$ cm^{-2} sulfur ions at $T_{irrad} = 20$ °C. The authors of [15] have observed the formation of a solid amorphous layer upon implantation of 40 keV sulfur ions atroom temperature in doses exceeding $3 \cdot 10^{13}$ cm^{-2}.

Still, the studies made by the authors of [16] have shown that the complete amorphization of InSb does not set in even after a Bi ion irradiation with a dose of 10^{15} cm^{-2}. With a dose in excess of the indicated one, a deposit formed on the surface, which could be

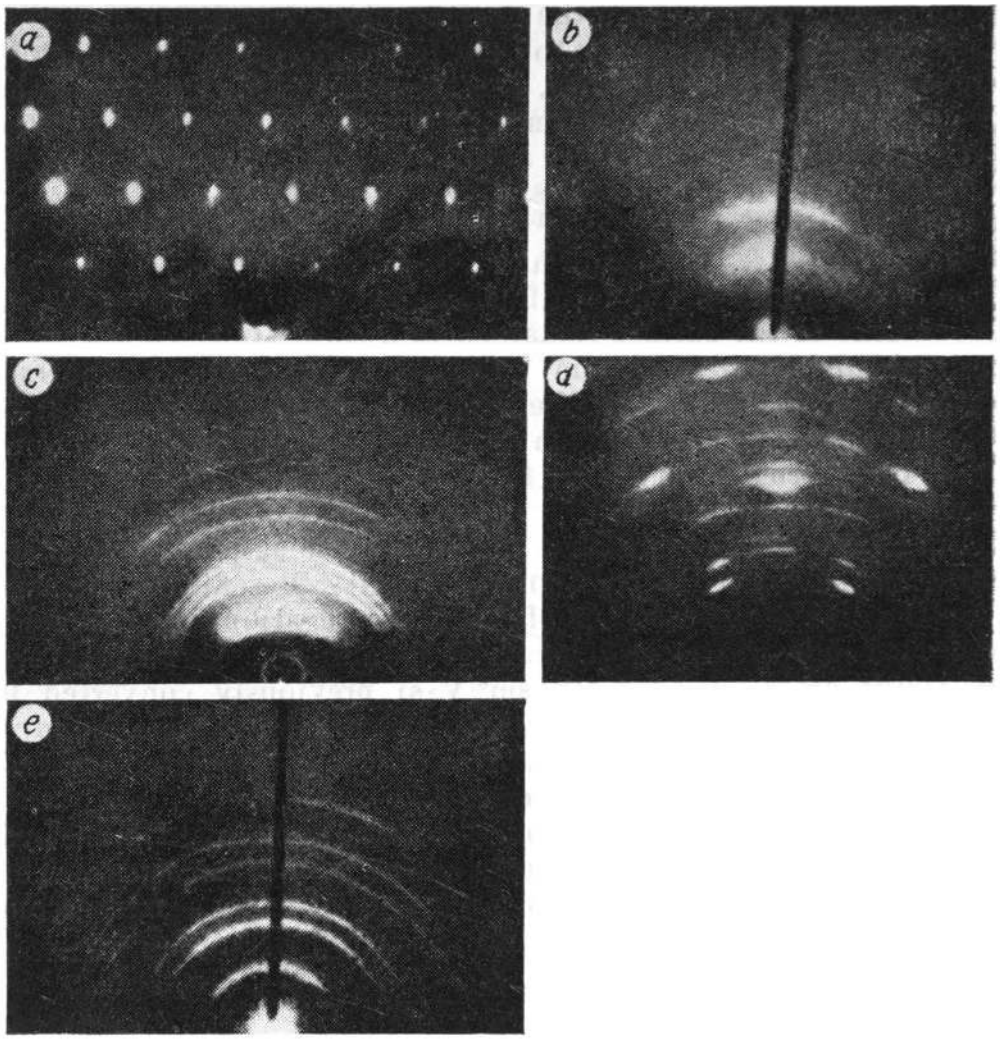

Fig. 6.5. Electron diffraction patterns of indium antimonide surface after argon ion irradiation under different conditions.
T_{irrad} = 20 °C; dose, cm^{-2}: *a*—$3 \cdot 10^{14}$; *b*—$5 \cdot 10^{15}$; *c*—10^{16}. Dose, $5 \cdot 10^{15}$ cm^{-2}, T_{irrad}, °C: *d*—250, *e*—20 + annealing at 200 °C for 15 min

neither annealed at temperatures below 450 °C nor removed by etching with HF. It follows from the foregoing that the understanding of the nature of the structural transformations in indium antimonide upon ion implantation and subsequent annealing is far from complete.

The authors of [17] made an attempt at finding out what the crystalline structure of implanted layers in indium antimonide was like, how it depended on the implantation conditions and restored its properties after annealing. The major electron diffraction patterns are shown in Fig. 6.5.

According to the data received, InSb amorphizes upon implantation of about 10^{15} cm^{-2} 60 keV ions of argon at room temperature. The thickness of the amorphous layer is about 200-300 Å with a mean free path of the argon ion equal to 470 Å. The amorphized layer expands with the growth in ion dose. It is curious that already with a dose of 10^{16} cm^{-2}, the irradiated area becomes crystalline. A repeated crystallization after a high-dose implantation was earlier observed in Si and Ge upon implantation of ions of some chemically active elements [18].

A dependence of the degree of disorder in InSb on the irradiation temperature was investigated within 20 to 450 °C upon implantation of $5 \cdot 10^{15}$ cm^{-2} 60 keV ions of argon. Irradiations with target temperatures of 20 and 100 °C resulted in amorphization of the material. With the irradiation effected at 150 to 300 °C, the implanted layer represented a textured polycrystal of indium antimonide. Such a behaviour of InSb is not quite usual, since a slight rise in the temperature during ion implantation in Si and GaAs impedes the amorphization [19, 20]. It is impossible to preserve the monocrystalline structure of InSb in the near-the-surface region even at the implantation temperature of 350 °C.

One of the very important parameters of ion implantation is the amorphous layer crystallization temperature. To clarify the role of this parameter, an isochronal annealing was performed of the samples amorphized by implantation of $5 \cdot 10^{15}$ cm^{-2} ions of argon, having an energy of 60 keV. The time of each stage of annealing was 20 min. No phase changes were observed at a temperature below 200 °C. Beginning from 200 °C, the layer turned monocrystalline. A polycrystalline structure was also observed after $T_{anneal} =$ 300, 400 and 450 °C. A combination of layer-by-layer etching with electron diffractometry has shown that at the two last-mentioned temperatures the polycrystal-monocrystal interface gradually shifts towards the surface. So, even at the annealing temperatures of the order of $0.9\ T_{melt}$, no complete recovery of amorphized InSb layers occurs. This is a feature that makes InSb quite different from such materials as Si, Ge and GaAs.

As indicated above, the radiation defects in indium antimonide, by virtue of a small width of the forbidden zone, strongly affect the conduction in the implanted layers of this material. Specifically, according to [21], the formation of *n*-layers after implantation of sulfur ions into *p*-InSb and annealing at a temperature below 350 °C is conditioned by the defects, and not by the doping impurity. At the same time, implantation of sulfur ions whose dose equals or exceeds $3 \cdot 10^{14}$ cm^{-2} at 280 °C results in the occurrence of *n*-layers, while the implantation of argon ions does not [22].

The authors of [23] made a study of the electrical properties of defects in indium antimonide after ion bombardment and isochronal

annealing at temperatures ranging from 20 to 450 °C. *p*-InSb samples were irradiated with 300 keV ions of H^+, N^+, Ne^+, Si^+, Ar^+ and Kr^+ to a dose of 10^{15} cm^{-2} within a dose range of 10^{13} to 10^{16} cm^{-2}.

With no annealing employed, stable and reproducible *n*-layers could be produced by proton bombardment only. The electron concentration in such layers amounted to $2 \cdot 10^{13}$ cm^{-2}, and the electron mobility was in excess of 10 000 $cm^2/V \cdot s$. Upon irradiation with heavier particles having the same energy and dose, the formation of *n*-layers was only observed in some instances. On the contrary, the bombardment usually resulted in *p*-layers with hole concentrations from 10^{12} to 10^{14} cm^{-2} and low mobility. A diagram of isochronal annealing of the irradiated samples is shown in Fig. 6.6. *n*-Type layers produced by proton bombardment show stability only below 100-150 °C. In *p*-type layers, hole conductivity is maintained only to a temperature of about 150 °C, following which, the *p*-type layers convert to *n*-type. The *n*-layers thus formed have electrical properties similar to those of the *n*-layers produced by proton bombardment but withstand heating to 350-400 °C.

Fig 6.7 shows isochronal annealing curves for InSb upon irradiation with different doses of 300 keV ions. In all the situations, the occurrence of layers with increased hole concentrations was observed. An increase in the dose caused an increase in the concentrations of free carriers in the *p*-layers. A rise in the annealing temperature was attended by the conversion of the *p*-layers to *n*-type. The conversion was the faster and the electron concentration the higher, the greater was the irradiation dose. With the minimum dose implantation of 10^{13} cm^{-2}, no *n*-type layers were observed throughout the investigated temperature range. Fig. 6.8 shows the distribution profiles of free carriers in *n*-layers produced by proton bombardment without annealing and by helium ion bombardment with subsequent annealing at 250 °C.

Reference [24] presents the results obtained from a study of near-the-surface layers in indium antimonide irradiated with argon and helium ions at target temperatures ranging from room temperature to 400 °C. The carrier concentration in layers versus irradiation temperature is illustrated in Fig. 6.9. The differences in absolute values of the layer concentrations after helium and argon ion irradiation are due to different thicknesses of the conducting layers (the calculated projective paths are 2 and 0.047 μm, respectively). The maximum increment in the concentration of free carriers is observed during low-temperature irradiation. With the target temperature increased to 250 °C, no conducting layer was formed.

In the study of the peculiarities inherent in the "hot" implantation technique, it is particularly important to find out what will be the effect of the irradiation temperature increase on the behaviour of radiation defects during subsequent annealing. Reference [24] de-

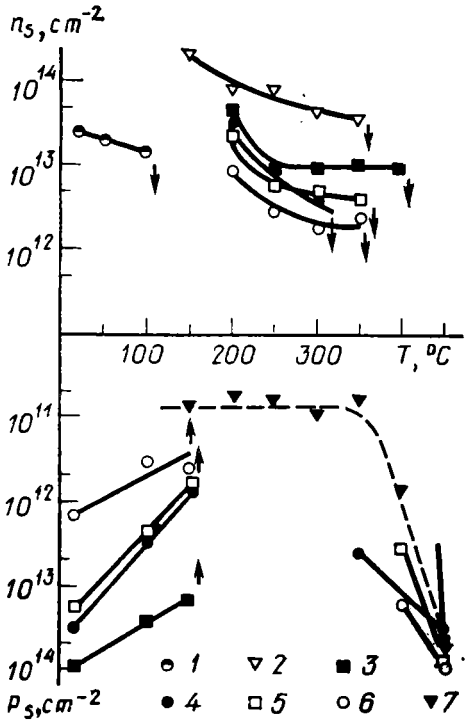

Fig. 6.6. Free carrier layer concentration vs isochronal annealing temperature (t_{anneal} = 20 min) after ion bombardment.

1—H; *3*—Si; *4*—N; *5*—Ar; *6*—Kr with an energy of 60 keV; dose, 10^{15} cm^{-2}; *2*—He with an energy of 300 keV; dose, 10^{16} cm^{-2}; *7*—annealing of non-irradiated sample. The arrows indicate conversion of conductivity type

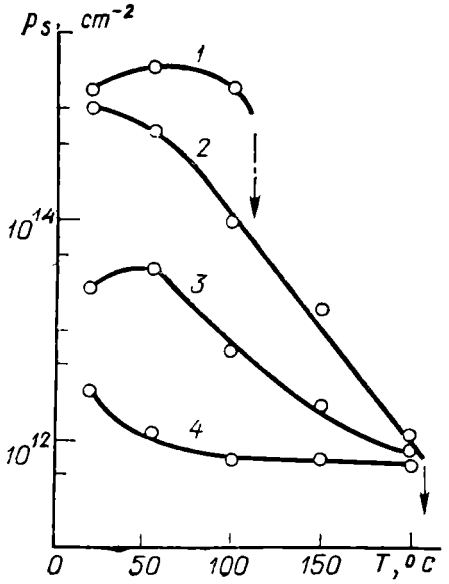

Fig. 6.7. Isochronal annealing of samples after 300 keV He ion irradiation. Dose, cm^{-2}: *1*—10^{16}; *2*—10^{15}; *3*—10^{14}; *4*—10^{13}

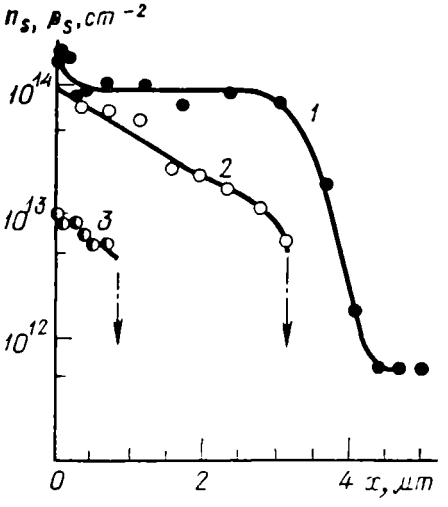

Fig. 6.8. Distribution profiles of hole (*1*) and electron (*2*, *3*) layer concentrations in irradiated layers.

1—He, 300 keV, 10^{15} cm^{-2}, without annealing; *2*—He, 300 keV, 10^{16} cm^{-2}, annealed at 250 °C; *3*—H, 60 keV, 10^{15} cm^{-2}, without annealing

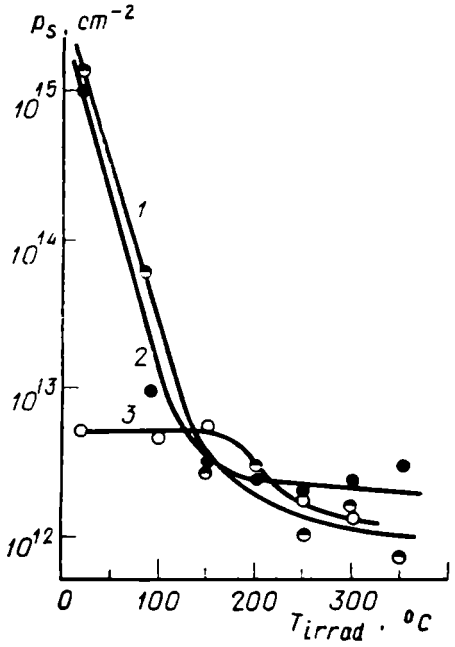

Fig. 6.9. A change in free carrier concentration in the near-the-surface layer as a function of temperature rise during helium (*1*—10^{15} cm^{-2}; *2*—10^{16} cm^{-2}) and argon (*3*) ion implantation.

scribes a set of experiments involving *p*-InSb samples irradiated with helium and argon ions at different temperatures and then isochronically annealed up to 400 °C. The results presented in Fig. 6.10 show that with the irradiation temperature not in excess of 200 °C a further isochronal annealing leads to the formation of *n*-layers stable up to 350 to 400 °C. Conversely, when the irradiation temperature reaches or exceeds 250 °C, no *n*-layers are formed.

The results obtained not only enable us to make an educated selection of the proper implantation and subsequent annealing temperatures for indium antimonide, but make it possible to have some insight into the nature of the defects arising in this material from medium-mass ion implantation. It seems that due to the low melting temperature and large mass of the atoms, the disordered regions in indium antimonide represent remelted and severely hardened sections measuring about 100 Å. According to [25, 26], such remelted sections have a structure different from that of the matrix. The presence of such sections leads, on the one hand, to the occurrence of acceptor levels after low-temperature implantation and, on the other hand, to the formation of *n*-layers due to annealing and transformation of similar regions at temperatures above 200 °C. It is curious that the indicated temperature has little dependence on the substrate temperature during irradiation. This means that disordered regions form not by a gradual accumulation of elementary defects but arise from a thermal flash under the action of a singular medium-mass ion.

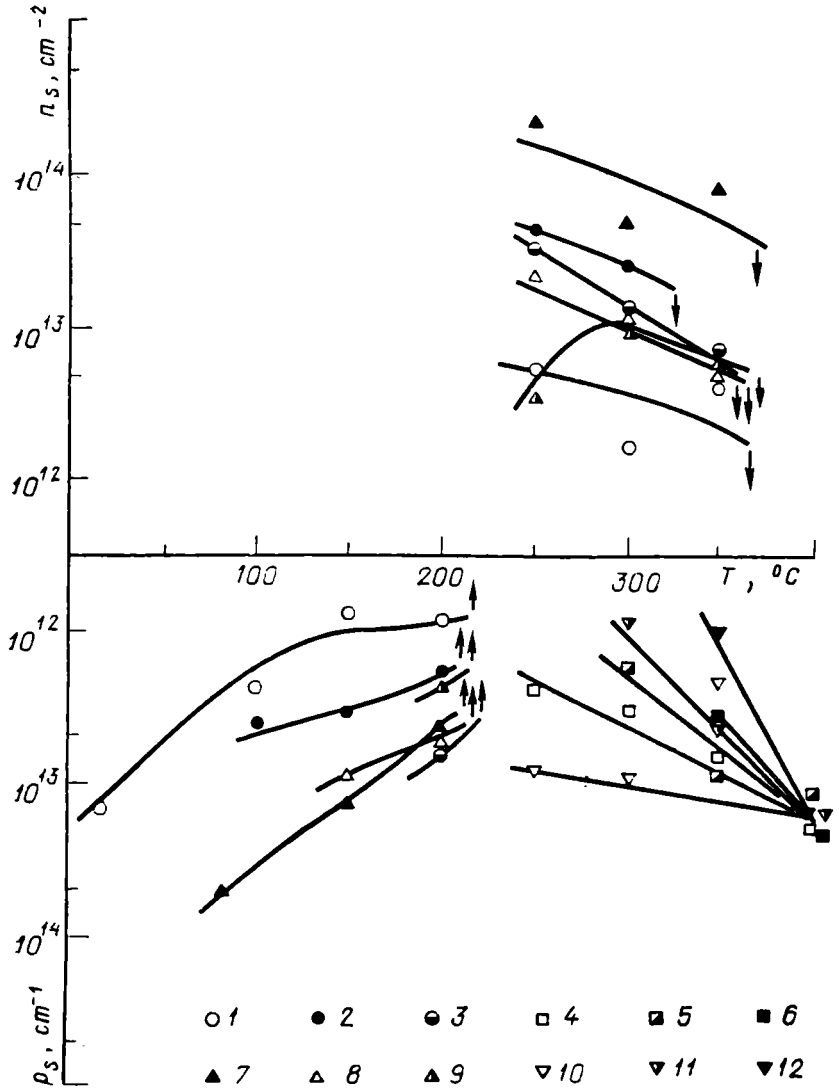

Fig. 6.10. Effect of irradiation temperature on nature of subsequent annealing with implantation of 10^{15} cm^{-2} argon (*1-6*) and 10^{16} cm^{-2} helium (*7-12*) ions in indium antimonide.

Irradiation temperature, °C: *1*—20; *2*—100; *3*—200; *4*—250; *5*—300; *6*—350; *7*—85; *8*—150; *9*—200; *10*—250; *11*—300; *12*—350

As to the donor centers observed in implanted layers heated at 200-350 °C, these are likely to be a product of annealing of disordered regions, representing relatively simple defect associations.

The above hypothesis of the formation of remelted sections is supported by a decrease in the current carrier mobility after the "cold" ion bombardment to the values normally associated with the scattering at large charged centers (Fig. 6.11) [27, 28].

Disordered regions anneal out intensively before 250°C when the electron mobility in the converted layers nears the value of the

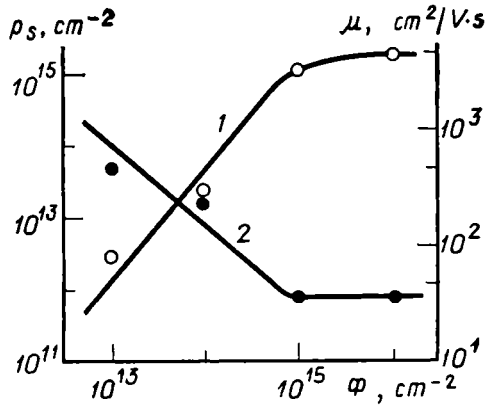

Fig. 6.11. Layer concentration (*1*) and mobility (*2*) vs 300 keV He ion irradiation dose.

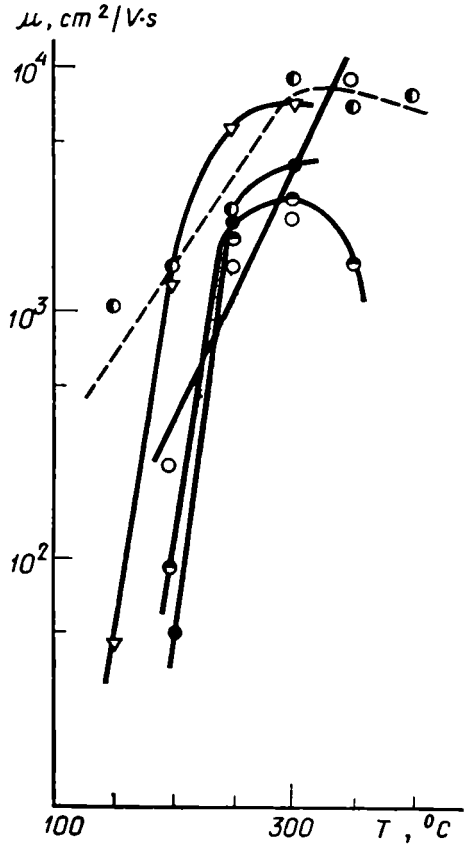

Fig. 6.12. Mobility of electrons in *n*-layers vs annealing temperature after irradiation with various ions (the dashed line—Ne; for explanation of other symbols, see Fig. 6.6).

mobility in the bulk material with a donor concentration of about 10^{18} cm^{-3} (Fig. 6.12).

In *n*-layers converted by annealing, relatively simple imperfections with donor properties are dominant. At the present time, the nature of the relationship between the defects in the layers converted during annealing and the donor centers arising from proton and neutron bombardments is not yet properly understood. In the two last-mentioned situations, the concentration of disordered regions is likely to be smaller than the concentration of simpler defects. As to *n*-layers arising from annealing at 150-350 °C, the formation of these requires a very high level of preliminary disorder.

The existence of *n*-type conduction before the temperature rises to 350 °C is of particular interest from the practical viewpoint, since it allows obtaining *n-p* junctions stable to heating.

Sec. 6.4. Behaviour of Implanted Impurities

The papers devoted to the study of the behaviour of the implanted layers in indium antimonide are not numerous.

The concentration profiles of sulfur implanted layers have been investigated with the aid of the Auger-spectroscopy and Hall effect

measurements [15]. The experimenters used p-type samples doped with germanium or manganese and containing an original impurity concentration of about 10^{13} cm^{-3}. The ion energy was 40 keV, current density, 2 μA/cm^2. The doses were varied from $6 \cdot 10^{14}$ to $6 \times \times 10^{15}$ cm^{-2}. In all the experiments, the target irradiation temperature was maintained at 280 °C. The selection of this temperature was dictated by two factors. On the one hand, heat-treatment of the crystals at temperatures above 300 °C resulted in abrupt changes in their bulk properties. On the other hand, the post-implantation annealing at temperature below 300 °C was insufficient for recrystallization of the solid amorphous layer emerging upon sulfur ion implantation at room temperature. At the same time, at $T_{irrad} = 280$ °C no solid amorphization was observed in the region near to the surface, while an inverted layer appeared beginning from a dose of $3 \cdot 10^{14}$ cm^{-2}.

From the correlation of the concentration profiles obtained with the aid of the Auger-spectroscopy and Hall effect measurements, it follows that the concentration of sulfur atoms is more than by two orders of magnitude greater than the concentration of free electrons. The latter approaches the limit of sulfur solubility in indium antimonide. Characteristic of such profiles is the fact that the concentration peaks of electrically active centers are located at the "tail" of the impurity distribution profiles (Fig. 6.13). The authors of [15] believe that in the region next to the surface, sulfur precipitates and new phases occur.

The results of the above work are in good agreement with the data obtained from the investigation of the "hot" bombardment of InSb with inert gas ions [24]. Indeed, with irradiation temperatures in excess of 200 °C, implantation of inert gas ions does not result in the occurrence of n-layers. Hence, the donor centers observed by the authors of [15] were associated with sulfur atoms. At a latter stage, the authors of [22] have effected, under the same conditions, "hot" implantation of sulfur and argon ions, which has shown that the emergence of the n-layers is associated with implantation of the impurity and not with the defects. The peculiarities of "hot" implantation have been also studied by the authors of [24]. In this work, zink was selected as the doping element. The ion energy was 40 keV, dose, 10^{15} cm^{-2}. The relationship between the layer concentration of holes and the zinc ion implantation temperature is shown in Fig. 6.14. The peak of the curve is located in the vicinity of 200 °C, while the value of p_s is about the same as the dose of the implanted impurity. The effective hole mobility in the layer was 100 cm^2/V·s. The layers were etched away to reveal the depth distribution profiles of acceptors (Fig. 6.15). A drop in the concentration of holes by one order of magnitude is observed after a layer 300 Å thick is etched

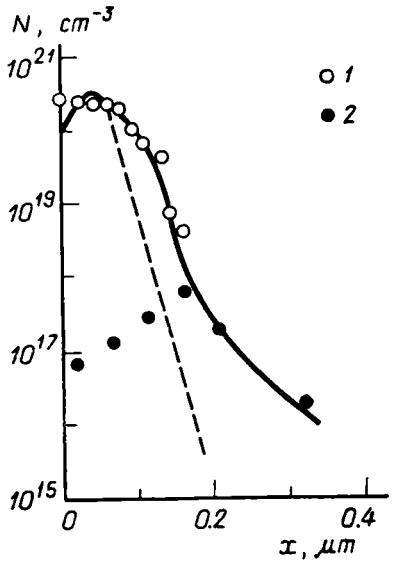

Fig. 6.13. Depth distribution of sulfur concentration (*1*) and active centers (*2*) in an inversion layer of indium antimonide bombarded with sulfur ions.

Energy, 40 keV; dose, $1.8 \cdot 10^{15}$ cm^{-2}; $T_{irrad} = 280$ °C. The calculated profile is shown by the dashed line

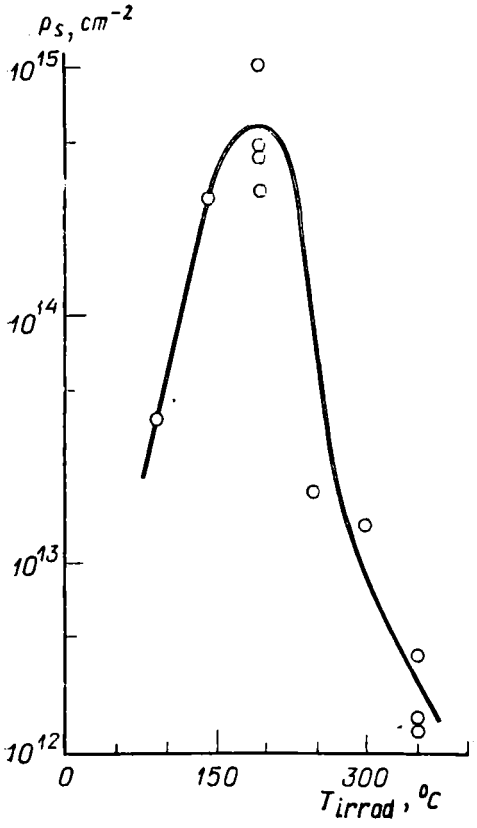

Fig. 6.14. Concentration of holes in a layer vs temperature of zinc ion implantation.

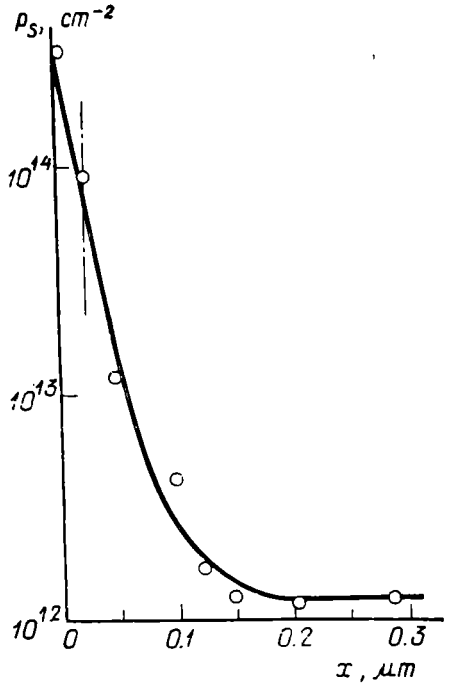

Fig. 6.15. Profile of hole concentration in a layer after zinc ion implantation at irradiation temperature of 200 °C (the dash-and-dot line shows the mean free path of zinc ions).

away, the fact that is consistent with the calculated projective path of 40 keV ions of zinc (220 Å).

To clarify the contribution made by defects and impurities to an increase in the layer concentration of holes, correlate the results indicated above with the data on the bombardment of indium antimonide with inert gas ions. Let us return to Fig. 6.9. It is obvious that irradiation of indium antimonide with ions of inert gases at temperatures ranging from 20 to 200 °C introduces additional acceptor levels. For this reason, a decrease in the coefficient of utilization of the impurity during a low-temperature implantation of acceptors is attributable not to electrical compensation but either to passive behaviour of the impurity atoms or to direct interactions between the impurity and defects.

As to a decrease in the efficiency of doping with rise in the irradiation temperature from 200 to 400 °C, such a decrease is most likely associated with evaporation of zinc from the implanted layer. Indeed, the solubility of zinc at 400 °C in InSb is so high that even with no account taken of the diffusion expansion of the doped layer, the entire implanted zinc can dissolve substitutionally in indium sublattice [29].

The experiments conducted at a later stage have shown that variation of the irradiation temperature from 20 to 200 °C leaves the efficiency of impurity utilization after annealing at 400 °C almost unaffected (Fig. 6.16). However, a further increase in the temperature of implantation results in a sudden drop in the post-implantation concentration of holes. This provides support for the assumption that at high-temperature implantation zinc evaporates from the substrate.

In fabrication of high-quality implanted *p-n* junctions, use is made normally of the enhanced diffusion of the implanted impurity. Of the compounds of the A_{III} B_V type, this method has been successfully applied to gallium arsenide in fabrication of photoconverters and light emitting diodes [30, 31]. In the works on the ion implantation in indium antimonide, no information is contained about the diffusion from the implanted layer during a subsequent annealing [14, 32]. This fact is somewhat unexpected, at least for the case of zinc ion implantation and subsequent annealing at 400 °C for two hours [14]. According to numerous papers, zinc diffuses in InSb at 400 °C quite easily [33-36].

The authors of [37] studied the diffusion of zinc implanted into InSb in doses ranging from 10^{14} to 10^{15} cm^{-2} with an energy of 40 keV. The irradiation temperature was varied from room to 400 °C. Fig. 6.17 shows the variation in layer conductivity, revealed by etching away the layers from the samples doped by zinc ion implantation at different temperatures. First, let us note the fact that the thickness of the doped layers largely exceeds the mean free path of

Fig. 6.16. Post-annealing concentration of holes vs zinc ion irradiation temperature.

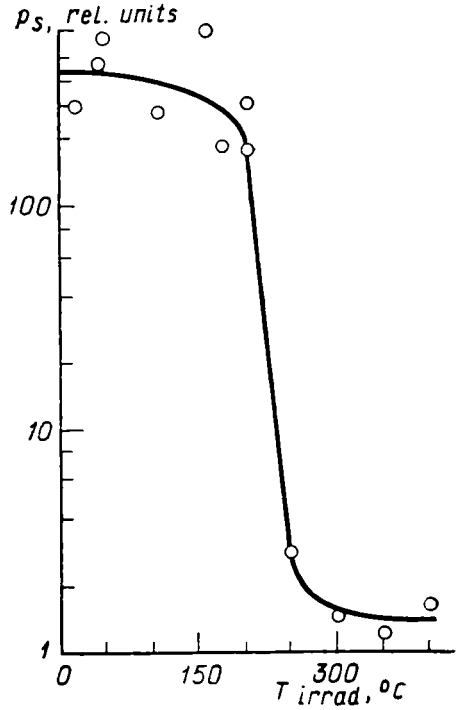

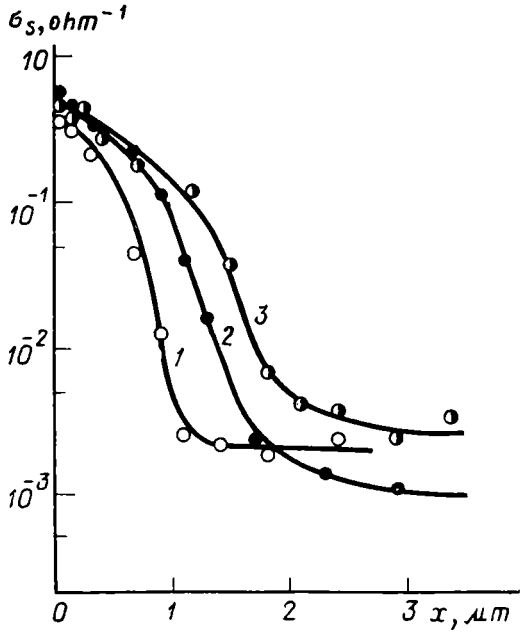

Fig. 6.17. A change in layer conductivity after zinc ion implantation at different temperatures.

Irradiation temperature, °C: *1*—20; *2*—50; *3*—200. The sample was annealed at 400 °C for 15 min to a dose of 10^{15} cm^{-2}

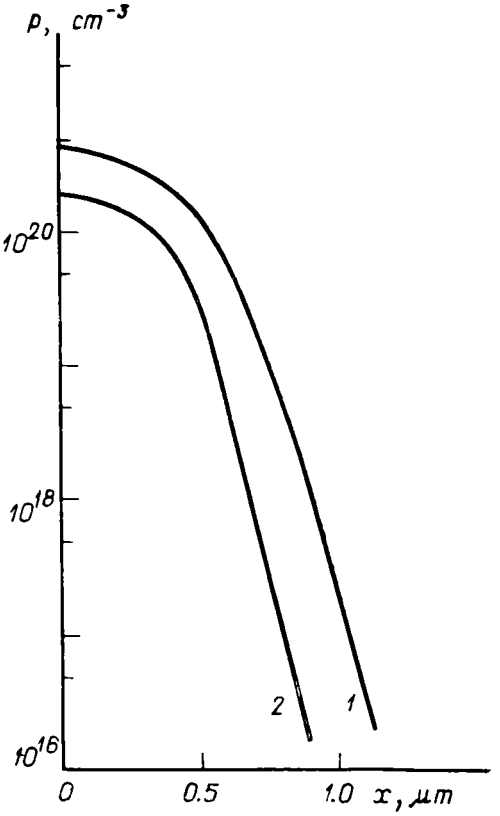

Fig. 6.18. Depth distribution of free holes after implantation of 10^{15} cm^{-2} (*1*) and $5 \cdot 10^{14}$ cm^{-2} (*2*) zinc ions and 15-min annealing at 400 °C.

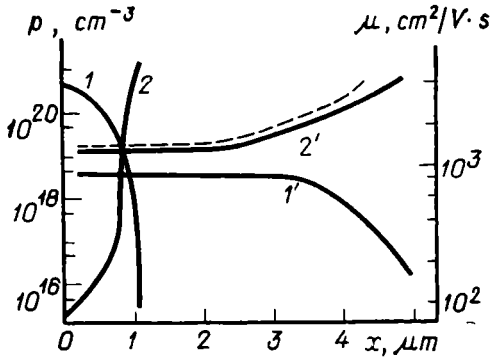

Fig. 6.19. Depth distribution of concentration (*1*, *1'*) and mobility (*2*, *2'*) of free holes vs implanted layer annealing conditions.
1, *2*—annealing at 400 °C for 15 min; *1'*, *2'*—same for 2 h. The dashed line shows the mobility calculated for the concentration curve. Dose, 10^{15} cm^{-2}

zinc ions (approx. 220 Å). This means that, at 400°C, zinc is capable of diffusing from the implanted layers of InSb. The dependence of zinc diffusion length on implantation temperature is comparatively weak, though a tendency exists towards increasing the thickness of the conducting layers with rise in irradiation temperature. The differences between the results obtained by the authors of [37] and the data given in [14] are likely to be due to different conditions of zinc ion implantation. According to [36], in indium antimonide zinc diffuses in two streams: the "fast" one—by interstitials, and the "slow" one—by vacancies. The earlier studies of diffusion of zinc implanted into gallium arsenide have shown that such an impurity transport mechanism is attended with an effect of retardation of diffusion from the implanted layer [38]. The reason lies in the absorption of fast interstitial atoms of zinc by excess vacancies. The degree of retardation is determined by the relation between the concentrations of the atoms and vacancies.

The author of reference [14] implanted 0.2-1.8 MeV ions of zinc in doses of 10^{13} and 10^{14} cm^{-2}. Because of the higher ion energy and smaller dose, the volume concentration of zinc turned out to be less than in the experiments described in [37]. It seems that this concentration is sufficient for complete capture of zinc by vacancies present in the implanted layer. To verify this assumption, an experiment was staged involving the annealing of layers implanted with a lesser dose ($5 \cdot 10^{14}$ cm^{-2}). As might be expected, a decrease in the dose resulted in a reduced thickness of the conducting layer (Fig. 6.18).

The distribution profiles of the volume concentration of holes and their mobility for different diffusion enhancement conditions are shown in Fig. 6.19. As can be seen, the annealing at 400 °C for 15 min is already sufficient to cause a marked increase in the thickness of the implanted layer. After a 2-hour annealing at 400 °C, the thickness of the implanted *p*-region reaches 4-5 μm. The hole mobility agrees with the one expected for the given concentration of acceptors, since the thickness of the *p*-layers is much in excess of the depth at which the defect distribution peak is situated.

Besides zinc, berillium and magnium ion implantation [32] was used in production of *p*-type layers. Layers with electron conduction were obtained after room-temperature irradiation of indium antimonide with protons [39]. The authors of [32, 39] did not make rigorous studies of the relationship between the electrophysical parameters of the layers and their production conditions. The results achieved by the authors of the above papers are discussed in the succeeding section, since they are directly related to the device structures fabricated by these methods.

Sec. 6.5. Production of Semiconductor Device Structures by Ion Bombardment

One of the first attempts to apply ion bombardment for production of photodetectors in InSb is described in reference [39]. The authors have discovered that the action of proton irradiation produces an *n*-layer at the surface of the *p*-type material. They suggested this method for production of *n-p* junctions.

The original material was *p*-InSb with an initial concentration of free carriers at 77 K equal to $5 \cdot 10^{15}$ cm^{-3}. The samples were bombarded at room temperature. The current density was 0.03 μA/cm^2 and the dose 10^{14} cm^{-2}. The Hall effect measurements performed at 77 K revealed an occurrence of *n*-layers with the volume concentration of free carriers 10^{17} cm^{-3} and mobility 15 000 cm^2/V·s.

For fabrication of photodetectors for the required area, a coat of photoresist was applied to the SiO_2 film with windows about 500 μm in diameter provided. The thickness of the photoresist coat exceeded the proton path and because of this the *n*-regions were limited to the sizes of the window openings. To secure a contact with the *n*-layer, additional windows were provided in SiO_2. These windows were 125 μm in diameter and were used for precipitation of gold on the surface of InSb.

The measurements of the volt-ampere characteristics of the structures produced have revealed that they possess good rectifying properties (Fig. 6.20). The inherent resistance of the junction near zero voltages amounted to several hundreds of kilohms. The capacitance of the diodes decreased with a rise in the applied backward voltage in accordance with the law $U^{-0.43}$, which points to the fact that the junctions have been not quite so abrupt. With no bias applied, the capacitance was of the order of 100 pF.

The photovoltaic properties of the structures were evaluated from the experiments involving measurements of detection sensitivity and relative wavelength dependence of photo response. The experiments on measurements of the detection sensitivity used a black body heated to 500 K as a source of irradiation. The modulation frequency was 900 Hz, the background temperature was assumed to be

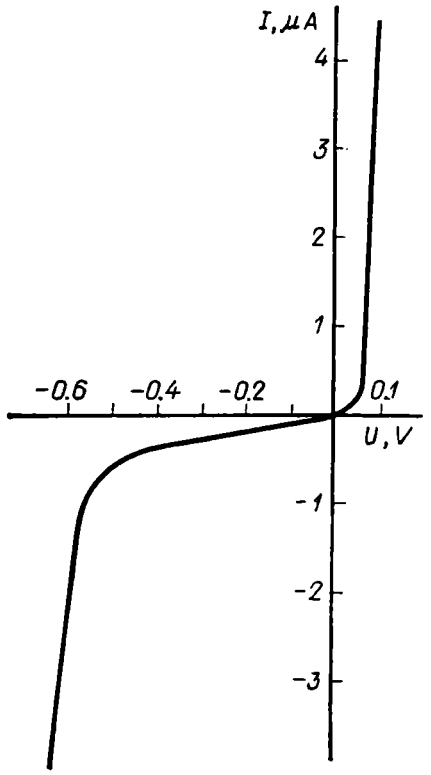

Fig. 6.20. Volt-ampere characteristics of *p-n* junctions at 77 K, produced by proton bombardment of *p*-InSb.

equal to 300 K. With the angle of view being 2π, the maximum detection sensitivity was $2 \cdot 10^{10}$ cm·Hz$^{1/2}$/W. The maximum photo response was attained on a wavelength of 4.9 μm. On the same wavelength, the quantum efficiency of the junctions, measured with reference to the short-circuit current amounted to 35%. The diodes were rather high-speed devices: their photo response rise and decay times were less than 20 ns. The structures fabricated in the form of a bar of 12 diodes possessed good reproducibility.

The basic disadvantage of the above devices resides in their low stability to temperature rise. The authors have found a drop in the quantum efficiency of *n-p* junctions after these have been annealed at 80°C for 460 hours. The replacement of the upper golden contact with one made of platinum allowed, however, the devices to withstand the indicated heat conditions. Still, as you see from Sec. 6.2, the donor centers caused by proton bombardment are fully annealed out at 150 °C, which significantly reduces the practical value of the device.

A much higher thermal stability is a characteristic feature of *p-n* junctions wherein the properties of the working regions are determined not by the structural defects but by implanted impurity atoms. Still it should be borne in mind that to avoid the influence of defects during ion implantation of indium antimonide is a task more difficult than in the case with silicon or gallium arsenide.

One can think of a number of variants of production processes minimizing the detrimental effects of the defects on the properties of *p-n* junctions (implantation of minimum doses, utilization of the lightest ions, acceleration of the impurity diffusion beyond the radiation damage region, ion implantation at elevated temperatures, etc.).

Some of the above variants have been realized practically. To build photodetectors, the author of reference [14] used a low-dose ($5 \cdot 10^{12}$ cm^{-2}) zinc ion implantation ($E = 400$ keV) in *n*-InSb. The

annealing was effected in an inert gas atmosphere at 400 °C for 2 hours. No impurity diffusion was found during the annealing, though it might be expected at such thermal treatment. The factors that cause diffusion retardation have been discussed in the preceding section.

The author of [14] used metal masks for fabrication of planar and mesa-diodes with an area of $1.5 \cdot 10^{-3}$ cm^{-2} and diode matrices. The detection sensitivity of the photodetectors was determined using the irradiation of a black body heated to a temperature of 500 K. The background temperature was 300 K. The measurements were taken at a frequency of 840 Hz, the photodetectors exposure angle was 180°, and the devices were kept at the nitrogen temperature. On the wavelength $\lambda = 5.3$ μm, the detection sensitivity of the photodetectors was within 10^{10} to 10^{11} cm·Hz$^{1/2}$/W. The reproducibility from diode to diode within one matrix was good.

Another approach to the problem of fabrication of photodetectors was demonstrated by Hurvitz and Donnely [32]. They used light ions of acceptor impurities, Be and Mg, for implantation into *n*-InSb. The substrate concentration of electrons was 10^{14}-$3 \cdot 10^{15}$ cm^{-3}. After a careful polishing, the samples were subjected to anode oxidation to a depth of 300-400 Å, following which, they were coated with a layer of photoresist 5 μm thick. The ion implantation was effected through windows 500 μm in diameter, opened in the photoresist layer. The ion energy was 100 to 400 keV and the doses ranged from $5 \cdot 10^{13}$ to 10^{15} cm^{-2}. The photoresist coat was removed after the implantation and the samples were annealed at 300-400°C for 5-6 min.

The further procedure of photodetector fabrication included a pyrolytic application of 1500 Å of silicon oxynitride and a cathode sputtering of 1000 Å of SiO_2. The coat of oxynitride assured a low density of the surface states, and SiO_2 a good stability. Then cathode sputtering was used for application of the potential rings used in adjustment of the surface potential and to compensate its variations by surface energy states.

To secure contact with the *p*-layer, the oxide films were provided with windows 120 μm in diameter for precipitation of Au and In to thickness of 0.5 and 1.5 μm, respectively. Indium was used as a base contact. A general view of the photodetector is shown in Fig. 6.21.

After the diodes have been fitted in standard holders, their properties have been investigated, both electrical and photoelectrical. No large difference was found in the characteristics of the devices fabricated by implantation of Be and Mg [32].

Quite similar were also the properties of the layers fabricated by ion implantation of these elements. Thus, the Hall measurements conducted at 77 K after implantation of $5 \cdot 10^{14}$ cm^{-2} ions of berillium

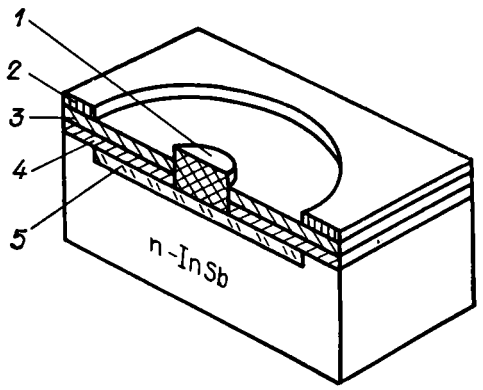

Fig. 6.21. A cross-sectional view of a photodetector (after [32]).
1—top contact (Au + In); *2*—guard ring; *3*—SiO_2 (0.10 μm); *4*—SiON (0.15 μm); *5*—*p*-layer

or magnium have shown that in both cases the impurity utilization coefficient was close to 50%. The depth of the *p-n* junctions was equal to 1.9 μm after Be implantation and 0.7 μm after Mg implantation. The two values are in good agreement with the calculations by the LSS theory which suggests that the ion distribution profiles are gaussian. The Hall measurements of hole mobility gave the results fitting the concentrations of carriers in *p*-layer. This points to the fact that the annealing of the post-implantation defects was rather complete.

The sensitivity of the photodetectors was measured at 500 Hz. The maximum photo response was achieved on the wavelength $\lambda = 5.3$ μm. With the exposure angle of 20° and background temperature of 300 K, the detection sensitivity was restricted by the background and amounted to $7.1 \cdot 10^{11}$ cm·Hz$^{1/2}$/W. The quantum efficiency of the diodes turned out to be equal to 67%, which is somewhat higher than theoretically conceivable, since 36% of the quanta are reflected from the air-indium antimonide interface. The authors of [32] explain this result with a brightening action of the oxide and silicon oxynitride.

The properties of photodetectors fabricated by ion implantation with a subsequent enhanced (accelerated) diffusion are described in reference [40]. Here, zinc was selected as a doping element, since it is a fast diffuser in indium antimonide and represents an effective acceptor. Unlike the case in reference [14], the implantation doses were comparatively large, about 10^{15} cm^{-2}. In accordance with [37], the depth of diffusion of zinc from the implanted layer increases with growth in dose. After a 30-min annealing at 400°C, the thickness of the *p*-layer was 1-2 μm, i.e. by two orders of magnitude greater than the mean free path of zinc ions ($E = 40$ keV). The possibility of obtaining a sufficiently great thickness of the upper layer is, in the given instance, the advantage offered by the diffusion enhancement method, since the calculations show that the quantum efficiency of *p-n* junctions remains high even for the layers 2 or 3 μm thick,

while the attachment of the contacts to the implanted layers becomes a much simpler procedure.

Upon removal of the protective coating under which the annealing was conducted, the contacts (Au and In) were applied to the *p*-region by vacuum sputtering technique. Then mesa-structures were formed by masking and chemical etching on the working surfaces of the samples. The area of the mesa-structures was $(3\text{-}4)\cdot 10^{-3}$ cm^{-2}, 50-60% of the area being occupied by sputtered contacts.

The volt-ampere characteristics of the mesa-structures were taken at the nitrogen temperature. The samples were screened against exposure by the walls of the Dewar flask. The backward branches of the volt-ampere characteristic had no saturation and were close to linear ones. The cut-off voltage determined by the straight branches was 140-150 mV. With a forward voltage in excess of 150 mV, the resistance of the structures was determined by that of the *n*-region (a material with $n = 2\cdot 10^{14}$ cm^{-3} and $\mu_n = 5\cdot 10^5$ cm^2/V·s). With a forward bias ranging from 120 to 150 mV, the current through the junction increased exponentially, while in the region with lesser voltage the dependence was linear. In general, the forward current at voltages up to 150 mV may be given by

$$j = j_0 (\exp qU/\beta kT - 1) + U/p,$$

where p is the structure resistance per unit area at low voltages. The coefficient, β, varied from 2 to 2.5. Similar characteristics were observed earlier in rediffusion and alloy diodes [41, 42].

The quantum efficiency of *p-n* junctions was evaluated against the n_0-load voltage with the known exposure and dark volt-ampere characteristics. Taking into account that about a third of total quanta are reflected from the surface, the segregation efficiency of the photogenerated pairs was about 0.9. This is indicative of the fact that the depth of the *p-n* junction and its properties are close to the optimum ones.

Experiments on determination of detection sensitivity of the photodetectors were staged at 77 K on a frequency of 1500 Hz. The pass band was 34 Hz. The angular aperture was 60°, and the background temperature was taken as 300 K. The relationship between the sensitivity, D^*, and wavelength is illustrated in Fig. 6.22. As may be seen from the figure, the maximum value of $D^* = 2\cdot 10^{11}$ cm·Hz$^{1/2}$·W^{-1} is attained with $\lambda \simeq 5.5$ μm. According to [9], the maximum possible value of D^* for the given measurement conditions is $2.4\cdot 10^{11}$ cm·Hz$^{1/2}$·W^{-1}.

It is evident from the aforesaid that implantation of zinc ions with subsequent enhanced diffusion of the impurity to a depth of 1-2 μm in InSb makes it possible to fabricate high-quality photodetectors with quantum efficiency and sensitivity close to the limit ones. At the same time, the analysis of the volt-ampere

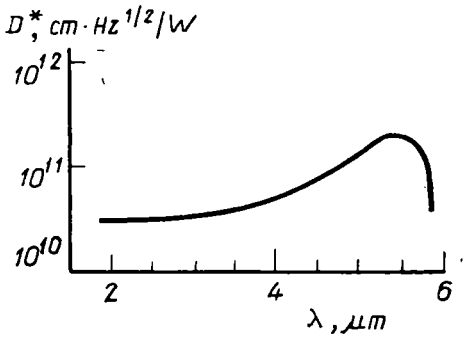

Fig. 6.22. Wavelength dependence of efficiency of photodetector fabricated by zinc ion implantation with subsequent enhanced diffusion.

characteristics shows that unprotected *p-n* junctions of InSb suffer from leakages that can prevent attaining high values of D^* at small angular apertures. Indeed, the calculations indicate that the main factor contributing to the noise inherent in *p-n* structures is the leakage current. Obviation of this disadvantage by protecting the surface outlet areas in *p-n* junctions will allow fabrication of photodetectors for background restricted applications.

The experimental evidence given in this section shows that using several techniques of the radiation technology makes it possible to fabricate IR-photodetectors of InSb, having characteristics close to the ideal ones. With regard to other types of device, there is no published information so far on the application of the radiation effects to production of real device structures. However, significant changes in the properties of InSb, caused by the action of laser, ion, proton and neutron beams, are indication of the fact that the potentialities of the radiation technology are far from being utilized in full.

References

1. Cleland, J., Crawford, J. H. Neutron irradiation of indium antimonide. *Phys. Rev.*, 1954, 95, 5, pp. 1176-1182.
2. Aukerman, L. W. Electron irradiation of indium antimonide. *Phys. Rev.*, 1959, 115, 5, pp. 1125-1132.
3. Eisen, F. N. Orientation dependence of electron radiation damage in InSb. *Phys. Rev.*, 1964, **135A**, 5 pp. 1394-1399.
4. Vavilov, V. S., Vodopyanov, L. K., Kurdiani, N. I. Effects of fast neutron and electron irradiation on electrical properties of indium antimonide. In: *Radiation Physics of Nonmetallic Crystals.* Kiev, Naukova dumka, 1967, pp. 200-206 (in Russian).
5. Mashovets, T. V., Khansevarov, R. Yu. Low-temperature gamma radiation and annealing of indium antimonide. In: *Radiation Physics of Non-Metallic Crystals.* Kiev, Naukova dumka, 1967, pp. 200-206 (in Russian).
6. Vitovsky, N. A., Vikhly, G. A., Galavanov, V. V., Mashovets, T. V., Khansevarov, R. Yu. Formation of radiation defects in indium antimonide at subthreshold irradiation energies. *Fizika i tekhnol. polupr.*, 1969, 3, 1, pp. 132-134 (in Russian).
7. Vitovsky, N. A., Mashovets, T. V., Khansevarov, R. Yu., Chelustka, B. A study of isochronal and isothermal annealing of InSb subjected to X-ray

and gamma irradiation. *Fizika i tekhnol. polupr.*, 1967, **1**, 5, pp. 766-773 (in Russian).
8. Vitovsky, N. A., Vikhly, G. A., Galavanov, V. V., Mashovets, T. V. On formation of defects in indium antimonide exposed to light. In: *Radiation Physics of Nonmetallic Crystals*, 3, part 2, Kiev, Naukova dumka, 1971, pp. 22-26 (in Russian).
9. Bogatyrev, V. A., Kachurin, G. A. Formation of low-ohmic *n*-layers on *p*-InSb by pulsed laser irradiation. *Fizika i tekhnol. polupr.*, 1977, **11**, 1, pp. 100-102 (in Russian).
10. Lyan' Chzhi-chyao., Nasledov, D. N. Electrical and galvanometric properties of *p*-type InSb crystals at low temperatures. *Fizika i tekhnol. polupr.*, 1961, 3, 5, pp. 1458-1464 (in Russian).
11. Gavrushko, V. V., Kosogov, O. V. On distribution of impurities in *p*-region of rediffusive *p-n*-junctions in indium antimonide. *Fizika i tekhnol. polupr.*, 1970, 6, 12, pp. 2373-2375 (in Russian).
12. Madelung, O. *Physics of III-V compounds.* London, 1964, 467 pages.
13. Ready, J. *Effects of high-power laser radiation.* New York-London, 1971, 433 pages.
14. McNally, P. J. Ion implantation in InAs and InSb. *Rad. Eff.*, 1970, 6, pp. 149-153.
15. Guseva, M. I., Mansurova, A. N., Stepanchikov, V. A., Konorova, E. A., Tkachenko, S. D. Auger spectroscopy and Hall effect studies of concentration profiles in indium antimonide layers doped with sulphur ions. In: *International Working Meeting on Ion Implantation in Semiconductors.* Budapest, 1975, pp. 510-521 (in Russian).
16. Langguth, G., Lang, E., Meyer, O. Lattice disorder and outdiffusion in ion implanted InSb and CdTe. In: *Ion Implantation in Semiconductors.* Ed. by Ruge, I. and Graul, J. Berlin, Springer-Verlag, 1971, pp. 228-234.
17. Chernysheva, N. Y., Kachurin, G. A., Bogatyryov, V. A. Amorphization and recrystallization of InSb ion implanted layers. *Phys. Stat. Sol(a)*, 1978, 47, pp. k5-k8.
18. *Physical Processes in Irradiated Semiconductors.* Ed. by L. S. Smirnov. Novosibirsk, Nauka, 1977, 256 pages (in Russian).
19. Mayer, J., Eriksson L., Davies, J. *Ion Implantation in Semiconductors. Silicon and Germanium.* New York-London. 1970, 280 pages.
20. Mazey, D. J., Nelson, R. S. Electron Microscope Investigation of Damage Structure in Gallium Arsenide Bombarded with Neon Ions. *Rad. Eff.*, 1969, 1, 4, pp. 229-239.
21. Wiedeburg, K. H., Betz, H., Kranz, H. Hall effects and sheet resistivity measurements on ion bombarded InSb. *Phys. Stat. Sol.*, 1975, **31a**, 1, pp. k69-71.
22. Guseva, M. I., Mansurova, A. N., Tikhonov, V. G., Khorvat, S. N. A study of hall effect in S ion implanted indium antimonide. *Fizika i tekhnol. polupr.*, 1976, **10**, 8, pp. 1469-1471 (in Russian).
23. Bogatyrev, V. A., Kachurin, G. A. Annealing of defects in ion bombarded indium antimonide. *Fizika i tekhnol. polupr.*, 1977, **11**, 7, pp. 1360-1363 (in Russian).
24. Bogatyrev, V. A., Kachurin, G. A., Smirnov, L. S. Ion implantation in indium antimonide at increased temperatures. *Fizika i tekhnol. polupr.*, 1978, **12**, 1, pp. 102-105 (in Russian).
25. Gonser, U., Okkerse, B. Radiation damage experiments and the nature of thermal spikes in III-V compounds. *Phys. Rev.*, 1958, **109**, 3, pp. 663-667.
26. Gonser, U., Okkerse, B. The question of radiation-induced phase changes. *J. Phys. Chem. Sol.*, 1958, 7, 1, pp. 55-57.
27. Gossik, B. R. Disordered regions in semiconductors bombarded by fast neutrons. *J. Appl. Phys.*, 1959, 30, 8, pp. 1212-1214.
28. Weisberg, L. Anomalous mobility effects in some semiconductors and insulators. *J. Appl. Phys.*, 1962, 33, 5, pp. 1817-1821.

29. Gusev, I. A., Murin, A. N. On diffusion of zinc in indium antimonide. *Fiz. tverd. tela.*, 1964, 6, 4 pp. 1208-1212 (in Russian).
30. Gavrilov, A. A., Kachurin, G. A., Smirnov, L. S. Solar cells fabricated by ion bombardment of gallium arsenide. *Geliotekhnika*, 1975, 6, pp. 20-24 (in Russian).
31. Gavrilov, A. A., Kachurin, G. A., Bogomyakov, N. P., Kovalev, I. K., Petrova, S. P. Light-emitting *p-n* junctions fabricated by Cd ion implantation in GaAs. *Mikroelektronika*, 1976, 5, 2, pp. 192-193 (in Russian).
32. Hurwitz, C. E., Donnelly, J. P. Planar InSb photodiodes fabricated by Be and Mg ion implantation. *Solid. St. Elect.*, 1975, 18, 9, pp. 753-756.
33. Sze, S. M., Wei, L. Y. Diffusion of zinc and tin in indium antimonide. *Phys. Rev.*, 1961, **124**, 1, pp. 84-89.
34. Wilson, R. B., Heasell, E. L. The diffusion of zinc and cadmium in indium antimonide. *Proc. Phys. Soc.*, 1962, 79, 508, pp. 403-408.
35. Pumper, E. Ya., Prostoserdova, I. V. Diffusion of zinc in indium antimonide. *Fiz. tverd. tela*, 1964, 6, 3, pp. 899-902 (in Russian).
36. Prostoserdova, I. V., Pumper, E. Ya., Troneva, N. V. On the mechanism of anomalous diffusion of zinc in indium antimonide. *Fiz. tverd. tela*, 1965, 7, 11, pp. 3255-3259 (in Russian).
37. Bogatyrev, V. A., Kachurin, G. A., Smirnov, L. S. Diffusion of zinc from implanted layers of indium antimonide. *Fizika i tekhnol. polupr.*, 1978, 12, 6, pp. 878-880 (in Russian).
38. Zelevinskaya, V. M., Kachurin, G. A., Pridachin, N. B., Smirnov, L. S. Gallium arsenide doping by zinc ion implantation. *Fizika i tekhnol. polupr.*, 1970, 4, 9, pp. 1784-1788 (in Russian).
39. Foyt, A. G., Lindley, W. I., Donnelly, J. P., *N-p.* junction photodetectors in InSb fabricated by proton bombardment. *Appl. Phys. Lett.*, 1970, 16, 9, pp. 335-337.
40. Bogatyrev, V. A., Gavrilov, A. A., Kachurin, G. A., Pusep, Yu. A., Smirnov, L. S. Photodetectors in InSb fabricated by zinc ion implantation with subsequent diffusion enhancement. *Fizika i tekhnol. polupr.*, 1978, 12, 11, pp. 2106-2109 (in Russian).
41. Marfaing, Y. Influence de l'etat de surface sur la sensibilité photoélectrique des jonctions *p-n* d'antimoniure d'indium. *Compt. Rend. Acad. Sci.*, 253, 4, 626-628, 1961.
42. Galavanov, V. V., Nasledov, D. N., Rzayev, M. A. Volt-ampere characteristics of alloyed *p-n* junctions in indium antimonide. *Radiotekhnika i elektronika*, 1963, 8, 7, pp. 1187-1192 (in Russian).

CHAPTER 7

HIGH DOSE AND CURRENT DENSITY EFFECTS IN ION IMPLANTATION OF SEMICONDUCTORS

Heat treatment or annealing of irradiated semiconductors, effected, say, for silicon, over a range of 600 to 1150 °C, is used most extensively for removal of the post-implantation damage. The efficiency of annealing out of defects in the ion implanted layer, the temperature of transition from the amorphous to monocrystalline state, as well as the number of imperfections that remain after the annealing reveal a strong dependence on the irradiation conditions (dose, current density, mass and species of ion, substrate temperature during the implantation) [1-12]. The temperature required to anneal out the defects and efffect the amorphous-to-crystalline transition in silicon is the higher, the greater the dose and energy of some ions (e.g., ions of inert gases) [3, 5, 9]. Under particular conditions of irradiation and annealing (or annealing only), the temperature of dissociation of the defects and crystallization of the amorphous layer decreases. This can be achieved through the use of additionally induced ionization [13-16], a metallic film on the ion-damaged semiconductor layer [17-21], generation of point defects [22-24], and implantation of the impurity to large concentrations [11-25], effected, when required, with high current densities [26-28]. Of the listed effects, in the present chapter we shall only consider the phenomena associated with high-dose ion irradiation of semiconductors. In the discussion, emphasis will be placed on the importance of current density.

By a convention, one may break the implanted ion dose scale into three distinctive sections. In the first the concentration of radiation defects exceeds that of the implanted impurity; in the second section, these concentrations are of the same order of magnitude and in the third section, the concentration of the implanted impurity becomes commensurate with the concentration of host atoms.

The term "high dose" applies to a dose range covering the second and third sections. These doses are usually in excess of those required for amorphization of irradiated semiconductor layers at room temperature.

Sec. 7.1. Attendant Factors Affecting High-Dose Ion Implantation

The important factors to be taken into account while discussing the processes involved in high-dose ion implantation of semiconductors are the target heating-up in the course of implantation, sputtering, blistering and exfoliation of the semiconductor material.

Target heating-up during ion implantation. In a number of instances, an impurity dose is to be implanted at a high rate, i.e., by using an increased density of current. The need for this is especially acute where ion implantation is to be included into the semiconductor device production practice and irradiation doses are sufficiently high. In such situations, the effects associated with ion beam heating are inevitable and often undesirable, since, for example, the electrical properties of the layers depend on the substrate temperature during the implantation and hence the reproducibility of the electrical characteristics will be a function of the irradiation conditions [29]. Therefore, it is essential to know the target surface temperature and control it during ion bombardment.

The temperature of the sample during irradiation is determined by its surroundings and by the parameters of the ion beam [30-33].

The energy, P_b, of a thermal flux incident on a semiconductor wafer of area A, is spent on increasing the temperature of the wafer (ΔT is the temperature increment), thermal radiation and heating-up of the wafer holder.

According to [32], ΔT occurring over the irradiation time Δt, is given by

$$\Delta T = (\Delta t/\rho A l c)\,[P_b - \alpha\,(T_w^4 - T_s^4) - \beta\,(T_w^4 - T_{wh}^4) - H\,(T_w - T_{wh})]. \tag{7.1}$$

Here, T_w, T_s, T_{wh} are the temperatures of the wafer, surroundings and wafer holder (substrate), respectively; ρ is the semiconductor density, c is the heat capacity and H is a coefficient characterizing a thermal flux from the wafer to the substrate, W/°C;

$$\alpha = \sigma A \varepsilon_w \varepsilon_s / [\varepsilon_s + \varepsilon_w\,(1 - \varepsilon_s)];$$

$$\beta = \sigma A \varepsilon_w \varepsilon_{wh} / [\varepsilon_{wh} + \varepsilon_w\,(1 - \varepsilon_{wh})],$$

where σ is the Stephan-Boltzmann's constant; ε_w, ε_s, ε_{wh} are emissive capacities of the wafer, surroundings and wafer holder (substrate), respectively.

The first term of the formula (7.1) is the energy absorbed by the semiconductor wafer per unit time. The second and third terms, respectively, stand for the radiant emittances of the bombarded surface of the wafer and its backside, and the fourth term, the thermal

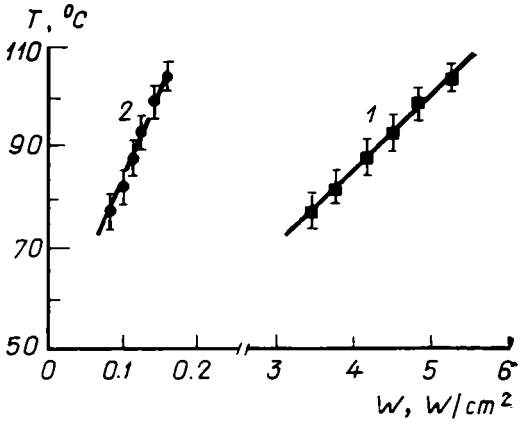

Fig. 7.1. Power dependence curves for surface temperature, obtained experimentally [31].
1—silicon sample on a brass substrate; *2*—sample devoid of thermal contact with the substrate

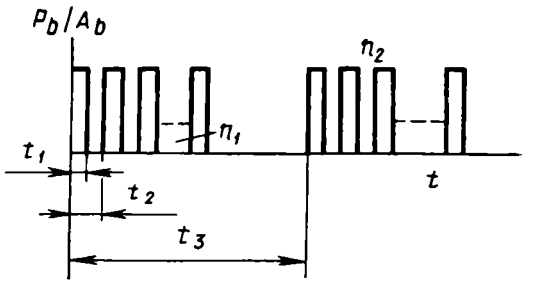

Fig. 7.2. A schematic representation of periodic pulses during ion irradiation [32].
P_b/A_b—instantaneous incident power per unit area, equal to the ratio of power of the beam to its cross-section on the plane of irradiated wafers; t_1—time during which the beam passes through the wafer in the "fast" direction; t_2—time between two passages of the beam in the "fast" direction; n_1—number of passages in the "fast" direction; t_3—time between scanning cycles in the "slow" direction; n_2—number of scans in the "slow" direction

flux from the wafer to the substrate, which occurs due to the contact between the two.

The authors of [32] used an infrared pyrometer to measure the temperature of a Si wafer, T_w, as a function of time. A satisfactory agreement was registered between the curves given by the formula (7.1) and the experimental data for $\varepsilon_s = 0.75 \pm 0.10$; $T_s = 135 \pm 35°$ C; $H = 10^{-3} + 2 \cdot 10^{-3}$ W/°C. These parameters, unlike all other used in the formula, do not lend themselves readily to direct experimental measurement. It appears that the value of T_s is largely determined by the construction of the ion-beam gun, particularly, by the position of the ion source with respect to the irradiatied wafer. The value of H turned out to be by an order of magnitude greater than that given above when a heat-conductive (in this case, organosilicon) paste was applied between the wafer and the holder.

The authors of [31] had simulated the conditions under which the energy was liberated during the ion bombardment and used the following technique to measure the temperature of the irradiated surface of the silicon wafer. A current of varying magnitude was passed through a conductive layer fabricated by implantation of boron into *n*-type Si and subsequent annealing. The heat liberated in the process was calculated for each value of current from the Joule-Lentz law, while the temperature was measured with the aid of

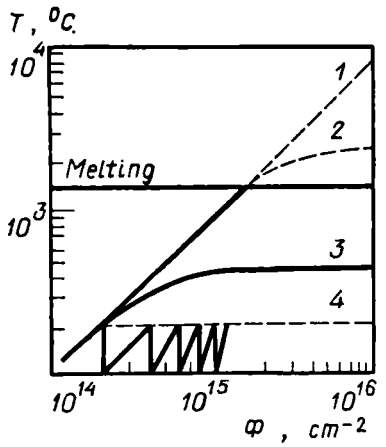

Fig. 7.3. Silicon wafer temperature vs irradiation dose [32].
1—without heat sink; *2-4*—heat sink due to irradiation (*2*—without beam scanning; *3*—scanning in the "fast" direction only; *4*—scanning in both the "fast" and "slow" directions)

strips of special compound applied to the wafer surface. The colour of the strips varied with temperature from white to black. The measurements thus performed have shown that in order for two samples, one of which is devoid of contact with the surroundings, while the other is placed on a substrate of brass, to attain equal temperatures, the power dissipated at one of them should be more than by an order of magnitude greater than at the other, that is, a greater power is required for the sample in contact with the substrate (Fig. 7.1). If, at that, thermal contact between the sample and the substrate is improved by, say, soldering them together with indium, the temperature of the sample remains about the same as room temperature for dissipated powers of the order of a few watts per square centimeter [33].

However, the technique in which a heat-conductive paste (or solder) is used to reduce the temperature of the ion-bombarded semiconductor wafer is technologically inefficient. A greater promise for the radiation technology is held by the technique based on the selection of the right speed for the ion beam scanning over a large number of semiconductor wafers [32]. If the ion beam is scanned at different speeds in two mutually perpendicular directions (or scanned at regular intervals over the irradiated object) a series of pulses acts upon a point selected on the water (Fig. 7.2).

Fig. 7.3 (curve *4*) shows the temperature of Si wafers versus dose for the above irradiation technique [32]. The calculations made from the formula (7.1) allowed for removal of heat by radiation, while the value of H was considered to be zero. The ion beam parameters were the following: $P_b/A_b = 200$ W/cm^2, $t_1 = 10^{-3}$ s, $t_2 = 5.8 \cdot 10^{-2}$ s, $t_3 = 60$ s ($n_1 = 308$, $n_2 = 20$ for a dose of $3 \times \times 10^{15}$ cm^{-2}). The oscillations of curve *4* are attributed to cooling of the wafer for the time t_3.

For comparison, Fig. 7.3 also shows the calculated silicon temperature versus irradiation dose for another beam scanning mode (curve

3), the temperature without beam scanning (curve *2*) and, finally, without taking heat abstraction into account (curve *1*). It is obvious that the selection of the proper beam scanning speed can be instrumental in decreasing the maximum temperature of the sample during ion irradiation. Still, if to obtain the dose Φ without beam scanning, one needs time $t_D = A_b De/I_b$, where e is the electron charge, and I_b the beam current, with the beam scanned over the area A_T, the same dose is obtained on the wafer for a time $t_T = t_D \cdot A_T/A_b$. Hence, the time during which the wafer is held in the ion accelerator will increase by a factor of A_T/A_b. For the mean time spent for treatment of one wafer not to be increased, the area A_T scanned by the beam should be filled with other wafers. As a result, using this technique we succeed in reducing the maximum temperature of the semiconductor being irradiated without changing the mean time spent for ion implantation of one wafer.

Material sputtering by ion irradiation. Sputtering or evaporation of solids by high-energy particles poses a special problem and many authors have dedicated their work to study it (see, e.g., [34, 35, 36]). The purpose of this section is to give the results of calculation of the sputtering yield, S, for elemental semiconductors, using the theory of [36] which takes into consideration the processes involved in quasi-elastic collisions of atoms in solids. Under particular conditions, the data supplied by this theory correlate fairly well with the experimental evidence.

The sputtering yield is the ratio of the number of atoms ejected from the unit area of a solid to the number of atoms incident on the surface [34]. As an ion penetrates into a solid, its first collision with a host atom does not usually result in sputtering. Due to a cascade of mutual collisions, for the ion falling even at right angles to the sample surface there may exist a target atom whose velocity component in the direction of exit from the bombarded target will be other than zero. The cascade of displacements may be located deep inside the target. During sputtering of amorphous or polycrystalline targets, only the processes by which energy is released in the near-the-surface region are important. Therefore, the calculations of the sputtering yield include the following operations: (1) determination of the amount of energy given off by the particle (incident ion or recoil atom) near the surface; (2) transfer of this energy to the number of low-energy recoil atoms; (3) determination of the number of atoms coming to the surface, (4) selection of the atoms capable of surmounting the energy barrier at the surface.

In sputtering of monocrystalline targets, a definite contribution is made by such factors as channelling of particles from a considerable depth and occurrence of focusons. These factors may be ignored as far as ion bombardment of crystals is concerned, as a noticeable part of the irradiated layer is sputtered with doses exceeding that

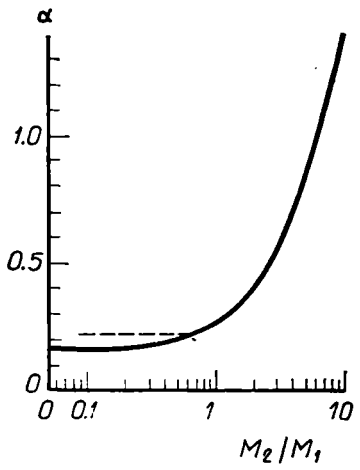

Fig. 7.4. Factor α as a function of mass ratio in the region of elastic collisions [36].

of amorphization (or a dose causing a significant disorder in the layer, if the irradiation is effected at elevated temperatures).

For heavy and medium-mass ions falling at right angles to the surface, the sputtering yield, S, is given by the formula [36]

$$S = 0.0420\ \alpha S_n\ (E)/U_0 \mathring{A}. \tag{7.2}$$

Here, $S_n\ (E)$ is the nuclear stopping power. Assuming that the interactions occur by the Thomas-Fermi statistics

$$S_n\ (E) = 4\pi Z_1 Z_2 e^2 a_{12}\ [M_1/(M_1 + M_2)]\ s_n\ (\varepsilon), \tag{7.3}$$

where ε is a dimensionless energy of an ion [1]

$$\varepsilon = [M_2 E/(M_1 + M_2)]/(Z_1 Z_2 e^2/a_{12}). \tag{7.4}$$

Here,

$$a_{12} = 0.8853 a_0\ (Z_1^{2/3} + Z_2^{2/3})^{-1/2}; \tag{7.5}$$

Z and M are the ordinal number of the element and its atomic weight; the index 1 relates to the ion, and index 2 to the target atom; a_0 is the Bohr radius ($0.529 \cdot 10^{-8}$ cm); e is the electron charge; $s_n\ (\varepsilon)$ is a function given in the form of Table 7.1; α is the factor depending on the ratio M_2/M_1 (Fig. 7.4), and U_0 is the binding energy at the surface.

Table 7.1

Elastic retardation cross-section $s_n\ (\varepsilon)$ referred to Thomas-Fermi interaction

ε	$s_n\ (\varepsilon)$	ε	$s_n\ (\varepsilon)$	ε	$s_n\ (\varepsilon)$	ε	$s_n\ (\varepsilon)$
0.002	0.120	0.04	0.311	0.4	0.405	10.0	0.128
0.004	0.154	0.1	0.372	1.0	0.356	20.0	0.0813
0.01	0.211	0.2	0.403	2.0	0.291	40.0	0.0493
0.02	0.261			4.0	0.214		

The formula (7.2) applies when the ion energy $E > E^*$, where $E^* = 6.62 \cdot 10^{-2} [(M_1 + M_2)/M_2] (a_{12}/\alpha^3 (Z_1 Z_2 e^2/a_{12})$.

The value of E^* is of the order of some hundreds of electronvolts.

Measurements of the sputtering yield of amorphous silicon bombarded by various ions ($E = 45$ keV) have shown that a good agreement with theory is attainable only for $U_0 = 7.83$ eV and low ion irradiation doses [37] (Table 7.2).

Table 7.2

Cathode sputtering yields calculated by formula (7.2) (S_{theor}) and measured experimentally (S_{exper}) for amorphous silicon, $E = 45$ keV

Ion	S_{exper}	S_{theor}	Ion	S_{exper}	S_{theor}	Ion	S_{exper}	S_{theor}
N	0.43	0.47	Zn	2.56	2.78	Te	3.9	4.0
Ne	0.85	0.77	Se	3.1	3.1	Xe	3.8	4.0
Al	1.12	1.06	Kr	3.3	3.3	Tm	5.0	4.4
Cl	1.35	1.55	Ag	4.0	3.7	Pb	4.8	4.6
Ar	1.75	1.67	Sn	4.4	3.9	Bi	4.8	4.6
V	2.16	2.12						

The influence of the dose of an impurity (Al^+, P^+, Zn^+, Sb^+, In^+) implanted into silicon on the rate of target sputtering has been treated in reference [38]. The sputtering was effected with Ar^+ ions having an energy of 500-1000 eV and with a beam current density of 0.1-0.3 mA/cm^2. It turned out that, say, for silicon irradiated with phosphorus ions at doses below 10^{17} cm^{-2}, the sputtering rate was about 100 Å/min. With a dose of P^+ ions equal to or in excess of 10^{17} cm^{-2}, the sputtering rate was reported to increase by a factor of 1.5-2.

Let us discuss the influence of sputtering on the accumulation of an implanted impurity and its depth distribution profile in a solid. We should focus our attention on a theoretical model. For experimental data, refer to Sec. 7.4.

The major assumptions of the model are as follows: the sputtering yield is constant and does not depend on dose, ionic current density and condition of the surface being bombarded; no impurity diffusion is observed during irradiation; the ion path in a target does not depend on ion dose; the ion beam falls with its density j at a right angle to the surface being irradiated; the target is essentially a half-space $x \geqslant 0$ [39-41]. Therefore, the sputtering process can be described in terms of the boundary motion parallel to the surface of the target.

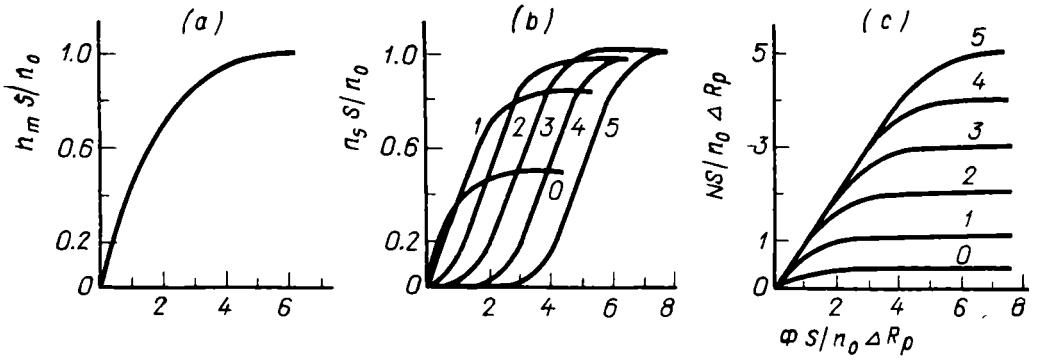

Fig. 7.5. Normalized concentration of implanted impurity in (*a*) distribution maximum, (*b*) concentration of impurity on the surface and (*c*) impurity accumulation curve vs corrected dose (the figures give the ratio $R_p/\Delta R_p$) [39].

In a particular case described by the model, it is assumed that the probability of stopping the particle within a range of x and $x + \Delta x$, equal to $p\,(x)\,dx$, is given by the Gauss function

$$p\,(x) = (1/\sqrt{2\pi}\Delta R_p) \exp\,[-\,(x - R_p)^2/2\Delta R^2_p], \tag{7.6}$$

where R_p and ΔR_p are the projected path of the particle and straggling, respectively, [1, 42]. Then the depth distribution profile, depending on dose, will take the form

$$n\,(x,\,\Phi) = (n_0/2S)\,[\mathrm{erf}\,((x - R_p + l)/\sqrt{2}\,\Delta R_p) - \mathrm{erf}\,((x - R_p)/\sqrt{2}\,\Delta R_p)], \tag{7.7}$$

where n_0 is the target density: the quantity $l = \Phi S/n_0$ is the thickness of the sputtered region; erf (z) is the error integral [43] given by

$$\mathrm{erf}\,(z) = (2/\sqrt{\pi}) \int_0^z \exp -(\eta^2)\,d\eta. \tag{7.8}$$

From (7.7), we can deduce useful expressions, say, those giving the concentration of impurity in the profile peak, n_m, depending on the dose:

$$n_m = (n_0/S)\,\mathrm{erf}\,(l/2\sqrt{2}\,\Delta R_p). \tag{7.9}$$

Very high doses result in equilibrium: every incident ion ejects an impurity atom. In this case, the maximum concentration of the implanted impurity in the layer remains constant and equal to

$$n^{\infty}_m = n_0/S, \quad \Phi \to \infty. \tag{7.10}$$

Variation of n_m with dose and attainment of the saturated state are shown in Fig. 7.5*a*.

Sputtering of the material upon irradiation causes a displacement of the impurity profile maximum towards the surface. The position of the maximum is given by

$$x_m = R_p - l/2 = R_p - \Phi S/2n_0, \tag{7.11}$$

that is, the maximum shifts a half-thickness of the sputtered layer. It follows from (7.11) that if a layer $l = 2R_p$ is sputtered, the maximum will emerge at the surface of the sample being irradiated.

The concentration of the implanted impurity at the surface, n_s, may be given by (7.7):

$$n_s = (n_0/2S)\,[\mathrm{erf}\,(R_p/\sqrt{2}\,\Delta R_p) + \mathrm{erf}\,((l - R_p)/\sqrt{2}\,\Delta R_p)], \tag{7.12}$$

and at $\Phi \to \infty$

$$n_s^{\infty} = (n_0/2S)\,[1 + \mathrm{erf}\,(R_p/\sqrt{2}\,\Delta R_p)]. \tag{7.13}$$

Variation of the normalized concentration of impurity at the surface and of the number of implanted atoms with dose is shown in Fig. 7.5*b*, *c*.

Blistering and exfoliation of material. The blister is a swelling at the surface of a solid. The occurrence of blisters was reported for high doses (over 10^{17} cm^{-2}) of gas (helium, hydrogen, argon) implants in semiconductors, insulators and metals (see, for example, [44-47]). Exfoliation of some irradiated fractions of irregular shape from the sample is also possible. An especially large body of data exists on the formation of blisters and exfoliation in metals, since the latter are used in fabrication of the walls of the chambers for controlled thermonuclear reactions as well of the walls of nuclear reactors. The formation of blisters and exfoliation of the material lead, in this case, to a heavy damage to the surfaces of the walls and, in thermonuclear reactions, to contamination of the plasma.

Two models exist explaining the formation of blisters and exfoliation of the material.

In the first model, a significant role is played by the occurrence, in the process of irradiation, of gas holes in a solid. It is believed that if the solubility of a gas implanted into the material is low (as is the case with, say, inert gases in metals), some gas may be trapped in microscopic pores arising from ion bombardment. Thus, gas cavities emerge in a solid, which grow in size with an increase in dose and, under suitable conditions, blow up at the surface, liberating the gas. According to the second model, it is assumed that the formation of blisters is attributable to the existence of large longitudinal stresses in ion bombarded layers. Such stresses are induced by the implanted impurity.

Sec. 7.2. Structural Changes in Layers During Irradiation and Annealing

Oriented crystallization effect. The essence of the effect is as follows. Under suitable conditions, an amorphous layer arising during the initial stages of ion bombardment of a semiconductor crystallizes [25-27, 48, 49]. Investigations of the effect have shown that it occurs where (1) a particular dose interval, (2) high local current density, (3) an orienting substrate and (4) the right sort of impurity are provided. Let us discuss all these factors in succession.

Dose. In the first experiments that disclosed the effect of oriented crystallization, the EPR method was used. The subject of the investigations was the accumulation of *VV*-centers, i.e., vacancy clusters with a number of vacancies of about 10 [48, 49, 50], in silicon irradiated with various species of ion. The paramagnetic defects grew in number with an increase in the dose of bombarding ions in accordance with a particular law showing dependence on the ion mass and sample temperature during the irradiation. The initial section of the curve illustrating the dose dependence of the number of *VV*-centers, N_{VV} (Φ), shows an increase in the *VV*-centers prior to amorphization of the irradiated layer (Fig. 7.6, section *1*).

With further irradiation of the amorphous layer, the character of the N_{VV} (Φ) curve depended on the species of ion: irradiation of the layer with ions of inert gases resulted but in a small increment in the number of *VV*-centers as the amorphous region had expanded [51], whereas the implantation of, say, P^+, B^+, or AS^+ ions lead to a decrease in N_{VV} (Φ) (Fig. 7.6, section *2*). Since the presence of *VV*-centers was associated with the presence of an amorphous phase [50, 51, 52], an experimental verification of the structure of the layer with the aid of fast electron reflection diffraction, was performed. As a result of simultaneous employment of these two methods, it has been established that a decrease in the number of *VV*-centers is associated with transition of the amorphous layer into a non-paramagnetic state.

A still greater increase in dose leads to a decrease in the thickness of the amorphous region due to crystallization of the layer at the interface with the monocrystalline substrate [25] (Fig. 7.6, section *3*). The dose range within which the oriented crystallization occurred was $2 \cdot 10^{16}$ to 10^{17} cm^{-2}. The doses in this range are rather high, therefore the crystallization effect is called a high-dose effect [27, 49]. It should be noted that the lower limit of the above range is largely dependent on other factors (such as ionic current density), while the upper limit is conditioned by new effects. Thus, if the dose exceeds 10^{17} cm^{-2}, another amorphous layer is likely to form. This latter layer is located deeper than the crystallized region and its occurrence is likely to be associated with accumulation of defects along the

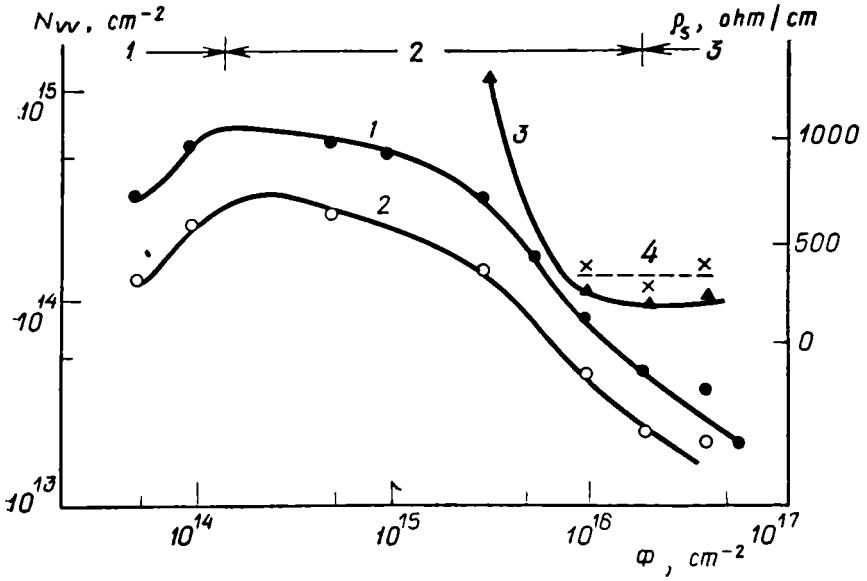

Fig. 7.6. Dose dependence of the number of *V-V* centers (curves *1* and *2*) and surface resistance (curves *3*, *4*) in silicon (*1*, *3*) and Si-SiO_2 structure (*2*, *4*) irradiated with phosphorus ions [27].
$E = 70$ keV; $j = 5$ μA/cm²; thickness of $SiO_2 \simeq 1000$ Å. Ions were implanted at room temperature

interface between the layer heavily doped by ion implantation and the lightly doped portion of the sample [53]. For example, in silicon irradiated with phosphorus ions ($E = 40$ keV, $\Phi = 2 \cdot 10^{17}$ cm^{-2}), the following irradiated layer structure was formed: an amorphous region extended from the surface to a depth of about 250 Å, a radiation-crystallized portion was formed at 400 Å, then another amorphous region was found at about 500 Å and, finally, followed the crystalline matrix. The local current density in this experiment was about 35 μA/cm², the ion beam scanning rate, 80 Hz.

Current density. It was found that the rate of crystallization was dependent on current density, j. With one and the same irradiation dose, the thickness of the remaining amorphous layer is the greater, the smaller j [26]. For example, at $\Phi = 6 \cdot 10^{16}$ cm^{-2}, for P^+ ions, $E = 50$ keV, the thickness of the amorphous layer, h, is 700 and 450 Å, respectively, for $\bar{j} = 1$ and 2 μA/cm² ($\bar{j}$ is the mean current density of the scanning beam).

The current density dependence of the effect in question was also established with the EPR method [27]. In this case, irradiation was effected with different values of $\bar{j}$, while the dose was maintained at a constant level and was selected so as to satisfy the following requirements: (1) the dose should correspond to the dipping section of the *VV*-center dose dependence curve and (2) the EPR signal should

be of intensity sufficient for measurement. The value of the signal decreased with rise in $\bar{j}$.

In most described experiments, use was made of a vertically scanning ion beam and the samples were secured to a rotating drum to assure mechanical scanning in the horizontal plane. For example, with irradiation effected with the aid of the Soviet-made equipment, type ИЛУ-3, the scanning rate in the vertical plane was 300 Hz (triangular sweep), the scanning amplitude was 24 cm, the beam measured 6×1.5 cm, the drum diameter was 18 cm and its rotational speed 20 rpm. In this case, a sample was acted upon by a series of pulses, schematically represented in Fig. 7.2, and the temperature was estimated to be not in excess of 100 °C. The current density, $\bar{j}$, was varied by changing the beam current and not the scanning area. A parameter of importance for the effect to occur is the local current density j. In the above technique involving scanning of both the beam and the sample, the local current density was 20-100 times as great as the value of $\bar{j}$. The authors of [53] used the experimental data analysis to determine the j range in which the crystallization effect was observed. It was found to be 30 to 100 $\mu A/cm^2$. It was experimentally proved that in irradiation effected without beam and sample scanning, when $\bar{j} = j = 1$ $\mu A/cm^2$, layer crystallization did not occur until the highest doses were attained.

Availability of orienting substrate. Investigations of the structure of ion bombarded silicon with the aid of fast electron reflection diffraction have shown that crystallization of the amorphous layer of implanted particles occurs at the interface with the monocrystalline substrate, with the layers thus formed retaining the matrix orientation. This process is heterogeneous in nature.

It would be natural to expect that the homogeneous growth of the crystal nuclei separated from the matrix would result in the occurrence of polycrystalline grains in the amorphous region. This, however was not observed.

The orienting influence of the substrate was checked by a special experiment. An amorphous silicon film produced by monosilane pyrolysis was P^+ ion irradiated under crystallization conditions. The thickness of the amorphous Si film was selected such as not to allow the ions to penetrate as far as the substrate (used as a substrate were pure silicon and silicon with a Si_3N_4 film). Upon irradiation of such samples with P^+ ions, the structure of the amorphous Si film did not change.

In another experiment [54], an amorphous layer was fabricated by 40 keV Si^+ ion bombardment of Si with subsequent 50 keV P^+ ion bombardment. In this case, the P^+ ions penetrated to a depth exceeding the thickness of the amorphous layer and crystallization was observed.

Sort of implanted impurity. The least understanding exists regarding the role of this condition, which seems to be due to the lack of knowledge of the processes involved in oriented crystallization.

According to the data currently available, the oriented crystallization effect is a well established fact observed during implantation into silicon of impurities such as P^+, B^+, As^+ as well as in P^+ ion bombarded Ge [25-27]. It is also reported that in S^+ ion bombarded InSb, the surface layer amorphization sets in at $\Phi = 3 \cdot 10^{13}$ cm^{-2} (room-temperature target) and after being irradiated with a dose exceeding $6 \cdot 10^{15}$ cm^{-2}, the surface gains a polycrystalline structure with a lattice of the ZnS type [55]. Superposition, on the electron diffraction patterns, of the reflexes from the non-irradiated area of the water on the polycrystalline rings of the irradiated crystal portion enabled the authors of the cited work to draw a conclusion that implantation of S^+ ions does not result in the occurrence of a new phase at the surface of InSb and the picture observed is not associated with a change in the structure of the sample being bombarded.

According to references [26, 49, 53] the amorphous layer crystallization mechanism is determined by solid-phased reactions with emergence and decay of semiconductor-impurity compounds. It is likely that such reactions release an additional energy required for epitaxial build-up of the crystallographic planes of the matrix at the crystallization front. Proceeding from the current density dependence of the crystallization process, the authors pointed to a significant role of an excited electronic subsystem. The influence of the high ionization level on structural changes in the amorphous semiconductor and on the activation of the implanted impurity was also noted in [15, 16].

The data existing on InSb, in contrast to the results obtained for Si and Ge, do not enable one to suggest a possible oriented crystallization of the entire layer being bombarded. They just point to the occurring structural changes caused by high irradiation doses, while oriented crystallization constitutes a macroscopic effect. One of the possible causes of formation of a polycrystal on InSb may reside in the high crystallization rate. The experimenters exploring the structure of P^+ ion bombarded silicon layers noted that the crystallization involving increased current densities (and, hence, high crystallization rates) resulted in the occurrence, near the crystallization front, of crystal twins and a polycrystalline interlayer. A decrease in the current density promotes formation of a more perfect structure [26].

Apart from the cited data, there are reports on the ordering of Si and InSb structures when irradiated with inert gas (Ar) ions [56, 57]. The results for InSb are similar to those achieved by its bombardment with S^+ ions. The ordering of the structure of Si when Ne^+ and Ar^+ ion irradiated to doses of $2\text{-}3 \cdot 10^{17}$ cm^{-2} was noted inside the amorphous region in a layer about 200 Å thick. With smaller doses

($\Phi > \Phi_a$), the layer remained amorphous (Φ_a is the amorphization dose).

This evidence is difficult to interprete in terms of the mechanism described above, since one hardly expects the formation of semiconductor-inert gas compounds. Therefore, it was supposed [56] that a rearrangement of the amorphous layer structure is conditioned by the stresses caused by ion implantation. The stresses may be induced, for example, by impurities implanted into the sample surface. The influence of the internal stresses on the structure and properties of the amorphous semiconductor was noted in references [58-60]. The authors of [58] have discovered a shock crystallization to occur when a film of amorphous germanium, fabricated by cathode sputtering and placed on a mica substrate, is brought under mechanical action of a sharp needle. The result was the transition from the amorphous to monocrystalline state. Special experiments with films in which stresses were relieved either through making a thin substrate or annealing the structure have shown that the shock crystallization in this case is nonexistent [60]. The difficulty in utilization of the results obtained resides in that so far no quantitative relationship has been discovered between the stress value and the structure of the amorphous semiconductor.

Proceeding from the data on the oriented crystallization effect, one can conclude that choosing a suitable sort of implant only makes the effect more pronounced (due to chemical properties of this implant) and does not constitute a factor of crucial importance for the effect.

Structural changes in layers during annealing. The influence of a high concentration of impurity on epitaxial crystallization of amorphous silicon layers fabricated by ion bombardment was investigated using the channelling effect of 2 MeV He^+ ions [11, 12]. At first, the silicon wafers were irradiated with Si^+ ions at $T = -180$ °C to cause the formation of the amorphous layer. Then P^+, As^+ and B^+ ions were implanted into amorphous silicon to produce an impurity concentration of 0.2-0.5 at%. The energy of P^+, As^+, B^+ ions was varied during the implantation to obtain a high concentration of impurity throughout the amorphous layer. Subsequent thermal annealing was effected in a vacuum of 10^{-6} mm Hg over a temperature range of 475 to 575 °C.

It was observed that with a concentration of P, B and As ions in excess of 10^{20} cm^{-3}, the rate of crystallization of the amorphous layer increased. For example, for the plane (100) of a silicon wafer, the presence of P and As enhances the crystallization rate at $T = 500$ °C by a factor of 6 as compared to that in silicon samples free of such impurities. Implantation of boron into the amorphous layer enhanced the crystallization rate by a factor of 20 (Fig. 7.7). Because of the nonuniform depth distribution of impurity, it was difficult to find the

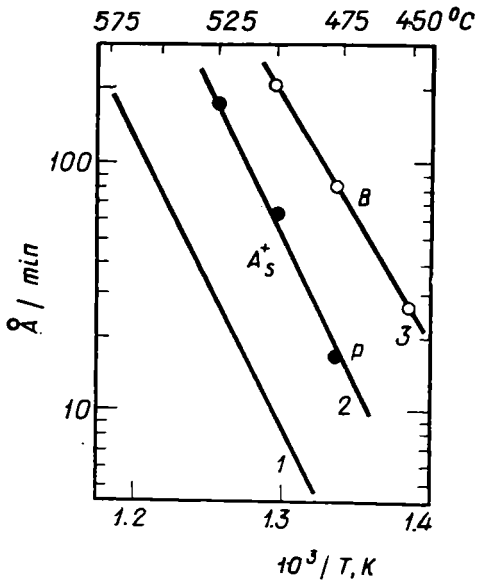

Fig. 7.7. Amorphous layer crystallization rate vs temperature [11].
1—pure Si (100); *2*—Si: P, Si: As; *3*—Si: B

exact value of the crystallization activation energy in the presence of impurity. The estimates of this energy are as follows: 1.9 eV for amorphous silicon with implanted boron and 2.35 eV for amorphous silicon free of impurity or containing phosphorus. Thus, most prominent crystallization enhancement effects were registered for boron-containing layers. As to phosphorus, though no reduction in the activation energy value was registered, an increase in the crystallization rate might be attributed to a change in the pre-exponential multiplier, C, in the equation $C \cdot \exp(-2.35/kT)$ giving the crystallization rate versus temperature (see Fig. 7.7).

Implantation into amorphous silicon of impurities such as C, N, O, Ne, Ar and Xe to concentrations of about 0.5 at.% reduced the layer crystallization rate. For example, in the event of implantation of oxygen, the crystallization rate reduced to one-tenth of its previous value at $T \simeq 550$ °C, while for an amorphous layer containing argon, it reduced to a value that could hardly be measured at the same annealing temperature [12].

Significant structural changes subsequent to annealing were noted for polycrystalline silicon irradiated with high-dose phosphorus ions [61]. Electron diffractometry studies were made of polycrystalline silicon films 0.6 μm thick, fabricated by pyrolysis of monosilane at $T = 800$ °C. Monocrystalline silicon wafers with a thermal oxide layer 1200 Å thick were used as substrates. The films were irradiated with P^+ and Ar^+ ions, $E = 150$ keV, $\Phi = 6.3 \cdot 10^{15}$-$6.3 \cdot 10^{17}$ cm^{-2}. Thermal annealing was effected in nitrogen at 800, 1050 and 1150 °C.

It was found that heat-treatment of phosphorus-containing films at $T > 800$ °C resulted in an increase in the size of the grain. Thus, the grain size increased from 3000-4000 Å to 1.3 μm after being an-

nealed for one hour at $T = 1150$ °C. In films non-bombarded or bombarded with Ar^+ ions, the grain size did not change after the same treatment. No oriented crystallization was reported by the authors of [61], probably, due to the absence of a monocrystalline substrate.

The constancy of the grain size in Ar^+ ion bombarded films was explained by the theory based on the assumption that the dissolved impurities impede the movement of the grain boundary due to elastic attraction of the impurity atoms towards the boundary. In such a situation, the boundary must "drag" these atoms as it moves with the result that its velocity is limited by the atomic diffusion rate [62]. Diffusion of Ar in Si over a temperature range of 967 to 1207 °C was not ascertained [63]. Great diffusive mobility of phosphorus is believed [61] to promote the growing of grains during annealing.

Sec. 7.3. Electrical Characteristics of Layers

Room temperature implantation of B^+, Al^+, Ga^+, In^+ ions into *n*-type Si and P^+, As^+, Sb^+, Bi^+ ions into *p*-type Si to high doses results in converted conductivity and occurrence of a conductive layer in the samples [64, 65]. Thus, a converted layer was reported for a phosphorus ion dose of about 10^{15} cm^{-2} [65]. With increase in the dose, the surface conductance, σ_s, sharply increased with respect to the number of implanted atoms and this growth continued to $\Phi \simeq$ $\simeq 4 \cdot 10^{16}$ cm^{-2} (the value of σ_s varied by three orders of magnitude over a dose range of 10^{15} to $4 \cdot 10^{16}$ cm^{-2}), following which, the value of σ_s remained constant over a dose range of $4 \cdot 10^{16}$ to 10^{17} cm^{-2}. It has been supposed that such a behaviour of conductance is associated with the radiation annealing of elementary defects, while the saturation of the $\sigma_s(\Phi)$ curve is explained by collection of defect complexes absorbing the phosphorus atoms and capturing the conducting electrons.

In further studies involving the EPR and fast electron reflection diffraction [3, 25-27, 48, 49], considerable structural rearrangements of the bombarded layer, up to its crystallization in the process of ion implantation, were reported (see Sec. 7.2). Sheet resistivity, ρ_s, measured with a four-point probe was reported by the authors of [65] to sharply decrease with increase in dose (Figs. 7.6 and 7.8).

The study [28] of the electrical characteristics of Ge bombarded with P^+ ions at room temperature gave a clear evidence of the ion beam current density. In *n*-type Ge with a resistivity of about 10 ohm · ·cm, the inversion of conductivity occurred at sufficiently high doses and current densities, while decreasing the current density to a particular value did not allow inversion of type of conductivity. Thus, with a density of current of 40 keV P^+ ions equal to 2 $\mu A/cm^2$, Ge retained its initial type of conductivity up to doses as high as $2 \cdot 10^{16}$

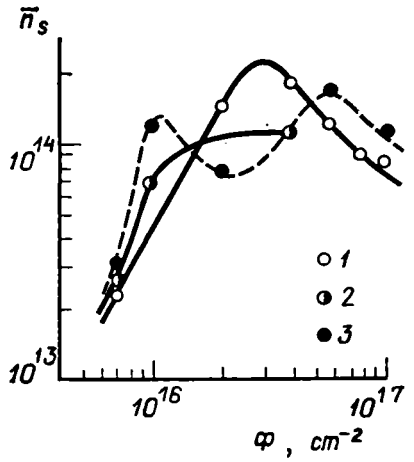

Fig. 7.8. Carrier concentration in a layer of silicon irradiated with 30 keV P ions vs dose of implanted impurity.
Ion current density, $\bar{j}$, μA/cm²: *1*—2; *2*—5; *3*—10

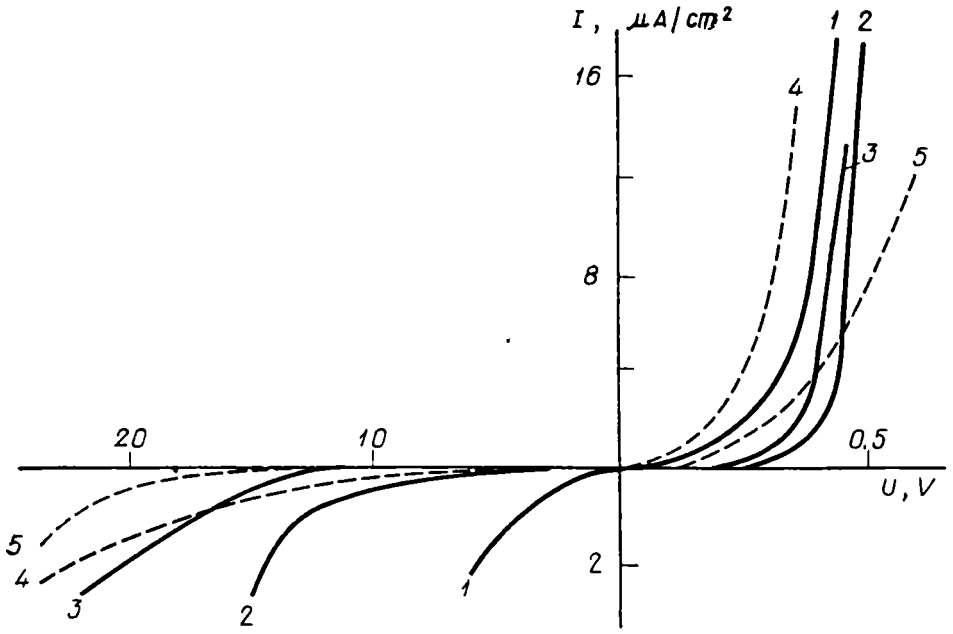

Fig. 7.9. Volt-ampere characteristics of *p-n* junctions produced in silicon irradiated with 30 keV P ions.
$\bar{j}$ = 2 μA/cm², Φ, cm⁻²: *1*—$2 \cdot 10^{16}$, *2*—$6 \cdot 10^{16}$, *3*—$4 \cdot 10^{16}$; Φ = $4 \cdot 10^{16}$, *j*, μA/cm²: *4*—5, *5*—10

cm^{-2}, while with $\bar{j} = 4$ μA/cm², the inversion of conductivity occurred at $\Phi = 5 \cdot 10^{15}$ cm^{-2}.

The structural rearrangement in the irradiated layer proved of help in understanding the occurrence of conductive regions, while concurrent stud es of the structural and electrical characteristics allowed ob ervation of new effects associated with implantation into semiconductors of high doses of ions [27]. Such effects include the phenomena occurring during implantation of impurities into amor-

phous semiconductors to high concentrations. In such an event, the amorphous layer becomes conductive. It is a common knowledge that amorphous semiconductors, unlike crystalline ones, do not readily lend themselves to doping, since the amorphous phase is thought of as a system with satisfied valence bonds [66].

Ion implantation of silicon allows obtaining an amount of impurity preventing silicon atoms from satisfying all chemical bonds of the impurity atoms. In this situation, the amorphous material becomes conductive.

A study of the volt-ampere characteristics of *p-n* junctions fabricated by room-temperature irradiation of semiconductors to high doses at various values of $\bar{j}$ was conducted on *p*-type silicon with ρ of about 1 ohm·cm [67]. The dose range was from 10^{16} to $6 \cdot 10^{16}$ cm^{-2}, current density $\bar{j} = 2.5$ and 10 μA/cm^2. The measurements were taken of mesa-structures about 0.5 mm in diameter. As a result, it was found that the maximum breakdown voltage, U_{br}, about equal to 10-12 V, was specified to *p-n* junction fabricated at $\bar{j} = 2$ μA/cm^2 and $\Phi = 4 \cdot 10^{16}$ cm^{-2}. An increase or decrease of the dose for $\bar{j} = 2$ μA/cm^2 resulted in an increase of the reverse current. Also, the reverse current of the *p-n* junction increased when $\bar{j}$ was increased to 5 and 10 μA/cm^2 (Fig. 7.9).

It seems that obtaining the best volt-ampere characteristics for minimum current density $\bar{j} = 2$ μA/cm^2 is associated with the fact that the rate of crystallization of amorphous silicon during irradiation is also a minimum (see Sec. 7.2), and, therefore, the number of residual defects in the vicinity of the *p-n* junction is less than that for $\bar{j} = 5$ and 10 μA/cm^2. As is clear from the discussion of Sec. 7.2, at $\bar{j} = 5$ μA/cm^2, twins were observed at the crystallization front and behind it, as viewed from the matrix, there was a polycrystalline silicon layer about 150 Å thick. Bombardment with lesser current densities, such as $\bar{j} = 1$ and 2 μA/cm^2 does not result in the formation of twins and a transition region, because monocrystalline silicon directly follows the crystallization front.

The fact that the dose of $4 \cdot 10^{16}$ cm^{-2} proved to be an optimum one is likely to be an evidence of insufficient structural rearrangement of the irradiated layer at $\Phi = 2 \cdot 10^{16}$ cm^{-2} and of too high a concentration of implanted impurity for $\Phi = 6 \cdot 10^{16}$ cm^{-2}. Since conductivity over this dose range remains practically constant with growth of Φ (see Fig. 7.8), the implanted atoms are essentially the defects present in the crystallized region. It seems that these defects cause an increase in the reverse currents of *p-n* junctions at $\Phi = 6 \cdot 10^{16}$ cm^{-2} for all values of $\bar{j}$.

Sec. 7.4. Impurity Profiles at Various Doses of Irradiation and Beam Current Densities

The discovery of oriented crystallization effects in semiconductor layers amorphized during the initial stages of bombardment and of electrical activation of impurity without additional annealing has prompted interest in investigating the impurity profiles in the presence of such effects. A study was made of silicon irradiated with 30 keV P^+ ions [41]. The dose range was $4.4 \cdot 10^{15}$ to 10^{17} cm^{-2}; current density $j = 2.5$ and 10 $\mu A/cm^2$.

The results obtained can be summarized as follows:

1. The P depth distribution peak, R_p^* shifts with increase in dose towards the surface of the sample for all known values of current density (see Fig. 7.10*a*, *b*).

2. With any dose selected, R_p^* is nearer to the surface when the current density, $\bar{j}$, is maximum, i.e., 10 $\mu A/cm^2$ (Fig. 7.11).

Under conditions of sputtering, the impurity profile is given by formula (7.7) which was deduced without making an allowance for the dose and current density dependence of the sputtering yield. Evidently, such assumptions presented no significant difficulties in comparison of the experimental evidence with the predictions of the simple theory explaining the effects of sputtering on the impurity profile (see Sec. 7.1), since it was already noted in our preceding discussion that in P^+ ion bombarded silicon the sputtering rate is independent of the phosphorus dose up to $\Phi \sim 10^{17}$ cm^{-2} [38]. The current density dependence of the sputtering yield was not observed up to the values in the vicinity of 30 $\mu A/cm^2$ [40].

If the distribution of the implanted impurity is gaussian and is presented by Mayer, Ericksson and Davies [1] in the form

$$n(x) = (\Phi/2.5 \cdot \Delta R_p) \exp[-(x - R_p)^2/\Delta R_p^2], \tag{7.14}$$

then, with sputtering of the boundary taken into account, the profile will be given by the expression

$$n(x, \Phi) = (\sqrt{\pi}\, n_0/5S)\,[\mathrm{erf}\,((x - R_p + \Phi S/n_0)/\Delta R_p) - \\ - \mathrm{erf}\,((x - R_p)/\Delta R_p)], \tag{7.15}$$

which differs from (7.7) only in a constant value because of another definition of the Gaussian distribution.

According to (7.11), the position of the profile peak is given by

$$R_p^* = R_p - S\Phi/2n_0. \tag{7.16}$$

This function can be applied for describing the variation of R_p^* with growth of Φ for $\bar{j} = 2$ and 5 $\mu A/cm^2$ when $S \simeq 1$ and R_p is close to the calculated value of 375 Å [1]. The value of S calculated

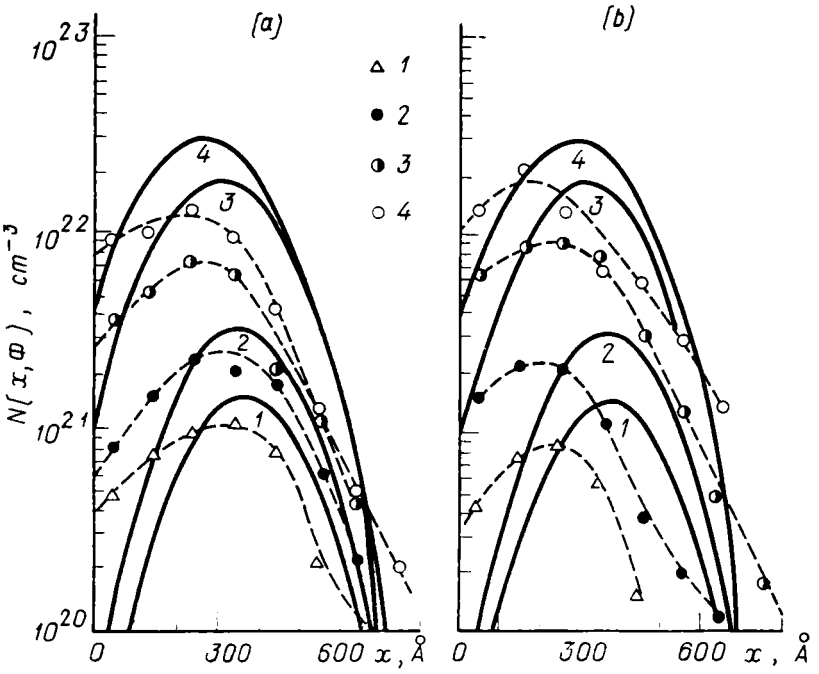

Fig. 7.10. Distribution of phosphorus implanted in silicon at $E = 30$ keV $\bar{j} = 2$ μA/cm² (*a*) and $\bar{j} = 10$ μA/cm² (*b*).
Dose, cm⁻²: *1*—$4.4 \cdot 10^{15}$; *2*—10^{16}; *3*—$6 \cdot 10^{16}$; *4*—10^{17}. The solid lines are the curves calculated by (7.15) with $S = 1$ [41]

Fig. 7.11. Position of distribution maximum of phosphorus implanted in silicon with an energy of 30 keV vs irradiation dose ($\bar{j}$, μA/cm²: *1*—2; *2*—5; *3*—10) [41].

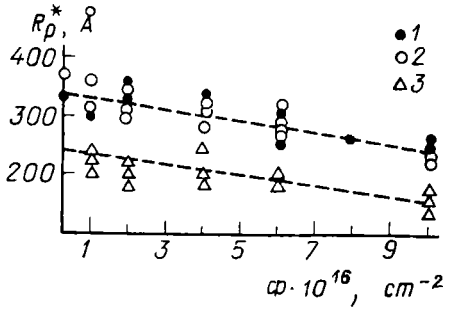

by formula (7.2) amounted to 1.3, which fits the experimental data fairly well.

It proved impossible to give the dependences $R_p^*(\Phi)$ for $\bar{j} = 10$ μA/cm² by simply increasing the value of S provided the value of R_p was close to the calculated one. A possible slope of the curve passing through all points gives, in this case, the value of $S \simeq 1$ (see Fig. 7.11).

Thus, the movement of R_p^* towards the surface with growth in the dose at $\bar{j} = 2$ and 5 μA/cm² can be determined with the aid of an impurity accumulation model, making an allowance for the material sputtering at $S \simeq 1$. The actual profile, however, significantly dif-

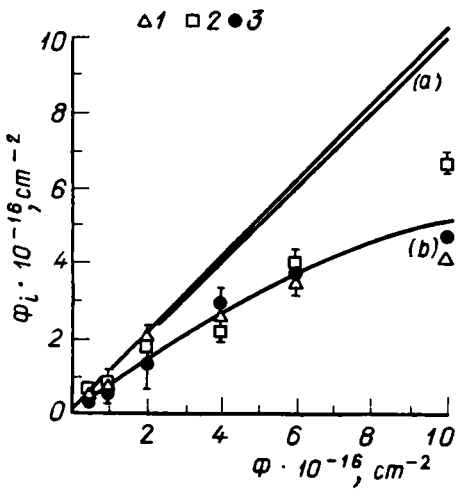

Fig. 7.12. Amount of phosphorus implanted in silicon and measured with neutron activation analysis vs irradiation dose [41].
a—calculated by (7.15); *b*—experimental data ($\bar{J}$, μA/cm²: *1*—2; *2*—5; *3*—10)

fers from that calculated by formula (7.15): in the experiment, a marked displacement of the profile towards the surface is observed (see Fig. 7.10). This effect as well as displacement of R_p^* towards the surface at $\bar{j} = 10$ μA/cm² and a great difference between the calculated amount of impurity implanted into the sample (with an allowance made for material sputtering) and the measured one (Fig. 7.12) have enabled the authors of [41] to draw a conclusion on a substantial diffusive displacement of phosphorus in the process of irradiation.

Fig. 7.12 shows the dose dependence of the number of ions, Φ_i, implanted into the samples per unit square (measured value). For comparison, a theoretical curve (*a*) is also depicted. This curve was provided by integration of formula (7.15) with respect to x. Deviation of this curve from linearity is caused by a loss of impurity due to sputtering. Juxtaposition of the calculated (*a*) and experimental (*b*) curves enables us to think that the main mechanism of losses of implanted ions is not represented by sputtering of the material boundary and the attendant loss of a fraction of phosphorus per se, but a combined action of the given mechanism and of radiation-enhanced diffusion of the impurity atoms towards the boundary. The process of diffusion in the course of implantation of ions into a solid, with a diffusion coefficient D^* independent of the coordinate and time, is theoretically described in reference [68]. In this case, the resultant impurity profile has a considerably larger half-width, while the position of the maximum remains unchanged and equal to the projection of the ion mean free path. As was noted above, the value of R_p^* shifts towards the surface with growth in dose and current density. Hence, the predictions of the theory given in reference [69] do not fit the experimental data. Rough agreement can be restored by assuming that the value of D^* left of R_p^* (i.e., near the boundary) is significantly greater than the value of the diffusion coefficient right of R_p^*.

From this it is inferred that the impurity diffusion during irradiation is most likely to be associated with the generation of point defects, caused by the implanted atoms. A major role of induced ionization in enhancement of impurity diffusion is also quite probable. Strong ionization changes the charge state of the implanted impurity and defects and, thus, influences the process of diffusion [70-72].

Diffusion of phosphorus in silicon seems to be insignificant in the process of its activation by neutron irradiation. This is supported by the facts that the shape of the profile does not depend on the neutron irradiation time (50 or 100 hours). Besides, it is known [73] that the phosphorus profiles in silicon, produced with the help of neutron-activation analysis and ion-beam microanalyzer, coincide.

To draw a more convincing conclusion on the nature of phosphorus diffusion in the process of irradiation, let us use formula (7.15) to evaluate the diffusion flux of atoms near the boundary ($x = 0$) and then integrate it with respect to the irradiation time $t = \Phi/\bar{j}$. Assume that the value obtained is equal to the observed difference: $\Delta\Phi = \Phi - \Phi_i$. The value of Φ_i versus dose may be given, for this evaluation, by a linear-quadratic function disregarding the current density dependence (see Fig. 7.12, curve *b*):

$$\Phi_i = (1 - \alpha)\,\Phi - \beta\Phi^2, \tag{7.17}$$

where α and β are the adjusting parameters that can be derived from the experimental data (see Fig. 7.12) by the method of least squares. In our case, $\alpha = 0.242$; $\beta = 0.24 \cdot 10^{-17}$ cm.

Formula (7.17) gives $\Delta\Phi = \Phi - \Phi_i = \alpha\Phi + \beta\Phi^2$. For the coefficient of radiation-enhanced diffusion of phosphorus in silicon, we obtain

$$D^* \simeq [\sqrt{\pi}\,(\Delta R_p)^3/R_p]\,(\beta + \alpha/\Phi)\,\bar{j}\exp(R_p/\Delta R_p)^2. \tag{7.18}$$

In the investigated range of doses and current densities, the value of D^* varies from $2 \cdot 10^{-15}$ to $5 \cdot 10^{-14}$ cm$^2 \cdot$s^{-1}.

Redistribution of phosphorus in the process of silicon irradiation with increased densities of current agrees with the idea of "pulling in" of impurity into the damaged region (see [49] and Ch. 3 of this book). This idea was conceived as a result of the experiments involving proton irradiation of ion-implanted layers. In these experiments, the peak of the impurity depth distribution profile shifted to the region with a high concentration of defects introducted by proton bombardment [49, 74, 75].

The effects described in the present chapter prove to be of technological value when it is required to significantly reduce the temperature of annealing of ion implanted layers. Often such a situation occurs when an operation aimed at fabrication of an implanted layer happens to be the last one, and heating up of the device structure is

quite undesirable, as this will strongly affect the characteristics of the structure. For example, a structure like a silicon film provided with a built-in *p-n* junction and placed on a metallic substrate may be heated to temperatures of $\simeq$500 °C. Higher temperatures will either cause diffusion of a metal into a semiconductor or result in the formation of a metal-semiconductor eutectics. At the same time, very often it is required to fabricate on this semiconductor film a low-ohmic layer to decrease the resistance at the point of contact with a subsequently sputtered metallic film. The use of the technique that provides for fabrication of a heavily doped layer without thermal annealing makes it possible to reduce the impedance of active components and increase their efficiency and output power.

As another example, we may mention a Soviet-made photo-target, type "Kremnikon", which, if annealed at high temperature, destroys the working portion of the wafer about 15 μm thick. Fabrication of a low-ohmic layer on this structure without thermal annealing also gives good results.

The effects discussed in this chapter may be applied to production of not only heavily doped layers but also of *p-n* junctions when these are planned to be used in low-voltage circuits, while high-temperature annealing is undesirable.

References

1. Mayer, J., Eriksson, L., Davies J. *Ion Implantation in Semiconductors. Silicon and Germanium.* New York-London. 1970, 280 pages.
2. *Ion Implantation in Semiconductors.* Ed. by S. Namba. New York-London, 1975, 742 pages.
3. Gerasimenko, N. N., Dvurechensky, A. V., Romanov, S. I., Smirnov, L. S. The study of defect formation in ion implanted silicon. In: *Radiation Damage and Defects in Semiconductors. Conf. Ser. No. 16*, Inst. of Phys. London-Bristol, 1972, pp. 72-80.
4. Kräutle, H. Study of the annealing behaviour of high dose implants in Si and Ge crystals. *Rad. Eff.*, 1975, **24**, 3-4, pp. 255-262.
5. Baranov, A. I., Dvurechensky, A. V., Gerasimenko, N. N., Smirnov, L. S. Annealing of vacancy clusters in silicon. In: *Radiation Effects in Semiconductors. Conf. Ser. No. 31*, Inst. of Phys. London-Bristol, 1977, p. 505.
6. Baeri, P., Campisano, S. U., Cianola, G., Foti, G., Rimini, E. Influence of implanted dose on the recrystallization of silicon amorphous layer. *Appl. Phys. Lett.*, 1975, **26**, 4, pp. 154-155.
7. Golansky, A., Fiderkiewicz, A., Rzewuski, H., Lefeld-Sosnovska, M., Gronkowski, J., Grötzschel, R., Kreissing, U., Bartseh, H. Particularities of crystalline to amorphous state conversion in Si heavily damaged by 140 keV Si^{++} ions. *Phys. Stat. Sol. (a)*, 1976, 38, 1, pp. 139-149.
8. Csepregi, L., Kennedy, E. F., Lau, S. S., Mayer, J. W., Sigmon, T. W. Disorder produced by high-dose implantation in Si. *Appl. Phys. Lett.*, 1976, **29**, 10, pp. 645-648.
9. Baranov, A. I., Gerasimenko, N. N., Dvurechensky, A. V., Smirnov, L. S. Annealing of large vacancy clusters. *Fizika i tekhnol. polupr.*, 1977, **II**, 1, pp. 94-99 (in Russian).

10. Vikhrev, B. I., Gerasimenko, N. N., Dvurechensky, A. V., Smirnov, L. S. Interactions of H atoms with defects produced by ion bombardment in silicon. *Fizika i tekhnol. polupr.*, 1974, 8, 7, pp. 1345-1348 (in Russian).
11. Csepregi, L., Kennedy, E. F., Gallagher, T. J., Mayer, J. W., Sigmon, T. W. Reordering of amorphous layer of Si implanted with P, As, B ions. *J. Appl. Phys.*, 1977, 48, 10, pp. 4234-4240.
12. Kennedy, E. F., Csepregi, L., Mayer, J. W., Sigmon, T. W. Influence of O, C, N and noble gases on the crystallization of amorphous Si layers. *J. Appl. Phys.*, 1977, 48, 10, pp. 4241-4246.
13. Picraux, S. T., Vook, F. L., Ionization, thermal and flux dependences of implantation disorder in silicon. *Rad. Eff.*, 1971, 11, 2, pp. 179-192.
14. Kimerling, L. C., Poate, J. M. Lattice defects in ion implanted semiconductors. In: *Lattice Defects in Semiconductors. Conf. Ser. No. 23*, Inst. of Phys. London-Bristol, 1974, pp. 126-148.
15. Suski, J., Krynicki, J., Rzewuski, H., Gyulai, J. Ionization enhanced annealing in P and As implanted Si layers. *Rad. Eff.*, 1976, 30, 2, pp. 125-126.
16. Suski, J., Csepregi, L., Gyulai, J., Rzewuski, H., Werner, Z. Electron irradiation assisted annealing of boron and phosphorus implanted Si layers. *Rad. Eff.*, 1976, 29, 3, pp. 137-141.
17. Oki, F., Ogawa, Y., Fujiki, Y. Effect of deposited metals on the crystallization of amorphous Ge films. *Japan. J. Appl. Phys.*, 1969, 8, p. 1056.
18. Barsnell, J. R., Voisey, U. C. The influence of contact materials on the condition crystallization temperature and electrical properties of amorphous Ge, Si and B films. *Thin Sol. Films*, 1970, 6, 3, pp. 161-166.
19. Lee, D. H., Hart, R. R., March, O. J. Effect of Al films on ion implanted Si. *Appl. Phys. Lett.*, 1972, 20, 2, pp. 73-75.
20. Herd, S. R., Chandhair, P., Brodsky, M. H. Metal contact induced crystallization in films of amorphous Si and Ge. *J. Non-Cryst. Sol.*, 1972, 7, 4, pp. 309-327.
21. Sigurd, D., Ottaviani, G., Marrelo, V., Mayer, J. W., MaCaldin, J. O. Crystallization of evaporated Si/Ag and Ge/Al films. *J. Non-Cryst. Sol.*, 1973, 12, 1, p. 135.
22. Gerasimenko, N. N., Dvurechensky, A. V., Kachurin, G. A., Pridachin, N. B., Smirnov, L. S. Radiation annealing of defects produced by ion bombardment of crystals. *Fizika i tekhnol. polupr.*, 1972, 6, 9, pp. 1834-1835 (in Russian).
23. Nelson, R. S. The clustering of defects in irradiated semiconductors. In: *Radiation Damage and Defects in Semiconductors, Conf. Ser. No. 16*, Inst. of Phys. London-Bristol. 1972, pp. 140-158.
24. Mordkovich, V. N., Solovyev, S. P., Temper, E. M., Kharchenko, V. A. On radiation annealing of defects in neutron irradiated silicon. *Fizika i technol. polupr.*, 1974, 8, 5, pp. 1024-1025 (in Russian).
25. Gerasimenko, N. N., Dvurechensky, A. V., Romanov, S. I., Smirnov, L. S. Interactions of defects and impurities in ion implanted silicon. *Fizika i tekhnol. polupr.*, 1972, 6, 10, pp. 1978-1981 (in Russian).
26. Gerasimenko, N. N., Dvurechensky, A. V., Romanov, S. I., Smirnov, L. S. On the effects of high-dose ion implants in semiconductors. *Fizika i tekhnol. polupr.*, 1973, 7, 11, pp. 2195-2199 (in Russian).
27. Dvurechensky, A. V., Gerasimenko, N. N., Romanov, S. I., Smirnov, L. S. High dose effects in ion implantation. *Rad. Eff.*, 1976, 30, 2, pp. 69-72.
28. Akimchenko, I. P., Krasnopevtsev, V. V., Milyutin, Yu. V. Role of ion beam current density in P ion implantation in GeO_2-Ge. *Electronnaya tekhnika. Ser. 2. Poluprovodnikovye pribory*, 1976, 7 (109), pp. 40-46 (in Russian).
29. Freeman, J. H., Chivers, D. J., Gard, G. A., Hinder, G. W., Smith, B. J., Stephen, J. Electrical behaviour of heavily-doped ion implanted layer in

silicon. In: *Ion Implantation in Semiconductors.* Science and Technology. N.Y.-London, Plenum Press, 1974, pp. 555-569.
30. Wada, Y., Usui, H., Ashikawa, M. Substrate temperature measurement during ion implantation. *Japan J. Appl. Phys.*, 1975, **14**, 9, pp. 1351-1356.
31. Furukawa, S., Inoue, O., Ishiwara, H. Experimental simulation of ion beam heating effects in ion implantation techniques. *Japan. J. Appl. Phys.*, 1973, **12**, 7, pp. 1075-1076.
32. Party, D. Target heating during ion implantation. *J. Vac. Sci. and Techn.*, 1976, **13**, 2, pp. 622-629.
33. Vasilyev, V. K., Zorin, E. I., Pavlov, P. V., Tetelbaum, D. I. On influence of ion current density on electrical conductivity of boron ion implanted silicon. In: *Fizicheskie osnovy ionno-luchevogo legirovaniya.* Part. 2. Gorky, 1972, pp. 183-185 (in Russian).
34. Pleshivtsev, N. V. *Cathode Sputtering.* Moscow, Atomizdat, 1968, 343 pages (in Russian).
35. Carter, G., Collington, J. S. *Ion Bombardment of Solids.* N.Y. Elsevier Publishing Co., 1968, 446 pages.
36. Sigmund, P. Theory of sputtering. I. Sputtering yield of amorphous and polycrystalline targets. *Phys. Rev.*, 1969, **184**, 2, pp. 383-416.
37. Andersen, H. H., Bay, H. Z. Heavy-ion sputtering yield of silicon. *J. Appl. Phys.*, 1975, **46**, 5, pp. 1919-1921.
38. Sowa, M., Sielanko, J., Meldizon, J., Żuk, W., Wasiak, A. The effect of high-dose implantation on the sputtering efficiency of silicon. In: *Proc. Internat. Conference on Ion Implantation in Semiconductors.* Reinhardsbrunn, 1977, Part 1, pp. 142-147.
39. Schultz, F., Wittmaack, K. Model calculation of ion collection in presence of sputtering. *Rad. Eff.*, 1976, **29**, 1, pp. 31-40.
40. Blank, P., Wittmaack, K., Schultz, F. The influence of sputtering. Range shortening and stress-induced out-diffusion on the retention of xenon implanted in silicon. *Nucl. Instrum. Meth.*, 1976, **132**, 1, pp. 387-392.
41. Baranov, A. I., Gerasimenko, N. N., Dvurechensky, A. V., Potapova, L. P. Profiles of phosphorus implanted in silicon versus ion dose and current density. *Electronnaya tekhnika. Ser. 2. Poluprovodnikovye pribory*, 1978, 4, pp. 33-39 (in Russian).
42. Zorin, E. I., Pavlov, P. V., Tetelbaum, D. I. *Ion Implantation in Semiconductors.* Moscow, Energiya, 1975, 129 pages (in Russian).
43. Yanke, E., Emde, F., Lesh, F. *Special Functions.* Moscow, Nauka, 1964, 344 pages (in Russian).
44. Primak, W., Radiation-induced cavities and exfoliation. *J. Appl. Phys.*, 1963, 34, 12, pp. 3630-3631.
45. Das, S. K., Kaminsky, M. Radiation blistering of polycrystalline niobium by helium ion implantation. *J. Appl. Phys.*, **44**, 1, p. 25-31.
46. Eer Nisse, E. P., Picraux, S. T. Role of integrated lateral stress in surface deformation of He implanted surfaces. *J. Appl. Phys.*, 1977, **48**, 1, pp. 9-16.
47. Evans, J. H., Mazey, D. J., Eyre, B. L., Erents, S. K., McCraken, G. M. A TEM study of gas bubbles and surface blisters in molibdenum bombarded with helium ions. In: *Application of Ion Beams to Materials*, 1975, Inst. of Phys. London, 1976, pp. 299-305.
48. Dvurechensky, A. V. Interactions of defects in ion bombarded silicon with one another and with impurities. An abstract on cand. dissert. Novosibirsk, 1973, 22 pages (in Russian).
49. *Physical Processes in Irradiated Semiconductors.* Ed. by L. S. Smirnov. Novosibirsk, Nauka, 1977, 256 pages (in Russian).
50. Gerasimenko, N. N., Dvurechensky, A. V., Smirnov, L. S. An EPR study of defect formation in ion implanted silicon. *Fizika i tekhnol. polupr.*, 1971, 5, 9, pp. 1700-1705 (in Russian).
51. Gerasimenko, N. N., Dvurechensky, A. V., Smirnov, L. S. On paramagnetic

centers formed as a result of ion irradiation of silicon. *Fizika i technol. poluprov.*, 1972, **6**, 6, pp. 1111-1114 (in Russian).
52. Crowder, B. L., Title, R. S., Brodsky, M. H., Pettit, G. D. ESR and optical absorption studies of ion implanted silicon. *Appl. Phys. Lett.*, 1970, **16**, 5, pp. 205-208.
53. Dvurechensky, A. V., Smirnov, L. S. Production and rearrangement of radiation defects in ion implanted semiconductors. *Rad. Eff.*, 1978, 37, 3, 4, pp. 173-178.
54. Romanov, S. I. Amorphization and crystallization of silicon by ion beams. An abstract of cand. dissertation, 1979, 13 pages (in Russian).
55. Brilliantov, E. I., Guseva, M. I., Koroleva, N. V., Korshunov, A. B., Makarov, A. G., Starinin, K. V. Sulfur ion implantation in *p*-InSb. In: *Interactions of Atomic Particles with Solids*. Moscow, 1972, pp. 397-400 (Proc. of II-nd All-Union Symposium) (in Russian).
56. Gerasimenko, N. N. Dvurechensky, A. V., Mashin, A. I., Khokhlov, A. F. Heterogeneity of amorphous layer produced by ion bombardment of semiconductors. *Fizika i tekhnol. polupr.*, 1977, **11**, 1, pp. 190-192 (in Russian).
57. Chernysheva, N. Y., Kashurin, G. A., Bogatyrev, V. A. Amorphization and recrystallization of ion implanted InSb. *Phys. Stat. Sol.* (a). 1978, **47**, 1, pp. k5-k8.
58. Takamori, T., Messier, R., Roy, R. New noncrystalline germanium which crystallizes "explosively" at room temperature. *Appl. Phys. Lett.*, 1972, **20**, 5, pp. 201-203.
59. Matsuda, A., Mineo, A., Kurosu, T., Kikuchi, M. Heat radiation from shock crystallization of sputtered amorphous Ge films. *Sol. St. Com.*, 1973, **13**, 8, pp. 1165-1166.
60. Mineo, A., Matsuda, A., Callanan, K. J., Kurosu, T., Kikuchi, M. Possible evidence of an internal stress contribution to the shock crystallization of a-Ge. *Sol. St. Com.*, 1973, **13**, 12, pp. 1945-1946.
61. Akulova, G. V., Kandyba, P. E., Krasovsky, V. M., Starikova, T. I. A change in polycrystalline silicon structure as a result of ion bombardment and subsequent thermal annealing. *Elektronnaya tekhnika. Ser. 3. Mikroelektronika*, 1977, 1 (67), pp. 86-89 (in Russian).
62. *Physical Metallurgy*. 3. Ed. by R. W. Cahn, Amsterdam, 1965, 1100 pages.
63. *Fundamentals of Silicon Integral Circuit Technology. Oxydation, diffusion, epitaxy*. Ed. by. R. Burger and R. P. Donovan, Englewood Cliffs (N. G.), 1967.
64. Gusev, V. M., Zadde, V. V., Landsman, A. P., Titov, V. V. A study of some characteristics of photo detectors with *p-n* junctions produced by ion bombardment. *Fizika tverd. tela.* 1966, 8, 6, pp. 1708-1712 (in Russian).
65. Gusev, V. M., Guseva, M. I., Kurinyi, V. I., Naumenko, V. G., Titov, V. V., Tsyplenkov, V. S. Effects of 30 keV P ion bombardment on electrical behaviour of silicon. *Fizika i tekhnol. polupr.*, 1968, **2**, 9, p. 1394.
66. Mott, F. L. Conduction in glassy and liquid semiconductors. *Disc. Faraday Soc.*, 1970, **50**, pp. 7-12.
67. Dvurechensky, A. V., Potapova, L. P. Volt-ampere characteristics of *p-n* junctions produced by bombardment of silicon with ions at different doses and current densities. *Elektronnaya tekhnika. Ser. 2. Poluprovodnikovye pribory*, 1979, 5, pp. 33-39 (in Russian).
68. Williams, J. S. The measurement of Pb^+ ion collection in Si by high depth-resolution Rutherford backscattering. *Phys. Lett.*, 1975, **51A**, 2, pp. 85-86.
69. Collins, R., Carter, G. The spatial distribution of ions implanted into solid subject to diffusion and surface sputtering. *Rad Eff.*, 1975, **29**, 3, pp. 181-191.
70. Bolotov, V. V., Vasilyev, A. V., Smirnov, L. S. On migration energy of elementary defects in germanium and silicon. *Fizika i tekhnol. polupr.*, 1974, 8, 3, pp. 518-521 (in Russian).

71. Bourgoin J., Peak, D., Corbett, J. W. Ionization enhanced diffusion: Ion implantation in semiconductors. *J. Appl. Phys.*, 1973, **66**, 8, pp. 3022-3027.
72. Bourgoin, J., Corbett, J. W. A new mechanism for interstitial migration. *Phys. Lett.*, 1975, **38A**, 2, pp. 135-137.
73. Burkhardt, F. Mertens, A., Wagner, C. Concentration profiles of implanted phosphorus in silicon. *Phys. Stat. Sol.* (a), 1974, **22**, 1, pp. K45-K47.
74. Baruch, P., Monnier, J., Blanchard, B., Casting C. Redistribution of boron in silicon through high temperature proton irradiation. In: *Ion Implantation in Semiconductors.* Ed. by. S. Numba. N. Y.-London, Plenum Press, 1974, pp. 189-192.
75. Gerasimenko, N. N., Obodnikov, V. I., Smirnov, L. S., Sokolov, S. A. Diffusion of phosphorus in silicon as a result of H ion irradiation at high temperature. *Fizika i tekhnol. polupr.*, 1975, **9**, 11, pp. 2220-2221 (in Russian).

CHAPTER 8

LASER ANNEALING OF IMPLANTED LAYERS

Of particular value to semiconductor technology would be a method in which the annealing of implanted layers could satisfy the following requirements:

(1) only a specified section of the substrate ranging from tens to units of microns in size is heated;

(2) various sections of one substrate can be subjected to controlled heating to different temperatures, without affecting the neighbouring region.

In principle, such problems can be solved through pulsed heating of the implanted regions with powerful light or electron beams. The essence of pulsed heating resides in the fact that with a pulse short enough to be completely absorbed in the near-the-surface layer 10^{-4} cm thick, heat has no time to propagate inside the bulk of the material during the time of the pulse, with the result that a considerable increase in the temperature of the layer is achieved with a relatively small expenditure of energy. Subsequent dissipation of the energy in the entire bulk will result in no marked heating of the material. As will be apparent from the discussion that follows, to accomplish this, the pulse length must not exceed a split microsecond. It is obvious that application of sharply focused beams allows localized annealing, that is, annealing that causes no heating of neighbouring sections. What is more, the use of pulsed heating is likewise an intriguing affair when the pulse time counts milliseconds, which is the usual duration of pulses produced by pumping flashtubes and lasers running free. In such situations, heat has time to spread over large distances, although its effects are but momentary and less injurious to the substrate and surrounding microcircuit components.

The increased temperature is not the only factor affecting the implanted layers during pulsed annealing. Under particular conditions, the results of annealing are influenced by ionization, shock waves and hardening. Consideration of these factors is essential not only to the selection of the required laser treatment conditions, but to taking an intelligent decision as to when the laser annealing is to be employed.

Pulsed annealing may be performed using a wide range of sources, from a flashtube to a charged-particle accelerator. The use of lasers offers certain advantages, which explains why lasers were involved in a large number of experiments. The present chapter will be dedicated to the questions of employment of laser annealing with due consideration of the new data left outside reference [1] describing the major advantages of laser annealing of ion implanted semiconductor layers and discussing the results of the first attempts at employment of the method.

Sec. 8.1. Major Factors Affecting Implanted Layers During Laser Annealing

Now, consider a temperature rise caused by the adsorption of the radiation flux whose density is insufficient for melting and evaporation of the matter. For the time of a nanosecond or millisecond pulse, the electrons and phonons present in the heated layer have a great number of collisions, the fact that enables one to believe that the local equilibrium exists throughout the pulse time. This makes it possible to use the concept of temperature and ordinary equations for thermal fluxes (the assumption that may be incorrect in the case of a picosecond pulse) [2].

The losses of heat in the heated near-the-surface layer are caused by the removal of heat inside the substrate, by reradiation and convection (unless the sample is in vacuum). It is believed that in most instances the energy losses occurring at the surface due to reradiation and convection are small. Even at high temperatures, thermal radiation from the surface of a solid substrate does not exceed 10^3 W/cm^2, while the densities of the laser radiation flux amount to 10^5-10^8 W/cm^2. The only exception are long pulses of radiation focused into a small-diameter spot. In this case, heat is transferred to a surface area much in excess of the spot diameter and the total radiant energy may prove to be comparable to the absorbed one. First of all, we shall be interested in the heating of the wafers irradiated uniformly over the entire surface with a powerful laser pulse. The problem, in this case, becomes one-dimensional, and the thermal flux equation assumes the form

$$d^2T/dz^2 - (1/\varkappa)\, dT/\partial t = -A\,(z,\ t)/k, \tag{8.1}$$

where T is the temperature; z is the depth; t is the time; $\varkappa$ is the coefficient of thermal diffusivity; k is the coefficient of thermal conductivity; A is the amount of heat released in unit volume per unit time depending on the coordinates and time. As a first approximation, the quantity A is related to power W incident on the wafer by the relation

$$A = (1 - R)\, W\,(t)\, \alpha \exp(\alpha z), \tag{8.2}$$

where R is the reflectivity and α, the absorptivity.

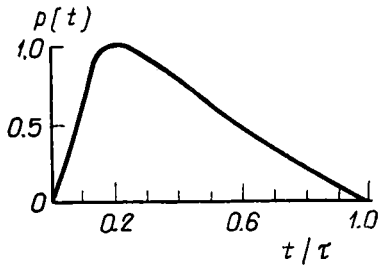

Fig. 8.1. Generalized form of laser pulse [2].

For rough estimates of the temperature at the depth z, the form of the laser pulse in time may be assumed to be rectangular. Then for a large absorptivity ($\alpha = 10^5$-10^6 cm^{-1}) the following relations are true

$$T(z, t) = [2W(1 - R)/k]\,(\varkappa t)^{1/2} i\,\mathrm{erfc}\,[z/2(\varkappa t)^{1/2}];$$
$$T(0, t) = [2W(1 - R)/k]\cdot(\varkappa t/\pi)^{1/2} \qquad (8.3)$$

(i erfc is the integral of the conjugate error function).

The actual form of the laser pulse is significantly different from the rectangular one. With many types of laser, the pulse normalized to unity in the maximum, has about the same form if the latter is regarded as a function of time referred to the pulse duration. This holds true both for millisecond and nanosecond pulses (Fig. 8.1). With due account taken of the real form of the pulse, the time dependence of temperature may be represented as a generalized curve good for any material. Such curves for heating with unfocused beams of millisecond and nanosecond lasers are shown in the monograph by Ready [2]. The basic quantitative characteristics of laser pulse action are given in Table 8.1. In calculating the values of parameters

Table 8.1

Tentative parameters specific to major pulsed annealing techniques (for Si) [51]

Parameter	White light	Ruby laser, $\lambda = 0.69\,\mu$m		Neodimium laser, $\lambda = 1.06\,\mu$m	
Pulse time τ, s	10^{-2}	10^{-3}	10^{-8}	10^{-3}	10^{-8}
Power W, W/cm^2	$5\cdot10^4$	$2\cdot10^5$	$5\cdot10^7$	$3\cdot10^5$	$5\cdot10^7$
Energy E, J/cm^2	500	200	0.5	300	0.5
Absorption depth, μm	0.2-2	3	3	30-100*	0.5**
Heating depth, μm	100	50	1	50*	0.7**
Ionization rate, pair/cm^3·s	10^{27}	10^{28}	$2\cdot10^{30}$	10^{28}**	$2\cdot10^{30}$
Ionization density, pair/atom	5	20	0.1	20*	0.1
Temperature gradient, deg/s	$2\cdot10^4$	$5\cdot10^4$	2.10^6	$5\cdot10^4$*	$3\cdot10^6$
Cooling rate, deg/s	$5\cdot10^4$	$2\cdot10^5$	$5\cdot10^5$	$2\cdot10^5$*	10^9

* Ion irradiation dose is less than amorphization dose.
** Irradiation absorption effect shows in amorphous region only.

such as the absorption depth, ionization rate, neodimium-glass laser radiation absorptivity of undamaged silicon was considered to be equal to 15-20 cm^{-1}. For silicon amorphized by ion bombardment, this factor rises to $(4\text{-}6)\cdot 10^3$ cm^{-1} [3, 26].

Ionization caused by pulsed laser irradiation was investigated by the authors of [4] through [8]. It was found that in silicon acted upon by a Q-switched laser having a maximum power of 10 MW, an increment in the concentration of free carriers amounted to about 10^{20} cm^{-3} at an excitation intensity of $9\cdot 10^{25}$ quant/$cm^2\cdot s$ [4]. This brought about an increase in the absorptivity of IR radiation at $\lambda = 1.66$ μm up to 10^3 cm^{-1}. The thickness of the absorbing layer was considered to be equal to 6 μm in accordance with the depth of penetration of a ruby laser light into silicon. In gallium arsenide, light is only absorbed in a layer 0.1 μm thick, thereby obviating the necessity to allow for the diffusion length of non-equilibrium carriers, which itself depends on the ionization level.

The estimates derived from experimental study of photoconductivity have shown that with an excitation intensity of about 10^{26} quant/$/cm^2\cdot s$, the concentration of free carriers approaches $7\cdot 10^{19}$ cm^{-3}. A rise in the reflectivity observed in gallium arsenide at intensities above $2\cdot 10^{25}$ quant/$cm^2\cdot s$ and not observed at the same intensities in silicon should not be attributed to an increase in the concentration of non-equilibrium carriers but to the onset of fusion of the near-the-surface layers [4]. In germanium, at irradiation intensities below the onset of the surface fusion an excess concentration of carriers amounts to $4\cdot 10^{18}$ cm^{-3} [5]. Using the I and II harmonics of a neodimium laser radiation spectrum, one can vary the depth of non-equilibrium carrier generation in silicon. According to reference [6], the first harmonic pulse ($\lambda = 1.06$ μm) with an intensity of 10^{23} quant/$cm^2\cdot s$ is capable of exciting about $2\cdot 10^{17}$ cm^{-3} carrier pairs, while the II harmonic pulse ($\lambda = 0.53$ μm) of the same intensity does $5\cdot 10^{18}$ cm^{-3} carrier pairs. When light is absorbed near the surface, a major role in non-equilibrium carrier recombination is played by surface states [7]. In a volume with high excitation levels, the zone-zone auger-recombinations dominate [8].

Strong ionization changes the charge states of the implanted impurity and radiation-induced defects and therefore affects the processes involved in implanted layer annealing. The theoretical aspects of the influence of ionization on the behaviour of impurities and defects were studied by many authors (see, for example, [9] through [13]). Experimental evidence for such influence may be found in a number of papers [14-17]. It should be, however, stressed that so far there is no quantitative theory allowing prediction of the course of this or other reaction in a semiconductor crystalline lattice.

Shock waves occur in the substrate due to abrupt thermal expansion of the near-the-surface layer under the influence of a laser pulse or

recoil effect resulting from scattering of the particles evaporating from the surface [18]. As the pulse power in laser annealing is insufficient to cause intensive evaporation of the material, the last-mentioned situation may be omitted from our discussion. A shock wave due to thermal expansion may arise when the energy supply time is short as compared to the shock wave propagation time [18].

It should be also noted that laser annealing of amorphized layers is affected by the release of the crystallization heat. For instance, in germanium, this heat amounts to 2.75 ± 0.20 kcal/g·atom [19]. For a crystallizing layer 10^{-5} cm thick, the amount of released heat reaches $0.84 \cdot 10^{-2}$ J/cm^2, making up 10% of energy produced by a Q-switched laser. According to [20], the crystallization of silicon layers amorphized by ion bombardment takes the time commensurable with the duration of the annealing pulse ($2 \cdot 10^{-8}$ s). After this, the electrophysical characteristics of the doped region become the same as those of thermally annealed samples. Hence, the power released during the crystallization also constitutes 10% of the laser annealing power.

Table 8.2

Comparative data on measurement of conductivity in ion implanted layers of Si, Ge and GaAs after laser (σ_l) and thermal (σ_{th}) treatments [24]

Sample. No.	Material	ρ, ohm-cm	Bombardment parameters			Laser irradiation parameters			Thermal annealing parameters		$\sigma_l \cdot 10^3$	$\sigma_{th} \cdot 10^3$	σ_l/σ_{th}
			ion species	E, keV	$\Phi \cdot 10^{-16}$, cm^{-2}	λ, μm	W·10^{-7}, W·cm^{-2}	$\tau \cdot 10^9$, s	T, °C	t, min	ohm^{-1}		
1	*p*-Si	7.5	P^+	210	0.06	1.06	2.5	15	800	30	20	11	1.82
2	*p*-Si	7.5	P^+	120	0.06	1.06	2.5	15	800	30	19.3	9.2	2.1
3	*p*-Si	7.5	Sb^+	120	0.6	0.69	2.5	20	800	30	14.5	6.5	2.23
4	*p*-Si	7.5	Sb^+	100	0.6	1.06	2.5	15	800	30	29	28	1.035
5	*n*-Si	7.5	B^+	30	0.06	0.69	2.5	20	800	30	4.9	3.6	1.36
6	*n*-Si	7.5	B^+	30	0.6	0.69	2.5	20	800	30	78	12	6.5
7	*n*-Si	7.5	B^+	30	6.0	0.69	2.5	20	800	30	81	11.7	6.92
8	*n*-Si	7.5	B^+	30	60	0.69	2.5	20	800	30	70	8	8.75
9	*n*-Si	7.5	B^+	30	0.06	0.69	2.5	20	1000	30	4.9	4.8	1.02
10	*n*-Si	7.5	B^+	30	0.6	0.69	2.5	20	1000	30	78	51	1.53
11	*n*-Si	7.5	B^+	30	6.0	0.69	2.5	20	1000	30	81	75	1.08
12	*n*-Si	7.5	B^+	30	60	0.69	2.5	20	1000	30	70	42.5	1.65
13	*p*-Ge	5.5	P^+	40	6.0	0.69	1.0	20	600	30	33	13.7	2.4
14	*p*-Ge	5.5	Sb^+	40	0.6	1.06	0.5	15	600	30	18	15	1.2
15	*n*-GaAs	10^{16}*	Zn^+	40	1.5	0.69	1.5	20	600	30	15	13	1.15

* Electron concentration, cm^{-3}.

As to the millisecond laser pulses, their energy is practically by four orders of magnitude greater than the value $0.8 \cdot 10^{-2}$ J/cm^2. One can estimate power from the released crystallization heat by using the following data. An amorphous silicon layer crystallizes epitaxially in a solid phase with an activation energy of 2.3 eV (see Ch. 7), and the maximum growth rate in the solid phase (i.e., at 1400 °C) is $2 \cdot 10^{-1}$ cm/s. Hence the crystallization time of silicon layer 10^{-5} cm thick is $0.5 \cdot 10^{-4}$ s. This means that the power generated by releasing the crystallization heat amounts to 160 W/cm^2, while the laser radiation power is 10^4 to 10^5 W/cm^2 (see Table 8.2).

Sec. 8.2. Laser Annealing of Implanted Silicon Layers

Experiments on laser annealing of implanted layers were run using both nanosecond and millisecond pulses [3], [20] through [30]. Now, consider the results obtained for the two ranges of irradiation pulse duration.

The authors of [21] performed laser annealing of implanted silicon layers with the use of material КДБ-10 doped with 30 keV P ions to a dose of $3 \cdot 10^{15}$ cm^{-2} at the target temperature of 20 °C. Pulsed laser radiation was effected at room temperature with the aid of a ruby laser Q-switched to a single pulse mode of operation. The pulse energy was 0.1-0.2 J, the duration $3 \cdot 10^{-8}$ s. A lens was used to defocus the light beam so that the entire surface of the sample would be illuminated. The diameter of the light spot on the sample plane was 10-15 mm.

It was found that one laser pulse was sufficient for annealing out the defects in implanted layers and for obtaining a high concentration of free carriers (up to $1.5 \cdot 10^{20}$ cm^{-3}). Electron diffractometry studies have shown that when subjected to laser pulse action an amorphized layer begins to recrystallize. It is interesting to correlate the data thus obtained with those of the experiments performed by the authors of [20, 23, 24] who annealed boron- and phosphorus-doped samples with the aid of ruby and neodimium glass-doped Q-switched laser pulses. According to [23, 24], the threshold power of annealing effected with a neodimium laser pulse amounts to $2.5 \cdot 10^7$ W/cm^2 when the pulse duration is $15\text{-}20 \cdot 10^{-9}$ s. Considering the lesser values of pulse duration and absorptivity as compared to those used in [21], an agreement of threshold energies in both cases may be thought of as good. The specified mode was optimum for efficient annealing. Unduly large energies resulted in destruction of the samples. The crystallization threshold could be recognized by the disappearance of the EPR signal associated with the amorphous phase. The threshold power of the neodimium laser pulse determined in this manner proved to be equal to $2 \cdot 10^7$ W/cm^2 ($\tau \simeq 15 \cdot 10^{-9}$ s). Simultaneously with the disappearance of the EPR signal associated with the amorphous

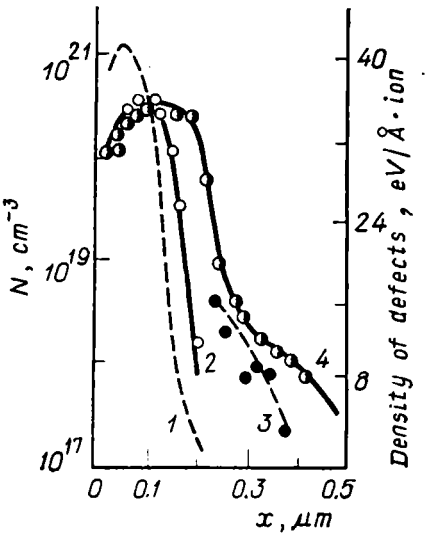

Fig. 8.2. Carrier concentration profiles in silicon bombarded with P ions ($\Phi = 6 \cdot 10^{15}$ cm^{-3}, $E = 100$ keV) [24]. *1*—distribution of radiation defects according to Brice theory [31]; *2*—laser annealing ($\lambda = 1.06$ μm, $\tau = 2 \cdot 10^{-8}$ s, $W = 2.5 \cdot 10^7$ W/cm^2); *3*—"tail" of impurity depth distribution profile in sample 2, revealed by additional thermal annealing ($T = 800$ °C, $t = 30$ min); *4*—thermal annealing ($T = 800$ °C, $t = 30$ min)

phase, a line appeared in the EPR spectrum, indicating the electron conduction in P-doped Si [25].

The comparative data on layer conductivity measurements in ion implanted silicon, germanium and gallium arsenide after thermal and laser annealings are given in Table 8.2 [24]. Before the annealing, the layers had low conductivity typical of strongly disordered semiconductors. Laser irradiation and thermal annealing resulted in inversion and sudden growth in layer conductivity. Comparison of conductivities σ_{laser} and $\sigma_{thermal}$ revealed a better conductivity for the layers subjected to laser beam annealing. This difference was notably less for high temperatures of thermal annealing. It is possible that the maximum semiconductor surface temperature caused by the laser action exceeded that of thermal annealing. This appears to be the reason why σ_{laser} exceeds $\sigma_{thermal}$. The Hall measurements have shown that with laser annealing the relations between the carrier concentration and mobility are similar to those of diffusion doped layers.

In the event of large light absorptivity, the effective thickness of the annealed layer may prove to be smaller than after thermal annealing. This suggests that even at a depth of 0.2-0.3 μm the temperature does not reach 600 °C and, therefore, at a depth of 1 μm the substrate is practically unheated. A similar situation arises when radiation absorptivity of the disordered semiconductor layer is high and that of the monocrystalline layer is low [24]. This holds for Si at $\lambda = 1.06$ μm. After a similar laser annealing of ion implanted silicon layers, the implanted impurity cannot be activated at the "tail" of its depth distribution profile. Additional heating of the sample reveals this impurity (Fig. 8.2).

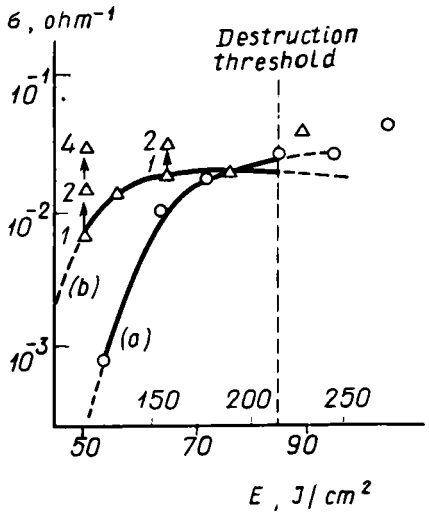

Fig. 8.3. Layer conductivity of P ion implanted silicon (E = 30 keV: Φ = = $6 \cdot 10^{15}$ cm^{-2}) vs laser pulse energy. *a*—$\tau = 10^{-2}$ s; *b*—$\tau = 0.8 \cdot 10^{-3}$ s. The top scale of the abscissa refers to *a*, the lower scale, to *b*. The numerals near the dots of the curve for $\tau = 0.8 \cdot 10^{-3}$ s give the number of irradiations of the sample with the pulses of the specified energy [28]

Measurements of the wavelength dependences of short-circuit currents in photoconverters fabricated with the use of laser annealing indicate that the carrier lifetime in the base does not become degraded [52]. This also points to a low-temperature heating-up of the base under selected treatment conditions.

The action of millisecond pulses was studied by the authors of [27, 28]. In the first place, it was interesting to learn in what way the changes in the electrical characteristics of the ion-implanted layer were related to the energy of the acting laser pulse. Figure 8.3 shows this relationship. It is nonlinear: at first, the layer conductivity grows fast with increase in the pulse energy, then it slows down. High radiation energies resulted in erosion of the sample surface. To prevent the erosion, the authors of [28] decreased the laser pulse energy but increased the number of pulses. With an increased number of pulses, the layer conductivity registered a rise (see Fig. 8.3).

The authors of [27] investigated laser annealing effects on the samples of silicon, type КДБ-10, doped with 80 keV P ions to a dose of 10^{16} cm^{-2}. For the purposes of annealing, use was made of the ГОР-300 ruby laser with pulses 6 ms long. In this case, the threshold energy of annealing was about 25 J/cm^2, which corresponds to an average power of 4 kW/cm^2. The annealing efficiency improved with an increase in the pulse energy. Computer-aided calculations show that maximum temperatures on the laser-irradiated and opposite surfaces differ for millisecond pulses by not more than 20%. This allows correlation of the results of pulsed annealing with the laser action applied to the face (ion-implanted side) and to the backside. In the former case, the implanted layer is subjected to both thermal and powerful light irradiations, while in the latter case, only to thermal irradiation. The time for rise and fall in the temperature was the same in both cases. The experiments were performed on samples

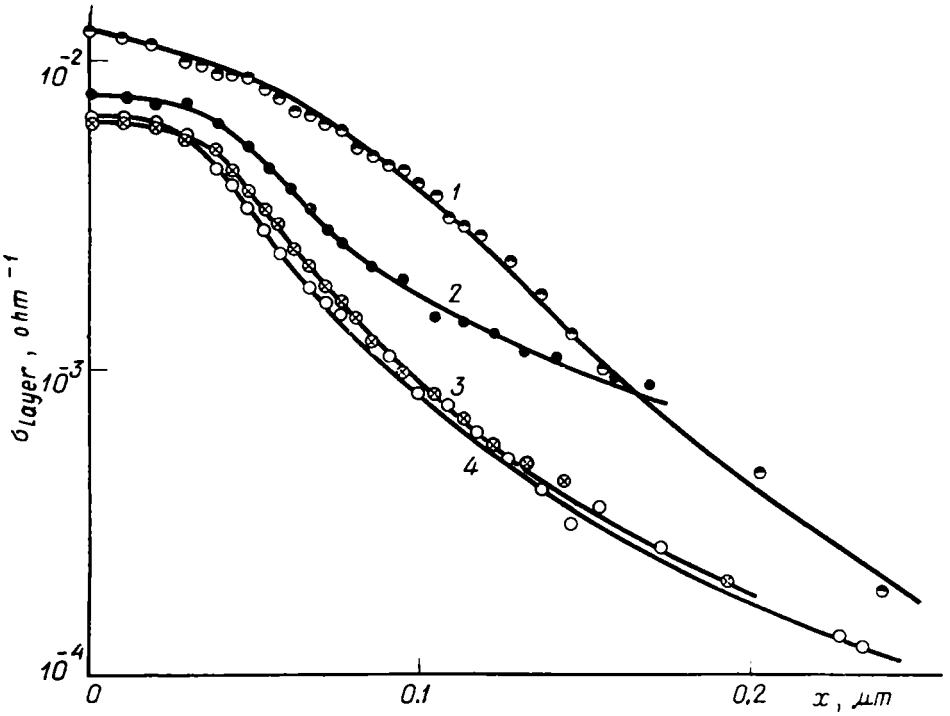

Fig. 8.4. Conductivity distribution profiles in P ion implanted silicon after annealing:
1—irradiation effected by millisecond laser pulse from implanted surface side; *2*—irradiation effected by a pumping flashtube; *3*—irradiation effected by millisecond laser pulse from the side opposite to the implanted surface; *4*—same as in *3* after additional thermal annealing at 200 °C.

270 μm thick, coated with a SiO_2 film from the side to be illuminated by the laser. The purpose of this film was to equalize the reflectivities of the amorphized and crystalline surfaces. A study of the electrophysical characteristics of the annealed layers have shown that with the same heating of the implanted surface the properties of the layers turned out to be about the same in both cases (Fig. 8.4).

The results of the experiments are evidence that heating plays the most important role in annealing of implanted layers with millisecond laser pulses. Although annealing with millisecond laser pulses does not rule out an increase in the substrate temperature, many advantages of the laser annealing method are preserved. These are the possibility of localized heating with the use of the focused beam, short duration (about 10^{-3} s), cleanliness. It should be emphasized that powerful light pulses 10^{-3} s long are produced by flashtubes used for excitation (pumping) of solid-state lasers. This feature makes them attractive for use in pulsed annealing of implanted layers. An experimental verification has shown that annealing with a light pulse derived from a pumping flashtube of type ИПСКХ 240/20 is as effective as that produced by a laser (see Fig. 8.4).

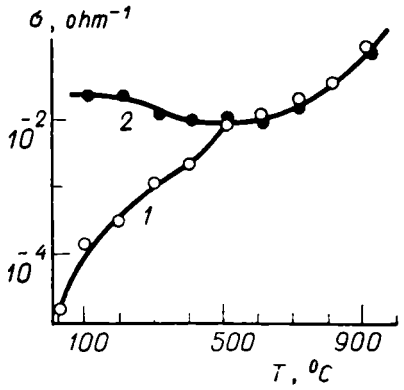

Fig. 8.5. Layer conductivity of silicon bombarded with P ions (E = 40 keV, $\Phi = 3.6 \cdot 10^{16}$ cm^{-2}) vs annealing temperature [28].
1—thermal annealing; *2*—isochronal annealing after neodimium-glass laser pulsed irradiation ($\tau = 0.8 \cdot 10^{-3}$ s; E = 70 J/cm^2)

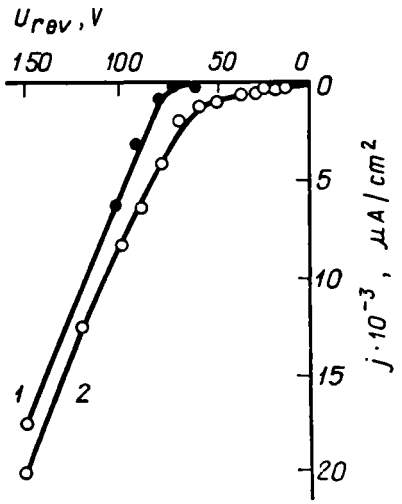

Fig. 8.6. Reverse branches of VAC curve for silicon p-n junctions fabricated by thermal (T = 900 °C, t = = 20 min) and laser annealing (neodimium-glass laser).
1—thermal annealing; *2*—laser annealing. n-Type silicon, $\rho \simeq 4.5$ ohm·cm, bombarded with B+ ions, E = 100 keV, $\Phi = 3.75 \cdot 10^{15}$ cm^{-2}

The effect of pulsed laser radiation on semiconductors is characterized by high rates of heating up and cooling, high energy released within a short time in a small volume (see Table 8.1). Under such conditions, the impurity-semiconductors system must be in a non-equilibrium state after cooling. This fact is supported by the results of thermal annealing of silicon layers, effected after the layers have been subjected to pulsed laser irradiation. In thermal annealing of such layers the conductivity decreases with temperature rise (Fig. 8.5), which appears to be associated with transfer of the system into the equilibrium state [28].

A study was made of the volt-ampere characteristics of p-n junctions fabricated by implantation of B^+ ions (E = 100 keV, Φ = 600 to 1200 μC/cm^2) into silicon (n-type, $\rho \simeq 4.5$ ohm·cm) with subsequent laser annealing. The results were compared with similar characteristics obtained for thermally annealed structures (T = 900 °C, t = 20 min). It turned out that the forward branches for thermal and laser annealing of implanted layers coincide. The value of breakdown voltage for laser-formed diodes was by 10-15 V less, i.e., from

50 to 60 V (Fig. 8.6). No marked changes were registered for the shape of the reverse VAC branch when neodimium and ruby lasers both Q-switched and free running were used. The smaller value of the breakdown voltage and greater reverse current in laser-annealed structures indicated a likely presence of unannealed defects in the vicinity of the *p-n* junction.

Sec. 8.3. Laser Annealing of Implanted Layers in Gallium Arsenide

Experiments on laser annealing of gallium arsenide were conducted with the use of a Q-switched ruby laser [21]. The pulse energy was 0.1-0.2 J and its duration $3 \cdot 10^{-8}$ s. Samples of semi-insulating gallium arsenide doped with 35 keV tellurium ions to a dose of 10^{15} cm^{-2} were subjected to annealing. To preclude possible evaporation of arsenic, the samples were coated with a transparent protective film 0.1 μm thick, produced by reactive cathodic sputtering of silicon.

It was found that a single laser pulse was sufficient to anneal out the compensating defects in the implanted layers to obtain a high concentration of free carriers. Measurements of electric conductance and Hall effect combined with precision etching-away of layers have disclosed that the volume concentration of electrons in a layer is 10^{18} cm^{-3} with a mobility of 1000 cm^2/V·s. Whenever the bombardment resulted in amorphization of the surface (low-temperature implantation), single laser pulse irradiation helped restore the crystalline structure. Increasing the number of pulses to ten did not result in marked changes in the electrical behaviour of the samples.

The depth distribution of a free carrier concentration after laser annealing is shown in Fig. 8.7. The threshold power of implanted layer annealing in gallium arsenide is lower than in silicon and amounts to about $3 \cdot 10^6$ W/cm^2 for nanosecond pulses of a ruby laser. This fact is partly explained by a greater absorptivity of GaAs. Localized annealing of amorphized GaAs with nanosecond pulses may be used for optical recording of information, as in its infrared region the amorphous layer has the absorptivity of $5 \cdot 10^3$ cm^{-1}, while the recrystallized one, 0.3-0.5 cm^{-1} [32].

Let us consider the millisecond pulse annealing results with reference to gallium arsenide implanted with zinc ions. *n*-Type GaAs samples with electron concentrations of $2 \cdot 10^{17}$ and $6 \cdot 10^{16}$ cm^{-3} were used as a starting material. The irradiation was effected with 35 keV Zn^+ ions. The irradiation temperature was 200 °C, implantation dose, 10^{16} cm^{-2}. The implanted layers were coated with a protective film produced by cathodic sputtering of silicon in residual gas atmosphere and were subjected to laser annealing using pulses 5 μs long ($\lambda =$ $= 0.694$ μm, $W = 10^4$ W/cm^2). During the annealing, the samples were kept at room temperature. The VAC and *CV*-characteristics of

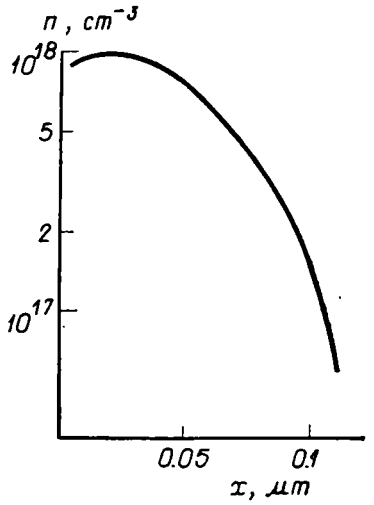

Fig. 8.7. Distribution profile of free electrons in tellurium ion implanted gallium arsenide after laser annealing.

the p-n junctions were measured on mesa-structures $5 \cdot 10^{-3}$ cm^{-2} in area. To study the hole distribution and mobility in the ion implanted layer, layers were etched away from the irradiated and annealed samples and simultaneous measurements of the Hall effect and conductivity were taken.

Ion implantation with subsequent laser annealing provides for obtaining on n-GaAs samples of a p^+-layer with a hole concentration $p = 10^{20}$ cm^{-3} (Fig. 8.8). The thickness of the ion implanted layer turns out to be somewhat greater than expected (according to the LSS theory, the mean projected path for 35 keV Zn^+ ions in GaAs is $\simeq$ $\simeq$ 0.01 μm), which may be due to the occurrence of a channelled "tail" right in the course of the bombardment [33].

Figure 8.9 shows the VACs of the structures obtained for the base material. It is evident that the series resistance in the mesa-structures fabricated with the aid of laser annealing is slightly greater than that of the structures prepared by thermal annealing. In all other respects, the forward branches of the VAC presented to a given scale do not have much of a difference.

A rigorous analysis of the forward VAC branches over a wide current variation interval has revealed that the properties of thermally annealed p-n junctions are similar to those of the diffused junctions described in reference [34]. Specifically, over the range of forward voltages from 0.3 to 0.9 V, the forward current density may be given by

$$j = j_0 \exp(eU/kT\beta), \qquad (8.4)$$

where $j_0 = (1 - 10) \cdot 10^{-10}$ A/cm^2 and $\beta = 2$ at room temperature. Approximation of the forward VAC branches of p-n junctions fabricated using laser annealing results in increased values of j_0 and β. The value of current with small reverse biases applied to these structures was higher (at $U = -1$ V, $j_{rev} = 10^{-6}$ A/cm^{-2}) than for

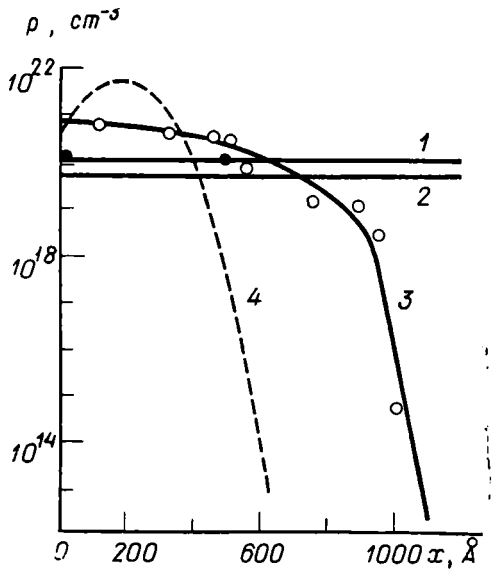

Fig. 8.8. Distribution profile of electrically active zinc in gallium arsenide. *1*—ion implantation with subsequent thermal annealing (750 °C, 20 min; depth of *p-n* junction, l = 0.7 μm); *2*—theoretical curve calculated for zinc diffusion in GaAs from an infinitely thin layer (T_{anneal} = 750 °C, t_{anneal} = 20 min, l = 4.5 μm); *3*—ion implantation with subsequent laser annealing; *4*—zinc distribution profile in GaAs according to LSS theory [50]

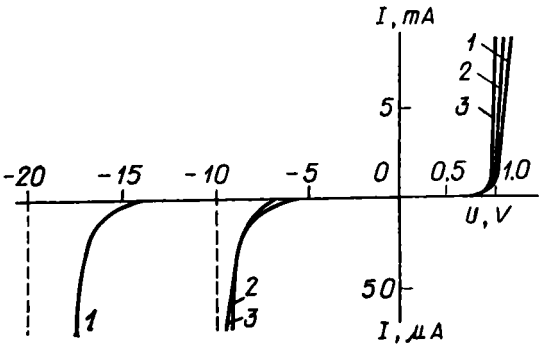

Fig. 8.9. VAC curves of mesa-diodes fabricated by implantation of zinc ions in GaAs with electron concentrations $n = 6 \cdot 10^{16}$ cm^{-3} (*1*) and $n = 2 \cdot 10^{17}$ cm^{-3} (*2*): subsequent laser annealing, $n = 2 \cdot 10^{17}$ cm^{-3} (*3*); subsequent thermal annealing.

thermally annealed *p-n* junctions. The breakdown voltage for implanted *p-n* junctions both after thermal and laser annealing approaches the calculated values of U_{fwd} for abrupt *p-n* junctions [35].

Measurements of *CV*-characteristics taken at a frequency of 1 MHz have shown that after laser annealing the *p-n* junctions, if not externally biased, have a space charge width $l \geqslant 0.6$ μm. With due account taken of large values of the hole concentration and of the gradient in the implanted layer, one can use the measurement data for calculation of the distribution profile of the electrically active donor impurity in the base. It is obvious from Fig. 8.10, that the laser-formed diodes are characterized by a partial compensation behind the p^+-layer. The structures fabricated by ion implantation with subsequent thermal annealing are close, by the character of variation of their volt-farad characteristics, to abrupt *p-n* junctions when the value of l is equal or close to 0.1 μm.

The occurrence of a compensating interlayer between the *p*- and *n*-regions was earlier observed in *p-n* junctions fabricated by implan-

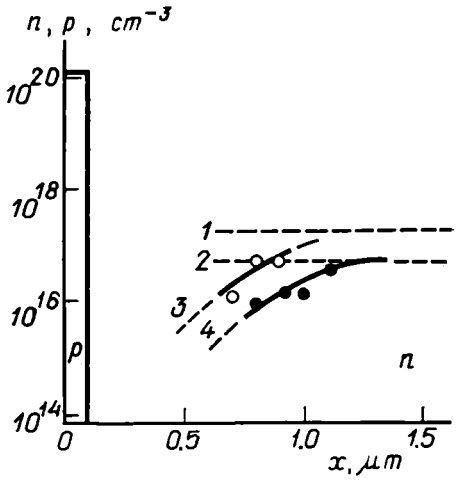

Fig. 8.10. Free carrier distribution profiles in GaAs *p-n* junctions fabricated by ion implantation with subsequent laser annealing.
1, 2—original concentrations in *n*-region; *3, 4*—concentrations calculated from *CV* measurements

tation of Zn^+ ions into GaAs followed by a low-temperature thermal annealing [36]. This result is explained by diffusion inside the crystal of the defects formed in the course of heavy damage annealing. It appears that a similar picture is observed during laser annealing. High as the temperature could be at the surface of the sample, the heating turned out to be insufficient for annealing out of compensating centers in the layers lying deeper. The annealing of deep-lying defects can be achieved, as it seems, by slightly increasing the power of the laser beam or by using a radiation with a greater penetrating power (for $\lambda = 0.7$ μm, the absorptivity is $3 \cdot 10^4$ cm^{-1}).

On the whole, the rectifying properties of *p-n* junctions fabricated with the use of laser annealing are equally sufficient for this material as well. At a voltage of 1 V, the rectification factor amounts to 10^5-10^6. This means that the method of laser annealing of implanted layers can be successfully employed for fabrication of *p-n* junctions without a prolonged heating of the base material.

Sec. 8.4. Redistribution of Impurity by Laser Annealing

Of particular interest is a problem of diffusion of impurity during laser annealing of implanted layers. Estimates show that for typical laser pulse lengths of 10^{-3} s (free running) and 10^{-8} s (Q-switched mode), the diffusive displacement, $(D\tau)^{1/2}$, of the main impurities in silicon does not exceed 10^{-7} and 10^{-9} cm, respectively, even when the layer temperature exceeds 1000 °C. Indeed, some experimenters did not find, after laser annealing, any expansion of the impurity distribution profile, that could be attributed to the specifics of laser action [23, 26, 37]. At the same time, there are reports on a quite pronounced displacement of impurity under the action of not only millisecond but nanosecond laser pulses [25, 38, 39]. Since it is impossible to account for the results obtained by ordinary diffusion, various mech-

anisms were suggested that would promote the migration of the impurity atoms. Particularly, there were reports on displacement of impurity during crystallization of the melted near-the-surface layer, enhancement of the diffusion due to the presence of an excess concentration of defects and the influence of the strongly excited electron gas.

To elucidate the mechanism of the diffusion, experiments were carried out on laser annealing of As^+, B^+ and P^+ ion irradiated Si in two modes, namely, those of "low" and "high" power ones [40]. These modes were established on the following basis.

The threshold power of implanted layer annealing is slightly different from the power causing visible surface damage. In addition, the threshold power depends on the duration, form and structure of the laser pulse as well as on the implantation parameters. All these factors complicate the work near the annealing threshold. To overcome the above difficulties, the investigations of impurity diffusion under the action of laser pulses with power close to the threshold one have been conducted as follows.

Implanted silicon samples were placed inside a block of aluminium and then irradiated with laser pulses having a fixed energy ($E = 90 \pm 10$ J/cm^2, $\lambda = 0.69$ μm, $\tau = 6 \cdot 10^{-3}$ s) insufficient for effective annealing of the ion implanted silicon layers under study. The degree of annealing could be adjusted by additionally heating the block containing the sample from 20 to 400 °C. This was the "low" power mode. In the "high" power mode, laser annealing was effected with powers in excess of the threshold one but lower than those causing surface damage (erosion). After the laser treatment, depth distribution of electrically active centers and impurity atoms was investigated.

The distribution of carriers was checked by Hall measurements and the impurity profile was taken by the methods of mass-spectrometry of secondary ions and by neutron-activation analysis. Layers were etched away by anode oxidation.

Upon irradiation of Si implanted with As^+ ions ($E = 100$ keV, $\Phi = 5 \cdot 10^{15}$ cm^{-2}) with "low" power laser pulses, diffuseness (spread) of the profiles in both directions from the maximum concentration of implanted ions was observed. An increase in the half-width of the profiles was noted caused by both a change in the distribution of the electrically active centers (Fig. 8.11) and a change in the As concentration measured by the neutron-activation analysis (Fig. 8.12). We know that the coefficient of diffusion of arsenic in silicon at 1400 °C is equal to 10^{-11} cm^2/s. Hence, we cannot explain the results obtained by ordinary diffusion. It is also a common knowledge that the expansion of the profiles cannot be ascribed to laser action (ionization, shock wave, etc.), as the effect is also observed after ordinary heating at 800 °C. Nor can we attribute the occurrence of

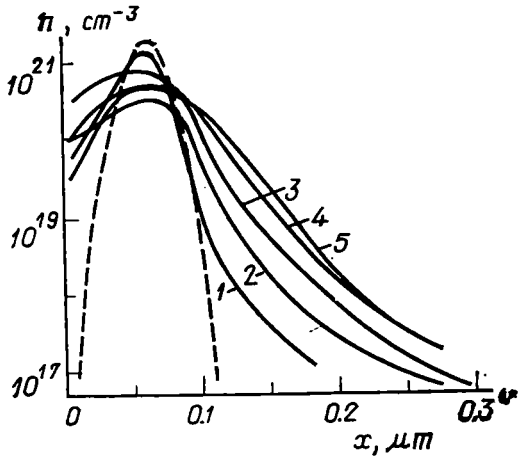

Fig. 8.11. Profiles of volume concentration of electrons in annealed layers [40].

Sample temperature prior to application of laser pulse, °C: *1*—20; *2*—200; *3*—350; *4*—400; *5*—thermal annealing at 800 °C for one hour. Dashed line shows calculated distribution of As ion paths

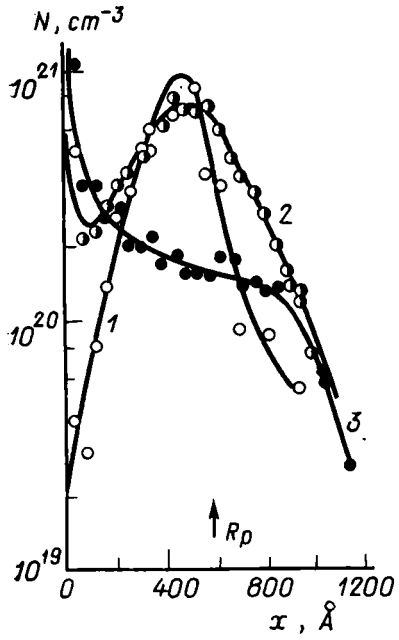

Fig. 8.12. Profiles of As implanted into Si (E = 100 keV; $\Phi = 5 \cdot 10^{15}$ cm^{-2}) after laser annealing with pulses of varying energy (laser ГОС-1001, λ = = 1.06 μm, τ = 1 ms) [40].

1—E = 0; *2*—$E = 0.8E_m$; *3*—$E = E_m$ = = 45 J/cm²

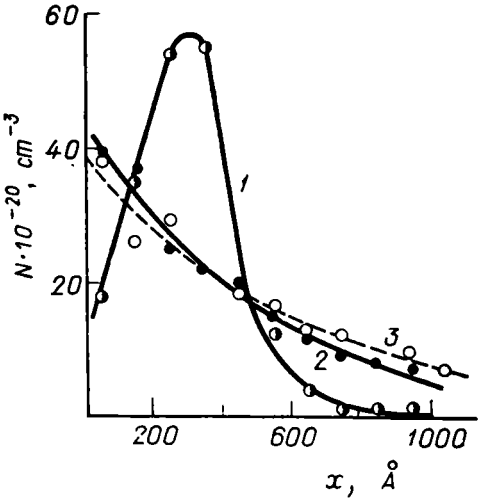

Fig. 8.13. Profiles of P atoms in Si bombarded by P ions (E = 30 keV, $\Phi = 1.6 \cdot 10^{16}$ cm^{-2}(before (*1*) and after application of neodimium (*2*) and ruby (*3*) lasers [25].

Neodimium laser: λ = 1.06 μm, τ = (15–20) 10^{-9} s, E = 0.4 J/cm²; ruby laser: λ = 0.69 μm, $\tau = 6 \cdot 10^{-3}$ s, E = 110 J/cm²

"tails" to the channelling effect. In the first place, the profiles spread at both sides. Secondly, when implanted into a cold target, a large portion of ions are capable of channelling to a dose of 10^{13} cm^{-2} only, whereas in our experiments the total concentration of donors at a depth of $\simeq$0.1 μm was in excess of 10^{14} cm^{-2}, and the observed ex-

pansion of the profiles reached the very top, the fact not appropriate to channelling.

The most probable cause of impurity migration is likely to be an enhancement of diffusion, that can be associated either with an excess concentration of vacancies or with interstitial displacement of the impurity. The vacancy mechanism of diffusion enhancement is characterized by concave diffusion profiles with an abrupt fall, since with an increase in the distance from the disordered layer the concentration of vacancies suddenly reduces and the effective rate of diffusion rapidly diminishes. In the event of interstitial diffusion, the profiles are extended, as the vacancies serve as traps for the impurity atoms and the effective rate of diffusion of the latter grows with an increase in the distance from the region filled with excess vacancies. An important role of interstitial diffusion in annealing of implanted layers was noted in reference [41]. Most likely that near the damage maximum the diffusion enhancement is associated with an excess concentration of vacancies, while the "tails" are caused by the interstitial migration of the impurity.

With ion implanted layers irradiated with "high" power laser pulses, the impurity profile registers a still greater change as compared with the initial distribution profile. In this case, the profile maximum occurred at the surface of the monocrystal, while the concentration at the "tail" of the distribution profile increased. Such a redistribution of impurity was observed in silicon layers irradiated with P^+, As^+, B^+ ions (see Figs. 8.12-8.14). The data on the depth distribution of concentrations of P and As were obtained by the method of neutron-activation analysis, while those on the B concentration, by means of an ion-beam microanalyzer. The amount of impurity that remained in Si after laser annealing differed from the original value by not more than 15-20%.

With usual thermal annealing, the impurity profile diffused without changing the position of the maximum (Fig. 8.15). A significant change in the impurity profile after laser annealing as compared to the original one was also observed in Si irradiated with Ga^+, In^+ and As^+ ions [42].

When analyzing the data obtained one whould take into account the following important condition: in all experiments described, laser annealing was effected on silicon samples which after annealing had a post-implantation near-the-surface layer comparable in thickness to the ion path. In experimental studies of the As profile, described in references [39] and [43], no amorphous layer was observed, which is likely to be associated with an increased temperature of the sample, caused by a high current density of the ion implantation process (about 40 $\mu A/cm^2$). The laser annealing results obtained by the authors of [39, 43] are different from those described above: the impurity distribution maximum shifts inside the sample with growth

Fig. 8.14. Impurity distribution profile obtained with ion-beam microanalyzer in boron implanted silicon samples ($E = 10$ keV, $\Phi = 6 \cdot 10^{14}$ cm^{-2}) [40].
1—original profile; *2*—profile after annealing with ГОР-300 laser ($\tau = 6 \cdot 10^{-3}$ s, $E = 110$ J/cm^2)

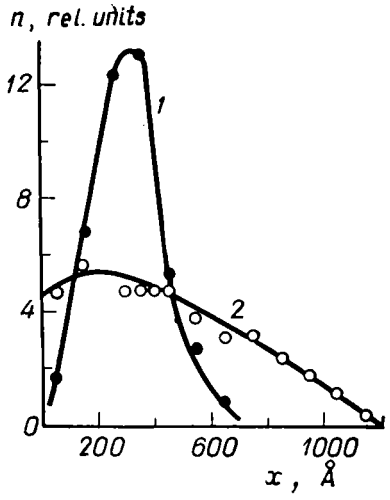

Fig. 8.15. Impurity distribution profile in arsenic implanted silicon samples ($E = 75$ keV, $\Phi = 6 \cdot 10^{15}$ cm^{-2}).
1—original profile; *2*—profile after thermal annealing (1000 °C, $t = 20$ min)

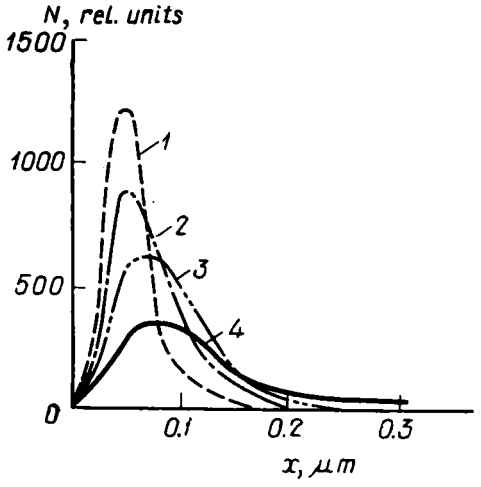

Fig. 8.16. Profile of arsenic in silicon irradiated with ruby laser pulses ($\tau = 2 \cdot 10^{-8}$ s) of varying power W [43].
1—original profile; W, W·cm^2; *2*—$2.3 \cdot 10^7$; *3*—$4.4 \cdot 10^7$; *4*—$7 \cdot 10^7$

in power of laser radiation (a ruby laser, $\tau = 20$ ns, $W = (2.3\text{-}7.0) \times \times 10^7$ W/cm^2) (Fig. 8.16). Backscattering of He atoms was used as the investigation method.

Thus, the comparison of the data on the profiles of implanted As in laser-annealed layers amorphized but retaining their monocrystalline structure in the process of ion implantation allows one to

assume that the presence of an amorphous layer during annealing is likely to promote redistribution of the impurity with shifting the profile maximum towards the surface. It is conceivable that the heating of an amorphous layer by pulsed radiation results in the occurrence of powerful streams of vacancies with the distribution maximum located near the surface. In this situation, an induced displacement of the impurity to the surface may be largely determined by the diffusion coefficient varying with depth [44] and increasing with the growth in the concentration of vacancies. The diffusion of As near the "tail" of the implanted impurity distribution profile may be attributed to the action of the interstitial mechanism [40, 45].

At present, there is an evidence, however, that does not altogether exclude the possibility of displacement of the impurity distribution profile maximum towards the surface due to the fact that the impurity is forced out of its position by the effect resulting from crystallization of the melted semiconductor layer, provided the energy of laser irradiation was sufficient for melting the material in the region next to the surface. This mechanism appears to be the most plausible when nanosecond pulses are used, since the volume of the sample in this case cannot heat up to high temperatures for the time of the pulse and the entire energy is spent to heat the region that absorbs the radiation. For the millisecond pulse range, the temperatures of the laser-illuminated and backside surfaces differ by not more than 20% [27], that is, the entire bulk of the sample is heated up to a high temperature.

From the aforesaid it follows that the problem of unambiguously determining the mechanism of impurity redistribution under various conditions of laser action still requires experimental investigations.

Sec. 8.5. Special Cases of Laser Treatment

It has been demonstrated by the experiments on laser annealing of implanted layers that recrystallization and electrical activation of implanted impurity last for a split microsecond. This suggests that scanning laser beams can be used to anneal out defects in implanted layers. The advantages of such annealing are obvious: a possibility of uniform or programmed annealing of large areas, high efficiency and employment of the zone recrystallization effect.

The authors of [46] investigated the electrophysical characteristics of implanted layers of silicon and gallium arsenide samples after these have been annealed with a scanning beam of an argon laser. Silicon КДБ-10 and semi-insulating *n*-type gallium arsenide (АГП) were used as the starting (source) materials. Silicon was implanted with arsenic ions (energy, 100 keV; dose, $5 \cdot 10^{15}$ cm^{-2}) at room temperature. Gallium arsenide (АГП) was implanted with 40 keV zinc

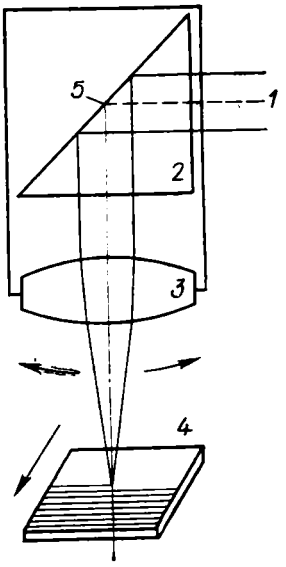

Fig. 8.17. Schematic representation of a laser beam scanner [46].
1—laser beam; *2*—prism; *3*—lens; *4*—sample; *5*—prism-lens system oscillation axis

ions to a dose of $5 \cdot 10^{14}$ cm^{-2}. Prior to annealing, all samples of gallium arsenide were coated with a protective film of SiO_2 1000 Å thick. The silicon samples were annealed both with and without the film. The annealing was effected at room temperature. The beam scanner principle is shown in Fig. 8.17. The beam *1* of a powerful CW (continuous wave) argon laser was passed through a system of rigidly interconnected prism *2* and lens *3*. The lens with a focal length of 40 mm allowed condensing the light beam to a diameter of 30 μm. An electric motor was used to swing the prism-lens system with respect to the oscillation axis with a period of oscillation of 3.6 s. The velocity of the light spot displacement was about 0.4 cm/s. Another electric motor shifted, through a helical gear, the sample in the direction normal to the scanning plane at a velocity of 10^{-3} cm/s. With such velocities of the beam spot travel, the average distance between two adjacent lines amounts to 20 μm, therefore, for reliable overlapping the minimum diameter of the light spot was confined to 100 μm. After the annealing, the samples were subjected to the Hall effect and conductivity measurements in combination with in-depth etching. Similar measurements were also taken on test samples which were annealed thermally.

An arsenic implanted silicon sample was annealed with a laser beam having a power of 3 to 15 W, focused into a spot 100 to 200 μm in diameter. By this means, the power density was varied from 10^4 to $2 \cdot 10^5$ W/cm^2, and the maximum exposure time, determined as the ratio of the maximum spot diameter to its velocity, was 50 μs. Although the power density shows a square-law dependence on the spot diameter, the general effect derived from a sharper focusing of the beam turns out to be not so significant due to a decrease in the laser action time.

The best annealing results have been achieved with a power density of about 10^5 W/cm^2. The annealed layers and resistance $\rho_{layer} =$ = 200-300 ohms, a concentration of free electrons, $6 \cdot 10^{14}$ cm^{-2}, and mobility about 50 cm^2/V·s. For the sake of comparison, let us recall that] conventional thermal annealing of similar samples at

600 °C for one hour gives $n_{layer} = 9 \cdot 10^{14}$ cm^{-2} and $\mu_{layer} = 100$ cm^2/V·s, and after a half-an-hour annealing at 900 °C and $t_{anneal} = 0.5$ h, $n_{layer} = 2 \cdot 10^{15}$ cm^{-2} and $\mu_{layer} = 45$ cm^2/V·s. A laser annealing with a pow r density of 10^4-$5 \cdot 10^4$ W/cm^2 did not result in recrystallization of amorphous silicon, while an increase in the power density above $1.5 \cdot 10^5$ W/cm^2 produced cracking and partial fusion of the surface. A sample of *n*-type gallium arsenide was annealed with powers of 2 to 8 W, the diameter of the light spot being 150-250 μm. The formation of *p*-layers was observed after annealing within a power range of 3 to 5 W (10^4-$2 \cdot 10^4$ W/cm^2). The concentration of free holes in the layer was 10^{13} cm^{-2}. The thickness of the annealed layer in gallium arsenide turned out to be less than in silicon, the fact explained by the difference in the mean free paths of doping ions and, to some degree, by a greater light absorptivity in GaAs ($9.5 \cdot 10^4$ cm^{-1} as compared to $1.1 \cdot 10^4$ cm^{-1} for silicon).

The results obtained have demonstrated that annealing of implanted layers can be successfully performed with the use of a scanning laser beam of sufficient power. The advantages of this method have been listed at the beginning of the chapter. At the same time, the action of a focused laser beam on a substrate kept at room temperature is accompanied with a thermal shock, which is recognized by cracking of the surface when the beam power slightly exceeds the optimum one. Because of this, it is most advantageous to combine the scanning laser annealing with additional slight heating up of the substrate. On the one hand, such a combination will alleviate the thermal shock, and, on the other hand, it will allow the use of smaller-power lasers and liberalize the requirements on the stability of their work. Also of interest is annealing effected with scanning electron beams, which makes it possible to have independent adjustments of electron energy and depth of penetration.

In some instances, thin layers containing high concentrations of free carriers can be only produced by laser action, i.e., without ion implantation [48, 49]. Particularly, the authors of reference [49] have found that pulsed laser irradiation of InSb results in the occurrence of low-ohmic surface *n*-layers with a volume concentration of electrons of 10^{18} cm^{-3} and the effective mobility in the layer, about $(1\text{-}2) \cdot 10^4$ cm^2/V·s at 77 K. The results of the experiments and causes of the occurrence of *n*-layers have been covered in Ch. 6.

Summarizing, the following conclusions can be drawn. The processes characterizing the annealing out of defects and electrical activity of impurity take a very short time (up to 10^{-8} s) when caused by high-power light pulses. Minimum powers required for annealing of implanted layers depend on the properties of the doped material and amount to 10^3-10^4 W/cm^2 for millisecond laser pulses and to 10^6-10^7 W/cm^2 for a Q-switched laser. Excessive increase in power (2-3 times the optimum one) results in injury to the surface.

The electrophysical parameters of implanted layers after laser annealing agree with those obtained after ordinary thermal annealing. Laser annealing is not accompanied with large diffusive expansion of the doped layer, still an insignificant redistribution of the implanted impurity takes place.

Along with the above-listed advantages, laser annealing has some limitations. Most limitations are not of great importance and stem from the complexity of the apparatus and its inability to meet the specified requirement, namely, to provide a uniform and well controlled irradiation of a relatively large area of a semiconductor wafer. Development of specialized laser equipments will obviate the difficulties caused by non-iniformity of irradiation and pulse-to-pulse variations of energy. Another problem faced in fabrication of *p-n* junctions with the use of ion-laser technology is incomplete annealing out of defects at great depth, i.e., in the vicinity of the *p-n* junction itself. In particular, this refers to nanosecond pulses. To solve this problem, a coordinated selection of pulse power, duration and absorptivity (wavelength) is required. Also promising is a combination of general thermal heating with localized laser annealing.

References

1. *Physical Processes in Irradiated Semiconductors.* Ed. by L. S. Smirnov. Novosibirsk, Nauka, 1977, 256 pages (in Russian).
2. Ready, J., *Effects of High-Power Laser Radiation.* New York-London, 1971, 433 pages.
3. Kazkaz Abdul-Ghaffar. Réalisation dans le silicium de dopages et de recuits de couches implantees par tir laser. *Thése doct. phys. Univ. sci. et méd.*, Grenoble, 1973, p. 91.
4. Blinov, L., Vavilov, V., Galkin, G. E. A change in optical properties and concentration of carriers in Si and GaAs upon intensive photoexcitation by ruby laser. *Fizika i tekhnol. polupr.*, 1967, 1, 9, pp. 1341-1357 (in Russian).
5. Bobrova, E. A., Vavilov, V. S., Galkin, G. N. Photoconductivity and photomagnetic effect in germanium irradiated with laser pulses. *Fizika i tekhnol. polupr.*, 1969, 3, 8, pp. 1232-1237 (in Russian).
6. Vaitkus, Yu., Grivatskas, V., Starosta, Yu. Electron-hole scattering and recombination of non-equilibrium carriers in silicon with high excitation level. *Fizika i tekhnol. polupr.*, 1975, 9, 7, pp. 1339-1344 (in Russian).
7. Zuev, V. A., Litovchenko, V. G., Glinchuk, K. D., Litovchenko, N. M., Sukach, G. A., Linnik, L. F. Processes of carrier recombination at the surface of Ge and Si upon laser excitation. *Fizika i tekhnol. polupr.*, 1972, 6, 10, pp. 1936-1944 (in Russian).
8. Blinov, L. M., Bobrova, E. A., Vavilov, B. S., Galkin, G. N. On recombination of non-equilibrium carriers in silicon at high levels of photoexcitation. *Fizika tverd. tela*, 1967, 9, 11, pp. 3221-3228 (in Russian).
9. Bourgoin, J., Corbett, J. W. A new mechanism for interstitial migration. *Phys. Lett.*, 1975, 38A, 2, pp. 135-137.
10. Bourgoin, J., Peak, D., Corbett, J. W. Ionization-enhanced diffusion: Ion implantation in semiconductors. *J. Appl. Phys.*, 1973, 66, 8, p. 3022-3027.
11. Lax, M. Cascade capture of electrons in solids. *Phys. Rev.*, 1960, Second. Ser., 119, 5, pp. 1502-1523.
12. Bolotov, V. V., Vasilyev, A. V., Smirnov, L. S. On migration energy of

elementary defects in germanium and silicon. *Fizika i tekhnol. polupr.*, 1974, 8, 3, pp. 518-521 (in Russian).
13. Oksengendler, B. L., Yunusov, M. S. Effects of static and dynamic recharges in semiconductors. *Izv. AN USSR*, 1974, 1, pp. 37-39 (in Russian).
14. Cheng, L. J., Lori, J. Electrical properties of gamma irradiated *p*-type silicon. *Phys. Rev.*, 1970, Third Series, 1, 4, pp. 1558-1563.
15. Barnes, C. E. Effects of Co^{60} gamma irradiation on epitaxial GaAs laser diodes. *Phys. Rev., B*, 1970, Third Series, 1, 12, pp. 4735-4747.
16. Gregory, B. L., Sander, H. H. Transient annealing of defects in irradiated silicon devices. *Proc. IEEE*, 1970, 58, 9, pp. 1328-1341.
17. Picraux, S. T., Vook, F. L. Ionization, thermal and flux dependences of Implantation disorders in Si. *Rad. Eff.*, 1971, 11, 2, pp. 179-197.
18. Mirkin, L. I., *Physical Fundamentals of Material Treatment by Laser Beams.* Moscow, 1975, Moscow State University, 384 pages.
19. Zakharov, V. P., Gerasimenko, V. S. *Structural Properties of Amorphous Semiconductors.* Kiev., Naukova dumka, 1976, 280 pages.
20. Shtyrkov, E. I., Khaibullin, I. B., Zaripov, M. M., Galyautdinov, M. F., Bayazitov, R. M., On mechanism of laser annealing of implanted layers. In: *Internat. Working Meeting on Ion Implant. in Semicond.* Budapest, 1975, pp. 247-262 (in Russian).
21. Kachurin, G. A., Pridachin, N. B., Smirnov, L. S. Annealing of radiation defects by pulsed laser irradiation. *Fizika i tekhnol. polupr.*, 1975, 9, 7, pp. 1428-1429 (in Russian).
22. Gerasimenko, N. N., Dvurechensky, A. V., Kachurin, G. A., Pridachin, N. B. Activation and redistribution of impurity in implanted Si and GaAs layers subjected to pulsed laser irradiation. In: *Intern. Working Meeting on Ion. Implant. in Semicond.* Budapest, 1975, pp. 263-267 (in Russian).
23. Shtyrkov, E. I., Khaibullin, I. B., Zaripov, M. M., Galyautdinov, M. F., Bayazitov, R. M. Localized laser annealing of ion implanted semiconductor layers. *Fizika i tekhnol. polupr.*, 1975, 9, 10, pp. 2000-2002 (in Russian).
24. Khaibullin, I. B., Titov, V. V., Shtyrkov, E. I., Zaripov, M. M., Strashko, V. P., Kuzmin, K. P. Laser annealing of implanted layers. In: *Intern. Working Meeting on Ion Implant. in Semicond.* Budapest, 1975, pp. 212-246 (in Russian).
25. Antonenko, A., Gerasimenko, N., Dvurechensky, A., Smirnov, L., Tzeitlin, G. Distribution of impurity implanted in silicon after laser annealing. *Fizika i tekhnol. polupr.*, 1976, 10, 1, p. 139 (in Russian).
26. Khaibullin, I. B., Shtyrkov, E. I., Zaripov, M. M., Galyautdinov, M. F., Bayazitov, R. M. Annealing of ion implanted layers by laser irradiation. Moscow, *VINITI*, dep. No. 2661-74, 32 pages (in Russian).
27. Kachurin, G. A., Nidayev, E. V. On efficiency of annealing of implanted layers by millisecond laser pulses. *Fizika i tekhnol. polupr.*, 1977, 11, 10, pp. 2012-2014 (in Russian).
28. Gusev, V. M., Titov, V. V., Kuzmin, K. M., Khaibullin, I. B., Shtyrkov, E. I., Bayazitov, R. M., Galyautdinov, M. F. Effects of various modes of laser annealing on profiles of implanted impurity in Si layers. In: *Intern. Conference on Ion Implantation in Semiconductors.* Rheinhardsbrunn (GDR), 1977, part 1, pp. 78-90 (in Russian).
29. Foti, G., Rimini, E., Vitali, G., Bertolirri, M. Amorphous-polycrystal transition induced by laser pulse in self-ion implanted silicon. *Appl. Phys.*, 1977, 48, 1, pp. 1-3.
30. Kachurin, G. A., Bogatyrev, V. A., Romanov, S. I., Smirnov, L. S. Annealing of defects in ion implanted layers by pulsed radiation. In: *Ion Implantation in Semiconductors.* Ed. by F. Chernov, J. Borders, D. K. Brice. N. V.-London, Plenum Press, 1977, pp. 445-451.
31. Brice, D. K. Spatial distribution of energy deposited into atomic processes in ion implanted silicon. *Rad. Eff.*, 1970, 6, 1-2, pp. 77-78.

32. Bolotov, V. V., Pridachin, N. B., Smirnov, L. S. Laser annealing of defects responsible for additional optical absorption in ion bombarded gallium arsenide. *Fizika i tekhnol. polupr.*, 1976, **10**, 3, pp. 556-567 (in Russian).
33. Gavrilov, A. A., Kachurin, G. A., Safronov, L. N. On deep penetration of defects in gallium arsenide irradiated with argon ions. In: *Arsenid Galliya*, Tomsk, 1975, 4, p. 99 (in Russian).
34. Ivanova, E. A., Nasledov, D. N., Tsarenkov, B. K. Electrical behaviour of diffused *p-n* junctions in gallium arsenide. *Radiotekhnika i elektronika*, 1965, **10**, 4, pp. 703-719 (in Russian).
35. Weinstein, M., Mlavsky, A. I. The voltage breakdown of GaAs abrupt junctions. *Appl. Phys. Lett.*, 1963, **2**, 5, pp. 97-99.
36. Kachurin, G. A., Pridachin, N. B. Special features of formation of *p-n* junctions in ion implanted GaAs. *Elektronnaya tekhnika. Ser. 2. Poluprovodnikovye pribory*, 1972, 1 (65), pp. 40-43 (in Russian).
37. Bogatyrev, V. A., Gavrilov, A. A., Kachurin, G. A., Smirnov, L. S. *p-n* junctions implanted in GaAs by pulsed laser annealing. *Fizika i tekhnol. polupr.*, 1976, **10**, 7, pp. 1392-1494 (in Russian).
38. Marquardt, C. L., Giuliani, J. F., Fraser, F. M. Observation of impurity migration in laser-damaged junction devices. *Rad. Eff.*, 1974, **23**, 2, pp. 135-139.
39. Geiler, H. D., Götz, G., Klinge, H. D., Triem, N. Backscattering measurements of As implanted Si after laser irradiation. In: *Materials of VIII All-Union Meeting on Physics of Interactions of Charged Particles with Monocrystals*. Moscow, 1976.
40. Dvurechensky, A. V., Kachurin, G. A., Antonenko, A. Kh. On the mechanisms of impurity redistribution at laser annealing of ion implanted semiconductors. *Rad. Eff.*, 1978, **37**, 3, 4, pp. 179-181.
41. Zelevinskaya, V. M., Kachurin, G. A., Smirnov, L. S. On the interstitial diffusion of impurity from implanted layers. *Fizika i tekhnol. polupr.*, 1975, 9, 8, pp. 1627-1629 (in Russian).
42. Grötzchel, R., Klades, R., Kreissig, U., Rüdiger, J., Voelskow, M., Krynicki, J., Suski, J. Laser annealing of heavily damaged silicon crystal surface layers. In: *Proc. of Intern. Conf. on Ion Implantation in Semiconductors*. Reinhardsbrunn (GDR), October, 23-29, 1977, part 1, pp. 103-110.
43. Geiler, H. D., Götz, G., Klinge, K. D., Triem, N. Investigation of laser induced diffusion and annealing processes in arsenic implanted Si crystals. *Phys. Stat. Sol.*, (*a*), 1977, **41**, 3, K171-K173.
44. Tsuchimoto, T., Tokuyama, T. Enhanced diffusion of Boron and Phosphorus in silicon during hot substrate ion implantation. *Rad Eff.*, 1970, **6**, 3-4, pp. 121-129.
45. Kachurin, G. A., Nidaev, E. V. On diffusion of impurity during laser annealing of implanted layers. *Fizika i tekhnol. polupr.*, 1977, **11**, 3 pp. 603-606 (in Russian).
46. Kachurin, G. A., Nidaev, E. V. Annealing of implanted layers by scanning laser beam. *Fizika i tekhnol. polupr.*, 1976, **10**, 10, pp. 1890-1893 (in Russian).
47. Alferov, G. N., Donin, V. I., Yurshin, B. Ya. Continuous-action argon laser with output power of 0.5 kW. *Pisma v ZhETF*, 1973, **18**, 10, pp. 629-631 (in Russian).
48. Tovstyuk, K. D., Plyatsko G. V., Orletsky, V. B., Kiyak, S. T., Bobitsky, Ya. V. Formation of *p-n* and *n-p* junctions in semiconductors by laser irradiation. *Ukr. fiz. zhurnal*, 1976, **21**, 11, pp. 1918-1920 (in Russian).
49. Bogatyrev, V. A., Kachurin, G. A. Formation of low-ohmic *n*-layers on InSb by laser irradiation. *Fizika i tekhnol. polupr.*, 1977, **11**, 1, pp. 100-102 (in Russian).
50. Mayer, J., Eriksson, L., Davies, J. *Ion Implantation in Semiconductors. Silicon and Germanium*. New York-London. 1970, 280 pages.
52. Kutukova, O. G., Streltsov, L. N. Laser annealing of implanted silicon. *Fizika i tekhnol. polupr.*, 1976, **10**, 3, p. 443-446 (in Russian).

CHAPTER 9

PRODUCTION OF THIN FILMS BY ION AND MOLECULAR BEAM DEPOSITION

Sec. 9.1. Basic Methods of Film Synthesis Using Ion and Molecular Beams

In our preceding discussion we have covered various techniques of application of radiation technology to modifying the properties of the existing and building new semiconductor device structures. This, however, does not exhaust the potentialities of radiation technology. The present chapter gives a summary of the main results achieved, over the last years, in application of ion and molecular beams to formation of active and passive layers in semiconductor materials. The interest in this problem is prompted by the advantages offered by the ion and molecular beam techniques of deposition of thin layers on the surface of a solid (high vacuum, permanent monitoring of the composition and intensity of the beams, possibility of checking the condition of the surface without unsealing the vacuum chamber, relatively low temperatures of synthesis, possibility of continuous and controlled variation of the growth conditions for formation of structures with desired characteristics).

At present, there exist, in a state of continuing development, at least four methods of production of thin films with the use of ion and molecular beams:

(1) implantation of accelerated ions into the substrate in doses sufficient for formation of a film of a new compound consisting of implanted and target atoms. Ion implantation can be effected both at elevated and at room (or below room) temperatures with subsequent annealing;

(2) implantation of accelerated ions into an interlayer deposited on the substrate. The interlayer may be both in a liquid or solid state. A new phase grows as a result of diffusion of implanted atoms towards the interlayer-substrate interface. When the interlayer is in a liquid state, the method is, in effect, a liquid-phase epitaxy with boost charging of the melt with an ion beam;

(3) deposition of films on the surface of a solid by low-energy beam epitaxy. It is supposed that in contrast to conventional vacuum sputtering the ion beam deposition will promote, to a greater degree, the processes of migration and interaction of atoms at the film growing surface, thus improving the structure and homogeneity of the films;

(4) molecular beam epitaxy (MBE). Over the last years, this method has been very successfully used in the production of various semiconductor devices. The MBE differs from ordinary vacuum sputtering in a higher degree of control over the composition and intensity of molecular beams, careful preparation of the substrate, in conducting the entire process in a high vacuum, checking the quality of the growing film without unsealing the working space, and introducing corrections into the film production conditions.

Formally, one can hardly relate MBE to the radiation methods since the particles of the beam possess the thermal energy and the formation of films is not attended with radiation effects. Still, from the technical viewpoint, MBE has much in common with the ion-beam technology, first of all in the ways the ion beams are checked, in the pre-epitaxial ionic cleaning of the surface, in the application of protonography and backscattering of light ions for analyzing the surface condition. Besides, MBE does not rule out preliminary ionization of atoms and molecules in the beam, their purification by mass-spectroscopy methods and their subsequent retardation or neutralization in the close vicinity of the substrate. Proceeding from the aforesaid as well as taking into account the progress made by MBE over the last years, we feel it appropriate to devote the present chapter to the discussion of this method of production of thin films.

Sec. 9.2. Synthesis of Compounds by Ion Implantation

In recent years, ion bombardment has been repeatedly and successfully used in synthesis of many compounds. The interest in ionic synthesis is accounted for by the fact that apart from widely known technical advantages typical of the ion-beam technology, this method also possesses quite valuable physical peculiarities. First it should be stressed that retardment of accelerated ions is attended with displacement peaks inside which there are momentary (about 10^{-11} s) occurrences of exceedingly high pressures (about 10^8 Pa) and temperatures [1]. This points to the potential use of ionic synthesis in fabrication of compounds whose formation under equilibrium conditions meets with difficulty [2, 3].

According to [4], ionic synthesis has the following distinguishing features:

1. The formation of new phases is observed over a wide dose range, including the small doses with the average concentration of implanted component being far from stoichiometric. In semiconductors, new molecular complexes arise already at doses of 10^{14}-10^{15} cm^{-2} and at irradiation temperature of 20 °C.

2. New compounds emerge through formation of elementary molecular complexes typical of the amorphous phase of the matter being synthesized.

3. Extended post-implantation annealing at elevated temperatures is, as a rule, essential to the ordering of structures, since the annealing involves an intensive redistribution of implanted atoms.

4. The substrate structure has a significant bearing on the crystallization of a new compound even when the lattice constants (spacings) of the base material and the material to be synthesized do not coincide.

5. Of particular importance to ionic synthesis is the dose accumulation rate (the density of the ion beam current).

Let us concentrate on the results obtained in ionic synthesis of semiconductor and dielectric films.

The authors of [5] have undertaken one of the first attempts at synthesis of dielectric coatings. They irradiated silicon with 60 keV ions of oxygen for 200 min. The ionic current density was 20 $\mu A/cm^2$. The occurrence of the SiO_2 film was recognized by a 9.4 μm band in the absorption spectrum. Though the films could withstand rather great breakdown voltages, the properties of the Si-SiO_2 interface were unsatisfactory. The capacitance of the MIS-structure was voltage independent within the range of ± 70 V. It should be noted that the postimplantation annealing was skipped.

Then followed some publications detailing the use of ion implantation for synthesis of dielectric (insulating) coatings (SiO_2 [6, 7] Si_3N_4 [6, 8, 9] and SiC [10, 11]) on silicon. Also produced were films of GeO_2 by implantation of O ions into Ge [12] and of SiC by Si ion irradiation of diamonds [13]. These experiments have demonstrated that ion implantation can be of help in controlled formation of dielectric coatings whose properties resemble those obtained by conventional methods. At the same time, the Si-SiO_2 and Si-Si_3N_4 interfaces turned out to be strongly populated with defects. Even after annealing performed at 1000 °C, the dependence of the MIS-structure capacitance on the voltage applied indicated a high density of surface states. In this respect, very interesting results were obtained by the authors of reference [11]. They irradiated silicon with 40 keV carbon ions at ionic current density of $(10\text{-}15)\cdot 10^{-6}$ A/cm^2. After the irradiation, the crystals were annealed at temperatures ranging from 600 to 1000 °C in a dry nitrogen environment. The occurrence of β-SiC was confirmed by the IR-absorption spectra and transmission data supplied by electron microscopy. The film thickness amounted to about 1900 Å. Of greatest significance was the fact that capacitance modulation by applied voltage was registered for both *n*- and *p*-type silicon samples (Fig. 9.1). The analysis of the *C-V*-characteristics indicated a density of states at the Si-SiC interface to be within $8\cdot 10^{11}$-10^{11} cm^{-2}. The properties of the Si-SiC heterojunctions were investigated by the authors of [14].

Of great interest are the experiments on the use of Si_3N_4 films synthesized by ion implantation for diffusion masking in silicon [9]. The authors of the reference irradiated an *n*-Si sample with 40 keV

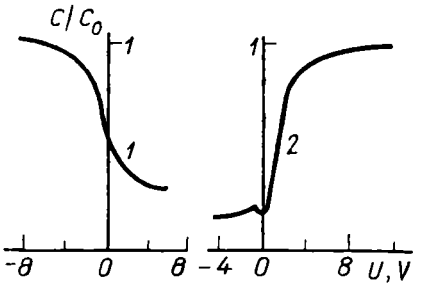

Fig. 9.1. *C-V* characteristics of Al-SiC-Si structures (*1*—*p*-Si substrate, *2*—*n*-Si substrate).

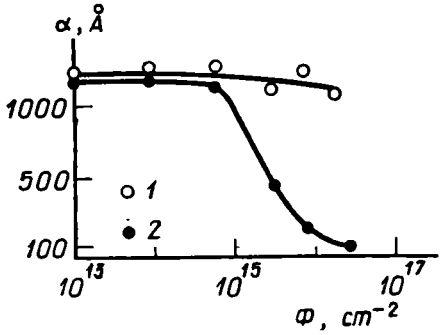

Fig. 9.2. Thickness of oxidized layer vs dose of preliminary irradiation with argon (*1*) and nitrogen (*2*) ions.

nitrogen ions at the ionic current density of about 200 μA/cm^2. The substrate temperature was varied from 20 to 500 °C. Oxygen was used as a diffusant and to achieve the desired effect, the samples were kept, after the irradiation, in a stream of dry oxygen at 1100 °C for one hour. Oxygen diffusion was monitored by measuring the thicknesses of oxide films with the aid of a laser photoelectric ellipsometer. It was found that already after a dose of about 10^{15} cm^{-2}, the growth of oxide films drastically decreased (Fig. 9.2). The indicated dose was obviously insufficient to produce a solid protective film of Si_3N_4. On the other hand, argon ion irradiation of samples over a dose range of 10^{13} to 10^{17} cm^{-2} did not result in appreciable reduction in the SiO_2 film growth rate. This means that the observed effect is not associated with the occurrence of a disordered layer. The authors of [15] who also observed a retardment of silicon oxidation rate upon implantation of insignificant doses of nitrogen suggested that this effect was conditioned by the occurrence of an oxinitride film. They believe that during annealing nitrogen is forced towards the surface of the sample where it forms Si-N bonds, while the external oxygen completes the structure to oxinitride. The effect is also observed in polycrystalline silicon [16], which allows one to use N-implanted polycrystalline films of silicon for masking purposes in planar MOS technology [17]. It should be noted that a decrease in the silicon oxidation rate may also be associated with a change in the absorptive properties of the irradiated surface [18].

Another important trend in ion synthesis studies is obtaining active semiconductor layers. Feasibility of producing semiconductor

compounds by ion implantation was first demonstrated in [3]. The authors irradiated tellurium films sputtered over glass substrates with cadmium ions. The target temperature in irradiation was 50 °C, and the ion energy ranged from 5 to 50 keV. The progress of the production of the compound was monitored by measuring the optical absorption spectra and photoconductivity. With a certain dose reached, the fringe of absorption and photoconductivity, typical for cadmium telluride (Fig. 9.3), was discovered.

Electron diffraction analysis of the film structure has confirmed the presence of cadmium telluride both in cubic and in hexagonal versions, though some reflexes of tellurium are also observed. The Hall effect measurements have shown that the films possess hole conductivity thus indicating an excess of tellurium in synthesized layers. The authors of the cited reference note that the rate of formation of the new phase can be stepped up through trapping the atoms adsorbed at the surface by the displacement peaks. It is possible that this effect is responsible for the production of cadmium telluride layers with small values of energy and dose of implanted ions.

At a later stage, the authors of [3] carried out successful experiments on synthesis of CdSe. Reference [19] informs about the synthesis (formation) of the ternary compound, $Hg_{1-x}Cd_xTe$, by Hg ion bombardment of cadmium telluride.

In recent years, interest in ternary compounds based on the III and V group elements, such as $GaAs_{1-x}P_x$, $Al_xGa_{1-x}As$, etc. increased. This is explained by an extraordinary promise held by these compounds for creation of irradiators and receivers of visible and near infra-red radiation. Since the properties of such compounds heavily depend on the parameter x and, in addition, in many instances it is desirable to have such compounds in the form of layers microns or less thick, ionic synthesis may prove to be quite suitable in satisfying these requirements. An example of production of layers of $Ga_{1-x}Al_xAs$ is provided by reference [20]. The authors used 30 keV Al ion implantation into GaAs substrates. After reaching a dose of $2 \cdot 10^{16}$ cm^{-2} and completing a four-hour annealing at 900 °C, the electroluminescent spectra of the irradiated surface revealed radiation with quantum energies largely exceeding the forbidden zone of gallium arsenide (Fig. 9.4). This is evidence that a wide-zone compound, $Ga_{1-x}Al_xAs$, has formed.

All this constitutes a sufficient proof of the possibility of successful employment of ionic synthesis for production of most diverse dielectric (insulating), semiconducting and conducting coatings. We have already mentioned the advantages of the ion beam method. Now, let us discuss some limitations of this method and outline the ways of their elimination.

The most unpleasant effect of ion implantation is the occurrence of radiation defects whose annealing often requires high-temperature

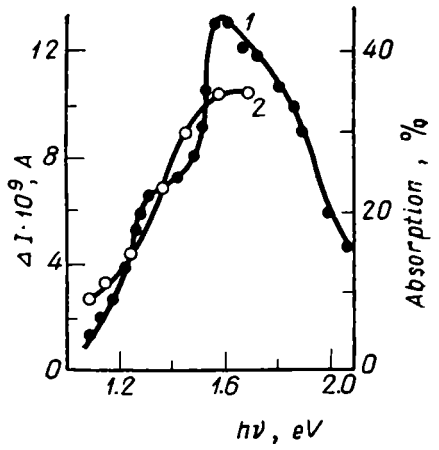

Fig. 9.3. Photoconductivity (*1*) and absorption (*2*) spectra of synthesized layers of cadmium telluride.

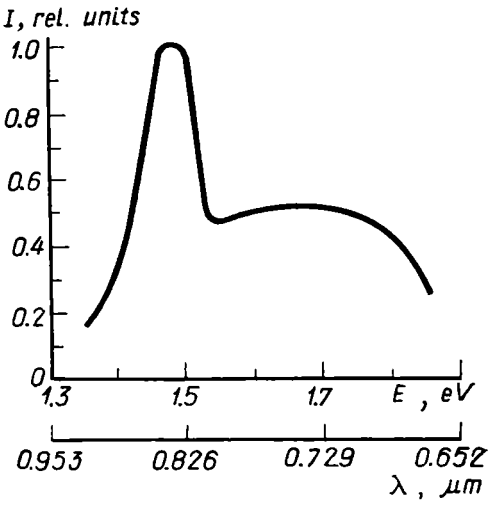

Fig. 9.4. Electroluminescence spectrum of $Ga_{1-x}Al_xAs$ structure obtained by implantation of aluminium into gallium arsenide with subsequent annealing.

heat treatment. Heating the samples to high temperatures is an undesirable option due to many reasons, and many researchers are currently engaged in the activities aimed at eliminating the annealing or, at least, reducing its temperature. One of the papers [21] suggests that we stimulate the annealing through simultaneous effects of temperature and light-particle irradiation. It is shown that electron and proton irradiations markedly enhance the reordering of disordered layers in Si and GaAs.

Also of interest is ion implantation at high temperatures. The traditional scheme of ion implantation, i.e., irradiation at a relatively low temperature and subsequent annealing at high temperature, is not always justifiable. For example, the authors of [22] bombarded gallium arsenide with P and Al ions at a temperature of about 500 °C with the result that the respective ternary compounds had been produced without additional annealing.

Let us recall that in the case of Al implantation into GaAs at room temperature, additional annealing at 900 °C was necessary to produce $Al_xGa_{1-x}As$ [20]. At a later stage, high-temperature ion implantation was used in synthesis of ternary compounds of the A_{III}-B_V type [23] and varizonal structures. It is quite probable that the dynamic properties of dislocations play a major role in high-temperature synthesis of compounds [23].

Finally, much promise is held by laser heating. Experiments have shown that annealing out of compensating defects and recovery of the crystalline structure under the action of nanosecond laser pulses occurs within so short a time that heat does not manage to spread over the crystal and heating affects a layer about 1 μm thick. Laser annealing may turn out to be of particular value to synthesis of compounds that decay easily.

Another difficulty one faces in ionic synthesis resides in that along with the useful compound the same elements may produce undesirable ones. Thus, implantation of N ions into GaAs to a dose of $2 \cdot 10^{7}$ cm^{-2} did not result in the formation of GaN despite the fact that it was proved that the entire implanted nitrogen was in the sample [26]. It is likely that the recovery of the GaAs structure and formation of molecules of N_2 (or other complexes) turned out to be more appropriate from the energy picture viewpoint than the formation of GaN. In such situations, one has to stimulate synthesis of the required compound. There are sufficient reasons to believe that the effect of capture of impurity atoms from the surface by the displacement peak [27], observed under suitable conditions, should enhance oversaturation of the material with the implanted component and set the course of the reaction in the desired direction. Another option for controlled reactions is through depletion of the surface layers of one component (an increase in the concentration of vacancies of the desired type). For example, synthesis of $GaAs_{1-x}P_x$ by implantation of phosphorus into GaAs is made easier with the GaAs samples preannealed in vacuum for evaporation of some arsenic and increase in the concentration of arsenic vacancies [28]. Likewise, the concentration of vacancies in one sublattice can be increased by implanting into it the ions making up another sublattice [29].

Sec. 9.3. Synthesis of Compounds by Ion Implantation of Components into an Interlayer

As has been stated in Sec. 9.1, the growth of a new phase during implantation of components into an interlayer occurs as a result of diffusion of implanted atoms towards the layer-substrate interface. This precludes the formation of radiation defects in the substrate and allows, in principle, the fabrication of substrate-synthesized

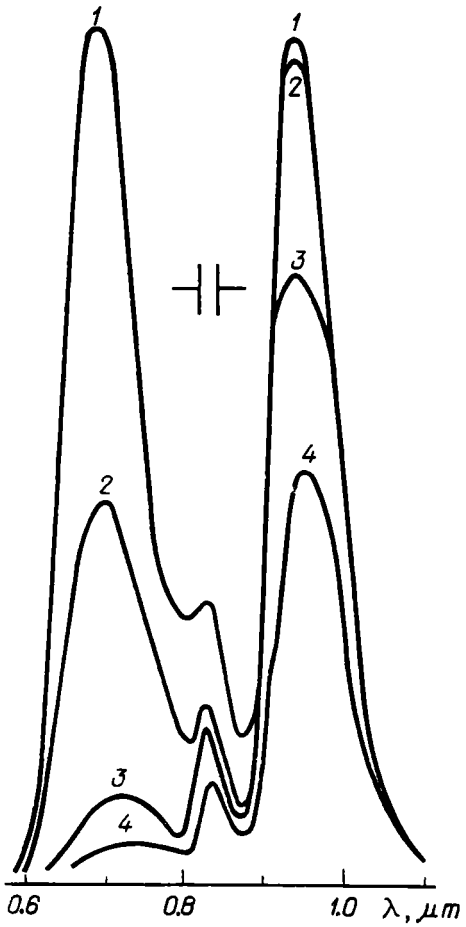

Fig. 9.5. Cathodoluminescence spectra of samples (90 K) for various energies of excitation electrons.
Excitation energy, keV: *1*—5; *2*—8; *3*—28; *4*—42

film interfaces with the properties appropriate to ordinary methods of epitaxial growth of heterostructures. The composition of the synthesized compound will depend on the growth conditions and, generally, may include implanted atoms, atoms of the matter making up the interlayer and substrate atoms if the latter are capable of penetrating into the interlayer by dissolution and diffusion.

Consider the results of the experiments performed in production and investigation of wide-band compounds which form in the course of P ion implantation into a thin layer of liquid gallium applied to the surface of a GaAs sample [30, 31].

The scheme of the experiment was as follows. A gallium film 0.8 μm thick was applied, by vacuum sputtering, to polished and etched monocrystalline samples of gallium arsenide. Then the samples were irradiated from the side of the sputtered film with 100 keV P ions to a dose of $6.3 \cdot 10^{16}$ cm^{-2}. The thickness of the gallium film and energy of P ions were selected so as to prevent the ions from reaching the surface of the GaAs sample, thus precluding the formation of radiation defects in the sample. Due to elevated temperature of the target in the course of irradiation, the gallium film was in a liquid state. After irradiation, the excess layer of gallium was etched away by heated hydrochloric acid.

The samples were studied with a Soviet-made electron diffractometer, type ЭР-100, using the reflection electron diffraction method. It was found that a new compound emerged as islands of epitaxial area on the surface of the GaAs sample. The polycrystalline phase was also observed. Analysis of electron diffraction patterns has shown that this compound has the zinc blende lattice type with the spacing $a_0 = 5.445 \pm 0.004$ Å, which agrees with the data on GaP.

In addition, studies were made of the cathodoluminescence spectra of the samples from the side of the synthesized film. The energy of exciting electrons was varied from 5 to 50 keV. By this means, the luminescence excitation area covered the film, a greater or lesser portion of the substrate of GaAs, depending on the energy of exciting electrons. Along with the impurity ($\lambda_{max} = 0.94$ μm) and "fringe" ($\lambda_{max} = 0.83$ μm) spectral bands of GaAs, the spectrum revealed a band of a shorter wavelength ($\lambda_{max} = 0.70$ μm) (Fig. 9.5). With a decrease in electron energy, the ratio of the short-wavelength and "fringe" band intensities in GaAs increased. This points to the fact that the red luminescence centers are located closer to the sample surface. The emergence of the spectral band with $\lambda_{max} = 0.70$ μm may be associated with the occurrence of GaP or $GaAs_{1-x}P_x$ having under suitable conditions a characteristic radiation in the given spectral region during recombination by impurity or defect levels.

The data supplied by electron diffractometry indicate domination of gallium phosphide. This means that the band with $\lambda_{max} = 0.70$ μm is likely to be associated with radiative recombination at imperfections of the GaP lattice.

Still later, layers of AlN up to 1200 Å thick and about 0.5 cm^2 in area were fabricated by N ion implantation into Al films applied to germanium and silicon samples [32].

Sec. 9.4. Deposition of Films by Ion Beams

This method is primarily applied for deposition of metal coatings although recent reports name it amongst the techniques used for fabrication of thin layers of semiconductor materials.

One of the problems in growing films by ion beams is relatively low rates of growth. Indeed, a time about 1 s is required in the ideal case for growing a monocrystalline layer at an ion beam current of the order of 100 $\mu A/cm^2$. In actual practice, however, only a fraction of all ions supplied by the ion beam condense on the substrate. Substantial losses result from reflection of ions from the surface, cathode sputtering, reevaporation and other factors. Therefore, progress in this field depends both on the headway made in the understanding of the mechanisms of film deposition by ion beams, and on the ability of constructing a special-function heavy-current ion-beam apparatus. The conventional ion guns employed for ion implantation are of little use in ion deposition.

Unfortunately, investigations carried out in this field are still at the initial stage of development, and the number of publications dedicated to the physics and techniques of ion deposition are still few.

The authors of [33] made a study of the process involved in the formation of layers on the surface of a solid irradiated with a flux

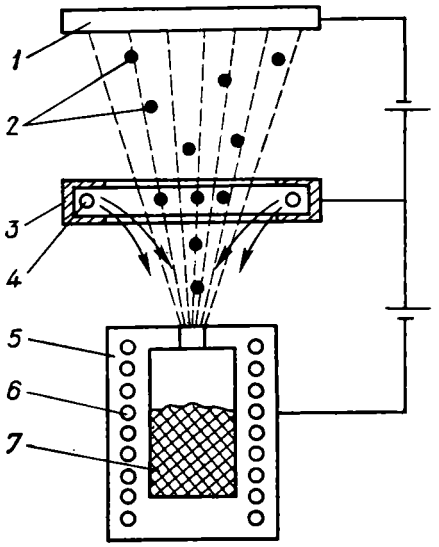

Fig. 9.6. Apparatus for ionized-cluster beam deposition
1—substrate; *2* — clusters; *3*—ionizer; *4*—cathode; *5*—crucible; *6*—heater; *7*—evaporated matter

of low-energy ions. They have deduced equations for estimating the quantity of absorbed particles versus time of bombardment of a target, its temperature and density, and the ion beam energy. Implantation of ions into the substrate, reflection of the ions back into vacuum, their decrement due to cathode sputtering, thermal evaporation from the surface and diffusion were taken into account. Precipitation of copper ions on aluminium was used for quantitative estimates. It was established by calculations that the most favourable conditions in this case are provided by the ion beam energy from 1 to 3 keV, substrate temperature below 200 °C, and maximum accessible ionic current density. Under such conditions, a practically linear time dependence of growth of the adsorption layer could be expected. According to the cited reference, it is preferable that the substrate be made of a material whose atomic weight is less than that of the bombarding ion. Then reflection of ions from the target surface can be neglected.

From general theory it follows that the film growing rate will increase with the ionic current density. However, the technique of producing high densities of low-energy ion beam current is difficult in itself, and in addition, the substrate is overheated by heavy ionic currents.

For this reason, the method of deposition of thin layers described in reference [34] is of particular interest. The essence of the method consists in that instead of ionizing single atoms, whole clusters of evaporated matter are subjected to ionization, comprising large quantities of atoms and molecules. An apparatus for realizing this method is schematically shown in Fig. 9.6. Microparticles varying in size are ejected from a heated source and are ionized on collision with electrons emitted by an orificed cathode. Since single-time ionization is most probable, the charge-to-mass ratio is low for polyatomic particles. This phenomenon permits a substantial increase in the actual beam density and, hence, in the rate of deposition. Moreover, the present method inherits a number of advantages peculiar to the ion-beam technology. In experiments described in

reference [34], the rate of deposition amounted to 1000 Å/min and more. Measurements taken with a transit-time analyzer showed that the masses of clusters were $5 \cdot 10^2$ to 10^3 atomic units. The authors noted good adhesion of films to the substrate surface.

A limitation of the above system resides in the absence of the mass-separator. One is tempted to fit an adapter into a conventional ion gun with a separated beam that would allow reducing the ion energy to tens of electronvolts without losses in the ionic current density. The construction of such an ion-optical system capable of retarding and focusing an isotope separator ion beam was reported in reference [35]. With this system, the energy of ions passing through a magnetic mass-analyzer was reduced from 20 keV to 50-60 eV. The system allows deposition of ions of any materials with pure spectrum for growing thin layers and device structures. The authors used wafers of monocrystalline silicon as a substrate, and chose copper and lead ions for deposition. Their choice is primarily attributed to the film analyzing technique utilizing the effect of small-angle Rutherford scattering of 2 MeV helium ions. In this technique, the ratio of the film and substrate atom masses must be high. The foregoing system provided for deposition of films with an area of up to 3 cm^2 at a rate of 100 Å/h. It was revealed by means of a scanning electron microscope that layers less than 150 Å thick appear in the form of islands. Thicker layers are continuous.

Germanium and silicon ion beams subjected to a mass analysis were used by the authors of [36] for fabrication of thin semiconductor layers. The substrates were made of polished and etched wafers of germanium and silicon. The ion energy was 100 eV, the ionic current density was 4 to 5 $\mu A/cm^2$, and the dose was 10^{18} cm^{-2}. The films 1500 to 3000 Å thick were built up by deposition during 5 hours at a substrate temperature of 350 °C. Under such conditions, the films of germanium grew directly in the form of a single crystal. If the temperature of the target was below 200 °C, the layers turned out to be amorphous, and if the temperature was subsequently elevated to 500 °C, the layer structure transformed to polycrystalline. Germanium films deposited at 200 °C became monocrystalline after annealing at a temperature above 300 °C. If the energy of germanium ions was raised above 500 eV, the result was sputtering of the substrate, and no films were formed. In depositing silicon films, the authors of [36] revealed heavy contamination of the growing layer with carbon atoms. Even high-temperature annealing (1200 °C) failed to effect crystallization of amorphous silicon layers. The authors of the work cited believe that contamination of silicon films with carbon is due to a high coefficient of capture of carbon atoms by the surface of silicon (with vacuum in the working volume amounting to 10^{-3} Pa). For improving the quality of the silicon film, the vac-

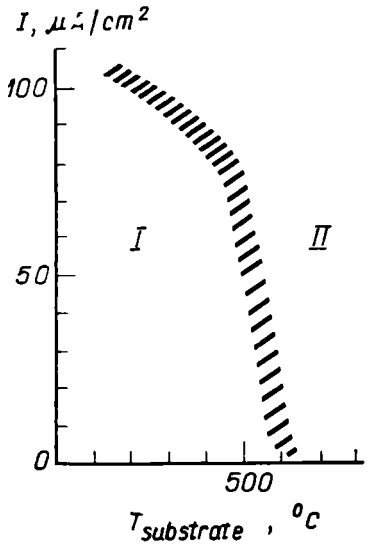

Fig. 9.7. Condition of Si film structure grown on ⟨111⟩ oriented silicon substrate by partially ionized beam vs ionic current density and substrate temperature.
Regions: *I*—amorphous structure and twin crystals; *II*—monocrystal

uum conditions must be improved and the current density of silicon ions must be increased.

The conditions described above were to some extent maintained during experiments of [37]. Getter ion and sublimation titanium pumps were employed to vacuumize the working system to a level of $7 \cdot 10^{-5}$ Pa.

The current density of silicon ions with an energy of 10 keV amounted to 100 μA/cm², though the gain in current density was at a sacrifice of the mass separator. The setup of the apparatus was nearly identical to that depicted in Fig. 9.6, and its function was to effect autoepitaxial vacuum growth of silicon films by a partially ionized beam. According to the authors of [37], the amount of the silicon ions was equal to 25% of the total quantity of the material applied to the substrate. The film growth rate was 4 Å/s. In the absence of ionization or with a low ionic current density, the deposited silicon layers were amorphous if the substrate temperature was below 600 °C (Fig. 9.7). If the ionic current density increased, the substrate temperature required for growing the monocrystalline film decreased. For example, at a current density of 80 μA/cm², the monocrystalline films grew on a substrate with the ⟨111⟩ orientation without additional heating. In this case, the ion beam with a power of 1 W/cm² heated the substrates to 400 °C (calculated estimate). As the grown films were high-ohmic, their resistance was to be reduced by annealing in the temperature range from 600 to 900 °C. The effect of stimulating the crystallization at high ionic current densities occurs partially due to general heating of the substrate, and partially due to liberation of the ion energy at the point of collision of ions. The latter factor is particularly important during

initial stages of growth when the substrate temperature is relatively low.

From the above results it follows that deposition of films by ion beams attracts greater attention of investigators. The method is quite promising, but ultrahigh-vacuum oil-free apparatus are to be provided for fabrication of high-quality semiconductor films. The substrate surface also requires more care in preparation. It is by drastic improvement of vacuum hygiene and better purification of the substrate that great progress was made in producing thin layers by molecular beam epitaxy (see the next section). There still exists a problem of constructing simple and convenient low-energy ion sources providing for a high ionic current density and mass separation. It should be noted however that good results can be achieved even without mass separators, provided all the other requirements, such as for cleanliness of vacuum volumes, substrate surface, crucibles and evaporating materials are satisfied.

Sec. 9.5. Molecular Beam Epitaxy

The MBE is generally defined as epitaxial growth of semiconductor compound films proceeding during interaction of molecular beams and crystalline substrate in ultrahigh vacuum [38]. The MBE is essentially a well-known vacuum deposition technique developed to a much higher level. The specific features of the MBE method are:

(1) superhigh vacuum (from 10^{-7} to 10^{-9} Pa);

(2) continuous qualitative and quantitative control of molecular beams;

(3) provision for quick interruption and resumption of introduction of molecules of the components and impurities permitting producing periodic structures with a spacing of about 10 Å;

(4) thorough preparation of the working surface directly inside the vacuum volume;

(5) control of the composition of the growing film without disturbing the high vacuum conditions.

The authors of work [39] made a great contribution to development of the MBE method by investigating the interaction of the Ga and As_2 beams with the gallium arsenide surface. They found that adsorption and desorption of atoms of gallium are characterized by a temperature-dependent constant τ:

$$\tau_{Ga} = 2.5 \cdot 10^{-14} \exp\left(\frac{2.6 \pm 0.2}{kT}\right) \text{ s for } \langle 111 \rangle \text{ oriented GaAs substrate.}$$

The value τ_{Ga} is the mean time over which the atoms of gallium stay on the substrate surface. For example, at a temperature of 885 K, this time amounts to 10 s for a ⟨111⟩ oriented GaAs substrate.

It was found that arsenic behaves in a more complicated manner. When no atoms of gallium were present, arsenic did not precipitate at all on the substrate at a temperature above 500 K. If the working surface was initially coated with gallium, the arsenic capture coefficient varied in proportion with the quantity of condensed free gallium. Thus the authors have arrived at the conclusion that arsenic can be adsorbed on a hot surface of GaAs only in case it reacts with the atoms of gallium. In other words, injection of ample quantities of arsenic suffices to fabricate a stoichiometric GaAs film by arsenic and gallium molecular beams.

In spite of the fact that at a later stage it was disclosed that the above assumptions were somewhat simplified, they proved to be helpful and correct as a whole. Such approach greatly contributed to a notable advance in synthesis of stoichiometric films grown from binary and ternary compounds. This is particularly true of the compounds of the A_{III}-B_V type. The electrical and optical parameters of the GaAs and $Al_xGa_{1-x}As$ films produced at present by the molecular beam epitaxy technique are commensurate with those of high-quality materials grown by conventional methods [38]. Another important factor promoting the development of the MBE method consists in construction of convenient and dependable ultrahigh-vacuum systems and elaboration of techniques of control of the beams and growing film without unsealing the working volume.

Fig. 9.8 shows schematically a cross-section of the MBE apparatus for growing multilayer structures. The principle component of the apparatus is a pressure chamber made of stainless steel where ion pumps reduce the pressure to $2 \cdot 10^{-7}$ Pa without heating. After an 8-hour heating period, the residual pressure becomes equal to 10^{-8} Pa. The components arranged inside the chamber include:

(a) crucibles *11* made of boron nitride serving to produce atomic and molecular beams, and incorporating individual heaters, thermocouples *10* and screens *9* cooled by liquid nitrogen. The temperature of each crucible is maintained automatically to within ± 2 °C. This feature implies that the intensity of beams is adjusted to an accuracy of $\pm 7\%$ for the majority of elements;

(b) an arrangement of externally-controlled shutters *8*, intended for quick interruption and resumption of supply of the components and impurities to the substrate;

(c) substrate holder *6* furnished with heating element *5* serving for adjustment of the predetermined epitaxy temperature (up to 650 °C). The holder is rotatable to permit various measurements to be taken without removing the sample from the pressure chamber;

(d) 3-keV electron gun *1* serving to conduct experiments with diffraction of electrons;

(e) ion gun *2* serving for preliminary purification of the substrate working surface and for in-depth cathode sputtering;

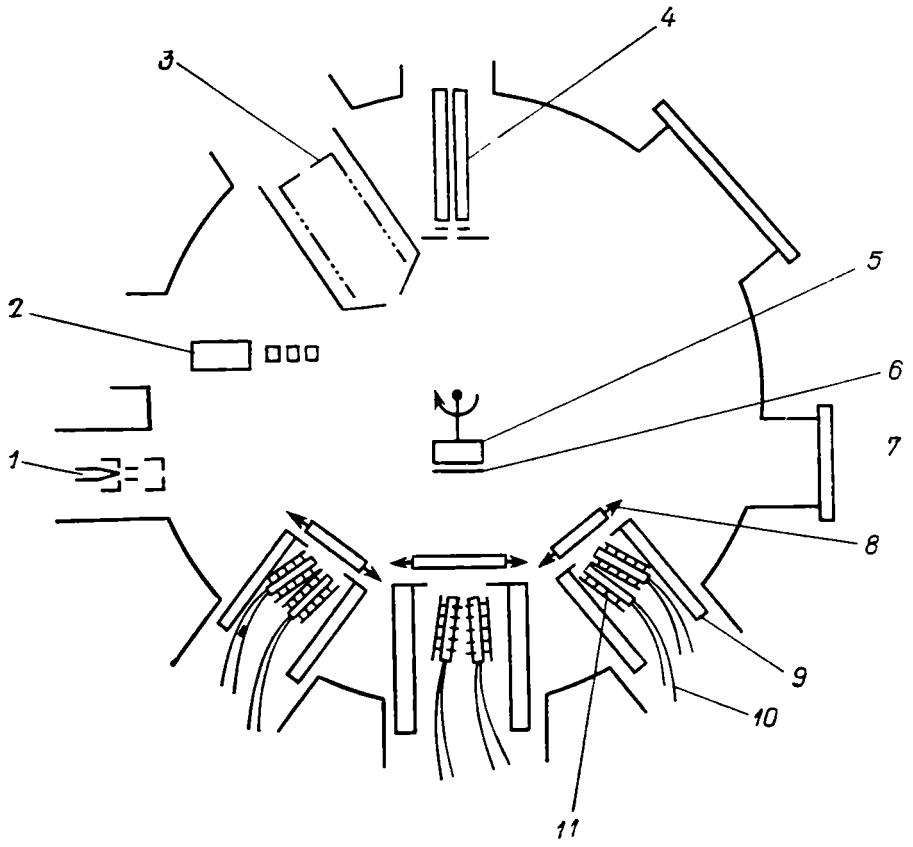

Fig. 9.8. Apparatus for growing films by molecular beam epitaxy.

(f) auger spectrograph *3* serving for analysing the chemical composition of the growing film;

(g) quadrupole mass spectrometer *4* serving to monitor the composition of residual gases and molecular beams;

(h) inspection hole *7* for visual monitoring and optical measurements.

In growing multilayer structures of the superlattice type with the number of layers running into hundreds, and with the thickness of each layer amounting to tens of angstroms, all the measuring apparatus and actuating members (such as heaters and shutters) are interconnected through a computer. An apparatus of this type is shown in Fig. 9.9 [40].

The apparatus comprises ultrahigh vacuum chamber *8* evacuated by twenty four ion pumps with a total capacity of 600 l/s and by a sublimation titanium pump with a capacity of 45 000 l/s. The pressure in the chamber after heating for one night at 250 °C amounts to 10^{-8} Pa. The molecular beams are produced by means of several crucibles *9* made of boron nitride and fitted with thermocouples and individual tantalum heaters. All crucibles are equipped with

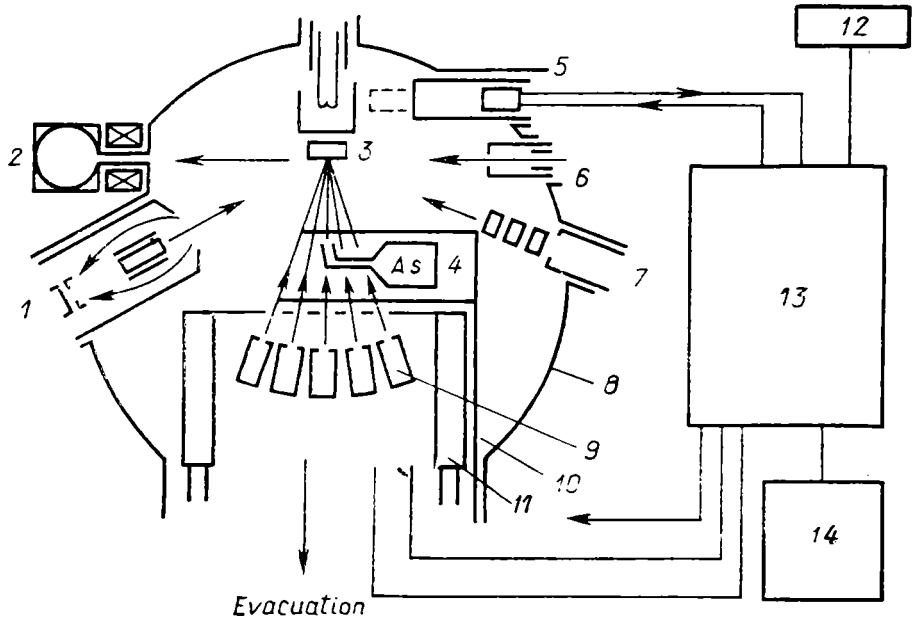

Fig. 9.9. Automated apparatus for fabrication of multilayer structures by molecular beam epitaxy.

controlled shutters *10* and surrounded by a single screen *11* cooled by liquid nitrogen. Since the purpose of the apparatus is to synthesize the $A_{III}B_V$ compounds with arsenic used as a source material, arsenic is evaporated from individual quartz crucible *4*. There is no need in maintaining the temperature of arsenic to a high accuracy, but it is essential that an excess amount of it should be supplied to the substrate. The substrate holder and heater *3* are movable. Auger analyzer *1*, scanning electron diffractometer *2*, quadrupole mass spectrometer *5* and electron gun *6* are built into the chamber to control the growth process. Ion gun *7* serves for purification of the substrate surface. The growth is controlled by computer *13* incorporating display *14* and printer *12*. The data pertaining to the composition of layers, deposition rate, layer thickness, sequence of deposition, etc., are entered into the computer program. The data are compared to the signals supplied from the measuring instruments, and appropriate control signals are forwarded to the heaters and shutters. The temperature of the crucible is maintained to an accuracy of ± 1 °C which is equivalent to the gallium beam intensity variation within $\pm 2\%$.

Some MBE apparatus incorporate additional means for reading the spectra of backscattering of the low-mass low-energy particles. The method used in the apparatus permits monitoring both the structure and the composition of the growing film. Since the quality of synthesized layers greatly depends on the preparation of the orient-

ing substrate surface, the surface preparation procedure is of particular importance. The samples are first finely ground, polished and treated by chemical etchants, and are then placed into the chamber where they are heated at 600 °C in high vacuum. Commonly, this procedure suffices to expel adsorbed oxygen, although heating fails to remove carbon from the surface. At the same time, a 20% carbon monolayer on the substrate surface results in occurrence of twin crystals because the film growth begins from many nuclei at a time. Efficient removal of atoms of carbon can be effected by cathode sputtering. If a flat surface of gallium arsenide sample is properly polished and etched, sputtering away of four to eight atomic layers is sufficient to reduce the carbon content below the detection capability of the auger spectrograph [38]. After ion bombardment, the defects are removed by short-time heating at a temperature of 350 °C.

The temperature required for growing films of gallium arsenide and ternary compounds based on it is generally from 500 to 600 °C. If the introduction of atoms of gallium limits the rate of growth, it can be given by

$$R = \alpha F_{Ga} \ \mu m/h$$

where $\alpha = (6.18 \cdot 10^{14})^{-1}$; F_{Ga} the current density of Ga atoms, cm^{-2}. In fabrication of doped films with desired electrophysical properties, the injection of the principal components is accompanied by evaporation of impurity from additional crucibles in accordance with the predetermined conditions. This procedure involves certain difficulties because doping results are affected not only by the solubility of the impurity, but also by its ability to adsorb at the surface and fit into the lattice. In addition, the behaviour of amorphous impurities (for example, germanium) depends on the ratio between the beam intensities of the basic components, that is, of gallium and arsenic.

Till now, the mechanisms of impurity adsorption and fitting into the lattice have not been fully understood. For simplicity, all the impurity elements may be divided into two classes, one characterized by a high capture coefficient ($S = 1$), and the other by a low capture coefficient ($S < 1$) [38]. The impurities with a high capture coefficient include Si, Ge, Sn, Mn and Te. These elements permit obtaining a concentration from 10^{18} to 10^{19} cm^{-3} of free carriers of the *n*- or *p*-type. The optimum introduction rate is 10^{11} $cm^{-2} \cdot s^{-1}$.

The impurities having a low capture coefficient (Zn, C, Mg) show poor adsorptivity at a hot GaAs surface. Hence, their incident intensity must be by some orders of magnitude higher than the intensity of impurity beams with $S = 1$. Thus, in experiments on doping the $Al_xGa_{1-x}As$ films with magnesium, the magnesium beam intensity was 10^{14} $cm^{-2} \cdot s^{-1}$, whereas the beam intensities of gallium and arsenic were 10^{15} and $5 \cdot 10^{15}$ $cm^{-2} \cdot s^{-1}$, respectively. Zinc is regarded

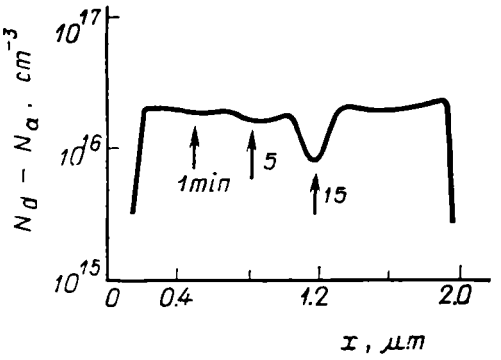

Fig. 9.10. Concentration profile in GaAs with growth interrupted for 1, 5 and 15 min while keeping the substrate heated to 560 °C.

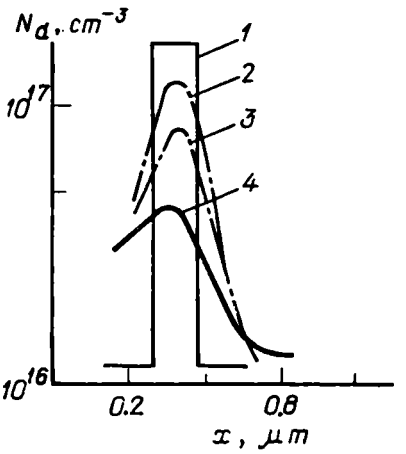

Fig. 9.11. Theoretical (*1*) and measured (*2-4*) profiles of donor concentrations for tin-doped GaAs (temperature of growth, °C: *2*—550, *3*—580, *4*—615).

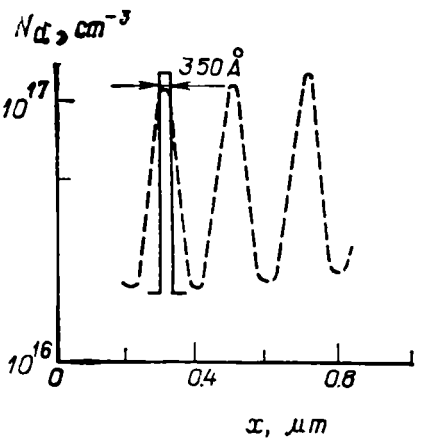

Fig. 9.12. Periodic profiles of donor concentrations for Ge doped GaAs (solid line gives the calculated profile).

unfit for doping of GaAs films fabricated by the MBE method because of its low adsorption energy (1.37 eV). In order for a concentration of zinc atoms on the substrate surface to be maintained at an acceptable level at a substrate temperature of 500 °C, the zinc incident intensity must reach $2.6 \cdot 10^{20}$ $cm^{-2} \cdot s^{-1}$ which is equivalent to a pressure of $1.6 \cdot 10^{2}$ Pa. So far there have been no reports on ion

implantation of impurities in the course of the MBE technique although combining these methods is likely to be advantageous, particularly for elements with $S < 1$.

In films fabricated by the MBE technique and intentionally not subjected to doping, the concentration and mobility of carriers are determined by the residual impurities contained in evaporated source materials. The maximum recorded electron mobility in gallium arsenide films at room temperature was 7600 $cm^2/V \cdot s$ for the concentration of $N_d - N_a = 1.3 \cdot 10^{15}$ cm^{-3}. In p-type films where $N_a - N_d = 2 \cdot 10^{14}$ cm^{-3}, the hole mobility at room temperature was 360 $cm^2/V \cdot s$. The resulting values are commensurate with the values typical for liquid epitaxy.

In growing thin films by any techniques, the transition layer and the constancy of properties of films with thickness always present certain problems. As regards the MBE technique, these problems were studied by the authors of [41]. It was found that a high-resistance layer about 0.2 μm thick (Fig. 9.10) exists at the substrate-film interface. The high-resistance layers occur in all cases when the introduction of components is interrupted, with the substrate remaining hot (at 560 °C). The longer the time of interruption, the higher is the resistance of the transition region in the film grown afterwards. The authors of [41] point out some probable causes of this phenomenon, including evaporation of arsenic from the film, reordering of the surface layers, and contamination of the surface with carbon. Although the actual causes of the occurrence of high-resistance layers were not found, the methods of preventing them were determined. The occurrence of the transition layer at the film-substrate interface can be precluded through additional doping conducted at the initial stages of growth. Another approach consists in that the film growth must proceed without interruptions. When a single pair of crucibles is not enough for synthesis of a film of required thickness, some more evaporators must be provided to be used when required.

Application of the MBE method for fabrication of device structures to a great extent depends on how accurate and controllable can be the doping of the films being grown. Ideally, the doping profile must be in the form of a rectangle whose width depends on the film growth rate and on the instants the impurity beam is turned on and off. In practice, the profiles are distorted due to diffusion, the distortion increasing with the substrate temperature (Fig. 9.11) [42]. The periodic structure obtained with gallium arsenide by successively switching on and off the impurity beam is illustrated in Fig. 9.12 [42]. In this structure, the spacing is 2000 Å. The authors of [43] reported producing a superlattice with a spacing of 1700 Å. There is also a review [40] containing information on fabrication of superlattices with a spacing reaching tens of angstroms.

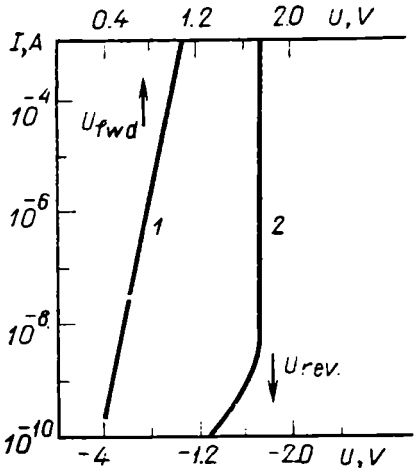

Fig. 9.13. Forward (*1*) and reverse (*2*) branches of *VAC* curve for *p-n* junction in GaAs film produced by the MBE method.

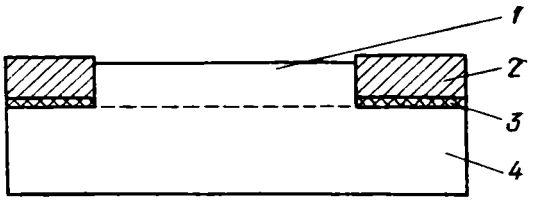

Fig. 9.14. Planar structure fabricated by the MBE method.
1—epitaxial monocrystalline film of GaAs; *2*—high-ohmic polycrystalline GaAs; *3*—SiO_2 film; *4*—substrate of semi-insulating GaAs

The results described above clearly point to the fact that the MBE method is very promising for production of semiconductor devices for wide application. Notable advances have already been made in this field. Thus, a reference [44] gives the results of investigation of the behaviour of the Schottky barrier and of the *p-n* junctions fabricated by the MBE technique with GaAs and $Al_xGa_{1-x}As$ used as source materials. The authors conclude that the properties of such junctions are not inferior to those of the devices fabricated by liquid or gas-transport epitaxy. To illustrate this, Fig. 9.13 shows the forward and reverse branches of the *VAC* curve peculiar of a mesa-diode measuring 100 μm in diameter and etched out in a gallium arsenide film incorporating a *p-n* junction produced by the MBE method. At a later stage, the molecular beam epitaxy was applied for manufacture of avalanche transit time diodes, varactors, mixer diodes, Schottky-barrier field effect transistors, and other kinds of device. These are described in a review [38] and in other original works.

The MBE planar technology proposed in reference [45] deserves special attention. Basically, it consists in that the working surface of a substrate made of gallium arsenide is coated with a SiO_2 film 2000 Å thick where windows of required geometry are etched. After that, the beams of components and impurity are directed to the whole working surface. In the areas protected by the SiO_2 film, a high-resistance polycrystalline gallium arsenide layer is grown

(Fig. 9.14). The impurities with a concentration of not more than 10^{18} cm^{-3} do not reduce the resistance of the polycrystalline material. The substrate located in the windows acts as an orienting agency, with the result that monocrystalline GaAs sections of desired properties grow in these areas. Thus, a planar system is produced consisting of active regions and a half-insulating layer around them. The planes of monocrystalline sections and polycrystalline layer differ in height by the thickness of the SiO_2 film (i.e., by 2000 Å), and in the case of the GaAs films some microns thick, there is no noticeable difference whatsoever. The authors of [45] point out that the proposed method features a good resolving power. In addition to the microelectronic elements, the molecular beam epitaxy permits producing semiconductor optoelectronic devices. According to recent reports, a low-loss waveguide has been constructed [46], and a heterolaser using GaAs-$Al_xGa_{1-x}As$ and running free at room temperature has been contrived [47].

The progress made within a comparatively short time due to application of the MBE method is so impressive that further rapid advances in this field are beyond any doubt.

References

1. Dienes, G., Vineyard, G. *Radiation Effects in Solids.* New York-London, Interscience publishers, 1957, 226.
2. Gorodetsky, A. E., Kachurin, G. A., Smirnov, L. S. Kinetics of new phase formation during ion bombardment. *Fizika i tekhnol. polupr.*, 1968, 2, 7, pp. 927-931 (in Russian).
3. Gorodetsky, A. E., Kachurin, G. A., Pridachin, N. B., Smirnov, L. S. On the feasibility of fabricating thin layers of semiconductor compounds by ion bombardment. *Fizika i tekhnol. polupr.*, 1968, 2, 1, pp. 136-137 (in Russian).
4. Akimchenko I. P., Krasnopevtsev, V. V. Synthesis of compounds by ion implantation: reality and prospects. In: *Proc. of the First USA-USSR Seminar on Ion Implantation.* Albany, USA, 1977, pp. 31-54.
5. Watanabe, M., Tooi, A. Formation of SiO_2 films by oxygen ion bombardment. *Japan J. Appl. Phys.*, 1966, 5, 8, pp. 737-738.
6. Blamires, N. G., Osborne, D. N., Owen, R. B., Stephen, J. *A preliminary study of semiconductor structures produced by ion implantation.* Grenoble, 1967, p. 669.
7. Gusev, V. M., Guseva, M. I., Kurinnyi, V. I., Titov, V. V., Tsyplenkov, V. S., Baranova, V. K., Streltsov, L. N. A study of the properties and employment for the *p-n* junction protection of the oxide film fabricated by oxygen ion implantation of silicon. *Radiotekhnika i elektronika*, 1971, 16, 8, pp. 1462-1467 (in Russian).
8. Astakhov, V. P., Karashev, T. B., Aranovich, R. M. On the mechanism of current conduction and properties of Si_3N_4 ion implanted layers on silicon. *Fizika i tekhnol. polupr.*, 1970, 4, 11, pp. 2128-2132 (in Russian).
9. Demyanov, E. A., Kachurin, G. A., Kuznetsov, O. N. The properties of silicon nitride produced by ion implantation. *Electronnaya tekhnika*, Ser. 2, 1973, 9 (81), pp. 26-28 (in Russian).
10. Borders, J. A., Picraux, S. T., Beezhold, W. Formation of SiC in silicon by ion implantation. *Appl. Phys. Lett.*, 1971, 18, 11.

11. Gerasimenko, N. N., Kuznetsov, O. N., Lezheiko, L. V., Lyubopytova, E. V., Smirnov, L. S., Edelman, F. L. Some properties of SiC films produced by ion implantation in Al-SiC-Si structure. *Mikroelektronika*, 1974, 3, 5, pp. 467-468 (in Russian).
12. Akimchenko, I. P., Galkin, V. V., Krasnopevtsev, V. V., Krasheninnikov, V. S., Milyutin, Yu. V. Optical absorption of germanium subjected to oxygen ion bombardment. *Fizika i tekhnol. polupr.*, 1972, 6, 6, pp. 1182-1184 (in Russian).
13. Akimchenko, I. P., Vavilov, V. S., Galkin, V. V., Ivanov, V. S., Krasnopevtsev, V. V., Milyutin, Yu. V. Synthesis of silicon carbide ion implantation of Si ions in diamond. *Fizika i tekhnol. polupr.*, 1972, 6, 6, pp. 1182-1184 (in Russian).
14. Lezheiko, L. V., Lyubopytova, E. V. The properties of *p-n* and *n-p* heterojunctions produced by ion implantation. *Fizika i tekhnol. polupr.*, 1976, 10, 9, pp. 1749-1751 (in Russian).
15. Fritzsche, C. R., Rothemund, W. Thermal oxidation of silicon after ion implantation. *J. Electrochem. Soc.*, 1973, 120, 11, pp. 1603-1605.
16. Wada, Y., Ashikawa, M. Oxidation characteristics of nitrogen implanted silicon. *Japan J. Appl. Phys.*, 1976, 15, 2, pp. 389-390.
17. Wada, V., Ashikawa, M. Silicon planar devices using nitrogen ion implantation. *Japan. J. Appl. Phys.*, 1976, 15, 9, pp. 1725-1739.
18. Khirny, Yu. M., Solodovnikov, A. P. The enhancement of corrosion resistance in metals irradiated with helium ions. *Dokl. AN SSSR*, 1974, 214, 1, pp. 82-83 (in Russian).
19. Foss, N. A. Formation of $Hg_{1-x}Cd_xTe$ by Hg ion bombardment of CdTe single crystals. *J. Appl. Phys.*, 1968, 39, 13.
20. Hunsperger, R. C., Marsh, O. J. $Ga_{1-x}Al_xAs$ produced by Al^+ ion implantation of GaAs. *Appl. Phys. Lett.*, 1971, 19, 9.
21. Gerasimenko, N. N., Dvurechensky, A. V., Kachurin, G. A., Pridachin, N. B., Smirnov, L. S. Radiation annealing of defects produced by ion bombardment of crystals. *Fizika i tekhnol. polupr.*, 1972, 6, 9, pp. 1834-1835 (in Russian).
22. Bely, I. M., Gumansky, G. A., Karas, V. I., Lomako, V. M., Tashlykov, I. S., Tishkov, V. S. A synthesis of $AlGa_{1-x}As$ and $GaAsP_x$ compounds by Al^+ and P^+ ion implantation in GaAs. *Fizika i tekhnol. polupr.*, 1975, 9, 10, pp. 2027-2029 (in Russian).
23. Kuznetsov, O. N., Lezheiko, L. V., Lyubopytova, E. V., Romanov, S. I. On the conditions of synthesis of structurally perfect layers by ion implantation of monocrystals. Dep. TsIII *Elektronika*, No. 5458/78, Moscow, 1978 (in Russian).
24. Vul, A. Ya., Vul., S. P., Lezheiko, L. V., Lyubopytova, E. V., Kuznetsov, O. N., Saidashev, I. I., Sharonova, L. V., Shik, A. Ya., Shmartsev, Yu. V. Experimental studies of photosensitivity of varizone structures. *Fizika i tekhnol. polupr.*, 1977, 11, 8, p. 1634-1637 (in Russian).
25. Kachurin, G. A., Pridachin, N. B., Smirnov, L. S. The annealing of radiation defects by pulsed laser annealing. *Fizika i tekhnol. polupr.*, 1975, 9, 7, pp. 1428-1429 (in Russian).
26. Kachare, A. H., Spitzer, W. G., Kahan, A., Euler, F. K., Whatley, T. A. Ion implanted nitrogen in gallium arsenide. *J. Appl. Phys.*, 1973, 44, 10, pp. 4393-4399.
27. Smirnov, L. S., Kachurin, G. A., Gorodetsky, A. E. Irradiation of thin CdTe layers with cadmium ions. *Fizika tverd. tela*, 1967, 9, 3, pp. 719-722 (in Russian).
28. Bobylev, B. A., Kachurin, G. A., Pridachin, N. B. Electrical reflection in gallium arsenide implanted layers. In: *Modulation Spectroscopy in Semiconductors and Dielectrics*. Tbilissi, 1975, pp. 86-92 (in Russian).
29. Pridachin, N. B., Kachurin, G. A., Smirnov, L. S. On the mechanism of

the radiation-enhanced diffusion in ion irradiated gallium arsenide. *Fizika i tekhnol. polupr.*, 1974, 8, 10, pp. 1996-1997 (in Russian).
30. Kachurin, G. A., Lezheiko, L. V., Romanov, S. I., Smirnov, L. S., Shmartsev, Yu. V. Epitaxial layer growth in a melt by ion bombardment. *Fizika i tekhnol. polupr.*, 1976, 10, 8, pp. 1549-1551 (in Russian).
31. Kachurin, G. A., Pridachin, N. B., Romanov, S. I., Smirnov, L. S. Production of semiconductor films by radiation methods. In: *Growth and Doping of Semiconductor Crystals and Films.* Novosibirsk, Nauka, 1977, pp. 227-230 (in Russian).
32. Kuznetsov, O. N., Lezheiko, L. V., Lyubopytova, E. V., Smirnov, L. S., Shmartsev, Yu. V., Edelman, F. L. AlN films on Si and Ge. *Fizika i tekhnol. polupr.*, 1976, 10, 11, pp. 2123-2126 (in Russian).
33. Gorbunova, N. A., Gulko, B. N. Formation of adsorption coating on the surface of a solid upon ion beam bombardment. *Elektronnaya tekhnika. Ser. 5*, 1969, 3, pp. 42-48 (in Russian).
34. Takagi, T., Yamada, I., Yanagawa, K. Ionized-cluster beam deposition. In: *Ion Implantation in Semiconductors.* Ed. S. Namba. N. Y.-London, Plenum Press, 1975, pp. 341-346.
35. Colligon, J. S., Grant, W. A., Williams, J. S., Lawson, R. P. W. Deposition of thin films by retardation of an isotope separator beam. In: *Applications of Ion Beams to Materials.* Ed. G. Carter, J. S. Colligon, W. A. Grant. Warwick, The Inst. of Phys., 1976, pp. 357-361.
36. Yagi K., Tamura, S., Tokuyama, T. Germanium and silicon film growth by low-energy ion beam deposition. *Japan J. Appl. Phys.*, 1977, 16, 2, pp. 245-251.
37. Itoh, T., Nakamura, T., Muromachi, M., Sugiyama, T. Low temperature silicon epitaxy by partially ionized vapor deposition. *Japan J. Appl. Phys.*, 1977, 16, 4, pp. 553-557.
38. Cho, A. Y., Arthur, J. R. Molecular beam epitaxy. In: *Progress in Solid-State Chemistry*, 1975, 10, Part 3, p. 157-191.
39. Arthur, J. R. Jr. Interaction of Ga and As_2 molecular beams with GaAs surfaces. *J. Appl. Phys.*, 1968, 39, 8, pp. 4032-4034.
40. Esaki, L., Chang, L. L. Superfine structures of semiconductors grown by molecular-beam epitaxy. *CRC Critical Reviews in Solid Sciences*, 1976, 6, 2, pp. 195-208.
41. Cho, A. Y., Reinhart, F. K. Interface and doping profile characteristics with molecular-beam epitaxy of GaAs: voltage varactor. *J. Appl. Phys.*, 1974, 45, 4, pp. 1812-1817.
42. Cho, A. Y. Impurity profiles of GaAs epitaxial layers doped with Sn, Si, and Ge grown with molecular beam epitaxy. *J. Appl. Phys.* 1975, 46, 4, pp. 1733-1738.
43. Cho, A. Y. Growth of periodic structures by the molecular-beam method. *Appl. Phys. Lett.*, 1971, 19, 11, pp. 467-468.
44. Cho, A. Y., Casey, H. C. Jr. Properties of Schottky barriers and *p-n*-junctions prepared with GaAs and $Al_xGa_{1-x}As$ molecular beam epitaxial layers. *J. Appl. Phys.*, 1974, 45, 3, pp. 1258-1263.
45. Cho, A. Y., Ballamy, W. C. GaAs planar technology by molecular beam epitaxy (MBE). *J. Appl. Phys.*, 1975, 46, 2, pp. 738-785.
46. Merz, J. L., Cho, A. Y. Low-loss $Al_xGa_{1-x}As$ waveguides grown by molecular beam epitaxy. *Appl. Phys. Lett.*, 1976, 28, 8, pp. 456-458.
47. Cho, A. Y., Dixon, R. W., Casey, H. C. Jr., Hartman, R. L. Continuous room temperature operation of GaAs-$Al_xGa_{1-x}As$ double-heterostructure lasers prepared by molecular-beam epitaxy. *Appl. Phys. Lett.*, 1976, 28, 9, pp. 501-503.

CHAPTER 10

DOPING BY NUCLEAR TRANSMUTATION

Electronics places new, often extremely hard requirements upon semiconductor materials. In particular, the demands on homogeneity and precision of doping cannot be satisfied by traditional techniques without obviating growing difficulties. In this connection, more emphasis is being placed nowadays on doping of semiconductors by nuclear transmutation. The doping by nuclear transmutation caused by gamma, neutron, proton, deuteron and alpha-particle irradiation has been known for more than half a century, though the lack of knowledge on radiation processes and behaviour of impurities restrained the application of this doping technique. With progress of radiation physics and accumulation of data pertaining to properties of doping impurities, experimental verification of the new doping technique has been made possible. In the first experiments on doping semiconductor materials by nuclear transmutation germanium was used. Then followed silicon and kinary compounds. Even the first tests revealed specific features of doping by nuclear transmutation. The most important of them include a larger content of radiation-induced defects and artificial radioactivity caused by irradiation. The above-mentioned peculiarities constitute a serious limitation of the technique.

However, the means for minimizing the foregoing limitations can be foreseen even at present. For example, in the case with silicon, a substantial reduction of radioactivity level can be achieved by thorough purification of the ingots of the impurities producing long-lived isotopes on irradiation. At the same time, the reduction of the number of radiation-induced defects requires optimum temperature conditions for irradiation and annealing.

The peculiarities inherent in nuclear transmutation doping also show up as the dependence of the doping results upon the kind of irradiation. Thus, any configuration of the doped region can be porvided by means of proton, neutron and alpha-particle beams. However, since the penetrating power of charged particles is low, the depth of the doped region will be calculated in microns. The use of slow neutrons characterized by a high penetrating power offers strong possibilities for uniform doping of large volumes of semiconductor materials. Practicability of large integral fluxes of slow neutrons is also worthy of notice.

Since neutron irradiation was used in most experiments on nuclear transmutation doping, we shall therefore be content in this chapter with a summary of the main results obtained.

Sec. 10.1. The Concept of Nuclear Reactions [1-7]

According to reference [1], it is assumed that neutrons are divided into groups depending on their energy. Table 10.1 presents the wavelengths and velocities of neutrons belonging to various groups.

Table 10.1

Wavelengths corresponding to various neutron energies [1]

E, eV	T, K	v, cm·s^{-1}	λ, cm	$\lambda/2\pi$, cm	Neutrons and their energies, eV
0.001	11.6	$4.37\cdot10^{4}$	$9.04\cdot10^{-8}$	$1.44\cdot10^{-8}$	Cold, below 0.01
0.025	290	$2.19\cdot10^{5}$	$1.81\cdot10^{-8}$	$2.88\cdot10^{-9}$	Thermal, ~ 0.01-0.1
1.0	$1.16\cdot10^{4}$	$1.38\cdot10^{6}$	$2.86\cdot10^{-9}$	$4.55\cdot10^{-10}$	Resonance, ~ 0.01-50
100	$1.16\cdot10^{6}$	$1.38\cdot10^{7}$	$2.86\cdot10^{-10}$	$4.55\cdot10^{-11}$	Slow, ~ 50-500
10^{4}	$1.16\cdot10^{8}$	$1.38\cdot10^{8}$	$2.86\cdot10^{-11}$	$4.55\cdot10^{-12}$	Moderate-energy, ~ 500-10^{5}
10^{6}	$1.16\cdot10^{10}$	$1.38\cdot10^{9}$	$2.86\cdot10^{-12}$	$4.55\cdot10^{-13}$	Fast, ~ 10^{5}-10^{7}
10^{8}	$1.16\cdot10^{12}$	$1.28\cdot10^{10}$	$2.79\cdot10^{-13}$	$4.43\cdot10^{-14}$	Ultrahigh-energy, ~ 10^{7}-10^{9}
10^{10}	$1.16\cdot10^{11}$	$2.99\cdot10^{10}$	$1.14\cdot10^{-14}$	$1.81\cdot10^{-15}$	Ultrafast (relativistic), above 10^{9}

Notes: 1. The distribution of thermal neutrons is given by

$$dn(v) = Av^2 \exp(-Mv^2/2kT), \tag{10.1}$$

where v is the velocity of neutrons; n is their number; M is their mass.

2. The wavelength of the neutron with the energy E (or velocity v and pulse P) is expressed by

$$\lambda = h/P \approx h/(2ME)^{1/2} \quad \text{when} \quad v \ll c, \tag{10.2}$$

where h is the Planck constant.

The majority of reactions involving neutrons occur in two stages, with a compound excited nucleus formed during the first stage, and with subsequent dissociation occurring during the second stage, that is

$$A + n \rightarrow C \rightarrow B + a \tag{10.3}$$

that can be reduced to

$$A\,(n,\ a)\,B. \tag{10.4}$$

There are several ways in which the compound nuclei formed in an excited state can disintegrate, for example, irradiation (n, γ), neutron scattering (n, n), and also emission of one or more particles. These processes compete, each being characterized by a mean life-

time τ_i (that is, by the lifetime that would be possessed by an excited state if all other disintegration mechanisms were impossible). The mean lifetime of an excited state

$$1/\tau = \sum_i 1/\tau_i \tag{10.5}$$

is related to the final width (energy diffuseness) of the compound nucleus excited level as follows:

$$\Gamma = \hbar/\tau, \tag{10.6}$$

where $\hbar = h/2\pi$; h is the Planck constant. Accordingly, the partial width corresponding to the i-th disintegration mechanism may be given by

$$\Gamma_i = \hbar/\tau_i. \tag{10.7}$$

Thus,

$$\Gamma = \sum_i \Gamma_i. \tag{10.8}$$

Assuming that the reaction involving neutrons occurs in two stages (formation of a compound nucleus, and subsequent emission of the particle a), the expression for the cross-section of the reaction (n, a) is

$$\sigma\,(n, a) = \sigma_c \Gamma_a/\Gamma. \tag{10.9}$$

The first factor σ_c denotes the cross-section of absorption of an incident neutron resulting in the formation of an excited compound nucleus, and the other factor gives relative probability of disintegration of the compound nucleus with emission of the particle a.

The cross-section of the formation of the compound nucleus shows a strong dependence on how close is the value of excitation energy to that of a level of the compound nucleus. When a single level of the compound nucleus is important, the dependence of the value σ_c upon the energy is expressed by the known resonance formula

$$\sigma_c = \lambda^2/(4\pi)\, f\Gamma_n\Gamma/((E - E_r)^2 + \Gamma^2/4), \tag{10.10}$$

whence

$$\sigma_a = \lambda^2/(4\pi)\, f\Gamma_n\Gamma_a/((E - E_r)^2 + \Gamma^2/4), \tag{10.11}$$

where E_r is the kinetic energy of a neutron at which the excitation energy is equal to the difference between the ground state energy and the energy of the compound nucleus level which determines the progress of the reaction; and f is the statistical weight depending on the neutron spin ($S = 1/2$), on the target nucleus spin I, and on the spin of the compound nucleus level of interest, J:

$$f = (2J + 1)/[(2I + 1)\,(2S + 1)] = (2J + 1)/(2I + 1)/2. \tag{10.12}$$

Apart from the resonance scattering, there exists another kind of elastic scattering described in terms of scattering from an impenetrable sphere, that is, potential scattering.

Turning to thermal neutrons, there is a case of special interest when the first resonance resides far above or below the region of thermal energies ($|E_r| \gg E_t$, $|E - E_r| \gg \Gamma$). In this case,

$$\sigma_t(n, a) = \lambda^2/(4\pi)\,\Gamma_n\Gamma_a/E_r^2. \tag{10.13}$$

Considering that $\lambda/(2\pi) \simeq E^{-1/2}$ and $\Gamma_n \simeq E^{1/2}$ provided that the value of Γ_a remains constant in the region of thermal energies, we arrive at the following expression for the cross-section

$$\sigma_t(n, a) = \sigma^*\,(E^*/E)^{1/2} = \sigma^*\,(v^*/v), \tag{10.14}$$

where σ^* is the cross-section specified for a certain optional energy E^* (velocity v^*). The above expression represents the well-known law $1/v$ for the cross-section of the reaction involving slow neutrons far from the resonance.

Let us now discuss the kinds of reactions involving neutrons.

Scattering (n, n). Since this reaction does not result in nuclear transmutation doping, we shall omit it.

Radiative capture (n, γ). In studying and practical application of radiative capture, the size of the cross-section of capture of thermal neutrons $\sigma_t(n, \gamma)$ is of particular interest. It is defined as mean cross-section of the reaction (n, γ) for slow neutrons whose energy distribution obeys the Maxwell law [ref. (10.1)]:

$$\sigma_t(n, \gamma) = \int_0^{E_1} \sigma(n, \gamma)\,d\varphi(E, E_0) \Big/ \int_0^{E_1} d\varphi(E, E_0). \tag{10.15}$$

The energy E_1 is chosen high enough with the result that only a minor portion of the Maxwell distribution corresponds to the energies $E > E_1$ (if a cadmium energy absorber is used, $E_1 \approx 0.4$ eV; with $E_0 = 1/40$ eV, the number of neutrons with the energy $E > E_1$ is less than 10^{-4}).

If the value of $\sigma(n, \gamma)$ versus energy E is known, the value of σ_t can be calculated directly. In the nuclei with the first resonance residing relatively far from the region of thermal energies, the cross-section of the reaction (n, γ) obeys the law $1/v$, that is

$$\sigma(n, \gamma) = \sigma_0 v_0/v$$

and then

$$\sigma_t = \sigma_0 v_0 \int_0^{E_1} v^2 \exp(-v^2/v_0^2)\,dv \Big/ \int_0^{E_1} v^3 \exp(-v^2/v_0^2)\,dv = \sqrt{\pi}\,\sigma_0/2. \tag{10.15a}$$

If the resonance resides in the thermal region, then the cross-section of the reaction (n, γ) for thermal neutrons does not obey the law $1/v$.

In case of light and medium-weight nuclei, the cross-section of the reaction (n, γ) turns out to be small for the intermediate-energy neutrons because $\Gamma_\gamma \ll \Gamma_n$. In case of heavy nuclei, the radiation capture cross-section is still quite significant in the above energy range.

Reaction with emission of charged particles. The reactions (n, p) and (n, α) are most frequent among other possible reactions. For a given reaction to compete advantageously with other types of reactions, the particle must have an energy high enough to provide for a marked probability of surmounting the Coulomb barrier. If slow neutrons are involved, the reactions (n, p) and (n, α) are practicable only with some light nuclei (see Table 10.2).

Table 10.2

Characteristics of some exoenergetic reactions (n, p) and (n, α) [1]

Reaction	Energy liberated in reaction, MeV	Isotope cross-section measured for $v_0 = 2200$ m/s, 10^{-24}, cm^2	Relative isotope content in natural mixture, %
He^3 (n, p) T^3	0.7637	5060±200	(1-10) 10^{-5}
Li^6 (n, α) T^3	4.785	910±100	7.4
B^{10} (n, α) Li^7	2.791	3837±110	18.83
N^{14} (n, p) C^{14}	0.626	1.76±0.05	100
Cl^{35} (n, p) S^{35}	0.62	~0.3	75.4

Reaction $(n, 2n)$. During the reaction $(n, 2n)$, the heat of the reaction is equal to the neutron binding energy in the target nucleus. The nucleus produced by such a reaction is an isotope of the target nucleus; it is found to be radioactive in many instances, and often disintegrates by emission of positrons.

According to the periodic table, the neutron binding energy varies from 1.85 MeV for Be^9 to about 20 MeV for C^{12}. The thresholds of the reaction $(n, 2n)$ for some elements [2] are tabulated below:

Nucleus	Neutron energy, MeV	Nucleus	Neutron energy, MeV
Be^9 . . .	1.85	Al^{27} . . .	13.2
Be^{10} . . .	9.4	Si^{28} . . .	17.4
B^{11} . . .	12.6	Si^{29} . . .	8.7
C^{12} . . .	20.3	P^{31} . . .	12.6
N^{14} . . .	11.3	S^{32} . . .	15.3
O^{16} . . .	17.3		

Most experiments on nuclear transmutation doping were conducted with use of reactors. In the reactor, the energy distribution $\varphi(E)$ of neutrons covers a wide range, from 0.001 eV up to 10 MeV. The peak of distribution falls on slow neutrons. We know that neutrons with energies above the threshold energy of the reactions (n, p), (n, α) and $(n, 2n)$ constitute but a minor fraction of the reactor emission, so we should expect that transmutations (n, γ) involving thermal and apithermal neutrons, and resonance absorption will dominate in doping of semiconductors by nuclear transmutation.

Sec. 10.2. Silicon Doping by Nuclear Transmutation

The feasibility of doping silicon by nuclear transmutation becomes obvious from the reactions (n, γ) involving slow neutrons and silicon nuclei:

$$Si^{28}(n, \gamma)Si^{29}; \quad Si^{29}(n, \gamma)Si^{30}; \quad Si^{30}(n, \gamma)Si^{31} \xrightarrow[2.62\ h]{\beta^{-1}} P^{31}. \tag{10.16}$$

It therefore follows that the resulting nonstable isotope Si^{31} disintegrates and forms a stable phosphorus isotope which constitutes a donor impurity in silicon and is widely used in practice. The isotope composition of silicon and the cross-section of the reaction (n, γ) are shown in Table 10.3.

Table 10.3

Cross-section of absorption of thermal neutrons by silicon isotopes [8]

Isotope	Isotope content in natural mixture, %	Effective cross-section, 10^{-24} cm^2	End product
Si^{28}	92.27	0.08±0.03	Si^{29}, stable
Si^{29}	4.68	0.27±0.09	Si^{30}, stable
Si^{30}	3.05	0.11±0.01	$Si^{31} \xrightarrow{\beta^{-1}} P^{31}$
Si	Total	0.13±0.03	

The content of injected phosphorus can be calculated by the formula

$$N_{P31} = Nk\sigma\varphi t, \tag{10.17}$$

where N is the quantity of silicon atoms per unit volume; k is the relative content of isotope Si^{30} in the natural mixture; σ is the activation cross-section of the reaction $Si^{30}(n, \gamma)Si^{31}$; φ is the slow neutron flux density; and t is the irradiation time.

Substituting the known values of N, k and σ, we can write

$$N_{P31} \approx 2 \cdot 10^{-4}\varphi t. \tag{10.18}$$

The amount of compensating impurities of aluminium and magnesium injected during the reactions (n, α) and $(n, 2n)$ is rather small because of the small cross-sections of the reactions and an insignificant fraction of fast neutrons in the general flux of the reactor neutrons [9].

The homogeneity of doping depends on three factors [10]:

(1) distribution of the neutron flux in the irradiation zone;

(2) scattering and partial absorption of the neutron flux by the crystal;

(3) contamination of the original material by doping elements.

In modern nuclear reactors of about 100 mm in diameter and not more than 500 mm in length, the homogeneity of the thermal neutron flux may be $\pm 5\%$ or better.

The results of variation of the neutron flux homogeneity in the ingots were experimentally verified by using ingots with a diameter of 50 mm and a length of 50 mm [10]. The maximum variation of activity of Si^{31} in the center of the ingot was found to be less than 1% both after irradiation by thermal neutrons alone, and after combined irradiation by thermal and fast neutrons. Similar results were obtained with silicon doped with boron ($\rho = 5.0$ ohm·cm) although the neutron capture cross-section in boron is large.

A high concentration of defects is revealed in the volume of silicon due to irradiation by fast neutrons, γ-radiation and β-decay. The atoms of silicon involved in the reactions (n, γ) provide quite an efficient means of defect production. The recoil energy imparted to the nucleus when a γ-quantum is emitted is expressed by the formula corollary of the laws of conservation of energy and pulse [8, 11]

$$E_{\text{recoil}} = .537\ (h\nu)^2/A, \tag{10.19}$$

where E_{recoil} is the nucleus recoil energy, eV; A is the recoil nucleus atomic weight; and $h\nu$ is the γ-quantum energy, MeV. Some authors [8, 11] estimate the mean recoil energy $R_{\text{mean recoil}}$ at 780 eV. The maximum recoil energy may reach 2010 eV [8].

The induced radioactivity of silicon presents certain problems. The surface radioactivity basically differs from the volume radioactivity of silicon. The surface radioactivity comprises the radioactivity of impurities remaining at the surface of a silicon sample, and the radioactivity of products of corrosion and the reactor materials sputtered during the reaction. As for the volume activity, it is caused by nuclear reactions with the existing impurities and atoms of the matrix. For minimizing the activity related to the presence of impurities, the material subject to nuclear transmutation doping should not contain nuclei producing long-lived isotopes during reactions.

The activity of Si^{31} formed by doping reduces to zero in three days. Among the doping impurities (such as boron and phosphorus), the

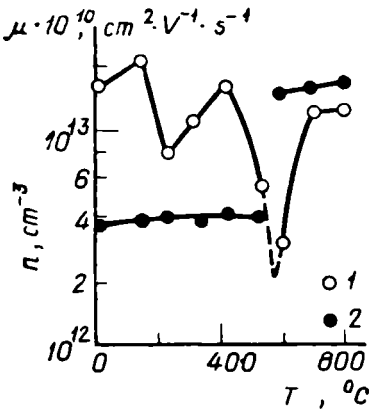

Fig. 10.1. Carrier concentration (*1*) and their mobility (*2*) in irradiated silicon vs annealing temperature [12]. Neutron dose, about $6 \cdot 10^{16}$ cm^{-2}, ρ_{orig} = = 3-6 kilohm·cm. Conversion of conductivity from *p* to *n* is observed at above 575 °C

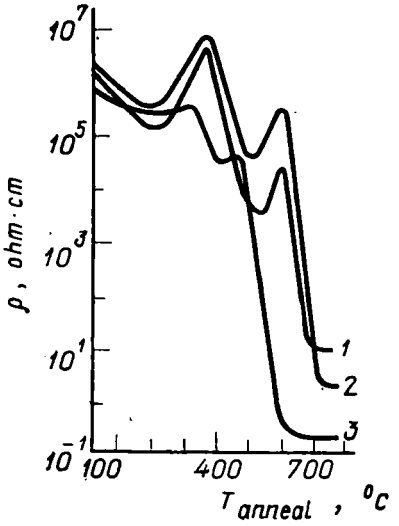

Fig. 10.2. Isochronal annealing of resistivity of *n*-type silicon samples irradiated at 50 °C [13]. *1*—ρ = 500 ohm·cm, $\Phi = 10^{18}$ cm^{-2}; *2*—ρ = 500, $\Phi = 10^{19}$; *3* — ρ = 0.3, $\Phi = 10^{18}$

long-lived isotope is inherent only in phosphorus (P^{32}). The production of phosphorus P^{32} by nuclear reactions is insignificant.

After their radioactive emission drops to a safe level, the irradiated samples of silicon are subjected to annealing at a temperature in the range from 700 to 1000 °C. Figs. 10.1 and 10.2 show the curves of isochronal annealing of changes in the basic parameters of the semiconductor material, including the resistivity, mobility and carrier concentration [12, 13]. Kinetics of annealing radiation defects is of particular interest of itself, but its discussion is beyond the scope of this chapter.

The annealing in the temperature range of 500 to 600 °C sharply reduces the resistance (see Fig. 10.2), the fact attributable to annealing of radiation defects. The temperature required for complete annealing of changes in the parameters of the material is $\geqslant$800 °C.

The comparison of phosphorus concentrations measured experimentally in terms of variation of the carrier concentration, with those estimated theoretically by formulae (10.17) and (10.18) shows a very close coincidence between the experimentally-measured and calculated concentrations in the case of silicon produced by zone refining (Fig. 10.3) [12-14]. At the same time, with silicon fabricated by the melt pulling technique, the concentration of electrons exceeds the calculated value, and increases with the concentration of oxygen in the original material. The authors of [13] ascribe the formation of additional donor centers to occurrence of defects which are stable up to $T \geqslant 1000$ °C and contain oxygen.

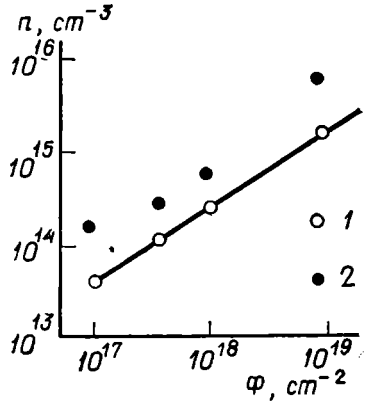

Fig. 10.3. Donor concentration is Si vs irradiation dose (after irradiation and annealing at $T = 800$ °C) [13].
1—silicon produced by zone refining; *2*—silicon produced by melt pulling. The solid line gives the theoretical accumulation of phosphorus as a result of reaction Si^{30} (n, γ) $Si^{31} \rightarrow P^{31}$

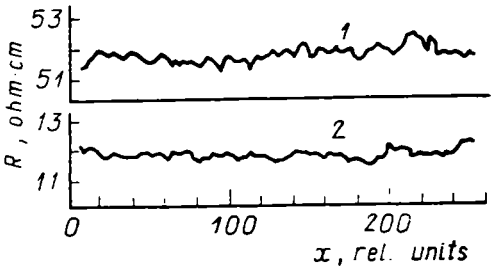

Fig. 10.4. Resistivity profile in radiation-doped silicon grown by crucibleless zone refining [9, 14]
1—$N_D/N_A \approx 20$, spread ±2%; *2*—$N_D/N_A \approx 14$, spread 4%

Measurements of resistivity microdistribution in radiation-doped silicon (Fig. 10.4) reveal a fairly uniform distribution of phosphorus in the volume of the samples [9, 10].

Production and annealing out of defects result in redistribution of the impurity, such as oxygen, contained in the original silicon

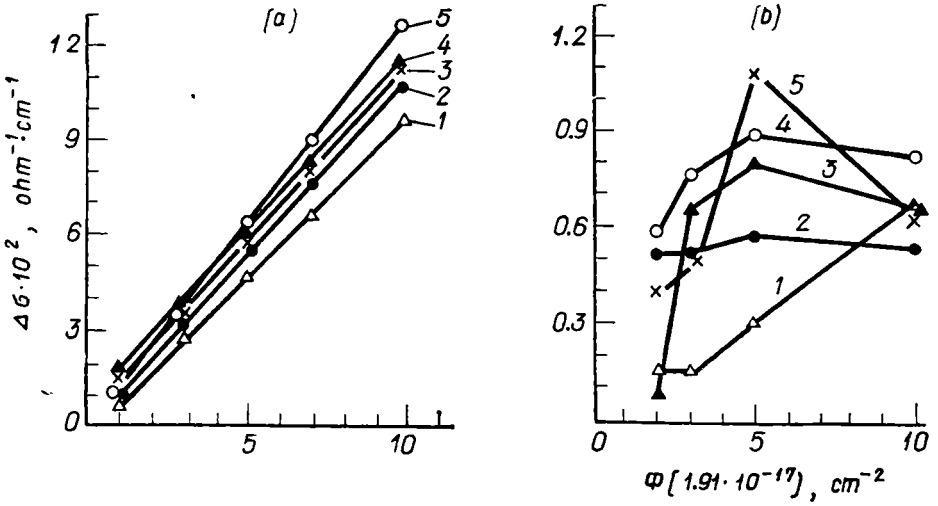

Fig. 10.5. Variations of Si crystal conductivity after reactor neutron irradiation without protection (*a*) and when placed inside a cadmium case (*b*) at $T_{anneal} = 1050$ °C [17].
Correspondence of the curves in the figure to the samples indicated in Table 10.4 is as follows: (*a*) *1*—1, *2*—6, *3*—3, *4*—4, *5*—theoretical calculation, (*b*) *1*—1, *2*—3, *3*—4, *4*—5, *5*—6

[15, 16]. The atoms of phosphorus injected by nuclear transmutation also undergo redistribution [17]. This process is due to a specific nature of doping by transmutation. Some atoms of Si^{31} formed by the reaction (n, γ) (10.16) remain in interstitial positions and can be attracted to sinks even before transmutation to the atoms of phosphorus. Fig. 10.5*a*, *b* illustrates the relationships between the conduction variation $\Delta\sigma$ and the dose of reactor neutrons for silicon samples grown under different conditions [17]. The characteristics of the samples are presented in Table 10.4.

The experimental values of $\Delta\sigma$ were found to be less than the theoretical ones determined by formula (10.17). It is assumed by the authors of [17] that when the growth rates are low, the impurities have enough time to condense at dislocations. In crystals grown at a rate of 8 mm/min, the diffusion of impurities toward grown defects is limited. In addition, since the impurity content in these crystals was low, one should agree with the supposition [17] that dislocations occurring in such crystals are more "refined", with the result that some fraction of atoms of phosphorus formed by the reaction (10.16) will precipitate there.

Table 10.4

Parameters of original crystals [17]

Sample No.	Rate, mm/min, and growing medium	Dislocation density, cm^{-2}	Resistivity, ohm·cm
1	8 (vacuum)	10^4	$6 \cdot 10^3$
2	2.2 (vacuum)	$\sim 5 \cdot 10^4$	180
3	3 ($90Ar + 10H_2$)	0	260
4	2 ($90Ar + 10H_2$)	0	90
5	2 ($90Ar + 10H_2$)	0	190
6	3.2 (vacuum)	$\sim 5 \cdot 10^4$	50

For some crystals within the initial portions of the curves shown in Fig. 10.5 the opposite was true, i.e. the experimental values of $\Delta\sigma$ exceeded the calculated ones. It is assumed that during irradiation and subsequent annealing, a fraction of atoms of phosphorus undergo activation although in the original crystal they remained in an electrically passive state. This phenomenon is illustrated in Fig. 10.5*b*. The deficient or excessive concentration of electrically active phosphorus in *n*-type silicon depends on the effects of two competing processes: in one case it is the decomposition of the "biographical" defects and transition of phosphorus to the active state, and in the other, it is the realization of the conditions favourable for the reverse process, that is, the formation of thermostable complexes at grown and radiation induced defects with the result that phosphorus bonds are satisfied. Some references [9, 18] point out that radiation-doped silicon is stable to subsequent radiation and thermal treat-

ment. According to reference [18], after two samples of n-type silicon ($N_A/N_D \approx 0.2$) with an initial concentration of electrons amounting to 12 and $5.1 \cdot 10^{12}$ cm^{-3} and with a conductance of 12.7 and $7.15 \cdot 10^{-4}$ ohm$^{-1} \cdot$cm^{-1} were subjected to gamma irradiation with a dose of $4 \cdot 10^{17}$ cm^{-2}, the parameters of the material have changed respectively to 10 and $4.6 \cdot 10^{12}$ cm^{-3}, and 10.6 and $6.45 \cdot 10^{-4}$ ohm$^{-1} \cdot$cm^{-1}. In the n-Si samples treated by conventional techniques and having initial parameters similar to those mentioned above, the concentration of electrons and conductance are affected quite substantially.

The lifetime values typical for carriers after radiation doping and annealing at a temperature of about 800 °C do not commonly exceed 10 to 15 μs for crucibleless silicon, and in the case of silicon produced by the Czochralski method, they are in the range from 25 to 50 μs [9]. However, the lifetime values for carriers of radiation-doped materials, as opposed to the so-called conventional silicon, do not essentially change during subsequent heat treatment in fabrication of p-n junctions, and are sufficiently high for production of semiconductors having good electrical parameters.

Sec. 10.3. Germanium Doping by Nuclear Transmutation

K. Lark-Horowitz was the first to discuss the feasibility of doping by nuclear transmutation [19]. He took part in experiments on irradiation of germanium by slow neutrons. The cross-section data are listed in Table 10.5. The concentration of atoms produced by each type of transmutation can be calculated by the formula similar to (10.17) by substituting the appropriate parameter values.

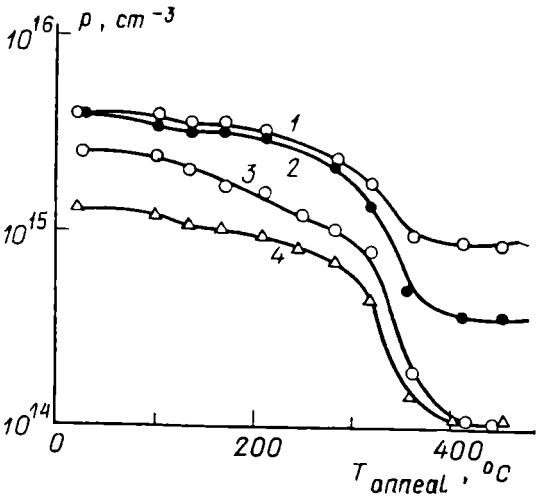

Fig. 10.6. Isochronal annealing of neutron irradiated germanium
1—sample ГДГ-15, $\Phi = 2 \cdot 10^{16}$ cm^{-2}, $T_{anneal} = 78$ K; *2*—sample ГЭМ-4, Φ and T_{meas} are as in *1*; *3*—sample ГД, pure, $\Phi = 5 \cdot 10^{15}$ cm^{-2}, $T_{meas} = 293$ K; *4*—same, $\Phi = 5 \cdot 10^{15}$ cm^{-2}, $T_{meas} = 78$ K (data supplied by the author)

In experiments conducted by K. Lark-Horowitz, the germanium monocrystals irradiated by slow neutrons were removed from the reactor and subjected to long-time annealing at a temperature of 450 °C. The isochronal annealing of similar samples is illustrated in Fig. 10.6. Like in the case with silicon, the annealing procedure

I. *Major reactions involving deuterons and slow neutrons*

	$(d, p), (n, \gamma)$	(d, n)
Ge^{70}	$Ge^{71} \xrightarrow{11.4\ days} Ga^{71}$	$As^{71} \xrightarrow{50\ h} Ge^{71} \xrightarrow{11.4\ days} Ga^{71}$
Ge^{72}	Ge^{73}	$As^{73} \xrightarrow{76\ days} Ge^{73}$
Ge^{73}	Ge^{74}	$As^{74} \xrightarrow{17.5\ days} \begin{cases} Ge^{74} \\ Se^{74} \end{cases}$
Ge^{74}	$Ge^{75} \xrightarrow{82\ min} As^{75}$	As^{75}
Ge^{76}	$Ge^{77} \xrightarrow{12\ h\ 59\ s} As^{77} \xrightarrow{40\ h} Se^{77}$	$As^{77} \xrightarrow{40\ h} Se^{77}$

II. *Major reactions involving fast neutrons*

	(n, p)	$(n, 2n)$	(n, α)
Ge^{70}	$Ga^{70} \xrightarrow{20\ min} Ge^{70}$	$Ge^{69} \xrightarrow{40\ h} Ga^{69}$	Zn^{67}
Ge^{72}	$Ga^{72} \xrightarrow{14.3\ h} Ge^{72}$	$Ge^{71} \xrightarrow{11.4\ days} Ga^{71}$	$Zn^{69} \xrightarrow{14\ h\ 52\ min} Ga^{69}$
Ge^{73}	$Ga^{73} \xrightarrow{5\ h} Ge^{73}$	Ge^{72}	Zn^{70}
Ge^{74}	$Ga^{74} \xrightarrow{?} Ge^{74}$	Ge^{73}	$Zn^{71} \xrightarrow{2.2\ min} Ga^{71}$
Ge^{76}	$Ga^{76} \xrightarrow{?} Ge^{76}$	$Ge^{75} \xrightarrow{82\ min} As^{75}$	$Zn^{73} \xrightarrow{< 2\ min} Ga^{73} \xrightarrow{5\ h} Ge^{73}$

III. *Major reactions involving alpha-particles*

	(α, n)	$(\alpha, 2n)$	(α, p)
Ge^{70}	$Se^{73} \xrightarrow{7.1\ h} As^{73} \xrightarrow{76\ days} Ge^{73}$	$Se^{72} \xrightarrow{9.7\ days} As^{72} \xrightarrow{26\ h} Ge^{72}$	$As^{73} \xrightarrow{76\ days} Ge^{73}$
Ge^{72}	$Se^{75} \xrightarrow{127\ days} As^{75}$	Se^{74}	As^{75}
Ge^{73}	Se^{76}	$Se^{75} \xrightarrow{127\ days} As^{75}$	$As^{76} \xrightarrow{26.8\ h} \begin{cases} Ge^{76} \\ Se^{76} \end{cases}$
Ge^{74}	Se^{77}	Se^{76}	$As^{77} \xrightarrow{40\ h} Se^{77}$
Ge^{76}	$Se^{79} \xrightarrow{?} Br^{79}$	Se^{78}	$As^{79} \xrightarrow{?} Se^{79} \xrightarrow{?} Br^{79}$

is intended for removing the radiation defects caused by gamma radiation and recoil nuclei.

The above Table gives is a summary list of possible reactions with germanium isotopes involving neutrons, deuterons and alpha-particles [19]. Irradiation with fast neutrons results in the formation of impurity atoms of lower atomic numbers. For example, the reaction (n, p) yields gallium turning later to germanium, and the reaction (n, α) yields zinc partly turning to gallium and partly changing into germanium. The procedure of irradiation of germanium with deuterons and alpha-particles involves for the most part injection

Table 10.5

Cross-section of capture of thermal neutrons by germanium isotopes [11, 19]

Isotope	Content, %	Cross-section of capture (n, γ), 10^{-24} cm^2	Recoil energy, eV	End product
Ge^{70}	20.45	3.4 ± 0.3	197	*Ga*
Ge^{72}	27.41	0.98 ± 0.09	161	*Ge*
Ge^{73}	7.77	14 ± 1	184	*Ge*
Ge^{74}	36.58	0.62 ± 0.06	149	*As*
Ge^{76}	7.79	0.36 ± 0.07	118	*Se*
Ge	Natural mixture	2.45 ± 0.20	—	—

of arsenic because this kind of irradiation is favourable for manufacture of materials possessing electron conduction. There is however a serious hindrance to germanium doping by nuclear transmutation consisting in long-time radioactivity of irradiated samples.

Sec. 10.4. Doping of Binary Compounds by Nuclear Transmutation

In discussing the doping of binary compounds by nuclear transmutation, let us consider an example of the $A_{III}B_V$ compounds, such as GaAs and InSb. When these semiconductors are irradiated with slow neutrons, the following (n, γ)-reactions take place

$$\begin{aligned}
&Sb^{121}(n, \gamma)\,Sb^{122} \xrightarrow{2.8\ \text{days}} Te^{122}; \quad Sb^{123}(n, \gamma)\,Sb^{124} \xrightarrow{60.4\ \text{days}} Te^{124};\\
&In^{113}(n, \gamma)\,In^{114} \xrightarrow{72\ \text{s}} Sn^{114}; \quad In^{115}(n, \gamma)\,In^{116} \xrightarrow{13.4\ \text{s}} Sn^{116};\\
&Ga^{69}(n, \gamma)\,Ga^{70} \xrightarrow{21.1\ \text{min}} Ge^{70}; \quad Ga^{71}(n, \gamma)\,Ga^{72} \xrightarrow{14.1\ \text{h}} Ge^{72};\\
&As^{75}(n, \gamma)\,As^{76} \xrightarrow{26.4\ \text{h}} Se^{76}.
\end{aligned} \tag{10.20}$$

Table 10.6 presents the cross-sections of absorption of thermal neutrons by stable isotopes of indium, gallium, antimony and arsenic.

Table 10.6

Absorption cross-section of thermal neutrons [20, 21]

Isotope	Isotope content, %	Absorption cross-section, 10^{-24} cm^2	End product
In^{113}	4.23	58±13	Sn^{114} (98%); Cd^{114} (1%)
In^{115}	95.77	200±20	Sn^{116}
Sb^{121}	57.25	5.7±0.5	Te^{122} (97%); Sn^{122} (3%)
Sb^{123}	42.75	3.9±0.3	Te^{124}
Ga^{69}	60.00	1.99±0.16	Ge^{70}
Ga^{71}	40.00	4.9±0.4	Ge^{72}
As^{75}	100.00	4.1±0.2	Se^{76}

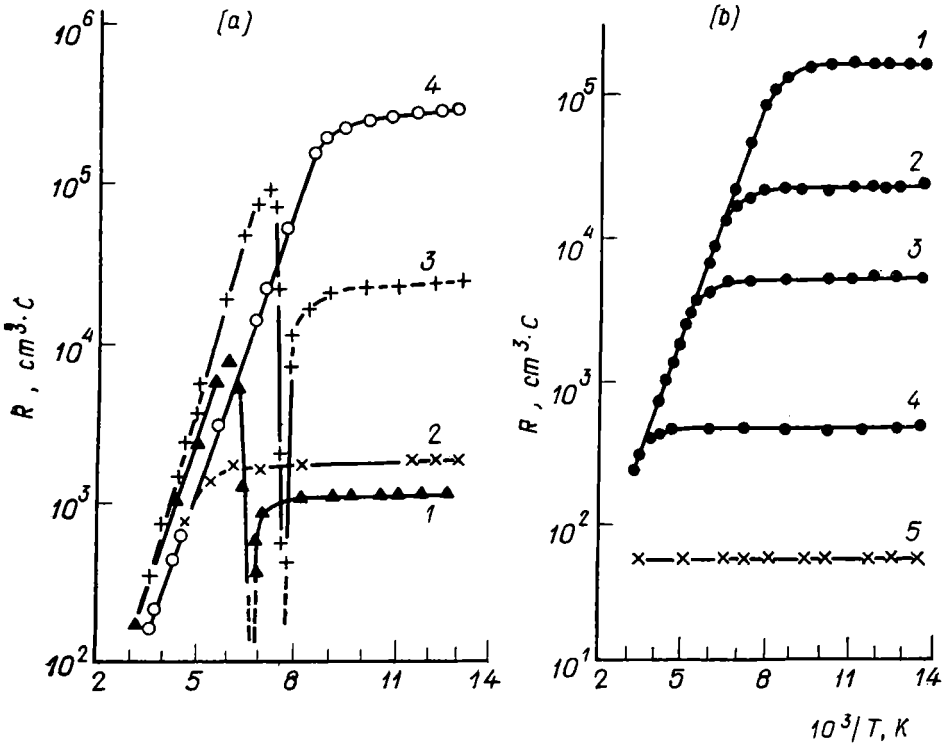

Fig. 10.7. Dependence of Hall constant on reciprocal of temperature for InSb of *p*- (*a*) and *n*-type (*b*), irradiated with slow neutrons [20].
(*a*) *1*—before irradiation; after irradiation with fluxes (cm^{-2}) and annealing: *2*—$1.04 \cdot 10^{16}$; *3*—$5.09 \cdot 10^{15}$, *4*—$5.34 \cdot 10^{15}$; (*b*) *1*—before irradiation; after irradiation with fluxes (cm^{-2}) and annealing: *2*—$4.35 \cdot 10^{14}$, *3*—$1.27 \cdot 10^{15}$; *4*—$1.02 \cdot 10^{16}$, *5*—$9.12 \cdot 10^{16}$

The results of irradiation of InSb crystals with neutrons described in work [20] are shown in Fig. 10.7*a*, *b*. The measurements were taken after long-time annealing in vacuum at 650 to 675 K (for the *p*-type samples) and at 620 K (for the *n*-type samples).

The resonance absorption of slow neutrons at isotopes of gallium and arsenic must also be taken into account in theoretical evaluation of the effects of doping GaAs by nuclear transmutation. Work [21] provides a comparison between the experimental data and the calculations considering the actual temperature of neutrons and the resonance absorption. An integral neutron flux was $2.94 \cdot 10^{18}$ cm^{-2}. Annealing was carried out at a temperature of 650 to 700 °C in arsenic environment. The experimental data are listed in Table 10.7.

The transmutative impurity content was greatly reduced in the samples kept under a radiation screen during irradiation. Sample 8 half protected by a cadmium and an indium screens (with an attenuation factor of 25) was one of those in which a *p-n* junction was produced by means of the screens. The junction region could be observed visually after appropriate etching [21]. The properties of such junctions are compatible with the properties of junctions manufactured by other methods.

Table 10.7

Results of GaAs doping by nuclear transmutation [21]

Sample	Conduction type	Before irradiation		Screen thickness, mm	Calculated transmutation concentration, 10^{-16} cm^{-3}		After irradiation and annealing			
							Unscreened		Screened	
		Concentration, 10^{-16} cm^{-3}	Mobility, 10^{-2} cm$^2 \cdot$ V$^{-1} \cdot$ s^{-1}		Unscreened	Screened	Concentration, 10^{-16} cm^{-3}	Mobility, 10^{-3} cm$^2 \cdot$ V$^{-1} \cdot$ s^{-1}	Concentration, 10^{-16} cm^{-3}	Mobility, 10^{-3} cm$^2 \cdot$ V$^{-1} \cdot$ s^{-1}
1	*n*	0.45	48.50	—	40.3	—	44.5	3.3	—	—
2	*n*	0.43	51.00	2 (Cd)	—	4.75	—	—	4.17	7.27
3	*n*	0.46	46.00	4 (Cd)	—	—	—	—	3.67	5.50
4	*n*	0.51	47.20	2 (Cd), 1 (In)	—	1.70	—	—	1.84	3.90
5	*p*	0.53	26.50	—	40.3	—	37.5	3.8	—	—
6	*p*	0.42	2.55	2 (Cd)	—	4.75	—	—	3.86	4.65
7	*p*	7.25	2.97	6 (Cd)	40.3	—	45.0	3.3	3.91	0.20
8	*p*	6.64	2.85	4 (Cd), 1 (In)	40.3	1.70	41.0	3.9	5.20	0.31
9	*p*	6.80	2.17	4 (Cd), 1 (In)	40.3	1.70	46.0	3.3	5.10	0.26
10	*p*	2.50	2.34	—	40.3	—	17.8	3.5	—	—
11	*p*	6.65	1.86	—	40.3	—	20.3	0.125	—	—

Sec. 10.5. Advantages and Disadvantages of Nuclear Transmutation Doping

Let us discuss now the substantial advantages and disadvantages of the method of nuclear transmutation doping. The advantages of the method are as follows:

1. *Predictability* of the results of doping, and *easy control* of the process. Transmutation doping completely depends on nuclear processes and may proceed independently of the irradiation conditions.

2. *Uniformity* of doping. In treating this problem, one should consider definite conditions, including the kind of irradiation, semiconductor material, required region of uniform doping. During irradiation with charged particles (protons, deuterons and alpha-particles), uniform doping should be expected to occur only in the layers with a thickness of units or tens of microns depending on the energy of the particles. Therefore, uniform doping of ingots is possible only if they are irradiated with neutrons. To provide for uniform doping, the crystals must be free from prehistoric defects.

3. *There are no limitations for concentration* of the injected impurity (over a wide range).

4. Application of screens permits obtaining any desired *configuration* of the doped region.

5. There are data indicative of high *resistance* of radiation-doped materials to subsequent heat treatment and exposure to radiation.

The disadvantages of the method include:

1. *Introduction of radiation-induced defects* during irradiation. For this reason, subsequent annealing is necessary. Probably, further development of the method will permit combining the irradiation and annealing procedures.

2. Annealing of radiation-induced defects results in a high concentration of vacancies which in turn leads to *enhanced diffusion* of impurities. Irradiation may yield similar results. In the final analysis, the enhanced diffusion brings about irregular distribution of impurities.

3. The process of nuclear transmutation doping results in formation of unstable isotopes and in *induced radioactivity*.

4. The *exposure time* is a limitation of purely practical nature in the way of doping some materials, such as silicon.

5. The type of impurity to be introduced is still another basic limitation worthy of consideration.

Nuclear transmutation doping permits injecting impurities in the form of the elements located in the periodic system beside the source material elements.

In spite of the foregoing limitations, the method of doping by nuclear transmutation is of great interest to the investigators because

it permits obtaining an impurity concentration easily controlled and uniformly distributed throughout the ingot volume. Further improvement will provide for its wide industrial application of the.

The selective nuclear transmutation doping with the use of charged particles may prove to be useful in modern semiconductor electronics which employs planar technology.

References

1. *Experimental Nuclear Physics.* 2. Ed. by E. Segre, 1955, 493 pages, N.Y.
2. *The Tables of Physical Quantities. A handbook.* Ed. by I. K. Kikoin, Moscow, Atomizdat, 1976, 1008 pages (in Russian).
3. Curtiss, L. F. *Introduction to Neutron Physics*, Princeton, 1959, 380 pages.
4. Beckurts, K., Wirtz, K. *Elementare Neutronenphysik.* Berlin, 1958, 243 pages.
5. Preston, M. A. *Physics of the Nucleus.* Addison-Wesley publ. co. 1962.
6. De Benedetty, S. *Nuclear Interactions.* New York, 1964, 636 pages.
7. *The Nuclear Handbook.* Consult. ed. O. R. Frish, London, 1958, 600 pages.
8. Chukichev, M. V., Vavilov, V. S. Formation of lattice defects by thermal neutrons during irradiation of silicon monocrystals in a nuclear reactor. *Fizika tverd. tela*, 1961, 3, 5 (in Russian).
9. Kharchenko, V. A., Solovyev, S. P. Radiation doping of silicon. *Fizika i tekhnol. polupr.*, 1971, 5, 8, pp. 1641-1643 (in Russian).
10. Haas, W. E., Schnöller, M. S. Silicon doping by nuclear transmutation. *J. Electronic Materials*, 1976, 5, 1, pp. 57-68.
11. Schweinler, H. C. Some consequences of thermal neutron capture in silicon and germanium. *J. Appl. Phys.*, 1959, 30, 8, pp. 1125-1126.
12. Konorova, L. Litovsky, M., Malkovich, R., *et al.* A study of radiation doped silicon. *Fizika i tekhnol. polupr.*, 1977, 11, 10, (in Russian).
13. Mordkovich, V. N., Solovyev, S. P., Temper, E. M., Kharchenko, V. A. Conductivity of neutron irradiated and annealed silicon. *Fizika i tekhnol. polupr.*, 1974, 8, 1, pp. 210-213 (in Russian).
14. Kharchenko, V. A., Solovyev, S. P. Silicon doping by radiation. *Izv. AN SSSR. Ser. Neorganich. mater.*, 1971, 7, 12 (in Russian).
15. Kharchenko, V. A., Solovyev, S. P., Voronov, I. N., Kuzmin, I. I., Smirnov, B. V. Defect structure etching study of fast neutron irradiated silicon. *Fizika i tekhnol. polupr.*, 1971, 5, 4, pp. 730-735 (in Russian).
16. Kharchenko, V. A., Smirnov, B. V., Solovyev, S. P., Fetisova, G. A., Voronov I. N., Bane V. E. Effects of heat treatment on electrophysical properties of radiation-doped silicon. *Izv. AN SSSR Ser. Neorganich. mater.*, 1971, 7, 12, pp. 2142-2145 (in Russian).
17. Gres'kov, I. M., Solovyev, S. P., Kharchenko, V.A. Effects of growth defects on a change in conductivity of neutron irradiated silicon. *Fizika i tekhnol. polupr.*, 1977, 11, 8, pp. 1598-1602 (in Russian).
18. Didkovsky, A. P., Saakova, A. K., Khivrich, V. I. Some electrical properties of high-ohmic radiation-doped silicon. *Fizika i tekhnol. polupr.*, 1976, 10, 3, pp. 543-545 (in Russian).
19. Lark-Horowitz, K. Bombardment of semiconductors by nucleons. In: *Semiconducting Materials.* Ed. by Henisch H. K. London, 1951, 281 pages.
20. Mirianashvili, Sh. M., Nanobashvili, G. I. Razmadze, Z. G. On feasibility of nuclear transmutation doping of indium antimonide. *Fizika tverd. tela*, 1965, 7, 12, pp. 3566-3570 (in Russian).
21. Mirianashvili, Sh. M., Nanobashvili, D. I. On feasibility of nuclear transmutation doping of gallium arsenide. *Fizika i tekhnol. polupr.*, 4, 10, (in Russian).

Printed in the Union of Soviet Socialist Republics